ABSTRACT

Reconstruction of Late Pleistocene Paleoenvironments
of the Lake Victoria Region using Paleosols and Freshwater Tufa

Emily J. Beverly, Ph.D.

Committee Co-Chairman: Steven G. Driese, Ph.D.
Committee Co-Chairman: Daniel J. Peppe, Ph.D.

Lake Victoria is the largest freshwater lake in the tropics by surface area (68,800 km^2) and is currently a biogeographic barrier between the eastern and western branches of the East African Rift. Lake Victoria has desiccated in the past at ~17 ka and at ~15 ka, but little is known about its history prior to the Last Glacial Maximum. The Middle to Late Pleistocene deposits exposed on the shoreline of eastern Lake Victoria, which preserve abundant vertebrate fossils and Middle Stone Age (MSA) artifacts, are ideal for paleoenvironmental and paleoclimatic reconstructions to understand the effect of changing environment during the migration of early modern humans within and out of Africa. Measured stratigraphic sections reveal fluvial and tufa deposits that directly overlie Miocene paleotopography. The ages (94.0±3.3, 111.4±4.2, and 455±45 ka) of these tufa deposits demonstrate that spring-fed rivers were a recurrent, variably preserved feature on the Pleistocene landscape for ~360 kyr, but tufa precipitation abruptly ceased at ~94 ka. Above the riverine tufas, three well-exposed and laterally continuous paleosols with intercalated tuffs allow for reconstruction of modern soil properties and estimates of

mean annual precipitation (MAP). The oldest paleosol is a smectitic paleo-Vertisol with vertic features and saline and sodic properties that indicate seasonal precipitation. Higher in the section, the paleosols are tuffaceous paleo-Inceptisols with Alfisol-like soil characteristics (illuviated clay). Paleosol MAP proxies indicate that MAP was 44% of modern between ~94 ka and >35 ka. These paleoprecipitation estimates were applied to a water budget model to understand the effects of prolonged aridity on the Lake Victoria region. When MAP is 44% of modern, Lake Victoria desiccates within centuries, but refills slowly (e.g., >10 kyr) until precipitation is >94% of modern, at which point it can be refilled in centuries. Therefore, it is likely that Lake Victoria was desiccated for most, if not all, of the interval between 94 and >35 ka. Prolonged desiccation would have removed a major barrier for the movement of fauna, including early modern humans, and provided a long-term dispersal corridor between the rifts and across the equator.

Reconstruction of Late Pleistocene Paleoenvironments of the Lake Victoria Region using Paleosols and Freshwater Tufa

by

Emily J. Beverly, B.A., M.S.

A Dissertation

Approved by the Department of Geology

____

Stacy C. Atchley, Ph.D., Chairperson

Submitted to the Graduate Faculty of
Baylor University in Partial Fulfillment of the
Requirements for the Degree
of

Doctor of Philosophy

Approved by the Dissertation Committee

____

Steven G. Driese, Ph.D., Co-Chairperson

____

Daniel J. Peppe, Ph.D., Co-Chairperson

____

Stephen I. Dworkin, Ph.D.

____

Joseph V. Ferraro, Ph.D.

____

Lee C. Nordt, Ph.D.

Accepted by the Graduate School
December 2015

____

J. Larry Lyon, Ph.D., Dean

Page bearing signatures is kept on file in the Graduate School.

TABLE OF CONTENTS

LIST OF FIGURES

LIST OF TABLES

ACKNOWLEDGMENTS

I would like to thank my co-advisors, Dr. Steven Driese and Dr. Daniel Peppe, for their outstanding examples of the type of professor that I hope to be. Thank you also to my committee members: Dr. Steve Dworkin, Dr. Joe Ferraro, and Dr. Lee Nordt who provided thoughtful discussion and review throughout this project. Thank to you to Dr. Christian Tryon, Dr. Tyler Faith, and Nick Blegen for their collaboration that I hope will continue into the future. I would like to thank Dr. Ren Zhang for his assistance with the stable isotope analyses. I would also like to thank the Kenyan field assistants, Stephen Longoria and Zach Ogutu, without whom none of this would have been possible, as well as those who worked in our camp Jackson Shaduma and Dickens Aketch. Thank you to my field and lab assistants Will Horner and Nicky Arellano for their tireless "munselling" and "shatterboxing." I am also indebted to Paulette Penney, Jamie Ruth, and Janelle Atchley for their help with all things Baylor. Thank you to the entire faculty who taught me so much over the past four years. I would also like to thank all of the graduate students for their support and friendship. Thank you to my parents Jane and Rex Beverly who offered continuous support for their daughter's desire to study dirt and rocks. This research was made possible by funding from the National Geographic Society Committee for Research and Exploration (9284-13 and 8762-10), the National Science Foundation (BCS-1013199 and BCS-1013108), the Leakey Foundation, the Geological Society of America, the Society for Sedimentary Geology (SEPM), the University of Queensland, Baylor University, the Baylor University Department of Geology Dixon Fund, New York University, Harvard University, and the American School for Prehistoric Research.

CHAPTER ONE

Introduction

Modern humans likely evolved in eastern Africa by 200 ka and by 80 to 60 ka had migrated throughout Africa and into Eurasia (Brown and others, 2012; Liu and others, 2006b; McDougall and others, 2005), but little empirical data on the climate or environment associated with archaeological sites are available from East Africa (Blome and others, 2012). Climate-driven environmental change is a commonly suggested mechanism for the dispersals of humans due to changes in biogeographic barriers and resource availability (Cowling and others, 2008; Eriksson and others, 2012; Rito and others 2013). The Lake Victoria region has the potential to provide critical paleoenvironmental and paleoclimatic data on equatorial East Africa to better understand this interval of human evolution. However, sediment cores from Lake Victoria only extend back to ~19 ka to the end of the Last Glacial Maximum (LGM), and paleoenvironmental data prior to the LGM is very limited (Blome and others, 2012; Johnson and others, 1996; Stager and others, 2002, 2011). Sediments deposited along the modern eastern shoreline of Lake Victoria near Karungu, Kenya are dated to between 455 ka and >33 ka and preserve abundant vertebrate fossils and Middle Stone Age (MSA) artifacts (Beverly and others, 2015a,b; Blegen and others, 2015; Faith et al., 2015; Tryon and others, 2010, 2012, 2014). The objectives of this research are to: i) use field descriptions and mapping, petrography and micromorphology, stable isotopes, bulk geochemistry to estimate paleoprecipitation, and paleopedology to reconstruct the environment through time, ii) provide context for the faunal and archaeological records, and iii) integrate the paleoclimate reconstruction into the broader understanding of Africa climate during the Late Pleistocene.

Chapter Two focuses on the oldest deposits at Karungu, which are riverine tufas deposited directly on top of Miocene bedrock. These riverine tufas or freshwater spring deposits are ideal for reconstructions because they record both paleoenvironmental information about the types of plants growing on the landscape in the carbon isotopes and paleoclimatic information about the source of precipitation in the oxygen isotopes. These tufas were constructed using a combination of field mapping, petrography, stable isotopes of carbon and oxygen, and U-series dating that indicate that these riverine tufas were deposited intermittently over an interval of ~355 ka. The large grain sizes indicates that rainfall was flashy and ephemeral due to the East African Monsoon, but perennial springs fed these rivers providing water for fauna such as hippopotamus and creating paludal areas where high abundances of C_3 plants, such as *Typha* were identified within an overall semi-arid C_4 grassland. This indicates that these spring-fed rivers were permanent water source for humans and associated fauna within an overall semi-arid environment.

Chapter Three focuses on one locality known as Kisaaka, which has the most laterally extensive (~2 km) and thickest (11 m) outcrops at Karungu. The deposits are primarily paleosols that provided critical paleoenvironmental information using paleosol proxies that can reconstruct paleoprecipitation and soil properties such fertility. Three paleosols are intercalated with tuffs that blanket the landscape and allow for lithostratigraphic correlation between outcrops, preserve the original topography, and allow for reconstruction of three distinct landscapes or catenas through time. The oldest catena formed between ~94 and 49 ka and has a well-developed and fertile, paleo-

Vertisol with salinity and sodicity problems that would have affected plant growth and limited the types of plants growing on the landscape. The upper two catenas are paleo-Inceptisols with an abundance of tephra, which weathered to form illuviated clay. The amount of illuviated clay (3-5%) suggests that these paleo-Inceptisols would have been in equilibrium with climate and supports the MAP estimates of 764±182 mm yr^{-1} for Vertisols (CALMAG) and 813 to 963±108 mm yr^{-1} for all other paleosols (CIA-K). There are no statistical changes between the paleosols throughout this interval between 94 and >33 ka, which indicates that climate was significantly drier than modern for an extended period. These are the first paleoprecipitation estimates for the region and likely would have resulted in a significant reduction in the size of Lake Victoria during the Late Pleistocene. This reduction in precipitation is supported by the saline-sodic conditions identified in the paleosols and C_4 grassland signature identified in fossil and pedogenic stable C and O isotope analyses (Faith and others, 2015; Garrett and others, 2015). This expansion of grassland suggests that the Serengeti may be an appropriate modern analog for this reconstructed series of landscapes at Kisaaka during the Late Pleistocene.

Chapters Two and Three focused on reconstructing the paleoenvironment to give context to the paleotology and archaeology identified at Karungu. Chapter Five combines the research from the first two chapters with additional data from paleosol paleoprecipitation proxies to understand the climate in a regional context. Thirteen Late Pleistocene paleosols indicate that paleopreciptation was 44% of modern between ~94 and >33 ka. At that precipitation, previous models indicated that Lake Victoria would be reduced to <10% of current surface area (Broecker and others, 1998: Milly, 1999), but these models do not include changes in temperature or insolation. These paleoprecipitation estimates from paleosols are applied to a water budget model to understand how a reduction in precipitation of this magnitude would affect the lake level and surface area of Lake Victoria, which is a currently a biogeographic barrier to migrations of humans and other fauna between the eastern and western branches of the East African Rift. This model suggests that Lake Victoria would have been desiccated between ~94 and >33 ka because precipitation was below a threshold that Lake Victoria could sustain itself. Grasslands would have expanded and enhanced the Nilotic corridor as an avenue for the migration of humans out of Africa and into Eurasia.

CHAPTER TWO

Recurrent spring-fed rivers in a Middle to Late Pleistocene semi-arid grassland: Implications for environments of early humans in the Lake Victoria Basin, Kenya

This chapter published as: Beverly, E.J., Driese, S.G., Peppe, D.J., Johnson, C.R., Michel, L.A., Faith, J.T., Tryon, C.A., and Sharp, W.D., 2015, Recurrent spring-fed rivers in a Middle to Late Pleistocene semi-arid grassland: Implications for environments of early humans in the Lake Victoria Basin, Kenya: Sedimentology, v. 62, 1611-1635.

Abstract

The effect of changing palaeoclimate and palaeoenvironment on human evolution during the Pleistocene is debated, but hampered by few East African records directly associated with archaeological sites prior to the Last Glacial Maximum (LGM). Middle to Late Pleistocene deposits on the shoreline of eastern Lake Victoria preserve abundant vertebrate fossils and Middle Stone Age artefacts associated with riverine tufas at the base of the deposits, which are ideal for palaeoenvironmental reconstructions. New data from tufas identified on Rusinga Island and on the mainland near Karungu, Kenya are provided from outcrop, thin-sections, mineralogical, stable isotopic, and U-series dating analyses. Tufa is identified at four sites: Nyamita (94.0±3.3 and 111.4±4.2 ka), Kisaaka, Aringo (455±45 ka), and Obware. The age ranges of these tufa deposits demonstrate that spring-fed rivers were a recurrent, variably preserved feature on the Pleistocene landscape for ~360 kyr. Poor sorting of clastic facies from all sites indicates flashy, ephemeral discharge, but these facies are commonly associated with barrage tufas, paludal environments with $\delta^{13}C$ values of ~10‰ indicative of C_3 plants and fossil *Hippopotamus,* all of which indicate a perennial water source. Other tufa deposits from Nyamita, Obware and Aringo have a mixed C_3/C_4 signature consistent with a semi-arid

C_4 grassland surrounding these spring-fed rivers. The $\delta^{18}O$ values of tufa from Nyamita are on average ~1‰ more negative than calcite precipitated from modern rainfall in the region, suggesting greater contribution of depleted monsoonal input, similar to the LGM. Microdebitage and surface collected artefacts indicate that early modern humans were utilizing these spring-fed rivers. The presence of spring-fed rivers would have afforded animals a reliable water source, sustaining a diverse plant and animal community in an otherwise arid environment.

Introduction

Homo sapiens likely evolved in eastern Africa by ~200 ka and by 80 to 60 ka had dispersed throughout Africa and into Eurasia (e.g. McDougall *et al*., 2005; Liu et al., 2006a; Brown *et al.*, 2012). Understanding the diversity of early human populations and the mechanisms underlying their dispersals continues to be a challenge because few empirical data on climate or environment associated with archaeological sites are available from East Africa prior to the Last Glacial Maximum (LGM) (e.g. Blome *et al.*, 2012). Changing palaeoclimate and palaeoenvironment is a commonly proposed mechanism for mediating human behavioral diversity and dispersals through their effects on population distributions and demographics, through the creation and removal of biogeographic barriers and through behavioral adaptations to resource availability (e.g. Ambrose & Lorenz, 1990; Scholz *et al.*, 2007; Cowling *et al.,* 2008; Eriksson *et al.*, 2012; Rito *et al.*, 2013). The Lake Victoria Basin has the potential to provide critical palaeoenvironmental and palaeoclimatic information in equatorial East Africa during this interval of human evolution (Fig. 2.1A). Although Lake Victoria provides excellent records during and after the LGM (e.g. Johnson *et al.*, 1996; Talbot & Laerdal, 2000;

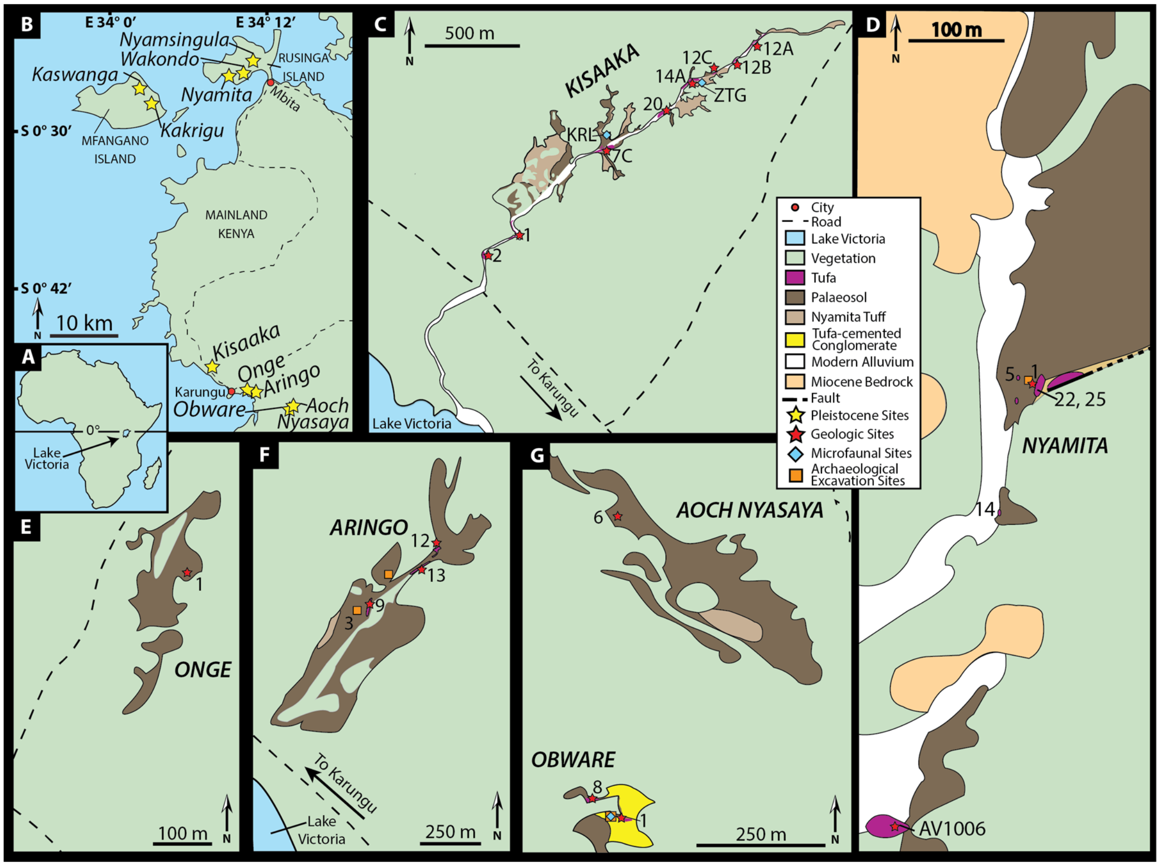

Figure 2.1: Location maps and Pleistocene exposures. (A) Inset shows the location of Lake Victoria in East Africa. (B) Location of Pleistocene sites along the eastern margin of Lake Victoria. (C), (D), (E), (F) and (G) Mapped lithologies exposed at the Kisaaka, Nyamita, Onge, Aringo, and Obware sites with key geologic, archaeological, and microfaunal locations identified. Note tufa denoted in magenta.

Stager *et al.*, 2002, 2011), there are few data available prior to the LGM. Recent work indicates that sediments and correlative tephra between ~455 and 45 kyr old are exposed on Rusinga and Mfangano Islands and on the mainland near Karungu, Kenya (Fig. 2.1B). These sediments preserve abundant vertebrate fossils and Middle Stone Age (MSA) artefacts (Owen, 1937; Tryon *et al.*, 2010, 2012, 2014; Faith *et al.*, 2015). Additional high-resolution geologic context would greatly expand the pre-LGM palaeoenvironmental and palaeoclimatic record of the region.

Tryon *et al.* (2014) and Van Plantiga (2011) previously identified freshwater tufas at Rusinga Island, and recent fieldwork at Karungu identified additional tufa deposits exposed near the base of the Pleistocene stratigraphic successions (Figs. 2.1 and 2.2). Rapidly accumulating, groundwater-fed riverine tufas are ideal for palaeoclimatic and palaeoenvironmental reconstructions, especially where these tufas are laminated and formed in barrage or paludal environments (Matsuoka *et al.*, 2001; Ihlenfeld *et al.*, 2003; Andrews & Brasier, 2005; Andrews, 2006). The importance of tufa in the palaeoanthropological record has been long recognized, but previously restricted to Early and Middle Pleistocene deposits (e.g. Wendorf, 1993; Haynes *et al.* 1997; Nicoll *et al.*, 1999; Smith *et al.*, 2004, 2007; Garcea & Giraudi, 2006; Barich & Garcea, 2008; Johnson *et al.*, 2009; Ashley *et al.*, 2009, 2010a,b,c, 2014; Johnson & McBrearty, 2012).

Following Pedley *et al.* (2003), tufa is defined here as a low-Mg carbonate precipitated under ambient temperatures from freshwater discharge and is preferred over travertine, which is usually reserved for carbonates produced by thermal waters. New data are presented on the tufas identified on Rusinga Island and Karungu (Fig. 2.1B). The objectives of this study are to: (i) use field descriptions, petrography, and stable isotopes of carbon and oxygen to characterize the depositional environments of riverine tufa deposits; (ii) combine new geologic data presented here with previous geological, archaeological, and palaeontological interpretations to provide better context for the faunal and archaeological record; and (iii) integrate this into the regional palaeoenvironment and palaeoclimate of the Middle and Late Pleistocene in East Africa, which will help to quantify the pressures that contributed to human evolution and migration.

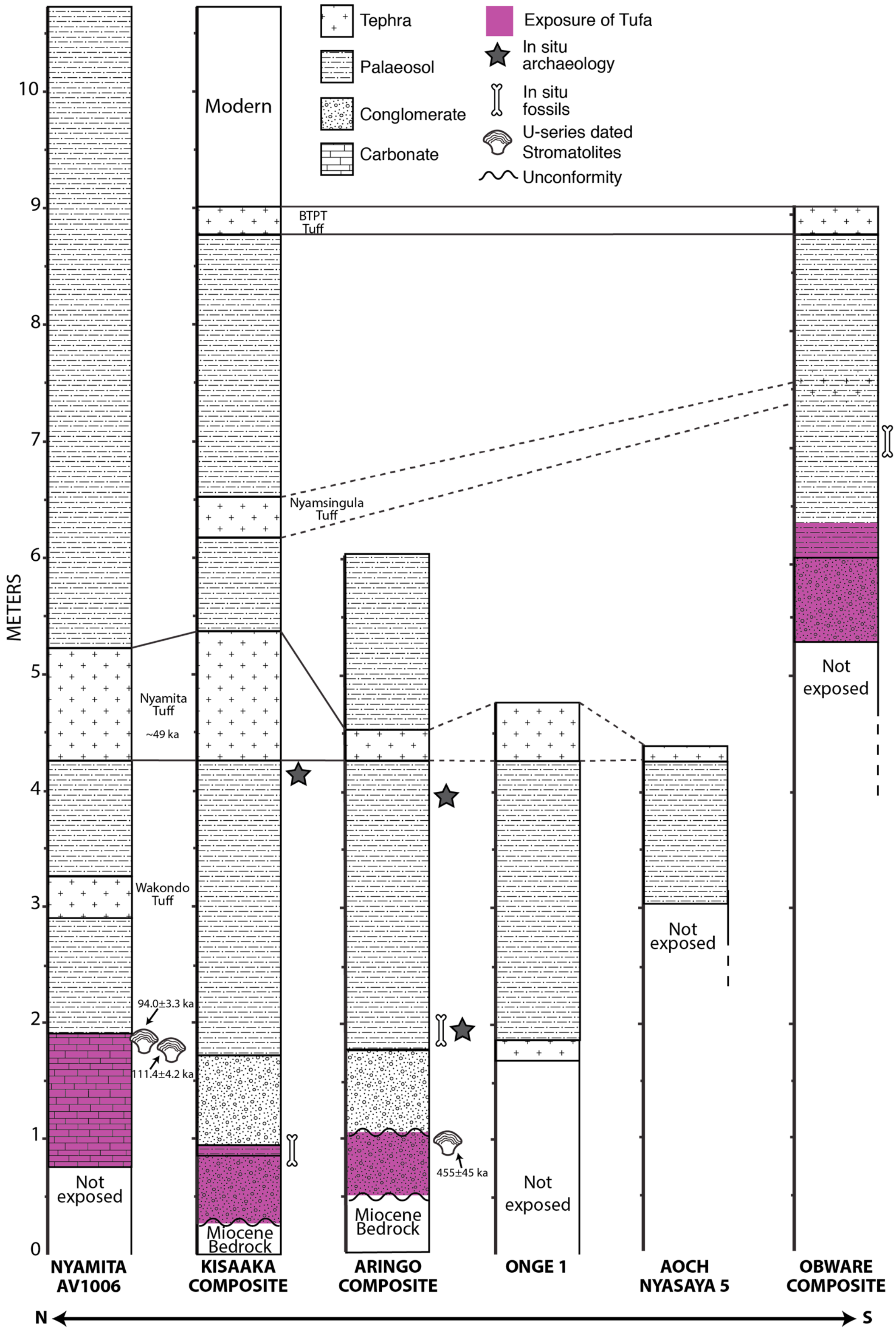

Figure 2.2: Stratigraphy from type sections at each site correlated using the base of the Nyamita Tuff and BTP Tuff as datum surfaces. Tufa is denoted in magenta and sites are arranged from north to south. See Fig. 2.1 for locations of sites. Locations of *in situ* archaeology and fossils are located on the stratigraphy as well as U-series dates. Tephrostratigraphic correlations from Blegen *et al.* (2015).

Setting

Lake Victoria Region

The research presented here focuses on the eastern margin of Lake Victoria in western Kenya (Fig. 2.1A and B). Lake Victoria spans the equator between the western and eastern branches of the East African Rift System (EARS) and is the largest freshwater lake in the tropics by surface area (~66,400 km^2; Crul, 1995; Stager & Johnson, 2008). The lake likely formed between ~1.6 and ~0.4 Ma due to back-ponding created by uplift of the western arm of the EARS that dammed westward-flowing rivers (Kent, 1944; Doornkamp & Temple, 1966; Bishop & Trendall, 1967; Ebinger, 1989; Johnson *et al.*, 1996; Talbot & Williams, 2009). Unlike the other African Great Lakes, Lake Victoria is not situated within a rift basin, and therefore, it is very shallow with a maximum depth of ~68 m (Stager & Johnson, 2008).

The lake is hydrologically open with two major inlets, the Kagera and Katonga Rivers, and the Victoria Nile as the primary outlet (Talbot & Williams, 2009). Up to 80% of the water input is from direct precipitation on the lake surface, and most of the water loss (up to 90%) is from evaporation (Crul, 1995). The Intertropical Convergence Zone (ITCZ) is the primary control on precipitation in the Lake Victoria region, and it crosses the region twice a year, first in March bringing long rains, and again in October, bringing shorter rains (Song *et al.*, 2004). Modern mean annual precipitation (MAP) of the entire Lake Victoria region is ~1600 mm yr^{-1}; however, there is variability in MAP across the lake (Crul, 1995; Fillinger *et al.*, 2004). At Mbita, which is proximal to the study area (Fig. 2.1B), MAP is ~1400 mm yr^{-1} (Crul, 1995; Fillinger *et al.*, 2004). The shallow depth and dependence on direct precipitation to maintain lake levels means that the Lake

Victoria region is very sensitive to changes in precipitation (e.g. Broeker *et al.*, 1998; Milly, 1999), making the region an ideal archive for equatorial East African palaeoclimatic and palaeoenvironmental research. Geological evidence suggests that during the Pleistocene the lake markedly increased in size (compared to modern) and desiccated multiple times, most recently at 16 ka (Heinrich Stadial 1; Johnson *et al.*, 1996; Talbot & Laerdal, 2000; Stager *et al.*, 2002, 2011).

Rusinga Island and Mainland Karungu

The Late Pleistocene geology, fossils, and MSA artefacts from Rusinga and Mfangano Islands have been the focus of research since 2009 (Tryon *et al.*, 2010, 2012, 2014; Van Plantinga, 2011; Faith *et al.*, 2011, 2012, 2014, 2015, in press; Blegen *et al.*, 2015). The Pleistocene deposits on Rusinga Island, informally designated the Wasiriya Beds by Pickford (1984), unconformably overlie a complex Miocene palaeotopography and are predominately comprised of tuffaceous alluvial and fluvial sediments intercalated with palaeosols that formed during periods of landscape stability, variably reworked tephra, and rare tufa deposits (Van Plantinga, 2011; Tryon *et al.*, 2010, 2012, 2014). The tephra deposits can be correlated between sites on the basis of geochemical compositional similarity (Tryon *et al.*, 2010; Van Plantinga, 2011; Blegen *et al.*, 2015).

On Rusinga Island there are three major Pleistocene fossil-bearing and artefact-bearing localities: Nyamsingula, Wakondo, and Nyamita (Fig. 2.1B). The deposits at Nyamita are the best exposed and most abundant, and it is the only site on Rusinga Island with tufa deposits (Van Plantinga, 2011; Tryon *et al.*, 2014). The tufa deposits are exposed at the base of the Pleistocene stratigraphic succession unconformably overlying the faulted Miocene bedrock (Fig. 2.2). At Nyamita, this faulting created an angular unconformity in the Miocene bedrock (mapped by Van Couvering, 1972) that is associated with the Pleistocene tufa at Nyamita 1 (Fig. 2.1D). The Wasiriya Beds are exposed along an ~1 km transect following a modern spring-fed channel, and are generally poorly sorted muds, sands, and gravels with weakly developed palaeo-Inceptisols and palaeo-Vertisols (Van Plantinga, 2011). Carbon isotopes from pedogenic carbonate indicate a significant local C_3 plant signal with ~64% woody cover at Nyamita, in what was otherwise a landscape dominated by C_4 grasses (Garrett *et al.*, 2015). The exposures range from 3 to 12 m thick and have been lithostratigraphically correlated along the transect using multiple marker tephra (Van Plantinga, 2011).

Based on geochemical composition, the tephra deposits are likely derived from Rift Valley sources that began erupting ~100 ka (maximum age) (Tryon *et al.*, 2010, 2012; Blegen *et al.*, 2015). At the Nyamita localities included in this study, two tuffs are exposed: the Nyamita Tuff and the Wakondo Tuff (Tryon *et al.*, 2010; Blegen *et al.*, 2015). AMS radiocarbon dates on gastropods that post-depositionally burrowed into the sediments at Nyamita provide a minimum age of ~45 kyr for the deposits (Tryon *et al.*, 2010). In addition, dates from optically stimulated luminescence (OSL) of deposits above and below the Nyamita Tuff indicate that it was deposited ~49 ka (Fig. 2.2; Blegen *et al.*, 2015). The Nyamita Tuff is thick and distinct, is found at almost all Pleistocene sites in this region (Blegen *et al.*, 2015). The Wakondo Tuff was deposited between ~100 and 50 ka based on optically stimulated luminescence (OSL) dates from overlying strata and tentative correlations to eruptions from Rift Valley volcanic sources with published age estimates of 100±10 kyr (Tryon *et al.*, 2010; Blegen *et al.*, 2015). The tufa is exposed at the base of the section below the Nyamita and Wakondo Tuffs, suggesting that the tufa is

~100 kyr old or older (Fig. 2.2). Below we present new U-series dates on the tufa that support these estimates.

More recently, this research has expanded to include Middle to Late Pleistocene deposits ~40 km to the south near Karungu, which can be correlated to those on Rusinga Island using tephrostratigraphy (Blegen *et al.*, 2015; Faith *et al.*, 2015). Abundant fossils and MSA artefacts have long been reported from Karungu (Owen, 1937; Pickford, 1984), but until recently only limited geological mapping and reconstructions of the palaeoclimate or palaeoenvironment have been conducted. Fieldwork conducted from 2012 to 2013 revealed deposits at Karungu similar to those from Rusinga Island (Faith *et al.*, 2015). These Pleistocene deposits are best exposed at five of the seven sites in the Karungu area mapped by Pickford (1984): Kisaaka, Aringo, Onge, Aoch Nyasaya, and Obware (Fig. 2.1B). Sediment thickness is variable and ranges from 3.5 to 10.5 m of deposition overlying Miocene bedrock with eroded topography similar to the Nyamita site (Blegen *et al.*, 2015; Faith *et al.* 2015). Although the Pleistocene stratigraphic succession varies with locality, at Kisaaka, Aringo, and Obware, the Nyamita Tuff blankets a palaeo-Vertisol that overlies a freshwater tufa commonly directly precipitated on the Miocene bedrock (Faith *et al.*, 2015).

Paleontology and Archaeology of Rusinga Island and Karungu

Previous research has shown that the Pleistocene deposits surrounding Lake Victoria yield an abundance of well-preserved fossils and MSA artefacts (e.g. Owen, 1937; Kent, 1944; Pickford, 1984; Behrensmeyer *et al.*, 1995; Ditchfield *et al.*, 1999; Plummer *et al.*, 1999; Tryon *et al.*, 2010, 2012, 2014; Van Plantiga, 2011; Faith *et al.*, 2011, 2012, 2013, 2014, 2015, in press; Garrett *et al.*, 2015). Stone artefacts from

Rusinga Island and Karungu include flakes, blades, retouched points, and Levallois cores, consistent with a MSA attribution (Tryon *et al.*, 2014; Faith *et al.*, 2015), the industry associated with the earliest modern humans.

Late Pleistocene palaeoenvironmental evidence from Rusinga Island and Karungu indicates an expansion of semi-arid grasslands during one or more intervals between ~100 and 45 ka (Faith *et al.*, 2012, 2014, 2015; Tryon *et al.*, 2012, 2014). The fauna are dominated by alcelaphine bovids (wildebeest and allies) and equids, suggesting environments that were grassier and probably drier than the evergreen bushland, thicket, and woodland found in the region today. Oryx (*Oryx beisa*) and Grevy's zebra (*Equus grevyi*), which prefer arid to semi-arid grasslands and shrublands, and extinct antelopes adapted to grazing in dry grasslands, indicate that the environment was significantly more arid than at present (Faith *et al.*, 2011, 2012, 2013, 2014, 2015; Tryon *et al.*, 2010, 2012, 2014). Carbon isotopes of mammalian tooth enamel indicate a diet of predominately C_4 grasses (Faith *et al.*, 2015; Garrett *et al.*, 2015). Several taxa also indicate freestanding water, such as the hippopotamus (*Hippopotamus amphibius*) and reduncine bovids like the southern reedbuck (*Redunca arundinum*). Overall the fauna identified at Rusinga Island and Karungu suggest generally open grasslands with localized areas of standing water.

Methods

Field Methods

Tufa was identified at four sites: Nyamita, Kisaaka, Aringo, and Obware (Fig. 2.1). All outcrops were recorded and mapped using GPS, multiple stratigraphic sections at each site were measured, and macroscale features were logged in detail and photographed. Representative samples from each outcrop were collected for mineralogical, stable isotope analysis, and U-series dating. Additional oriented samples were collected for micromorphological analysis of representative features.

Laboratory Methods

Samples were pulverized using a Spex SamplePrep 8515 enclosed shatter box for analysis of mineralogy. Mineralogical analysis of 9 representative samples was conducted at Baylor University on a Siemens D-5000 θ-2θ X-ray diffractometer (XRD) using Cu Kα radiation at 40Kv and 30mA. Samples were scanned from 2 to 60º 2θ, at a 0.05º step per 1.5 seconds. Seventeen thin-sections were prepared commercially by Spectrum Petrographics, Inc. Three thin-sections were double-polished to enhance imaging. Petrographic study of tufas was conducted at Baylor University using techniques developed by Riding (2000) and Freytet & Verrecchia (2007), and references therein, on an Olympus BX-51 polarized-light microscope equipped with a 12.5 MPx digital camera and ultraviolet fluorescence (UVf) attachment. Changes in organic matter content were visually estimated by subjecting the thin section to UVf causing the organic matter to autofluoresce. Photomicrographs were taken using three different UVf wavelength filters, NU, NB, and TXRED, in addition to cross-polarized light (XPL) and plane-polarized light (PPL) of unique and representative features. A Relion Industries® cathodoluminescence (CL) microscope was used to determine changes in redoximorphic environments of the carbonates and assess diagenetic alteration of the calcite. Carbonate forming in a shallow reducing environment with higher manganese to iron ratios will luminesce, whereas carbonate forming in an oxidizing environment will be non-luminescent (Barnaby & Rimstidt, 1989; Machel *et al.*, 1991).

Thin sections were used also to determine areas with little detrital input to sample for U-series dating. One sample from Aringo and two from Nyamita were used for U-series dating due to minimal detrital contamination and dense micrite. Tufa from the Kisaaka and Obware sites contained too much detrital contamination. Analyses were performed at the Berkeley Geochronology Center using a Thermo NEPTUNE *Plus* Multi-Collector-Inductively-Coupled-Mass-Spectrometer (MC-ICP-MS). Samples from stromatolitic tufas were drilled from oversized thin section chips using a moat-and-spall technique that yielded intact chips consisting of lamina selected based on examination of the facing thin section. The chips were cleaned by repeated cycles of ultrasonic treatment and rinsing in de-ionized water. Samples weighing *ca* 20 mg were totally dissolved using sequential treatment with HNO_3 and concentrated HF + perchloric acid and then were equilibrated with a mixed spike containing ^{229}Th, ^{233}U, and ^{236}U. The spike was calibrated against solutions of NBL CRM 145 and solutions prepared from a 69 Myr old U ore that has been demonstrated to yield concordant U/Pb ages [Schwartzwalder Mine, Colorado, USA (hereafter, SM); Ludwig *et al.*, 1985] and sample-to-sample agreement of $^{234}U/^{238}U$ and $^{230}Th/^{238}U$ ratios. U and Th were separated using two stages of HNO_3–HCl cation exchange chemistry followed by reaction with HNO_3 and $HClO_4$ to remove any residual organic material from ion exchange resins. Measured peak heights were corrected for multiplier dark noise/Faraday baselines, background intensities, ion counter yields, peak-tail contributions, and interfering spike isotopes. Mass fractionation was determined using the gravimetrically determined $^{233}U/^{236}U$ ratio of the spike. The external reproducibility of $^{234}U/^{238}U$ and $^{230}Th/^{238}U$ ratios of SM solutions measured during each mass spectrometry session was better than 0.2 % (2σ). Ages were calculated using the half-lives of Jaffey (1971) for ^{238}U, Holden (1990) for ^{232}Th, and Cheng *et al.* (2013) for ^{230}Th and ^{234}U. Uncertainties of corrected mean ages for each site are stated at the 95% confidence level and include measurement uncertainties as well as uncertainties associated with the initial isotope corrections. Complete U-Th analytical data are available in Table 2.1. Two sub-samples of each sample were analyzed to check the reproducibility of their U-series dates, and in all cases good agreement between such sub-samples was observed, increasing our confidence in the dates.

Tufa samples were micro-drilled using a 1 mm diameter drill. The features identified in thin section guided sampling of tufa facies. Each unique carbonate feature was sampled in replicates of three to ensure reproducibility. The $\delta^{13}C$ and $\delta^{18}O$ values of carbonate samples were analyzed at Baylor University's Stable Isotope Laboratory. Samples were loaded into a Thermo Scientific Gasbench II and reacted with 100% phosphoric acid before being introduced into a continuous-flow Thermo Scientific Delta-V mass spectrometer. Repeat isotope analysis of an in-house standard gives an analytical uncertainty of ± 0.16‰ for carbon and ± 0.07‰ for oxygen. The $\delta^{13}C$ and $\delta^{18}O$ results are expressed as the standard per mil (‰) and are normalized using two standards relative to the Vienna PeeDee Belemnite (V-PDB). These data are available in Appendix A.

Results

Tufa is exposed at the base of four sites at Karungu and Rusinga: Nyamita, Kisaaka, Aringo, and Obware (Fig. 2.1). XRD analyses of bulk-powdered samples indicate that all samples are low-Mg calcite with variable amounts of detrital clay and quartz. The CL studies indicate non-luminescent to very weakly luminescent carbonate in all samples, suggesting that the tufas formed in a generally oxidizing environment and are unaffected by diagenesis. Carbonate cement is non-luminescent and is interpreted as syndepositional. The XRD and CL petrography reveal no diagenetic alteration or inclusion of Miocene carbonate grains and suggest that all features identified are primary.

Figure 2.2 shows the exposures of tufa using the base of the Nyamita Tuff as the datum, or the Bimodal Trachyphonolitic (BTP) Tuff where the Nyamita Tuff is not exposed. Based on tephra geochemical correlations by Blegen *et al.* (2015) and measured sections and geologic mapping in 2011-2013, the tufa deposits are not considered time equivalent (Fig. 2.2), which is confirmed by U-series dates. Two samples from the tufa at Nyamita were dated. Sample CRJ-11-15 was collected from the upstream or north face of the barrage tufa and has a weighted mean age of 111.4±4.2 kyr BP (95% CI; Table 2.1). Sample CRJ-11-14 from the south or downstream face has a weighted mean age of 94.0±3.3 kyr BP (95% CI; Fig. 2.3D). This is consistent with growth direction of the barrage tufa. In contrast, the tufa from Aringo is significantly older with a weighted mean age of 455±45 kyr BP (95% CI). Detrital contamination of samples from Obware and Kisaaka precluded accurate dating.

Facies and Facies Associations

Facies descriptions follow Pedley (1990), Arenas-Abad *et al.* (2010), and Miall (2010), and the seven carbonate facies and three clastic facies cemented by syndepositional calcite are summarized in Table 2.2.

Table 2.1: U-Th isotopic data and ages for carbonate stromatolites

Sample Name	Sample wt. (mg)	U (ppb)	^{232}Th (ppb)	(^{230}Th /^{232}Th)	(^{232}Th /^{238}U)	± (%)	(^{230}Th /^{238}U)	± (%)	(^{234}U /^{238}U)	± (%)	Uncorrected Age, Error (ka)		Corrected Age, Error (ka)		Initial (^{234}U /^{238}U), ± (abs.)	
13-AR-TS1a	19.08	3199	508.0	22.78	0.051685	0.29	1.1775	±0.27%	1.1379	±0.26%	480	±10	477	±68	1.554	±0.087
13-AR-TS1b	19.63	2605	485.0	20.00	0.060470	0.32	1.2095	±0.34%	1.1673	±0.55%	441	±22	438	±61	1.606	±0.081
												Mean	***455***	***±45***		
CRJ-11-14a	16.56	1541	421.2	10.23	0.088539	0.23	0.9057	±0.52%	1.4660	±0.23%	98.2	±1.1	93.1	±5.7	1.654	±0.047
CRJ-11-14b	16.95	1545	290.8	14.00	0.060996	0.26	0.8540	±0.43%	1.3882	±0.34%	98.2	±1.1	94.5	±4.2	1.534	±0.027
												Mean	***94.0***	***±3.3***		
CRJ-11-15a	17.96	1359	378.1	10.90	0.090256	0.27	0.9834	±0.38%	1.4249	±0.30%	117.7	±1.3	112.5	±6.1	1.631	±0.047
CRJ-11-15b	21.01	1375	378.7	11.14	0.089165	0.30	0.9936	±0.36%	1.4533	±0.31%	115.5	±1.3	110.5	±5.9	1.668	±0.049
												Mean	***111.4***	***±4.2***		

All isotope ratios are activity ratios. Uncertainties are given at 2 standard deviations, except for mean ages, which are 95% C.I. Uncorrected ages are calculated without correction for U and Th from detritus. Corrected ages are calculated assuming detritus with (^{232}Th/^{238}U) = 1.2 ±0.6, (^{230}Th/^{238}U) = 1.0 ±0.1, and (^{234}U/^{238}U) = 1.0 ±0.1. Initial (^{234}U/^{238}U) is back-calculated from the measured ratios using the corrected ages. Decay constants are those of Jaffey (1971) for ^{238}U and Cheng et al. (2013) for ^{230}Th and ^{234}U.

Carbonate facies. Two distinct stromatolite facies occur at Nyamita and Aringo: the barrage stromatolite (Ls1); and the isolated stromatolite (Ls2). Facies Ls1 is a hemidomic boundstone with high-angle undulatory and planar laminations that nucleated on a conglomerate (Figs. 2.3D and 2.4D). The barrage stromatolite facies covers an area approximately 10 m^2 at Nyamita AV1006 (Fig. 2.1D). The laminations are alternating light-coloured and dark-coloured, dense micrite (α-lamina), as well as porous micrite (β-lamina) with very little volcaniclastic detritus (Fig. 2.4D and E; Freytet & Plet, 1996). Cyanobacteria filaments are preserved most commonly in these dense laminations (Fig. 2.4D). Dissolution surfaces can be identified by undulating surfaces of insoluble organic matter and FeMn (Fig. 2.4D). The porosity in Fig. 2.4E is most likely created by aquatic larval insects such as pyralids (moths), which create rectangular marquee-like structures (Carthew *et al.*, 2002); desiccation cracks can be identified in some areas (Fig. 2.4F). At Nyamita AV1006, the barrage stromatolite facies is associated with the bioclastic limestone (Lbg), which is a laminated wackestone with abundant gastropod fragments and volcaniclastic detritus. The facies is a lenticular deposit behind the barrage stromatolite.

The isolated stromatolite facies (Ls2) is much smaller (~1 m), consists of localized boundstones nucleated on cobbles of nephelinite or indurated Miocene bedrock and grew in asymmetrical domes or bulbs aligned with flow direction (Fig. 2.3C, H and I). This facies is identified at Nyamita 5, Nyamita 14, and Aringo 9 (Fig. 2.1D and F). Similar to the barrage stromatolites, the isolated stromatolites have alternating laminae of light and dark, dense and porous micrite, with minimal volcaniclastic detritus. The laminations are generally planar but can occasionally be undulatory (Fig. 2.4F). An ultra-

Table 2.2: Facies model and interpretation of sedimentary facies. Nomenclature follows Pedley (1990), Arenas-Abad et al. (2010), and Miall (2010).

Facies	Geometry	Textural Characteristics	Sedimentary Structures	Biologic Content	Associated Facies	Depositional Environment	Site
Carbonate facies							
Barrage stromatolite (Ls1)	- Hemidomic - 2 to 3 m thick - ~5 m wide	- Boundstone nucleated on conglomerate - Alternating lamina of dense and porous micrite - Average lamina thickness 30 μm up to 5 mm - Minimal silt-sized volcaniclastic detritus	- High angle bedding - Undulatory and planar laminations - Desiccation cracks - Dissolution surfaces	- Cyanobacteria filaments	Lbg, Gh	Fast-flowing fluvial barrage	Nyamita AV1006
Isolated stromatolite (Ls2)	- Asymmetrical domes aligned with flow direction or bioherm - 0.05 to 1 m thick and extent	- Localized boundstones nucleating on coarse pebbles of basalt or indurated Miocene bedrock - Alternating lamina of dense and porous micrite - Average lamina thickness 30 μm up to 5 mm - Minimal silt-sized volcaniclastic detritus or clay	- Undulatory to planar laminations - Desiccation cracks	- Cyanobacteria filaments	Lph, Lo, Gh	Slow-flowing fluvial channel (except during flooding)	Aringo 9; Nyamita 5, 14
Phytoherm limestone (Lst1)	- Tabular - 10-20 cm thick - Larger lateral extent up ~1200 m^2	- Amount of volcaniclastic material variable - Tephra clasts weathering to clay - Pedorelicts and clay infilling pores	- Bioturbation - Carbonate nodules in macrophytes root pores - Reworked tufa clasts - Syndepositional micrite cement	- Decomposing roots - Charcoal - Bovid teeth, horn corn and other bone fragments	Gh, P	Paludal or inter-barrage pool	Kisaaka 20; Aringo 13

Table 2.2: Continued

Facies	Geometry	Textural Characteristics	Sedimentary Structures	Biologic Content	Associated Facies	Depositional Environment	Site
Phytoclastic limestone (Lph)	- Bioherm - 10-20 cm thick - 1-2 m lateral exposure	- Boundstone of plant fragments - Fragments up to 2 mm in size coated with micrite - Abundant porosity	- Structureless - Syndepositional calcite cement precipitated around decayed plant material	- Leaf and stem molds - Gastropods	Ls2, Lo	Paludal or inter-barrage pool	Nyamita 5
Bioclastic limestone (Lbg)	- Lenticular - 1-2 m thick - ~20 m^2 area	- Wackestone of gastropod fragments and volcaniclastic detritus	- Laminated - Syndepositional micrite cement	- Gastropod fragments	Ls1	Inter-barrage pool	Nyamita AV1006
Intraclastic limestone (Li)	- Tabular - 65 cm thick - ~5 m lateral extent	- Packstone of pisoids and volcaniclastic detritus, and pedorelicts - Pisoids (>2 mm) nucleating on tephra or pedorelicts - Detrital grain size ranges from silt to coarse sand	- Structureless - Syndepositional micrite cement			Paludal	Nyamita 22, 25
Oncolitic limestone (Lo)	- Bioherm - 10-20 cm thick - 1 to 2 m lateral exposure	- Boundstone - Cylindrical with diameter of ~5 cm	- Structureless - Syndepositional micrite cement	- Nuclei of oncoids likely plant stems or other organic matter	Ls2, Lph	Slow-flowing fluvial channel	Nyamita 5

Table 2.2: Continued

Facies	Geometry	Textural Characteristics	Sedimentary Structures	Biologic Content	Associated Facies	Depositional Environment	Site
Clastic facies							
Conglomerate (Gh)	- Can be channel-shaped - 0.5 to 2 m thick - ~1200 m^2 (Kissaka) ~6000 m^2 (Obware)	- Clast-supported, crudely bedded gravel - Clast sizes range from granules to cobbles - Dominantly basalt and quartz at Kisaaka and Obware, respectively	- Structureless to horizontal bedding - Syndepositional micrite cement		Sh, P, Ls1, Ls2, Lst1	Fluvial channel	Obware 1; Kisaaka 1, 2,12A, 12B, 12C, 20; Aringo 9
Sandstone (Sh)	- Channel-shaped - 1 to 2 m thick - ~70 m of lateral exposure	- Clast-supported, crudely bedded sandstone - Grain size ranges from medium to coarse sand - Angular to subangular grains, dominantly quartz - Microdebitage - Pedorelicts	- Structureless to horizontal laminations - Occasional gravel lag deposits - Syndepositional micrite cement	- Decomposed root fragments	Gh	Fluvial channel	Obware 1
Paleosol (P)	- Tabular - 0.5-1 m thick - <10 m lateral exposure	- Mudstone - Dominantly clay	- Structureless - Pedogenic carbonate rhizoliths and nodules - Syndepositional cement		Gh	Paludal or floodplain	Kisaaka 20, 14A, 12B; Aringo 12

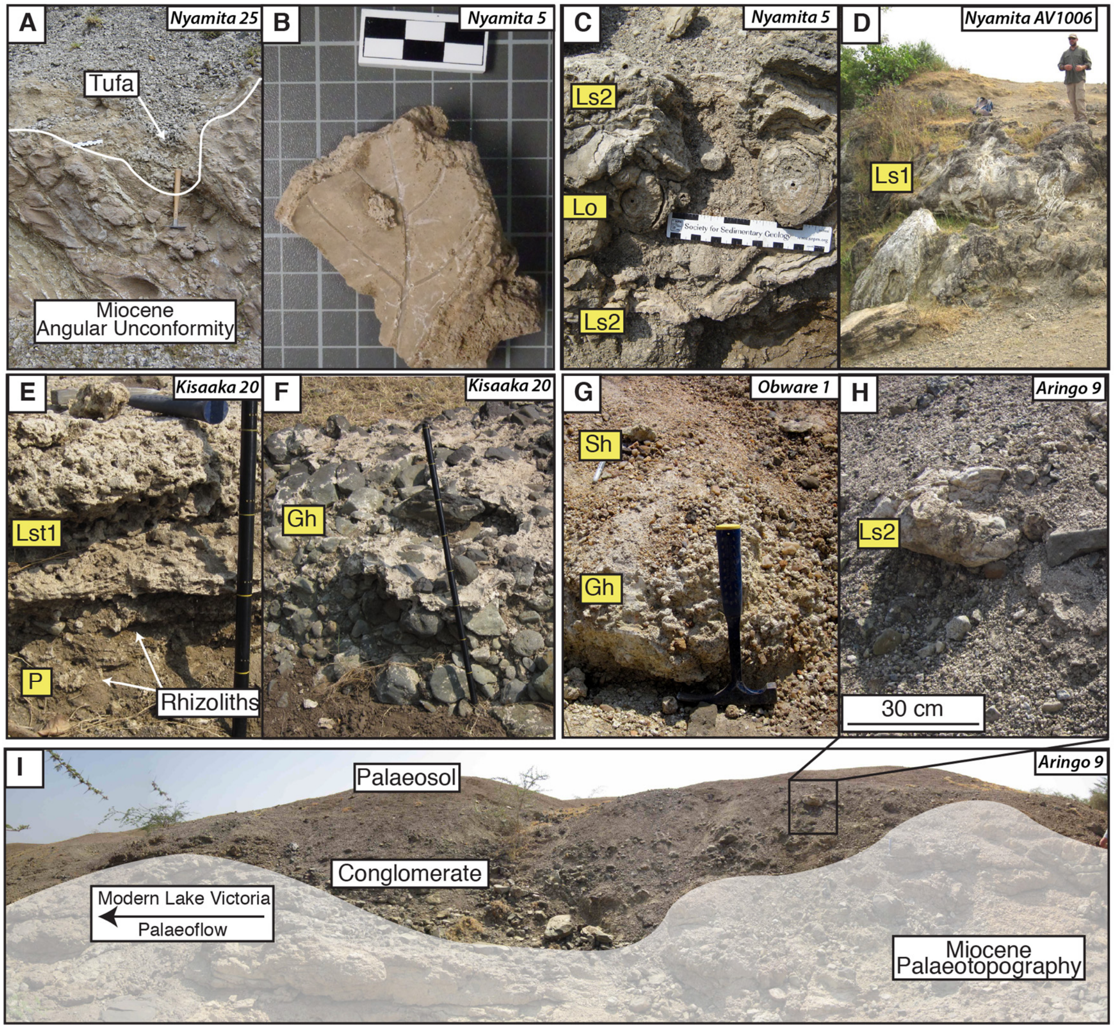

Figure 2.3: Field photographs of key features and tufa facies. See Table 2.2 for a description of the tufa facies and Fig. 2.1 for location. (A) Miocene angular unconformity indicated by white line with tufa draping the unconformity; rock hammer for scale. (B) Example of dicotyledonous angiosperms. (C) Oncolite facies (Lo) nucleating on roots or stems preserved by isolated stromatolites (Ls2); 15 cm scale. (D) Barrage stromatolite (Ls1); person for scale. (E) Phytoherm limestone facies (Lst1) with macrophytes preserved by syndepositional cement and the palaeosol facies (P) with rhizoliths and syndepositional calcite cement; 10 cm Jacob's staff for scale. (F) Clast-supported and crudely bedded conglomerate facies (Gh) with syndepositional calcite cement; 10 cm Jacob's staff for scale. (G) Clast-supported and crudely bedded sandstone facies (Sh) with syndepositional calcite cement overlying facies Gh; hammer for scale. (H) Facies Ls2 with asymmetrical domes aligned with flow direction. (I) Panorama of Aringo 9 with the Miocene bedrock shaded in white illustrating the palaeotopographic highs and lows that created environments ideal for tufa precipitation.

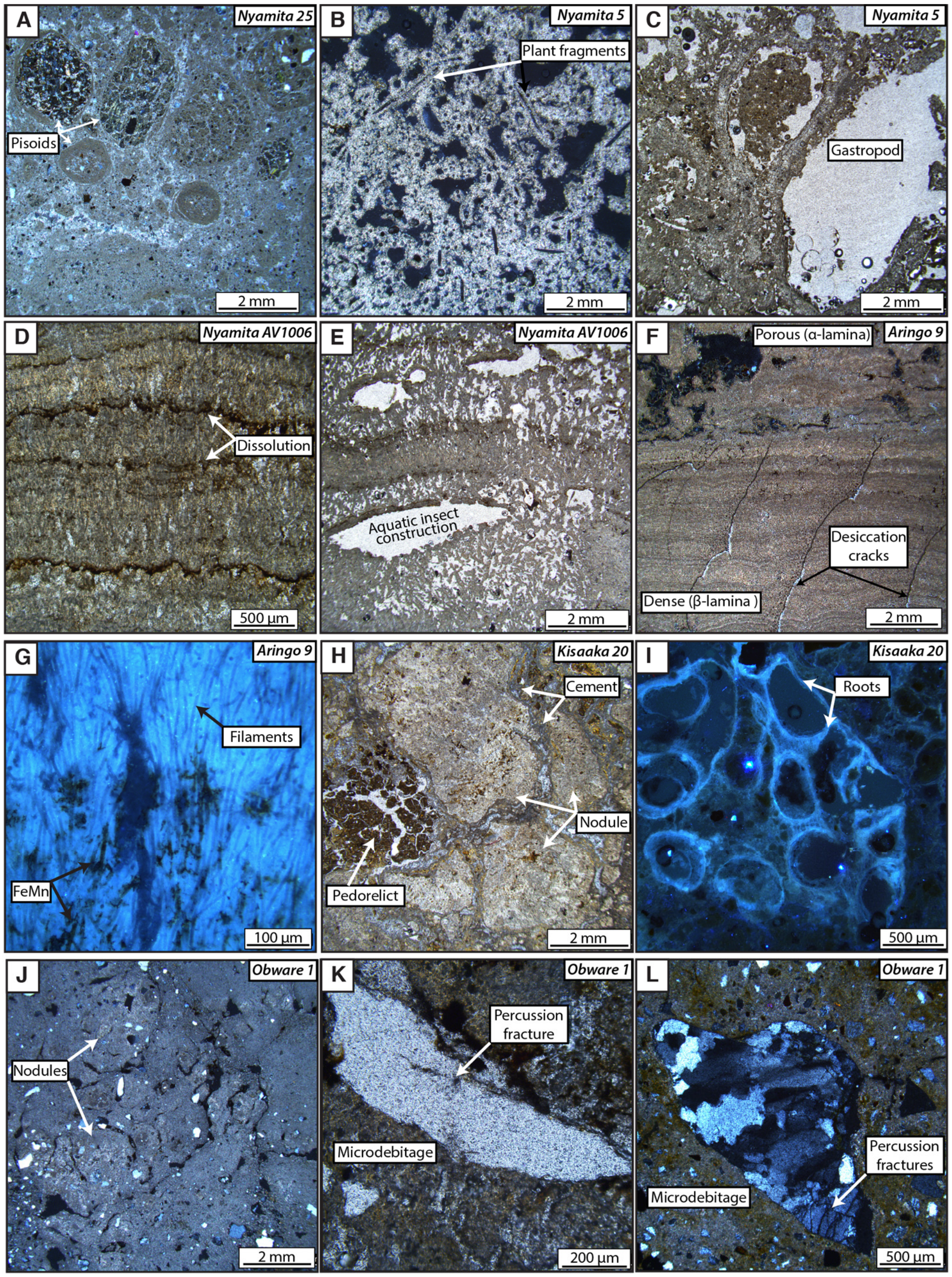

Figure 2.4: Photomicrographs of key microstructures and biologic features. (A) Pisoids nucleating around volcaniclastic detritus and tephra clasts; Facies Li; 1.25x XPL. (B) Syndepositional calcite cement precipitated around decayed plant material; Facies Lph; 1.25x XPL. (C) Gastropod shell with abundant volcaniclastic detritus and clay cemented by syndepositional micritic cement; Facies Lph; 1.25x PPL. (D) Dense micritic lamina with preserved cyanobacteria filaments and dissolution surfaces; Facies Ls1; 4x PPL. (E) Alternating dense and porous lamina with pyralid marquee-like structures; Facies Ls1; 1.25x PPL. (F) Desiccation cracks in dense micritic laminations; 1.25x XPL. (G) Extremely well preserved cyanobacteria filaments in dense micritic lamina only visible using UV fluorescence; 20x NU. (H) Nodules forming in association with roots and pedorelicts; 1.25x PPL. (I) Representative of organic matter (likely a root) found throughout the sites; 4x Nu. (J) Curved cracks are likely nodules surrounded by syndepositional calcite; 1.25x XPL. (K) and (L) Likely examples of microdebitage due to angular, elongate shape and large grain size in comparison to surrounding grains as well as possible percussion fracture; 10x PPL and 4x XPL, respectively.

polished thin-section sample (13-AR-TS5) from this facies at Aringo 9 had improved optics that revealed extremely well preserved cyanobacteria filaments only visible with UVf (Fig. 2.4G). Desiccation cracks are also present in this facies (Fig. 2.4F). These isolated stromatolites can be associated with localized bioherms of phytoclastic limestone (Lph) and oncolitic limestone (Lo) at Nyamita 5 and 14 (Fig. 2.1D). The phytoclastic limestone is a boundstone in which syndepositional calcite cement precipitated around gastropods and now-decayed plant material (Fig. 2.4B and C). The associated oncolitic limestone likely nucleated around plant stems or roots (Fig. 2.3C). Isolated stromatolites (Ls2) are identified above and below both the phytoclastic limestone and oncolitic limestone (Lph and Lo; Fig. 2.3C).

Closest to the Miocene fault mapped at Nyamita (Fig. 2.1D), an intraclastic limestone (Li) was identified at Nyamita 22, 25 (Fig. 2.3A). The intraclastic limestone is a packstone with volcaniclastic detritus and pedorelicts that often form the nucleus for pisoids that are cemented by syndepositional calcite cement (Fig. 2.4A). Most pisoids have a single lamination, but several have multiple generations with variable amounts of organic matter that are not visible without UVf. This facies is unique to this location.

Tabular phytoherm limestones (Lst1) with a lateral extent of up to ~1200 m^2 were identified at Kisaaka 20 and Aringo 13. This facies is 10 to 20 cm thick, with variable amounts of volcaniclastic material and pedorelicts (Figs 2.3E and 2.4H). Carbonate nodules formed in macrophyte root pores that are cemented by syndepositional calcite cement are abundant (Fig. 2.4H). Using UVf an abundance of organic matter was visible; however, the specific type is difficult to identify. Figure 2.4I is representative of this organic matter identified throughout the Kisaaka thin sections and is likely a decomposing root. Pleistocene bovid teeth, a reedbuck (*Redunca arundinum*) horn core, and other unidentifiable bone fragments were found in the tufas at Kisaaka.

Clastic facies. Three clastic facies are associated with the carbonate facies at these sites: conglomerates (Gh), sandstones (Sh), and palaeosols (P). The conglomerate facies is a clast-supported, poorly bedded gravel with clasts ranging from very fine pebble-size to cobble-size (Miall, 2010). This facies is identified at Kisaaka 1, 2, 12A-C, and 20, as well as Obware 1. The clasts are dominantly nephelinite and quartz at Kisaaka and Obware, respectively, and they are cemented by syndepositional calcite (Fig. 2.3F and G). Facies P is a mudstone palaeosol with an abundance of pedogenic carbonate rhizoliths and nodules cemented by syndepositional calcite (Figs 2.3E and 2.4H). The carbonate phytoherm limestone facies is commonly associated with the palaeosol (Fig. 2.3E) and conglomerate facies (Fig. 2.3F).

The sandstone facies is associated with the conglomerate facies at Obware and is clast-supported and crudely bedded, typically with only horizontal laminations and occasional gravel lag deposits (Fig. 2.3G). The sandstone is dominantly quartz-rich with sparse pedorelicts and a few decomposed root fragments. In some areas, these sandstones contain dominantly syndepositional cement precipitated around nodule-like features (Fig. 2.4J). The sandstone facies at Obware 1 has unique quartz grains with features that suggest microdebitage, resulting from on-site stone tool production. The grains are much larger in comparison to the rest of the sand-sized fraction, are fresh and unaltered, and are very angular (Fig. 2.4K and L). These grains also contain curved faces and percussion fractures typical of microdebitage (Angelucci, 2010).

Stable Isotopes

Stable isotopes of C and O from tufa are presented in bivariate plots of $\delta^{18}O$ vs. $\delta^{13}C$ and are organized by site (Fig. 2.5A). Isotopes from the four sites are variable in both C and O. The $\delta^{13}C$ values from the majority of the Nyamita samples generally range from -7‰ to -3‰. Values from Aringo and Kisaaka are more positive than those from Nyamita, ranging from -5‰ to -1‰, and values from Obware are slightly more negative, ranging from -9‰ to -7‰. The isotopic values circled by a dotted line were sampled from nodules formed in macrophyte root pores and are distinct from the rest of the Kisaaka samples, which were sampled from the syndepositional cement (Fig. 2.4H). The $\delta^{18}O$ values of the Kisaaka nodules range from -7.3‰ to -4.5‰ and the $\delta^{13}C$ values range from -9.2‰ to -10.2‰. Both the carbon and oxygen isotopes are substantially more negative (5‰ and 2‰, respectively) in the nodules than in the syndepositional cement, although both are non-luminescent in CL (Fig. 2.5A). The mean $\delta^{13}C$ value from the Kisaaka nodules is -10.9‰ whereas the mean value from the Kisaaka tufa samples is -3.8‰ (Table 2.3).

The values from Nyamita circled in a solid black line were sampled from the intraclastic limestone and included both pisoids and syndepositional cement from Nyamita 22, 25 (Figs 2.1D, 2.4A and 2.5A). The results from Nyamita are further subdivided in Fig. 2.5B to illustrate these differences. Values from the intraclastic limestone at Nyamita 22, 25 are in dark blue boxes, isolated stromatolites from Nyamita 5 are in purple boxes, and barrage stromatolites from AV1006 are in orange boxes. The oxygen isotope values at Nyamita 22, 25 are within the range of those found at the rest of the Nyamita localities; however, the carbon isotopes values are consistently more

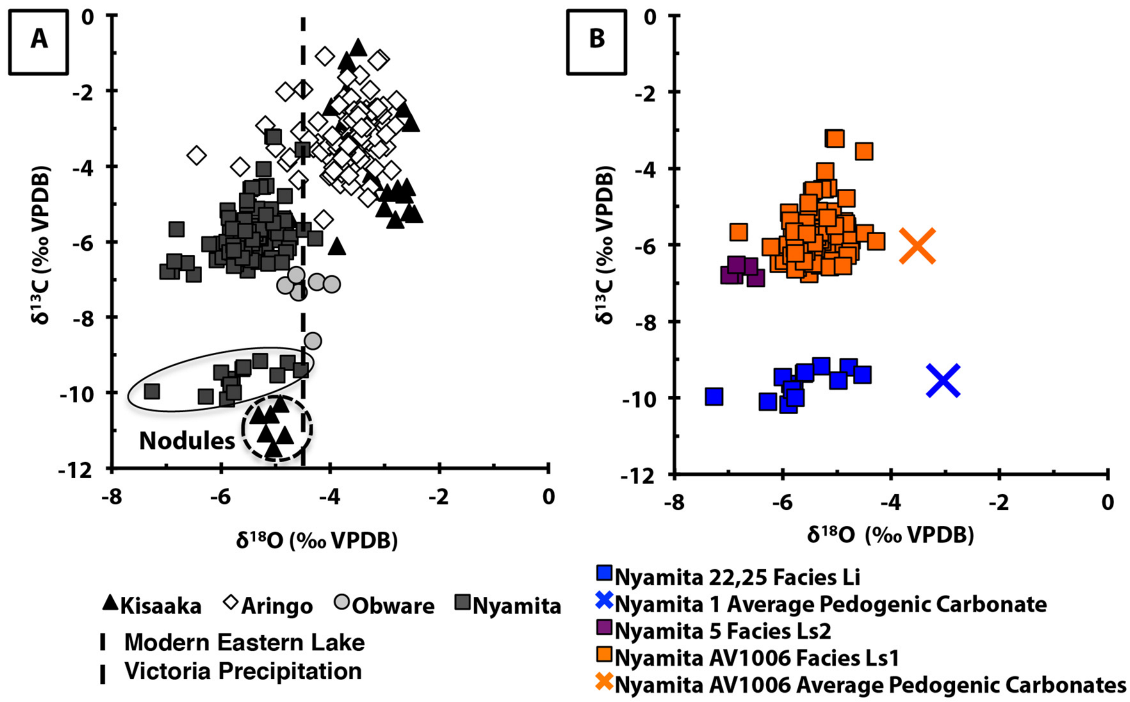

Figure 2.5: Stable isotopes of carbon and oxygen from tufa. (A) The $\delta^{18}O$ vs. $\delta^{13}C$ values of tufa separated by site. The vertical dotted line illustrates the average value of modern Eastern Lake Victoria precipitation. The samples from Nyamita circled in the solid black line are from the Nyamita 1 site <5 m from the source of the spring. The samples from Kisaaka circled by the dotted black line are rhizoliths of macrophytes and the $\delta^{13}C$ values are ~5‰ more negative than the syndepositional cement analyzed in all other Kisaaka samples. (B) The $\delta^{18}O$ vs. $\delta^{13}C$ values of tufa from the Nyamita site only grouped by locality (See Fig. 2.1). Those in dark blue are closest to the source of the spring and have a range of $\delta^{18}O$ values, but consistently very negative $\delta^{13}C$ values of -10‰. The Nyamita 5 and AV1006 samples are ~40 m and ~450 m away from the spring source, respectively. The average pedogenic carbonate sample from each site is identified by the X and indicates the shift in the $\delta^{13}C$ values (Pedogenic carbonate data from Garrett *et al.* (2015))

negative than those from the rest of the samples from Nyamita. The mean $\delta^{13}C$ value from Nyamita 22, 25 is -9.6‰ whereas the AV1006 samples have a mean of -5.8‰ (Table 2.3). Nyamita has a range of oxygen isotope values between -7.3‰ and -4.3‰, whereas Kisaaka ranges from -4.0‰ to -2.5‰ and Obware ranges from -4.8‰ to -4.0‰ (Fig. 2.6A). Aringo also has a wide range of $\delta^{18}O$ values between -6.5‰ and -3.0‰. On average, the oxygen isotopes at Nyamita are the most negative and become increasingly more positive at Obware, Aringo, and Kisaaka (Table 2.3).

Table 2.3: Averaged oxygen and carbon isotopes.

Site or Locality	Mean $\delta^{13}C$ (‰VPDB)	Mean $\delta^{18}O$ (‰VPDB)	n
Nyamita 22,25 Facies Li	-9.6	-5.7	14
Nyamita AV1006 Facies Ls1	-5.8	-5.5	103
Nyamita 1 average pedogenic carbonate	-9.6	-3.0	3
Nyamita AV1006 average pedogenic carbonate	-6.0	-3.1	4
Kisaaka nodules	-10.9	-5.1	6
Other Kisaaka	-3.8	-3.2	23
Aringo	-3.2	-3.7	109
Obware	-7.4	-4.4	6

Discussion

Stable Isotopes

Analysis of the stable isotopes indicates that palaeoenvironmental and palaeoclimatic changes were recorded in the riverine tufas identified at Rusinga Island and Karungu. The stable isotope results can be used to further understand the environmental context of the associated archaeological and palaeontological sites. It is well established that riverine tufas can record information about the palaeoclimate and palaeoenvironment using stable isotopes of carbon and oxygen (Andrews *et al.*, 1997, 2000; Matsuoka *et al.*, 2001; Ihlenfeld *et al.*, 2003; Andrews & Brasier, 2005; Andrews, 2006; Arenas-Abad *et al.*, 2010; Brasier *et al.*, 2010). Oxygen isotope values of riverine tufas are mainly a function of the water temperature in which the calcite precipitates, the $\delta^{18}O$ value of the aquifer, and evaporation (Andrews & Brasier, 2005; Andrews, 2006). In tropical East Africa, the amount, elevation, and source of precipitation have the greatest influence on $\delta^{18}O$ values (Dansgard, 1964; Rozanski *et al.*, 1996).

The $\delta^{13}C$ values are commonly more variable than the $\delta^{18}O$ values (Arenas-Abad *et al.*, 2010) and the sources for dissolved inorganic carbon (DIC) in the stream or spring generally have the greatest effect on the $\delta^{13}C$ values (Andrews *et al.*, 1993, 1997; Andrews, 2006). The relative contributions of isotopically light CO_2 from soil organic matter (SOM) and isotopically heavy CO_2 from dissolution of a marine carbonate aquifer have the biggest influence on the DIC (Chafetz *et al.*, 1991; Andrews *et al.*, 1993; Andrews, 2006). This is further modified by in-stream calcite precipitation and equilibration of the spring or stream with atmospheric CO_2 (Matsuoka *et al.*, 2001; Andrews & Brasier, 2005). Progressive degassing downstream can also affect the carbon isotopic composition as well as preferential degassing in high-velocity and turbulent currents that can increase $\delta^{13}C$ values slightly (Pentecost & Spiro, 1990; Chafetz *et al.*, 1991; Andrews *et al.*, 1993; Ortiz *et al.*, 2009; Arenas-Abad *et al.*, 2010).

The interpretations of the isotopic changes from the Lake Victoria Basin are complex but are supported by field observations and micromorphology. The dominant contributor to the DIC is likely the photosynthetic pathway of C_3 vs. C_4 plants affecting SOM (Smith *et al.*, 2004; Andrews, 2006; Arenas-Abad *et al.*, 2010; Lee *et al.*, 2013). To estimate the $\delta^{13}C$ values of a calcite precipitated with a dominantly SOM source for DIC, several assumptions must be made to simulate conditions in the Middle to Late Pleistocene. The average $\delta^{13}C$ values from C_3 (-27.4‰) and C_4 plants (-12.5‰) in East Africa are used (Cerling *et al.*, 2003), and the soil CO_2 is ~4.5‰ heavier than the plant biomass (Cerling *et al.*, 1991). A temperature-independent 1‰ enrichment factor for calcite-bicarbonate must be added in addition to a temperature-dependent enrichment factor for calcite-CO_2 (Romanek *et al.*, 1992). Due to the depostition of tufa over a period of ~360 ka, a range of mean annual temperatures (MAT) is assumed using the modern MAT of 21.6°C from nearby Entebbe, Uganda (Rozanski *et al.*, 1993, 1996) and maximum 3°C cooler MAT temperature estimated from the LGM (Gasse *et al.*, 2008). This range of temperatures applied to the calcite-CO_2 enrichment equation results in an enrichment factor of 9.4‰ to 9.7‰. This would result in calcite precipitating from a SOM source for the DIC having a $\delta^{13}C$ value of -12.5‰ to -12.2‰ for pure C_3 and 2.4‰ to 2.7‰ for pure C_4. In comparison, calcite precipitated directly from a pre-Industrial atmosphere would have a $\delta^{13}C$ value between 2.9‰ and 3.3‰ (Romanek *et al.*, 1992; Rozanski *et al.*, 1996, 1993). The $\delta^{13}C$ values of the tufa from Rusinga Island and Karungu range from -12‰ to -1‰ and suggest strong soil zone, and not atmospheric influence on the carbon isotopes.

Additional evidence is demonstrated at Nyamita by comparing the carbon isotopes of the riverine tufa and pedogenic carbonates of the same age. The Nyamita tufas have distinct $\delta^{13}C$ values based on facies, and although still debated, it is unlikely that the more positive $\delta^{13}C$ values in the riverine tufa are due to photosynthetic fractionation by cyanobacteria or algae because these organisms act as surfaces for nucleation of calcite rather than as direct calcifiers (Andrews *et al.*, 1993, 1997; Andrews & Brasier, 2005; Arenas-Abad *et al.*, 2010). Pedogenic carbonates from palaeosols at Nyamita 1 (<10 m from Nyamita 22, 25; Fig. 2.1D) have a very similar $\delta^{13}C$ value of -9.6‰ compared to -9.6‰ from the intraclastic limestone facies at Nyamita 22, 25 (Table 2.3; Garrett *et al.*, 2015). A similar pattern is identified in the pedogenic carbonates from Nyamita AV1006, which have an average $\delta^{13}C$ value of -6.0‰ compared to the -5.8‰ average for the barrage stromatolite. The more positive $\delta^{18}O$ values of the palaeosols can be attributed to evaporation affecting the composition of the soil water (Zimmerman *et al.*, 1967).

Tufas precipitated where C_3 vegetation dominates generally have a $\delta^{13}C$ value of -8‰ (Andrews, 2006; Arenas-Abad *et al.*, 2010) whereas semi-arid areas with C_4 vegetation commonly have more positive $\delta^{13}C$ values between -6‰ and -2‰ (Smith *et al.*, 2004). When combined with the pedogenic carbonate isotopes, the carbon isotopic offset in the tufas at Nyamita provides strong evidence that the C_3 vs. C_4 pathway had the strongest influence on the DIC from which the tufa precipitated. It is therefore likely that the depleted $\delta^{13}C$ values Nyamita 22, 25 are a result of dominantly C_3 vegetation, and the more positive values at Nyamita AV1006 are a result of more mixed C_3/C_4 contribution. This likely applies to other sites in the region, although data from pedogenic carbonates are currently only available from Nyamita. Kisaaka also has evidence for depletion in tufa nodules with an average of -10.9‰, probably due to high concentrations of C_3 plants, such as the wetland plant *Typha* that is widespread in eastern Africa today. Evidence from tufas in Croatia, China, and Spain suggests that pools with encrusted macrophytes such as *Typha* will have more negative $\delta^{13}C$ values (Pavlović *et al.*, 2002; Horvatinčić *et al.*, 2003; Z. Liu *et al.*, 2006b; Ortiz *et al.*, 2009).

In general, Aringo and other samples from Kisaaka have much more positive $\delta^{13}C$ and $\delta^{18}O$ values that could be linked to changes in the $\delta^{18}O$ of precipitation, changes in the plant composition, or changes in evaporation processes. Because all of the sites are at similar elevations (1150 to 1190 m), evaporation is the most likely cause for the more positive $\delta^{13}C$ and $\delta^{18}O$ values. At Nyamita, the source (faulted Miocene bedrock) of the Pleistocene spring can be identified less than 5 m from tufa deposits at Nyamita 22, 25.

The spring discharged into the axial drainage to supply the barrage tufa at Nyamita AV1006 (Fig. 2.1D). However, a Pleistocene source of the spring is neither exposed at Kisaaka nor at Aringo, suggesting that evaporation and degassing might have a greater influence on the stable isotopes at these sites. The increases in both $\delta^{13}C$ and $\delta^{18}O$ values at Kisaaka and Aringo compared to Nyamita indicates that tufa precipitation was also likely affected by evaporation processes and degassing, which produce more positive values of both ^{18}O and ^{13}C, similar to hydrologically closed lakes (Talbot, 1990; Smith *et al.*, 2004; Ordóñez *et al.*, 2005; Ortiz *et al.*, 2009), rather than due to changes in plant populations. Although the effect of evaporation of $\delta^{18}O$ is generally considered small in most riverine tufas, evaporation in semi-arid regions can cause $\delta^{18}O$ enrichment, commonly >1‰ (Zamarreño *et al.*, 1997; Ihlenfeld *et al.*, 2003; Smith *et al.*, 2004; Andrews & Brasier, 2005; Andrews, 2006).

Obware is slightly different than Aringo, Kisaaka, or Nyamita (Fig. 2.6A). With an average $\delta^{13}C$ value of -7.4‰, Obware data indicate a stronger C_3 signal than at Nyamita (excluding the intraclastic limestone facies), Kisaaka and Aringo. The $\delta^{18}O$ values of Obware fall between those of Nyamita and the Aringo-Kisaaka grouping, and may reflect a change in the $\delta^{18}O$ of palaeoprecipitation.

Palaeoenvironmental Reconstruction

When the overall trends in the stable isotopes are combined with other palaeoenvironment information from the identified facies and facies associations, a reconstruction is possible. Based on stratigraphic measurements, tephrostratigraphy and U-series dating, the sites are not time-equivalent, but evidence suggests that similar depositional environments existed, at least intermittently, over a ~360 kyr interval between 455 and 94 ka. The poor sorting and lack of sedimentary structures suggests flashy discharge likely associated with wet seasons of the East African monsoon. Grain sizes can reach up to 30 cm (very coarse pebbles) and estimations using a Hjulstrom diagram indicate that it would have required flow velocities of between 6 and 12 m s^{-1} to transport grains this size (Fig. 2.3F; Sundborg, 1956). However, most of the time the rivers likely had little flow from precipitation, and the ecosystem was supported by perennial spring discharge. Cyanobacteria would have stabilized these coarse-grained deposits, forming barrages and interbarrage pools behind them (Fig. 2.6A). The Miocene palaeotopography also provided surfaces for nucleation by cyanobacteria in the fast-flowing areas of the channel and marshy, paludal environments in the calmer areas of slack water (Fig. 2.6A and B).

In addition, the fauna from both Rusinga Island and Karungu suggest the presence of a freestanding or perennial water source. Hippopotamus and reedbuck need freestanding water, and bushbuck (*Tragelaphus scriptus*) and duiker (*Sylvicapra grimmia*) (Tryon *et al.*, 2010, 2012, 2014; Faith *et al.*, 2015) require dense shrubby vegetation that indicates a perennial source of water. On Rusinga Island, hippopotamus are found at Nyamita within ~50 m of the tufa deposits and carbon isotopes from Nyamita pedogenic carbonates indicate that C_3 plants were abundant near the spring with ~64% woody cover (Garrett *et al.*, 2015). The Nyamita tufa deposits also suggest a mixed C_3/C_4 plant source for DIC. In contrast, isotopes from teeth from fauna such as wildebeest, hartebeest (*Alcelaphus buselaphus*), zebra, and oryx found at Rusinga and Karungu suggest a dominantly C_4 diet from a semi-arid grassland (Faith *et al.*, 2015; Garrett *et al.*, 2015). This evidence is summarized in a reconstruction of Nyamita,

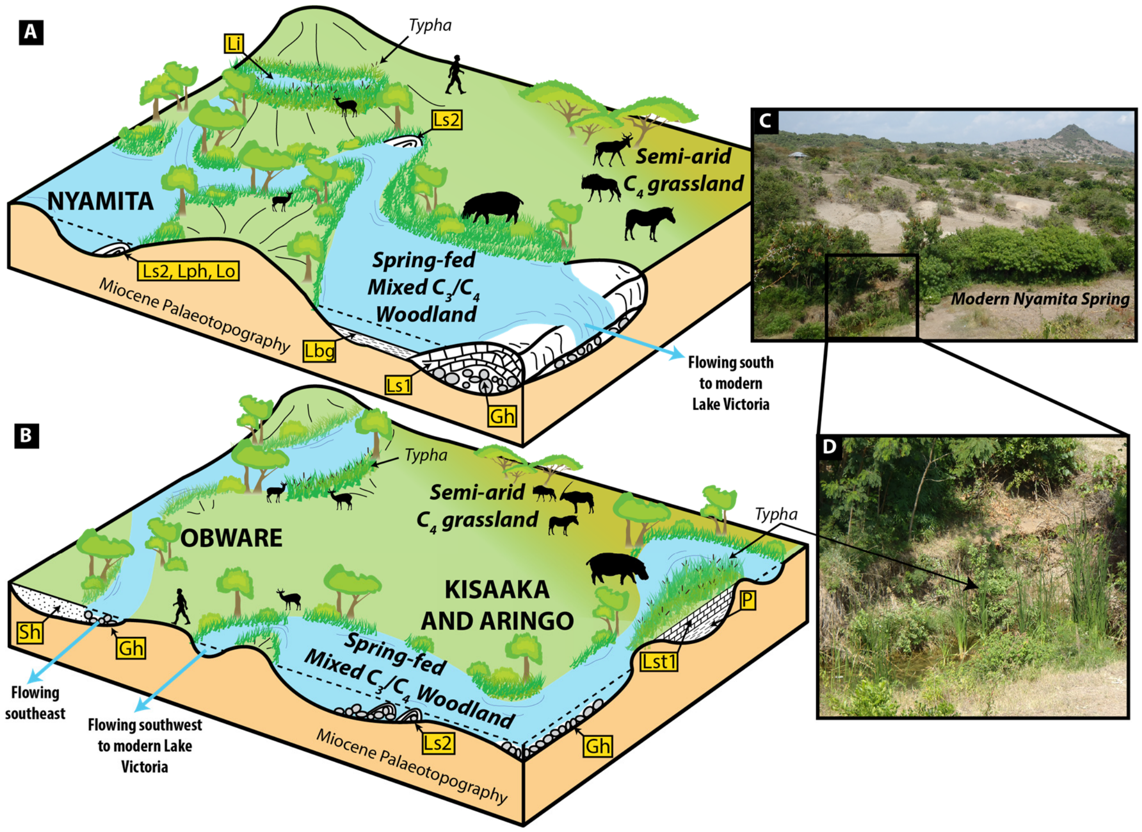

Figure 2.6: Diagrammatic summary showing conceptual model for distribution of lithofacies and environments across Middle to Late Pleistocene palaeolandscapes in the Rusinga Island and Karungu study areas (not to scale). See text for discussion.

Kisaaka, Aringo, and Obware during Pleistocene time (Fig. 2.6A and B). It is not meant to be a literal representation of the sites, but an idealized conceptual model demonstrating that spring-fed rivers with a mixed C_3/C_4 vegetation area surrounded by a semi-arid C_4 grassland were a long standing feature on the landscape that existed intermittently between 455 and 94 ka (Fig. 2.6A and B).

Nyamita. Riverine tufa was deposited at Nyamita at 4 localities over a lateral transect of ~500 m. At Nyamita, the tufa generally precipitated directly on Miocene bedrock that is not exposed at every locality. The tufa (deposited between ~111 and 94 ka) is conformably overlain by a palaeosol deposited between ~100 and 49 ka (Fig. 2.2;

Blegen *et al.*, 2015). The intraclastic limestone (Li) at Nyamita 22, 25 is interpreted as deposits of a paludal environment forming near the likely source of the spring only several metres away from where tufa drapes the Miocene fault (Figs 2.1D and 2.3A and B). This fault likely tapped into subsurface aquifers during movement and provided a continual source of water. The pisoid textures identified in thin-sections using UVf are indicative of low-energy biologic mediation rather than inorganic deposition in high-energy environments. There is no evidence for drying, such as the desiccation cracks found in other facies, and the carbon isotopes for the intraclastic limestone are extremely negative (-9.6‰ on average) suggesting that the DIC was dominately influenced by a C_3 plant such as the wetland plant *Typha* and other riparian herbs, shrubs, and tree species (Fig. 2.6A and D). In addition, macrofossils from Nyamita suggest the presence of wetland plants, such as *Typha.* Modern climate is much wetter at Nyamita today, but a spring is still present on the landscape. A modern spring flowing into the axial drainage is located ~50 m west of the Late Pleistocene tufa (Fig. 2.6C). These modern springs currently have *Typha* growing within paludal areas (Fig. 2.6D).

This low-energy paludal area drained into a stream that was likely ephemeral. The stream, which drained the local highlands that lay up to 260 m above the site, experienced flashy discharges capable of moving pebbles to cobbles during the rainy season and was spring-fed during the dry season. In arid and semi-arid environments, highly variable flow regimes can cause erosional phases and deposition of clastic sediments intercalated with carbonates (Viles *et al.*, 2007; Lee *et al.*, 2013; Martini & Capezzuoli, 2014) similar to those identified at Rusinga Island and Karungu. On the edges of the channel, where water flow was slower, small, asymetrical domal stromatolites (Ls2) nucleated on Miocene palaeotopographic highs or cobbles where it is likely that turbulent flow over these obstructures during a flood caused CO_2 to degas and form a cement that stabilized the sediments and created a substrate for cyanobacteria (Fig. 2.1D). These localized stromatolites are commonly associated with phytoclastic limestone and oncolitic limestone facies (Lph and Lo) in paludal areas forming along the calmer edges at Nyamita 5 and 14 (Figs 2.3C and 2.6A). The leaf impressions of dicotyledonous angiosperms in these facies indicate trees or shrubs were growing along the stream (Figs 2.3B and 2.6A), and that plant material was abundant (Fig. 2.4C). The carbon isotopes of these facies indicate a more mixed C_3/C_4 signal of ~ -6.5‰ (Fig. 2.5B).

Further downstream at the Nyamita AV1006 locality, a fluvial barrage formed a large deposit (Figs 2.1D and 2.3E). A conglomerate (Gh) was deposited during flooding and created a barrier where turbulent flow caused CO_2 to degas and cement the conglomerate, similar to what occurred elsewhere at Nyamita. Cyanobacteria took advantage of this large conglomeratic deposit and over time created a stromatolite barrage (Ls1) that dammed flow and formed an interbarrage pool where a bioclastic limestone with abundant gastropods (Lbg) was deposited (Fig. 2.6A). Based on the structures identified in thin section using UVf, the stromatolites were likely formed by cyanobacteria such as *Schizothrix*, *Phormidium,* or *Scytonema* (Chafetz & Folk, 1984; Freytet *et al.*, 1996; Freytet & Verrecchia, 1998; Arenas *et al.*, 2014), which have branching or dendritic filaments covered with micrite, but further identification is difficult to determine despite the exceptional preservation (Fig. 2.4D and G).

U-series dates indicate that this barrage tufa was present for at least 17 kyr between ~111 and 94 ka. Marquee structures similar to those contructed by larval pyralids (moths) were identified in a thin section prepared from a sample near the back of the barrage, and provide further evidence that this was an interbarrage pool (Fig. 2.4E). Larval pyralids often create these structures on a pool bank near a waterfall with intermediate to high stream flow, or where there are pulses of lapping water along bank (Carthew *et al.*, 2002, 2006). These marquee structures occur between cyanobacteria colonies and were identified by Carthew *et al.* (2002) in a similar monsoonal environment in northern Australia (Fig. 2.4E). The carbon isotopes of the barrage stromatolies are also indicative of a mixed C_3/C_4 contribution to the DIC.

Kisaaka. Riverine tufa deposits were identified across the ~2 km exposure at Kisaaka. At Kisaaka, a palaeosol and the Nyamita Tuff overlie the Kisaaka tufas and indicate that the tufa is >100 ka, but it is unknown whether this is a conformable contact because detrital contamination prevented U-series dating (Fig. 2.2). Although Kisaaka is ~40 km south of Nyamita, the site is similar to Nyamita in that an ephemeral river flowed across the Miocene palaeotopography (Figs 2.1C and 2.6B). A similar depositional system developed where turbulent flow over both the Miocene palaeotopography and nephelinite cobbles deposited during flooding caused preferential degassing of CO_2 and the precipitation of syndepositional cement (conglomerate facies). In lower areas created by the Miocene palaeotopography where the river was calmer, a paludal environment formed. Where the water was perennial, macrophytes grew and nodules nucleated around roots and were later cemented by syndepositional cement (Phytoherm limestone facies). In comparison with the syndepositional cement, these nodules have very negative carbon isotopic values of -10.9‰ that indicate a very strong C_3 riparian vegetation influence on the DIC (Fig. 2.5A and Table 2.3). The palaeosol facies is also interpreted as a paludal environment that commonly experienced subaerial exposure that allowed for soil ped formation (Fig. 2.6B).

Aringo. The Aringo tufa (~455 ka) precipitated directly on the Miocene bedrock and is unconformably overlain by conglomerates, palaeosols, and finally the Nyamita Tuff (~49 to 100 ka), which indicates that a significant uniformity exists at this location (Fig. 2.2). Riverine tufa is exposed at Aringo over a ~400 m transect where the Miocene topography affected the types of tufa that were deposited. In the calmer areas with subaerial exposure, weakly developed palaeosols were deposited in a paludal environment. Where the water permanently flooded the landscape in Miocene palaeotopographic lows, macrophytes grew and were later cemented by syndepositional cement (Phytoherm limestone facies). In the slow-flowing areas of the fluvial channel, cyanobacteria adhered to nephelinite cobbles where Miocene palaeotopography created turbulent flow and degassing of CO_2 enhanced stromatolite formation (isolated stromatolite facies). These stromatolites indicate an environment where the DIC is greatly influenced by C_4 plants because the average $\delta^{13}C$ for the Ls2 facies is -3.2‰.

Obware. The tufa at Obware is overlain by a palaeosol and the BTP Tuff, but it is unclear whether this is a conformable contact because U-series dating was not possible. Obware has a similar conglomerate and sandstone facies (Gh and Sh) to the other sites; however, larger grain sizes of sand to gravel with very little clay indicates a much more dynamic landscape. This dynamic landscape created turbulent flow that caused the precipitation of syndepositional cement in the fluvial channel (Fig. 2.6B). This calcite cement has a $\delta^{13}C$ average value of -7.4‰, indicating a mixed C_3/C_4 plant community. Although there is no macroscale evidence for plants, likely due to the high energy of the fluvial channel, UVf reveals unidentifiable organic matter similar to that identified at Kisaaka, Nyamita, and Aringo. Obware is the only site with *in situ* artefacts preserved in the tufa. The uniquely shaped and unaltered quartz grains with curved faces and percussion fractures have been cited elsewhere as indicative of microdebitage (Angelucci, 2010). This is consistent with our recovery of quartz stone tool-making debris (cores and flakes) from Obware, many retaining the smoothed and rounded outer surfaces characteristic of the stream pebbles and cobbles from which they were made, suggesting on-site cobble acquisition and reduction for tool production. Combined with the surface-collected artefacts at Obware (Faith *et al.*, 2015), this suggests that humans were actively utilizing the spring-fed rivers on this landscape during the Late Pleistocene.

Palaeoclimate

The riverine tufas at Nyamita and Aringo provide a unique opportunity to reconstruct the palaeoclimate of the area. Evidence from cores indicates that the $\delta^{18}O$ composition of palaeoprecipitation has varied in comparison to modern values (Beuning *et al.*, 1998, 2002). Few modern temperature or isotopic data are available for the Lake Victoria region, but MAT for nearby Entebbe, Uganda is 21.6°C with an annual mean of -2.3‰ VSMOW for $\delta^{18}O$ of precipitation and ranges from -7‰ to 3‰ (Rozanski *et al.*, 1993, 1996). The $\delta^{18}O$ VPDB of calcite precipitated from precipitation with $\delta^{18}O$ values similar to Entebbe would have an average value of -4.6‰ (labeled with a dashed line on Fig. 2.5A) and could range from -8.5‰ to 1.2‰ (Faure, 1986). The oxygen isotopes from

Rusinga Island and Karungu all fall within this range. The Nyamita tufa is more negative on average (-5.5‰) and the Aringo and Kisaaka tufas are more positive on average (–3.7‰ and -3.2‰, respectively) than tufa precipitated from modern precipitation (Figs 2.5A and 2.7; Table 2.3). These differences between the sites are most easily explained by changes in the moisture source and evaporation.

Changes in the moisture source may be the cause for the more negative $\delta^{18}O$ values at Nyamita. Data from cellulose $\delta^{18}O$ values used to reconstruct lake-water $\delta^{18}O$ indicate a shift to more negative values during the LGM (Beuning *et al.*, 1997, 2002), probably reflecting precipitation sources with lower $\delta^{18}O$ values (Beuning *et al.*, 1997, 2002). This may be a result of changes in the moisture source, such as greater contribution of more negative monsoonal rains (Dansgard, 1964; McKenzie, 1993; Rozanski *et al.*, 1993, 1996). Lake Victoria is very sensitive to changes in precipitation, and the loss of direct precipitation due to a decrease in lake size would greatly reduce the amount of more positive catchment rainfall (Beuning *et al.*, 1998, 2002). Faunal evidence from Rusinga Island and Karungu also indicate drier conditions during the deposition of the Nyamita tufa than present, possibly similar to the LGM (Tryon *et al.*, 2014; Faith *et al.*, 2015). A shift in $\delta^{18}O$ caused by arid conditions, similar to that documented during the LGM (Beuning *et al.*, 1998, 2002), may account for the more negative $\delta^{18}O$ values at Nyamita during Late Pleistocene with enrichment of isotopically heavy ^{18}O due to evaporation at Kisaaka and Aringo.

Implications of Recurrent Spring-fed Rivers in East Africa

The spring-fed rivers of the Lake Victoria Basin add to the record of palaeoanthropological sites associated with tufa previously restricted to the Early and

Middle Pleistocene (Wendorf, 1993; Haynes *et al.* 1997; Nicoll *et al.*, 1999; Smith *et al.*, 2004, 2007; Garcea & Giraudi, 2006; Barich & Garcea, 2008; Johnson *et al.*, 2009; Ashley *et al.*, 2009, 2010a,b,c, 2014; Johnson & McBrearty, 2012). The aquifers stored water during times of high rainfall, allowing for continual spring discharge, which in turn allowed the landscape to host more diverse plant and animal communities (Cuthbert & Ashley, 2014). These spring-fed rivers could have functioned as a refugium for water-dependent fauna (i.e. hominins) similar to the Turkana Basin (Quinn *et al.*, 2007, 2013; Joordens *et al.*, 2011, 2013), the Olduvai Basin (Ashley *et al.*, 2009, 2010a,b,c, 2014; Cuthbert & Ashley, 2014), or the Olorgesailie Basin (Lee *et al.*, 2013). Time equivalent palaeosol deposits from Nyamita (Tryon *et al.*, 2010) and microdebitage and surface-collected artefacts from Obware suggest that early modern humans were utilizing this landscape during tufa deposition.

The U-series dates suggest that these spring-fed rivers were a recurrent feature and possible refugium on the landscape between ~455 and 95 ka before deposition became distinctively more fluvial. Springs still exist in the area today but have much smaller discharges unable to produce equivalent features. It seems that in this active and erosive landscape, springs were long-lived due to fault-controlled groundwater recharge and were present for at least 17 kyr at Nyamita, but variably preserved due to the high energy and variable climate of this system. In general, spring discharge is controlled by both climate and active tectonics shifting the water pathways, but there is no evidence for active faulting during the Middle to Late Pleistocene at Rusinga Island and Karungu.

It is likely that MAP decreased enough to cross a critical recharge threshold during the Late Pleistocene. With a decreased or nonexistent recharge, the spring system became choked with fluvial sediments and tufa precipitation ceased at ~94 ka. The termination of tufa precipitation occurs simultaneously with an expansion of C_4 grasslands beginning at ~100 ka, identified by the presence of alcelaphine antelopes and zebras and carbon isotopes of fossil teeth at Rusinga Island and Karungu (Faith *et al.*, 2012, 2014, 2015; Tryon *et al.*, 2012, 2014; Garrett *et al.*, 2015). At 95 ka, climate was variable across Africa. North Africa was wet, while tropical and southern Africa was dry, and East Africa entered a dry period (Blome *et al.*, 2012, and references therein). The Lake Victoria region is on the boundary between east and tropical Africa, and this suggests that the disappearance of the spring-fed rivers may be related to aridity identified at other sites across east and tropical Africa.

Conclusions

Riverine tufas identified from Rusinga Island and the mainland near Karungu have similar depositional environments, although the sites are almost 40 km apart and the tufas were deposited intermittently over an interval of ~355 ka. Poor sorting and large grain sizes indicate flashy and ephemeral discharge associated with the East African Monsoon, but a perennial water source is evident with fauna such as hippopotamus, barrage tufas created by cyanobacteria, paludal areas with high abundances of C_3 plants, possibly *Typha,* and evidence from $\delta^{13}C$ values of pedogenic carbonates suggesting ~64% woody cover. The combined evidence indicates that these spring-fed rivers were supplying a continual source of water within a semi-arid grassland (Fig. 2.6A and B).

Riverine tufa from Nyamita indicates that the $\delta^{18}O$ of palaeoprecipitation was more negative than modern, which suggests a greater contribution of depleted monsoonal input, similar to the LGM. Kisaaka and Aringo have positive increases in both oxygen and carbon isotopes, suggesting that evaporation and CO_2 degassing had a greater effect on tufa precipitating at Karungu due to distance from the spring source. Isotopic evidence indicates that the climate was significantly drier than modern and would have stressed humans and other mammals living on the landscape, making a perennial source of water very important. Microdebitage identified in thin section and fossil remains in the tufa deposits indicate that early modern humans and associated fauna were using these recurrent spring-fed rivers as a permanent water source within an overall semi-arid environment.

References

Ambrose, S.H. and **Lorenz, K.G.** (1990). Social and ecological models for the Middle Stone Age in southern Africa. In: *The emergence of modern humans: an archaeological perspective* (Ed. P. Mellars), pp. 3-33. Edinburgh University Press, Edinburgh.

Andrews, J., Riding, R., and **Dennis, P.** (1997) The stable isotope record of environmental and climatic signals in modern terrestrial microbial carbonates from Europe. *Palaeogeogr. Palaeoclimatol. Palaeoecol.,* **129**, 171–189.

Andrews, J.E. (2006) Palaeoclimatic records from stable isotopes in riverine tufas: Synthesis and review. *Earth-Sci. Rev.,* **75**, 85–104.

Andrews, J.E., and **Brasier, A.T.** (2005) Seasonal records of climatic change in annually laminated tufas: short review and future prospects. *J. Quat. Sci.,* **20**, 411–421.

Andrews, J.E., Pedley, M., and **Dennis, P.** (2000) Paleoenvironmental records in Holocene Spanish tufas: a stable isotope approach in search of reliable climatic archives. *Sedimentology,* **47**, 961–978.

Andrews, J.E., Riding, R., and **Dennis, P.F.** (1993) Stable isotopic compositions of recent freshwater cyanobacterial carbonates from the British Isles: local and regional environmental controls. *Sedimentology,* **40**, 303–314.

Angelucci, D.E. (2010) The recognition and description of knapped lithic artifacts in thin section. *Geoarchaeology,* **25**, 220–232.

Arenas, C., Vázquez-Urbez, M., Pardo, G., and **Sancho, C.** (2014) Sedimentology and depositional architecture of tufas deposited in stepped fluvial systems of changing slope: Lessons from the Quaternary Añamaza valley (Iberian Range, Spain). *Sedimentology,* **61**, 133-171.

Arenas-Abad, C., Vázquez-Urbez, M., Pardo-Tirapu, G., and **Sancho-Marcén, C.** (2010) Fluvial and Associated Carbonate Deposits. In: *Carbonates in Continental Settings: Facies, Environments, and Processes* (Eds A.M. Alonso-Zarza and L.H. Tanner), pp. 133–175. Elsevier, New York.

Ashley, G., Tactikos, J., and **Owen, R.** (2009) Hominin use of springs and wetlands: Paleoclimate and archaeological records from Olduvai Gorge (~1.79–1.74 Ma). *Palaeogeogr. Palaeoclimatol. Palaeoecol.*, **272**, 1–16.

Ashley, G.M., Domínguez-Rodrigo, M., Bunn, H.T., Mabulla, A.Z.P., and **Baquedano, E.** (2010a) Sedimentary geology and human origins: A fresh look at Olduvai Gorge, Tanzania. *J. Sed. Res.*, **80**, 703–709.

Ashley, G.M., Barboni, D., Domínguez-Rodrigo, M., Bunn, H.T., Mabulla, A.Z.P., Diez-Martin, F., Barba, R., and **Baquedano, E.** (2010b) A spring and wooded habitat at FLK Zinj and their relevance to origins of human behavior. *Quaten. Res.*, **74**, 304–314.

Ashley, G.M., Barboni, D., Domínguez-Rodrigo, M., Bunn, H.T., Mabulla, A.Z.P., Diez-Martin, F., Barba, R., and **Baquedano, E.** (2010c) Paleoenvironmental and paleoecological reconstruction of a freshwater oasis in savannah grassland at FLK North, Olduvai Gorge, Tanzania. *Quatern. Res.*, **74**, 333–343.

Ashley, G.M., Bunn, H.T., Delaney, J.S., Barboni, D., Domínguez-Rodrigo, M., Mabulla, A.Z.P., Gurtov, A.N., Baluyot, R., Beverly, E.J., and **Baquedano, E.** (2014) Paleoclimatic and paleoenvironmental framework of FLK North archaeological site, Olduvai Gorge, Tanzania. *Quatern. Int.*, **322-323**, 54-65.

Barich, B.E. and **Garcea, E.A.A.** (2008) Ecological Patterns in the Upper Pleistocene and Holocene in the Jebel Gharbi, Northern Libya: Chronology, Climate and Human Occupation. *Afr. Archaeol. Rev.,* **25**, 87–97.

Barnaby, R.J. and **Rimstidt, J.D.** (1989) Redox conditions of calcite cementation interpreted from Mn and Fe contents of authigenic calcites. *Geol. Soc. Am. Bull.*, **101**, 795-804**.**

Behrensmeyer, A., Potts, R., and **Plummer, T. (**1995) The Pleistocene locality of Kanjera, Western Kenya: stratigraphy, chronology and paleoenvironments. *J. Human. Evol.*, **29**, 247–274.

Beuning, K.R.M., Kelts, K., Ito, E., and **Johnson, T.C.** (1997) Paleohydrology of Lake Victoria, East Africa, inferred from $^{18}O/^{16}O$ ratios in sediment cellulose. *Geology,* **25**, 1083–1086.

Beuning, K.R.M., Kelts, K., and **Stager, J.C.** (1998) Abrubt climate changes associated with the arid Younger Dryas interval in Africa. In: *Environmental Change and Response in East African Lakes* (Ed J.T. Lehman), pp. 147–156, Kluwer Academic Publishers.

Beuning, R.M., Kelts, K., Russell, J., and **Wolfe, B.B.** (2002) Reassessment of Lake Victoria-Upper Nile River paleohydrology from oxygen isotopes records of lake-sediment cellulose. *Geology,* **30**, 559–562.

Bishop, W.W., and **Trendall, A.F.** (1967) Erosion-surfaces, tectonics and volcanic activity in Uganda. *Q. J. Geol. Soc.,* **122**, 385–420.

Blegen, N., Tryon, C.A., Faith, J.T., Peppe, D.J., Beverly, E.J. Jacobs, Z., and **Bo, Li** (2015) Distal tephras of the eastern Lake Victoria Basin, Equatorial East Africa: Correlations, chronology and a context for early modern humans. *Quatern. Sci. Rev.*

Blome, M.W., Cohen, A.S., Tryon, C.A., Brooks, A.S., and **Russell, J.** (2012) The environmental context for the origins of modern human diversity: A synthesis of regional variability in African climate 150,000-30,000 years ago. *J. Human. Evol,* **62,** 563-592.

Brasier, A.T., Andrews, J.E., Marca-Bell, A.D., and **Dennis, P.F.** (2010) Depositional continuity of seasonally laminated tufas: Implications for δ18O based palaeotemperatures. *Global. Planet. Change,* **71**, 160–167.

Broecker, W.C., Peteet, D., Hajdas, I., and **Lin, J.** (1998) Antiphasing between rainfall in Africa's Rift Valley and North America's Great Basin. *Quatern. Res.,* **50**, 12- 20.

Brown, F.H., McDougall, I., and **Fleagle, J.G.** (2012) Correlation of the KHS Tuff of the Kibish Formation to volcanic ash layers at other sites, and the age of early Homo sapiens (Omo I and Omo II). *J. Human. Evol.* **63**, 577–585.

Carthew, K., Taylor, M., and **Drysdale, R.** (2002) Aquatic insect larval constructions in tropical freshwater limestone deposits (tufa): preservation of depositional environments. *Gen. Appl. Entomol,* **31**, 35–42.

Carthew, K.D., Taylor, M.P., and **Drysdale, R.N.** (2006) An environmental model of fluvial tufas in the monsoonal tropics, Barkly karst, northern Australia. *Geomorphology,* **73**, 78–100.

Cerling, T.E. (1991) Carbon dioxide in the atmosphere: evidence from Cenozoic and Mesozoic paleosol. *Am. J. Sci.* , **291**, 377-400.

Cerling, T.E., Harris, J.M., and **Passey, B.H.** (2003) Diets of East African bovidae based on stable isotope analysis. *J. Mammal.,* **84**, 456–470.

Chafetz, H., and **Folk, R.** (1984) Travertines: depositional morphology and the bacterially constructed constituents. *J. Sed. Petrol.,* **54**, 289–316.

Chafetz, H., Rush, P., and **Utech, N.** (1991) Microenvironmental controls on mineralogy and habit of $CaCO_3$ precipitates: an example from an active travertine system, *Sedimentology,* **38**, 107–126.

Cheng, H., Edwards, R.L., Shen, C.-C., Polyak, V.J., Asmerome, Y., Woodhead, J., Hellstrom, J.,Wang, Y., Kong, X., Spotl, C., Wang, X., and **Alexander E.C., Jr**. (2013) Improvements in ^{230}Th dating, ^{230}Th and ^{234}U half-live values, and U-Th isotopic measurements by multi-collector inductively coupled plasma mass spectrometry. *Earth Planet. Sci. Lett.,* **371-372**, 82-91.

Cowling, S.A., Cox, P.M., Jones, C.D., MAslin, M.A., Peros, M., and **Spall, S.A.** (2008) Simulated glacial and interglacial vegetation across Africa: implications for species phylogenies and trans-African migration of plants and animals, *Glob. Change Biol.,***14**, 827-840.

Crul, R.C.M. (1995) Limnology and hydrology of Lake Victoria (Studies & Reports in Hydrology. In: *Comprehensive and Comparative Study of Great Lakes*, pp. 79, UNESCO.

Cuthbert, M.O. and **Ashley, G.M.** (2014) A Spring Forward for Hominin Evolution in East Africa. *PLoS ONE*, **9**, 1–9**.**

Dansgard, W. (1964) Stable isotopes in precipitation. *Tellus,* **16**, 436–468.

Ditchfield, P., Hicks, J., Plummer, T., Bishop, L.C., and **Potts, R.** (1999) Current research on the Late Pliocene and Pleistocene deposits north of Homa Mountain, southwestern Kenya. *J. Human. Evol.*, **36**, 123–150.

Doornkamp, J.C., and **Temple, P.H.** (1966) Surface, drainage and tectonic instability in part of southern Uganda. *Geogr. J.* **132**, 238–252.

Ebinger, C.J. (1989) Tectonic development of the western branch of the East African rift system. *Geol. Soc. Am. Bull.,* **101**, 885–903.

Eriksson, A., Betti, L., Friend, A.D., Lycett, S.J., Singarayer, J.S., von Cramon-Taubadel, N., Valdes, P.J., Balloux, F., and **Manica, A.** (2012) Late Pleistocene climate change and the global expansion of anatomically modern humans. *P. Natl. Acad. Sci. USA,* **109**, 16089-16094.

Faith, J.T., Choiniere, J.N., Tryon, C.A., Peppe, D.J., and **Fox, D.L.** (2011) Taxonomic status and paleoecology of Rusingoryx atopocranion (Mammalia, Artiodactyla), an extinct Pleistocene bovid from Rusinga Island, Kenya. *Quatern. Res.* **75**, 697–707.

Faith, J.T., Potts, R., Plummer, T.W., Bishop, L.C., Marean, C.W., and **Tryon, C.A.** (2012) New perspectives on middle Pleistocene change in the large mammal faunas of East Africa: Damaliscus hypsodon sp. nov. (Mammalia, Artiodactyla) from Lainyamok, Kenya. *Palaeogeogr. Palaeoclimatol. Palaeoecol.,* **361-362**, 84–93.

Faith, J.T., Tryon, C.A., Peppe, D.J., and **Fox, D.L.** (2013) The fossil history of Grevy's zebra *(Equus grevyi)* in Equatorial East Africa. *J. Biogeogr.,* **40,** 359-369.

Faith, J.T., Tryon, C.A., Peppe, D.J., Beverly, E.J. and **Blegen, N.** (2014) Biogeographic and evolutionary implications of an extinct late Pleistocene impala from the Lake Victoria Basin. *J. Mamm. Evol.,* **21**, 213-222.

Faith, J.T., Tryon, C. a., Peppe, D.J., Beverly, E.J., Blegen, N., Blumenthal, S., Chritz, K.L., Driese, S.G., and **Patterson, D.,** (2015) Paleoenvironmental context of the Middle Stone Age record from Karungu, Lake Victoria Basin, Kenya, and its implications for human and faunal dispersal in East Africa, *J. Human Evol.*, **83**, 28–45.

Faith, J.T., Tryon, C.A., and **Peppe, D.J.** (in press) Environmental change, ungulate biogeography, and their implications for early human dispersals in equatorial East Africa. In: *Africa from MIS 6-2: Population Dynamics and Paleoenvironments* (Eds S.C. Jones and B.A. Stewart), Springer.

Faure, G. (1986) Oxygen and hydrogen in the lithosphere. In: *Principles of Isotope Geology*, pp. 460-462, Wiley & Sons, New York.

Fillinger, U., Sonye, G., Killeen, G.F., Knols, B.G.J., and **Becker, N.** (2004) The practical importance of permanent and semipermanent habitats for controlling aquatic stages of Anopheles gambiae sensu lato mosquitoes: operational observations from a rural town in western Kenya, *Trop. Med. Int. Health.,* **9**, 1274–1289.

Freytet, P., and **Plet, A.** (1996) Modern freshwater microbial carbonates: The Phormidium stromatolites (tufa-travertine) of Southeastern Burgundy (Paris Basin, France). *Facies,* **34**, 219–237.

Freytet, P., Kerp, H., and **Broutin, J.** (1996) Permian freshwater stromatolites associated with the conifer shoots Cassinisia orobica Kerp et al . - a very peculiar type of fossilization. *Review of Palaeobotany and Palynology*, **91**, 85-105.

Freytet, P. and **Verrecchia, E.P.** (2007) Lacustrine and palustrine carbonate petrography: an overview. *J. Paleolimnol.,* **27**, 221–237.

Garcea, E.A.A. and **Giraudi, C.** (2006) Late Quaternary human settlement patterning in the Jebel Gharbi. *J. Human. Evol.,* **51**, 411–421.

Garrett, N. D., Fox, D.L., McNulty, K.P., Tryon, C.A., Faith, J.T., Peppe, D.J., and **Van Plantinga, A.** (2015) Stable isotope paleoecology of late Pleistocene Middle Stone Age humans from the equatorial East Africa, Lake Victoria basin, Kenya. *J. Human. Evol.,* **82**, 1-14.

Gasse, F., Chalié, F., Vincens, A., Williams, M.A.J., and **Williamson, D. (**2008) Climatic patterns in equatorial and southern Africa from 30,000 to 10,000 years ago reconstructed from terrestrial and near-shore proxy data. *Quatern. Sci. Rev.*, **27**, 2316–2340.

Haynes, C.V., Maxwell, T.A., Hawart, A.E., Nicoll, K.A., and **Stokes, C.E. (1997).** An Acheulian site near Bir Kiseiba in the Darb el Arb'in Desert, Egypt. *Geoarchaeology*, **12,** 819–832**.**

Holden, N.E. (1990) Total half-lives for selected nuclides. *Pure and Applied Chem.,* **62**, 941–958.

Horvatinčić, N., Krajcar Bronić, I., and **Obelić, B.** (2003) Differences in the ^{14}C age, δ^{13}C and δ^{18}O of Holocene tufa and speleothem in the Dinaric Karst. *Palaeogeogr. Palaeoclimatol. Palaeoecol.,* **193**, 139–157.

Ihlenfeld, C., Norman, M.D., Gagan, M.K., Drysdale, R.N., Maas, R., and **Webb, J.** (2003) Climatic significance of seasonal trace element and stable isotope variations in a modern freshwater tufa. *Geochim. Cosmochim. Acta,* **67**, 2341–2357.

Jaffey, A.H., Flynn, K.F., Glendenin, L.E., Bentley, W. C., and **Essling**, **A.M.** (1971) Precise measurement of half-lives and specific activities of ^{235}U and ^{238}U. *Phys. Rev. C*, **4**, 1889–1906.

Johnson, T.C., Scholz, C.A., Talbot, M.R., Kelts, K., Ricketts, R.D., Ngobi, G., Beuning, K.R., Ssemmanda, I., and **McGill, J.W.** (1996) Late Pleistocene dessication of Lake Victoria and rapid evolution of cichlid fishes, *Science* **273**, 1091–1093.

Johnson, C.R., Ashley, G.M., De Wet, C.B., Dvoretsky, R., Park, L., Hover, V.C., Bernhart Owen, R., and **Mcbrearty, S.** (2009) Tufa as a record of perennial fresh water in a semi-arid rift basin, Kapthurin Formation, Kenya. *Sedimentology*, **56**, 1115–1137.

Johnson, C.R. and McBrearty, S. (2012) Archaeology of middle Pleistocene lacustrine and spring paleoenvironments in the Kapthurin Formation, Kenya. *J. of Anthropol. Archaeol.*, **31**, 485–499.

Joordens, J.C. a., Vonhof, H.B., Feibel, C.S., Lourens, L.J., Dupont-Nivet, G., van der Lubbe, J.H.J.L., Sier, M.J., Davies, G.R., and **Kroon, D.** (2011) An astronomically-tuned climate framework for hominins in the Turkana Basin. *Earth Planet. Sci. Lett*., **307**, 1–8.

Joordens, J.C. a, Dupont-Nivet, G., Feibel, C.S., Spoor, F., Sier, M.J., van der Lubbe, J.H.J.L., Nielsen, T.K., Knul, M. V, Davies, G.R., and **Vonhof, H.B.** (2013) Improved age control on early Homo fossils from the upper Burgi Member at Koobi Fora, Kenya. *J. Human. Evol.*, **65**, 731–745.

Kent, P.E. (1944) The age and tectonic relationships of East African Volcanic Rocks. *Geol. Mag.,* **81**, 15–27.

Lee, R.K.L., Owen, R.B., Renaut, R.W., Behrensmeyer, A.K., Potts, R., and **Sharp, W.D. (**2013) Facies, geochemistry and diatoms of late Pleistocene Olorgesailie tufas, southern Kenya Rift. *Palaeogeogr. Palaeoclimatol. Palaeoecol.,* **374**, 197-217.

Liu, H., Prugnolle, F., Manica, A., and **Balloux, F.** (2006a) A geographically explicit genetic model of worldwide human-settlement history. *Am. J. Hum. Genet.,* **79**, 230–237.

Liu, Z., Li, Q., Sun, H., Liao, C., Li, H., Wang, J., and **Wu, K.** (2006b) Diurnal Variations of Hydrochemistry in a Travertine-depositing Stream at Baishuitai, Yunnan, SW China. *Aquat. Geochemistry,* **12**, 103–121.

Ludwig, K.R., Wallace, A.R. and **Simmons**, **K. R. (**1985) The Schwartzwalder uranium deposit, II: age of uranium mineralization and Pb-isotope constraints on genesis. *Econ. Geol.,* **80**, 1858-1871.

Machel, H.G., Mason, R.A., Mariano, A.N., and **Mucci, A.** (1991) Causes and emission of luminescence in calcite and dolomite. In: *Luminescence Microscopy and Spectroscopy: Quatitative and Qualitative Applications (SC25)* (Eds C.E. Barker and O. C. Kopp), pp. 9-25, SEPM.

Martini, I., and **Capezzuoli, E.** (2014) Interdigitated fluvial clastic deposits and calcareous tufa testifying an uplift of the catchment area: An example from the Pianizzoli area (southern Tuscany, Italy). *Sediment. Geol.,* **299**, 60–73.

Matsuoka, J., Kano, A., Oba, T., Watanabe, T., Sakai, S., and **Seto, K.** (2001) Seasonal variation of stable isotopic compositions recorded in a laminated tufa, SW Japan. *Earth Planet. Sci. Lett.,* **192**, 31–44.

McDougall, I., Brown, F.H., and **Fleagle, J.** (2005) Stratigraphic placement and age of modern humans from Kibish, Ethiopia. *Nature*, **433**, 733-736.

McKenzie, J. (1993) Pluvial conditions in the eastern Sahara following the penultimate deglaciation: implications for changes in atmospheric circulation patterns with global warming. *Palaeogeogr. Palaeoclimatol. Palaeoecol.,* **103**, 95–105.

Miall, A.D. (2010) Alluvial deposits. In:, *Facies Models 4* (Eds N.P. James and R.W. Dalrymple), pp. 105-107, Geological Association of Canada, Newfoundland.

Milly, P.C.D. (1999). Comment on “Antiphasing between rainfall in Africa's Rift Valley and North America's Great Basin." *Quat. Res.,* **51**, 104-107.

Nicoll, K., Giegengack, R., and **Kleindienst, M. (**1999) Petrogenesis of artifact-bearing tufa deposits from Kharga Oasis, Egypt. *Geoarchaeology* **14,** 849–863.

Ordóñez, S., González Martín, J.A., García del Cura, M.A., and **Pedley, H.M.** (2005) Temperate and semi-arid tufas in the Pleistocene to Recent fluvial barrage system in the Mediterranean area: The Ruidera Lakes Natural Park (Central Spain). *Geomorphology,* **69**, 332–350.

Ortiz, J.E., Torres, T., Delgado, A., Reyes, E., and **Diaz-Bautista, A.** (2009) A review of the Tagus river tufa deposits (central Spain): age and palaeoenvironmental record. *Quat. Sci. Rev.,* **28**, 947–963.

Owen, W.E. (1937) Draft of tentative preliminary report on the July 1937 investigations at Ng'ira Karungu, Unpublished manuscript housed in the archives of the Natural History Museum, London.

Pavlović, G., Prohić, E., Miko, S., and **Tibljaš, D.** (2002) Geochemical and petrographic evidence of meteoric diagenesis in tufa deposits in Northern Dalmatia (Zrmanja and Krupa Rivers, Croatia). *Facies,* **46**, 27–34.

Pedley, H.M. (1990) Classification and environmental models of cool freshwater tufas, *Sediment. Geol.* **68**, 143–154.

Pedley, M., Martín, J.A.G., Delogado, S.O., and **García del Cura, M.A.** (2003) Sedimentology of Quaternary perched springline and paludal tufas: criteria for recognition, with examples from Guadalajara Province, Spain. *Sedimentology,* **50**, 23–44.

Pentecost, A., and **Spiro, B.** (1990) Stable carbon and oxygen isotope composition of calcites associated with modern freshwater cyanobacteria and algae. *Geomicrobiol. J.,* **8**, 17–26.

Pickford, M.H. (1984) An aberrant new bovid (Mammalia) in subrecent deposits from Rusinga island, Kenya. *Proceedings of the Koninjlijke Nederlandsche Akademie van Wettenschappen B87,* **87**, 441–452.

Plummer, T., Bishop, L.C., Ditchfield, P., and **Hicks, J**. (1999) Research on Late Pliocene Oldowan Sites at Kanjera South, Kenya. *J. Human. Evol*, **36**, 151–170.

Quinn, R.L., Lepre, C.J., Wright, J.D., and **Feibel, C.S.** (2007) Paleogeographic variations of pedogenic carbonate δ^{13}C values from Koobi Fora, Kenya: implications for floral compositions of Plio-Pleistocene hominin environments.: *J. Human. Evol.*, **53**, 560–573.

Quinn, R.L., Lepre, C.J., Feibel, C.S., Wright, J.D., Mortlock, R. A, Harmand, S., Brugal, J.-P., and **Roche, H.** (2013) Pedogenic carbonate stable isotopic evidence for wooded habitat preference of early Pleistocene tool makers in the Turkana Basin. *J. Human. Evol.***, 65,** 65–78**.**

Riding, R. (2000) Microbial carbonates: the geological record of calcified bacterial-algal mats and biofilms. *Sedimentology,* **47**, 179–214.

Rito, T., Richards, M.B., Fernandes, V., Alshamali, F., Cerny, V., Pereira, L., and **Soares, P**. (2013) The first modern human dispersals across Africa. *PLoS ONE,* **8**, 1-16.

Romanek, C.S., Grossman, E.L., and **Morse, J.W.** (1992) Carbon isotopic fractionation in synthetic aragonite and calcite: Effects of temperature and precipitation rate. *Geochim. Cosmochim. Acta* **56**, 419–430.

Rozanski, K., Araguas-Araguas, L., and **Gonfiantini, R.** (1993) Isotopic patterns in modern global precipitation. *Geophys. Monogr,* **78**, 1–36.

Rozanski, K., Araguas-Araguas, L., and **Gonfiantini, R.** (1996) Isotope patterns of precipitation in the East African Region. In: *The Limnology, Climatology and Paleoclimatology of the East African Lakes* (Eds T.C. Johnson and E.O Odada)*,* pp. 79–93, Gordon and Breach Publishers, Netherlands.

Scholz, C.A., Johnson, T.C., Cohen, A.S., King, J.W., Peck, J.A., Overpeck, J.T., Talbot, M.R., Brown, E.T., Kalindekafe, L., Amoako, P.Y.O., Lyons, R.P., Shanahan, T.M., Castenada, I.S., Heil, C.W., Forman, S.L., McHargue, L.R., Beuning, K.R., Gomex, J., and **Pierson, J.** (2007). East African megadroughts between 135 and 75 thousand years ago and bearing on early-modern human origins. *P. Natl. Acad. Sci. USA,***104**, 16416-16421.

Smith, J., Giegengack, R., and **Schwarcz, H.** (2004) Constraints on Pleistocene pluvial climates through stable-isotope analysis of fossil-spring tufas and associated gastropods, Kharga Oasis, Egypt. *Palaeogeogr. Palaeoclimatol. Palaeoecol.,* **206**, 157–175.

Smith, J.R., Hawkins, A.L., Asmerom, Y., Polyak, V., and **Giegengack, R.** (2007) New age constraints on the Middle Stone Age occupations of Kharga Oasis, Western Desert, Egypt. *J. Human. Evol.,* **52**, 690–701.

Song, Y., Semazzi, F.H.M., Xie, L., and **Ogallo, L.J.** (2004) A coupled regional climate model for the Lake Victoria Basin of East Africa. *Int. J. Climatol.,* **24**, 57–75.

Stager, J.C., and **Johnson, T.C.** (2008) The late Pleistocene desiccation of Lake Victoria and the origin of its endemic biota. *Hydrobiologia,* **596**, 5–16.

Stager, J.C., Mayewski, L., and **Meeker, L.D.** (2002) Cooling cycles, Heinrich event 1, and the desiccation of Lake Victoria. *Palaeogeogr. Palaeoclimatol. Palaeoecol.,* **183**, 169–178.

Stager, J.C., Ryves, D.B., Chase, B.M., and **Pausata, F.S.R.** (2011) Catastrophic drought in the Afro-Asian monsoon region during Heinrich Event 1. *Science,* **331**, 1299–1302.

Sundborg, A. (1956) The River Klaralven: A Study of Fluvial Processes. *Geogr. Ann.,* **38**, 238–316.

Talbot, M.R. (1990) A review of the palaeohydrological interpretation of carbon and oxygen isotopic ratios in primary lacustrine carbonates. *Chem. Geol. Isot. Geosci. Sect.,* **80**, 261–279.

Talbot, M.R., and **Laerdal, T.** (2000) The late Pleistocene - Holocene palaeolimnology of Lake Victoria, East Africa, based upon elemental and isotopic analyses of sedimentary organic matter. *J. Paleolimnol.,* **23**, 141–164.

Talbot, M.R., and **Williams, M.A.J.** (2009) Cenozoic evolution of the Nile Basin. In: *The Nile: Origin, Environments, Limnology and Human Use* (Ed H.J. Dumont)*,* pp. 37–60, Springer Science.

Tryon, C.A., Faith, J.T., Peppe, D.J., Fox, D.L., McNulty, K.P., Jenkins, K., Dunsworth, H., and **Harcourt-Smith, W.** (2010) The Pleistocene archaeology and environments of the Wasiriya Beds, Rusinga Island, Kenya. *J. Human. Evol.,* **59**, 657–671.

Tryon, C.A., Peppe, D.J., Faith, J.T., Van Plantinga, A., Nightingale, S., Ogondo, J., and **Fox, D.L.** (2012) Late Pleistocene artefacts and fauna from Rusinga and Mfangano islands, Lake Victoria, Kenya. *Azania Archaeol. Res. Africa,* **47**, 14–38.

Tryon, C. A., Faith, J.T., Peppe, D.J., Keegan, W.F., Keegan, K.N., Jenkins, K.H., Nightingale, S., Patterson, D., Van Plantinga, A., Driese, S., Johnson, C.R., and **Beverly, E.J.** (2014) Sites on the landscape: Paleoenvironmental context of late Pleistocene archaeological sites from the Lake Victoria basin, equatorial East Africa. *Quat. Int.* **331**, 20-30.

Van Couvering, J.A. (1972) Geology of Rusinga Island and Correlation of the Kenya Mid-Tertiary Fauna: PhD Dissertation, Cambridge University, 208 pp.

Van Plantinga, A. (2011) Geology of the Late Pleistocene artifact-bearing Wasiriya beds at the Nyamita Locality, Rusinga Island, Kenya, Master's Thesis, Baylor University, 97 pp.

Viles, H.A., Taylor, M.P., Nicoll, K., and **Neumann, S.** (2007) Facies evidence of hydroclimatic regime shifts in tufa depositional sequences from the arid Naukluft Mountains, Namibia. *Sediment. Geol.,* **195**, 39–53.

Wendorf, F. (Ed) (1993) Egypt During the Last Interglacial: The Middle Paleolithic of Bir Tarfawi and Bir Sahara East, Plenum Press, 596 pp.

Zamarreño, I., Anadón, P., and **Utrilla, R.** (1997) Sedimentology and isotopic composition of Upper Palaeocene to Eocene non-marine stromatolites, eastern Ebro Basin, NE Spain. *Sedimentology,* **44**, 159–176.

Zimmerman, U., Ehhalt, D., and **Münnich., K.O.** (1967) Soil-water movement and evapotranspiration: changes in the isotopic composition of the water. In: Isotopes in Hydrology, pp. 567–585, International Atomic Energy Agency, Vienna.

CHAPTER THREE

Reconstruction of a semi-arid Late Pleistocene
paleocatena from the Lake Victoria region, Kenya

This chapter published as: Beverly, E.J., Driese, S.G., Peppe, D.J., Arellano, L.N., Blegen, N., Faith, J.T., and Tryon, C.A., 2015, Reconstruction of a semi-arid Late Pleistocene paleocatena from the Lake Victoria region, Kenya: Quaternary Research.

Abstract

The effect of changing environment on the evolution of *Homo sapiens* is heavily debated, but few data are available from equatorial Africa prior to the Last Glacial Maximum. The Karungu deposits on the northeast coast of Lake Victoria are ideal for paleoenvironmental reconstructions and are best exposed at the Kisaaka site (94 to >33 ka) where paleosols, fluvial deposits, tufa, and volcaniclastic deposits (tuffs) are exposed over an ~2 km transect. Three well-exposed and laterally continuous paleosols with intercalated tuffs allow for reconstruction of a succession of paleocatenas. The oldest paleosol is a smectitic paleo-Vertisol with saline and sodic properties. Higher in the section, the paleosols are tuffaceous paleo-Inceptisols with Alfisol-like soil characteristics (illuviated clay). Mean annual precipitation (MAP) proxies indicate little change through time, with an average of 764±108 mm yr^{-1} for Vertisols (CALMAG) and 813±182 to 963±182 mm yr^{-1} for all paleosols (CIA-K). Field observations and MAP proxies suggest Karungu was significantly drier than today, consistent with the associated faunal assemblage, and likely resulted in a significantly smaller Lake Victoria during the Late Pleistocene. Rainfall reduction and associated grassland expansion may have facilitated human and faunal dispersals across equatorial East Africa.

Introduction

Climate-driven environmental change is a commonly proposed mechanism for the dispersals of humans within and out of Africa through its effects on population distributions and demographics, biogeographic barriers, and resource availability (e.g., Ambrose and Lorenz, 1990; Cowling et al., 2008; Blome et al., 2012; Eriksson et al., 2012; Rito et al., 2013; Scholz et al., 2007; Soares et al., 2012; Faith et al., in press). The earliest fossil remains of *Homo sapiens* are known from eastern Africa at ~195 ka, and by as early as 80 to 60 ka populations had dispersed throughout Africa and also into Eurasia (e.g., Brown et al., 2012; McDougall et al., 2005; Rito et al., 2013; Soares et al., 2012). Few empirical data on climate or environment at relevant spatial or temporal scales are associated with archaeological or early human fossil sites from equatorial East Africa prior to the Last Glacial Maximum (LGM) (e.g., Blome et al., 2012), which limits understanding the ecology of early human populations and the mechanisms underlying their dispersals. Sediment cores from Lake Victoria provide continuous records of regional hydrology and vegetation back to the LGM (Kendall, 1969; Johnson et al., 1996; Talbot and Laerdal, 2000; Stager et al., 2002, 2011; Berke et al., 2012), but paleoenvironmental data prior to the LGM are sparse.

Deposits identified along the northeastern shores of Lake Victoria near Karungu, Kenya, dated to between 94 ka and >33 ka (Tryon et al., 2010; Beverly et al., 2015; Blegen et al., in 2015; Faith et al., 2015), have the potential to provide fundamental paleoenvironmental and paleoclimatic information about equatorial East Africa during this critical interval of human evolution and dispersal (Figs. 3.1A and 3.1B). The sediments at Karungu preserve abundant vertebrate fossils and Middle Stone Age (MSA) artifacts (Faith et al., 2015; Owen, 1937; Pickford, 1984), which are considered the archaeological signature of early *Homo sapiens* in East Africa (McBrearty and Brooks, 2000; Tryon and Faith, 2013). The pre-LGM Karungu dataset complements, refines, and expands those from correlative deposits on Rusinga and Mfangano Islands ~40 km to the north (Tryon et al., 2010, 2012, 2014; Van Plantinga, 2011; Faith et al., 2011, 2012, 2014, 2015; Garrett et al., 2015). Previous evidence from MSA archaeological and paleontological sites from Rusinga and Mfangano Islands suggests that the contraction of Lake Victoria and expansion of grasslands during the Late Pleistocene may have facilitated the dispersal of large bodied mammals, including humans, across Africa (e.g., Faith et al., 2015, in press). However, the modeled reduction in the size of Lake Victoria requires a reduction in precipitation (Broecker et al., 1998; Milly, 1999), for which we had no direct evidence. Here, we provide the first quantitative estimates of paleoprecipitation through a multi-proxy analysis of paleosols from Kisaaka (Fig. 3.1C), one of seven Pleistocene artifact- and fossil-bearing sites at Karungu, originally noted by Owen (1937, 1938, 1939), later mapped by Pickford (1984) and the focus of fieldwork by our team over the last several years (Faith et al., 2015).

The deposits at Kisaaka are predominantly made up of paleosols, which are invaluable records of paleoenvironmental information through the use of paleosol paleoclimate proxies (reviewed in Sheldon and Tabor, 2009; Tabor and Myers, 2015). In addition, correlative tuffs blanketing the landscape allow for lithostratigraphic correlation between outcrops and in some instances the preservation of the original topography (Figs. 3.1C, 3.2, and 3.3A; Faith et al., 2015; Blegen et al., 2015). Milne (1935) originally defined the relationship of soil development to changes in topography as a catena, and

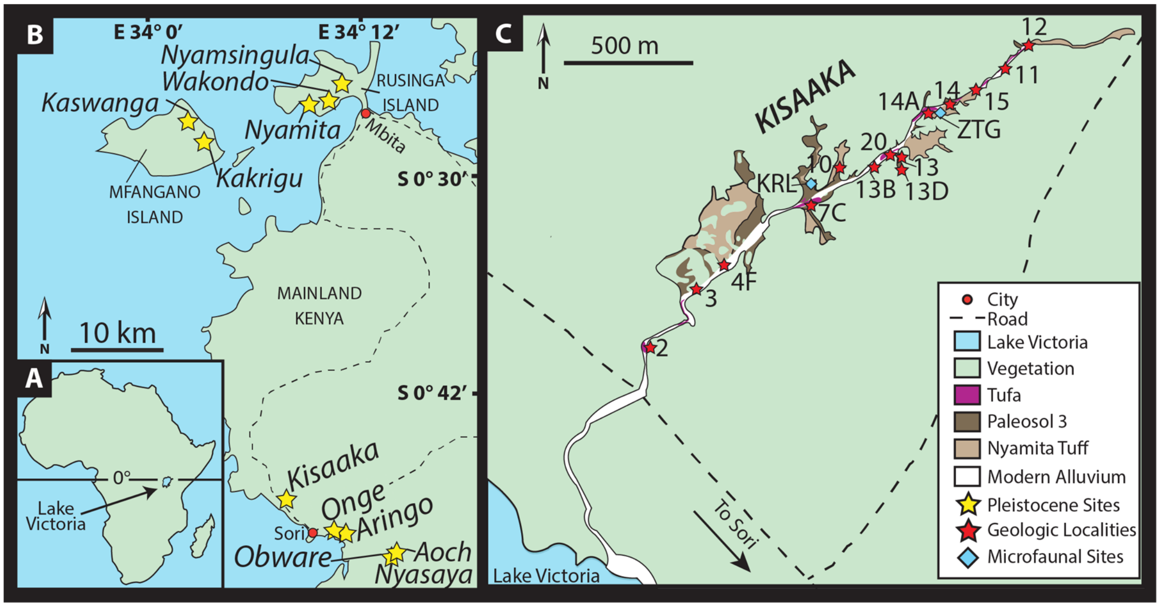

Figure 3.1: Location maps. A) Inset shows the location of Lake Victoria in East Africa. B) Location of Pleistocene sites along the eastern margin of Lake Victoria. C) Mapped lithologies exposed at the Kisaaka site with key geologic and microfaunal locations identified. Modified from Beverly et al. (2015).

soil properties can change dramatically across a landscape with topography due to changes in hydrology (Birkeland, 1999). The correlative volcanic ashes burying these surfaces form a succession of paleocatenas at Kisaaka. The objectives of the present study are to: 1) use field and micromorphological descriptions of paleosols and paleoenvironmental proxies or pedotransfer functions derived from their bulk geochemical composition to reconstruct a series of paleocatenas at Kisaaka, 2) provide context for faunal and archaeological records at Kisaaka, and 3) integrate paleoprecipitation estimates into the regional paleoclimate and paleoenvironment of the Late Pleistocene in equatorial East Africa to quantify some of the factors that may have contributed to human evolution and dispersal in the Late Pleistocene.

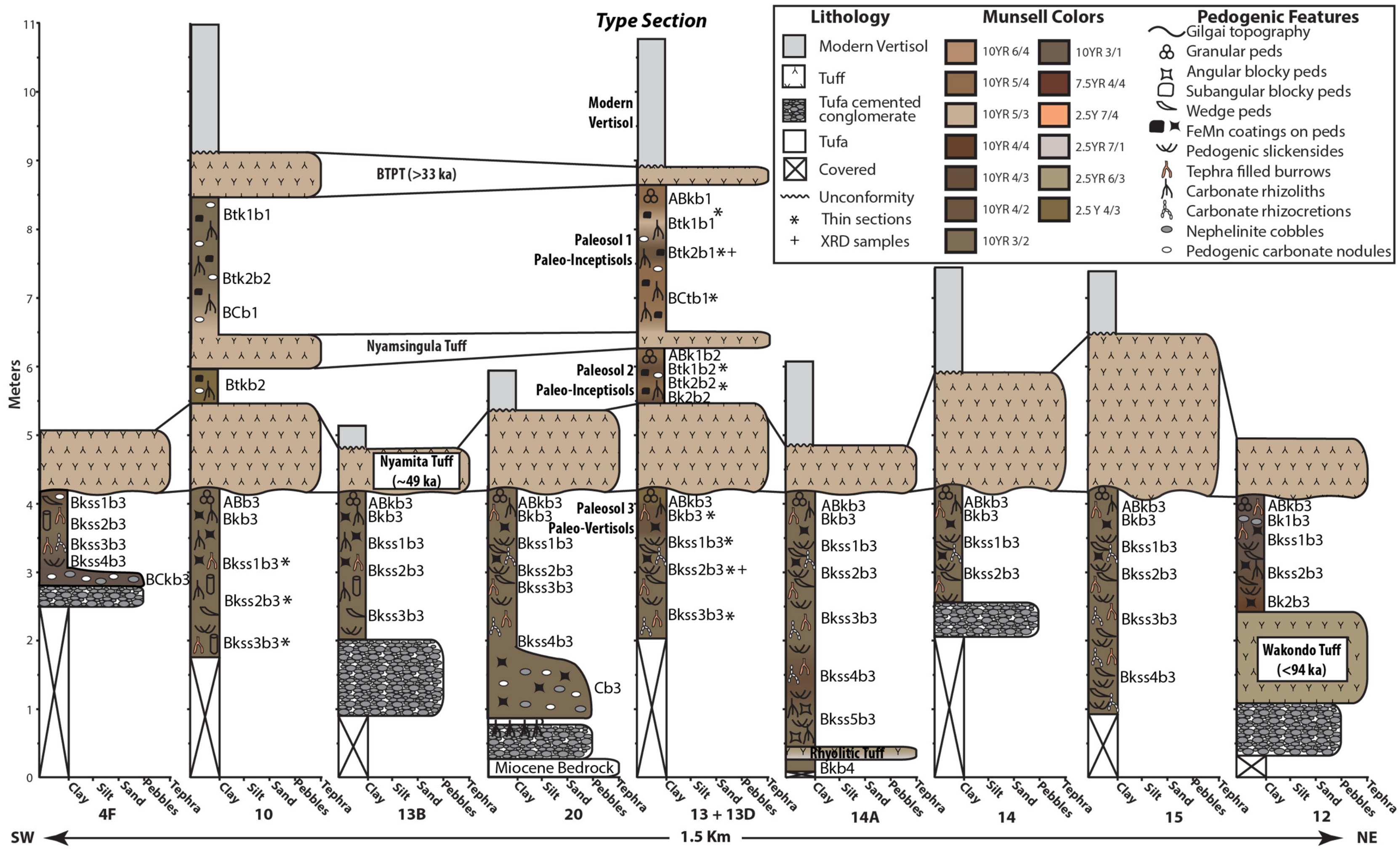

Figure 3.2: Measured stratigraphic sections from Kisaaka correlated using the base of the laterally extensive Nyamita Tuff as the datum and tephrostratigraphy by Blegen et al. (2015). Localities are arranged from north to south over 1.5 km transect. See Figure 3.1 for location of sites. Pedogenic features, soil and tuff colors, soil horizons, and lithology are described in detail with three paleosols identified.

Background

Lake Victoria Basin

Lake Victoria is the largest freshwater lake in the tropics by surface area (~66,400 km^2), spanning the equator in a depression between the eastern and western branch of the East African Rift System (EARS). The lake is very shallow with a maximum depth of ~68 m (Stager and Johnson, 2008) in comparison to the other African Great Lakes, Lakes Malawi and Tanganyika, which are 700 and 1470 m deep, respectively (Bootsma and Hecky, 2003). Lake Victoria likely began to form between ~1.6 and ~>0.4 Ma when uplift associated with of the western arm of the EARS began to dam westward-flowing rivers, causing ponding between the western and eastern arms of the EARS (Bishop and Trendall, 1967; Doornkamp and Temple, 1966; Ebinger, 1989; Johnson et al., 1996; Kent, 1944; Talbot and Williams, 2009).

The Intertropical Convergence Zone (ITCZ) is the primary control on precipitation in the Lake Victoria region, which today crosses the region twice a year with long rains in March and shorter rains in October (Song et al., 2004). Mean annual precipitation (MAP) at Mbita, Kenya, which is proximal to the study area (Fig. 3.1B), is ~1400 mm yr^{-1} (Crul, 1995; Fillinger et al., 2004). Up to 80% of the water input is from direct precipitation on the lake surface, and most of the water loss (up to 90%) is from evaporation (Crul, 1995). Thus, small changes in precipitation likely have a significant influence on water input and lake volume (Broecker et al., 1998; Milly, 1999).

Geological evidence suggests that Lake Victoria increased in size compared to present surface area and desiccated multiple times, with the most recent desiccation occuring at 16 ka (Heinrich Event 1) (Johnson et al., 1996; Talbot and Laerdal, 2000;

Stager et al., 2002, 2011). The desiccation at 16 ka led to the formation of a paleo-Vertisol across much of the basin that has been identified in multiple cores across Lake Victoria, and none of the cores penetrated more than a few cm beneath it (Johnson et al., 1996; Stager et al., 2002, 2011). This 16 ka paleo-Vertisol surface can be identified in seismic profiles across the entire lake basin, and similar underlying surfaces identified in the seismic data suggest that the lake desiccated multiple times prior to Heinrich Event 1 (Johnson et al., 1996; Stager et al., 2002, 2011).

Karungu

Karungu (0.84°S, 34.15°E) is located on the Kenyan margin of Lake Victoria (Fig. 3.1), ~40 km south of Pleistocene localities on Rusinga and Mfangano Islands that have been the focus of research by our team since 2009 (Tryon et al., 2010, 2012, 2014; Faith et al., 2011, 2012, 2014; Van Plantinga, 2011; Garrett et al., 2015; Beverly et al., 2015). The Pleistocene deposits at Karungu are exposed at seven sites around the town of Sori. They were originally noted by Owen (1937) and mapped by Pickford (1984). The best-exposed sites (Kisaaka, Aringo, Onge, Obware, and Aoch Nyasaya) were further investigated and mapped in greater detail by Beverly et al. (2015), Faith et al. (2015), and Blegen et al. (2015). The Kisaaka locality has the most laterally extensive (~2 km) and thickest (2.5 to 11 m) outcrops at Karungu, and the paleosols identified in these deposits are the focus here (Fig. 3.3A). The stratigraphy varies across Kisaaka, but generally, freshwater tufa that precipitated on Miocene bedrock of conglomerates and breccias forms the base of the sequence and is overlain by conglomerates, paleosols, and tuffaceous sediments (Beverly et al., 2015; Faith et al., 2015; Blegen et al., 2015).

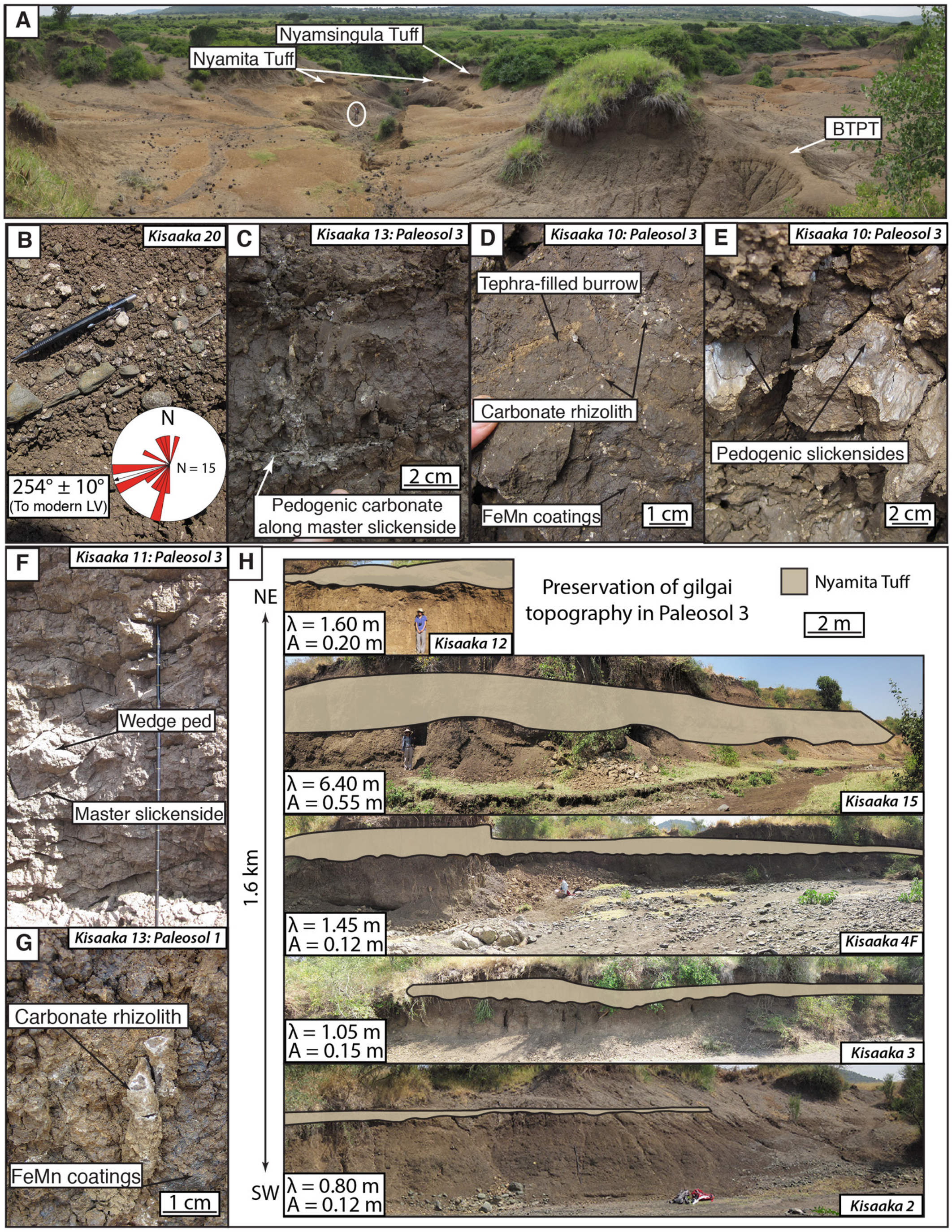

Figure 3.3: Field photos of key features described in Figure 3.2. See Figure 3.1 for location. A) Panoramic view of Kisaaka 13 with correlative tuffs identified and person circled for scale. B) Imbricated cobbles used to determine a mean paleocurrent direction of 254°N flowing towards modern Lake Victoria. C) Paleosol 3: Pedogenic carbonate precipitating along a master slickenside. D) Top view Paleosol 3: Tephra filled burrows, carbonate rhizoliths, and FeMn coatings visible. E) Paleosol 3: Well developed pedogenic slickensides. F) Paleosol 3: Extremely well developed vertic features with wedge peds and master slickenside. G) Paleosol 1: Carbonate rhizoliths and FeMn coatings are visible with subangular blocky peds. Representative of both Paleosols 1 and 2. H) Preservation of gilgai topography due to deposition of Nyamita Tuff. λ= wavelength of gilgai. A = amplitude of gilgai.

There are five compositionally distinct tuffs exposed at Kisaaka. As a result of a comprehensive program of geochemical characterization by electron microprobe analyses of 50 samples, the tuffs at Karungu can be correlated with those to the north at Rusinga and Mfangano Islands where they have been dated by multiple radiometric methods (Tryon et al., 2010; Van Plantinga, 2011; Blegen et al., 2015; Beverly et al., 2015; Faith et al., 2015; Garrett et al., 2015). As summarized in Fig. 3.2, the lowermost tephra, the Wakondo Tuff and an unnamed rhyolitic tuff were deposited between ~49 and 94 ka based on U-series dates on underlying tufa (Beverly et al., 2015) and OSL dates on overlying sands (Blegen et al., 2015; Faith et al., 2015). The Nyamita Tuff was deposited at ~49 ka based on OSL dates on sand deposits bracketing the tephra (Blegen et al., 2015; Faith et al., 2015). The Nyamsingula Tuff is overlain by the Bimodal Trachyphonolitic Tuff (BTPT), and both were dated between >33 and 49 ka based on their stratigraphic relationship with the underlying Nyamita Tuff and AMS radiocarbon dates on gastropod shells that post-depositionally burrowed into the sediment (Tryon et al., 2010; Blegen et al., 2015). These gastropods (*Limicolaria* cf. *martensiana*) are only found in the upper sediments in life position. Therefore, these gastropods, which likely burrowed into the sediment after deposition, but before lithification, represent a minimum age for these deposits.

At Kisaaka, three paleosols are identified (Fig. 3.2), separated by tuffs that allow their correlation over a ~2 km transect and preserve the topography of the paleocatenas. The Nyamita Tuff, the Nyamsingula Tuff, and the BTPT Tuff can be laterally traced between numerous outcrops across Kisaaka, with additional correlations among discontinuous exposures confirmed on the basis of geochemical composition (Faith et al., 2015; Blegen et al., 2015). Two outcrops preserve the entire stratigraphic sequence (Kisaaka 10 and 13; Fig. 3.1C). Kisaaka 13 is the representative section for the stratigraphic sequence at Kisaaka (Figs. 3.2 and 3.3A). From bottom to top, Kisaaka 13 has a 2 m thick paleosol (Paleosol 3) that is overlain by 1 m of the Nyamita Tuff. Above the Nyamita Tuff is a thin (0.8 m) paleosol unit capped by the Nyamsingula Tuff, which is designated Paleosol 2. The youngest paleosol, designated Paleosol 1, is 2.2 m thick and is overlain by the BTPT Tuff.

Methods

In order to use the Kisaaka paleosols to infer past environmental conditions, all outcrop locations were recorded and mapped using hand-held GPS (Appendix B), the exposures were trenched to expose bedding unaffected by modern processes, and the stratigraphic sequence measured and described at the cm scale. All lithologic and pedogenic features were recorded and photographed. Wavelength and amplitude of gilgai topography, typical of soils affected by shrinking and swelling of clays, were measured in the field and averaged by location for comparison across the landscape. Paleocurrent measurements on imbricated cobbles were collected from seven locations. Samples were collected for bulk geochemistry and clay mineralogy at 10 cm vertical intervals through the paleosols, and where applicable, samples were collected from gilgai topography micro-lows where erosion is less likely and pedogenic processes are greatest (Driese et al., 2000, 2003). Oriented samples for micromorphological analysis were collected from each identified soil horizon.

Samples were pulverized for mineralogical and geochemical analysis. Paleosol mineralogical analysis was conducted at Baylor University on a Siemens D-5000 θ-2θ X-ray diffractometer (XRD) using Cu Kα radiation at 40Kv and 30mA. Samples were scanned from 2 to 60º 2θ, at a 0.05º step per 1.5 seconds for bulk powder and < 2 μm fraction of four oriented aggregate treatments (MgCl, MgCl plus glycerol, KCl at 25 °C, KCl heated to 550 °C for 24 hours) using the Millipore system described in Moore and Reynolds (1997).

Bulk geochemical samples were sent for commercial analysis to ALS Geochemistry (Reno, NV) for major, rare, and trace element analyses using a combination of inductively coupled plasma atomic emission spectroscopy (ICP-AES) and inductively coupled plasma mass spectrometry (ICP-MS). The complete geochemical analyses of all samples are available in Appendix C. All bulk geochemical data were normalized to molecular weight for application to molecular weathering ratios and pedotransfer functions developed to reconstruct soil properties of paleo-Vertisols after Retallack (2001) and Nordt and Driese (2010a), respectively. Molecular weathering ratios can be used to examine relative changes in weathering such as hydrolysis or salinization down profile (Retallack, 2001). Pedotransfer functions were developed to relate the bulk geochemistry of paleosols to physical and chemical properties determined by the USDA-NRCS using regression based transfer functions (Nordt and Driese, 2010a).

Bulk geochemical data were also used to calculate paleoprecipitation using the chemical index of alteration minus potassium (CIA-K) for all soil types (Sheldon et al., 2002), and the CALMAG proxy, specific to paleo-Vertisols (Nordt and Driese, 2010b). CIA-K is defined as Al_2O_3/ (Al_2O_3 +CaO + Na_2O) x 100 and is a weathering index that measures clay formation and base loss associated with feldspar weathering and was designed to be universal for all paleosol types in which there has been sufficient time of soil formation to equilibrate with climate conditions (Sheldon et al., 2002). The application of the CIA-K proxy to Vertisols can be problematic because CIA-K measures the hydrolysis of weatherable minerals, and hydrolysis in Vertisols is very limited due to the stability of the smectite and illite clay minerals. The smectitic clay is often pre-weathered in Vertisols due to inheritance of clays from the parent material. Therefore, the CALMAG weathering index was developed specifically for paleo-Vertisols, which is defined as $Al_2O_3/(Al_2O_3 + CaO + MgO) \times 100$ where all oxides are normalized to their molar ratios. CaO and MgO accounts for 90% of the variation with climate in Vertisols and therefore MgO is substituted for Na_2O. This subsitution also reduces the influence of primary sodium-bearing minerals. The CIA-K and CALMAG weathering indices in modern soils have a strong correlations to MAP and these indices can be used to estimate paleo-rainfall using stepwise linear regression.

Nineteen thin-sections were prepared commercially by Spectrum Petrographics, Inc. Oriented samples were stabilized in the field and lab with epoxy and then vacuum-impregnated with epoxy prior to thin section preparation. Micromorphological study of paleosols was conducted at Baylor University according to techniques established by Fitzpatrick (1993) and Stoops (2003) on an Olympus BX-51 polarized-light microscope equipped with a 6.5 MPx Leica digital camera and an ultraviolet fluorescence (UVf) attachment. Changes in organic matter content were visually estimated by subjecting the thin section to UVf causing the organic matter to autofluoresce. Photomicrographs of unique and representative features were taken using three different UVf wavelength filters, NU, NB, and TXRED, in addition to those taken with cross-polarized light (XPL) and plane-polarized light (PPL).

Results

Field and Micromorphological Descriptions

Of the sequence of three paleosols at Kisaaka, Paleosol 3 is the easiest to identify and correlate because the Nyamita Tuff forms a thick, locally distinctive marker bed that caps it throughout the Kisaaka locality (Figs. 3.2 and 3.3H). Paleosol 3 varies in thickness from 1.5-3.5 m, and where the base of the stratigraphy is exposed, it overlies a tufa-cemented conglomerate, the rhyolitic tuff, or the Wakondo Tuff. This conglomerate is part of a fining upward sequence and is often imbricated allowing for paleocurrent measurements (Fig. 3.3B). The measurements indicate that the paleoflow direction was generally to the west (N 254°±10°) in the direction of modern Lake Victoria, paralleling modern drainage patterns. Paleosol 3 is identified as a paleo-Vertisol in outcrop by the medium to coarse wedge peds, pedogenic slickensides with angles up to 45°, master slickensides, and gilgai topography (Figs. 3.3C-F, H). The wavelength (λ) and amplitude (A) of these gilgai varies significantly across the landscape (Fig. 3.3H). At the northeast (Kisaaka 12) and southwest (Kisaaka 2, 3, and 4F), the average λ ranges from 0.8 to 1.6 m and the average A ranges from 0.12 to 0.20 m. At the Kisaaka 15 site, the average λ is 6.4 m and the average A is 0.55 m.

Vertic features are also present in thin section. The oriented birefringent clay (b-fabric) is identified as pedogenic slickensides in the micromorphology (Fig. 3.4B) by the lack of laminations and identical grain size between oriented clay and the matrix (Stoops et al., 2010). This is best illustrated by contrasting the oriented clay in XPL and PPL (Fig. 3.4B). Parallel striated and granostriated b-fabrics are also common in the Bkss horizons and with some areas of more developed cross-striated b-fabric (Table 3.1).

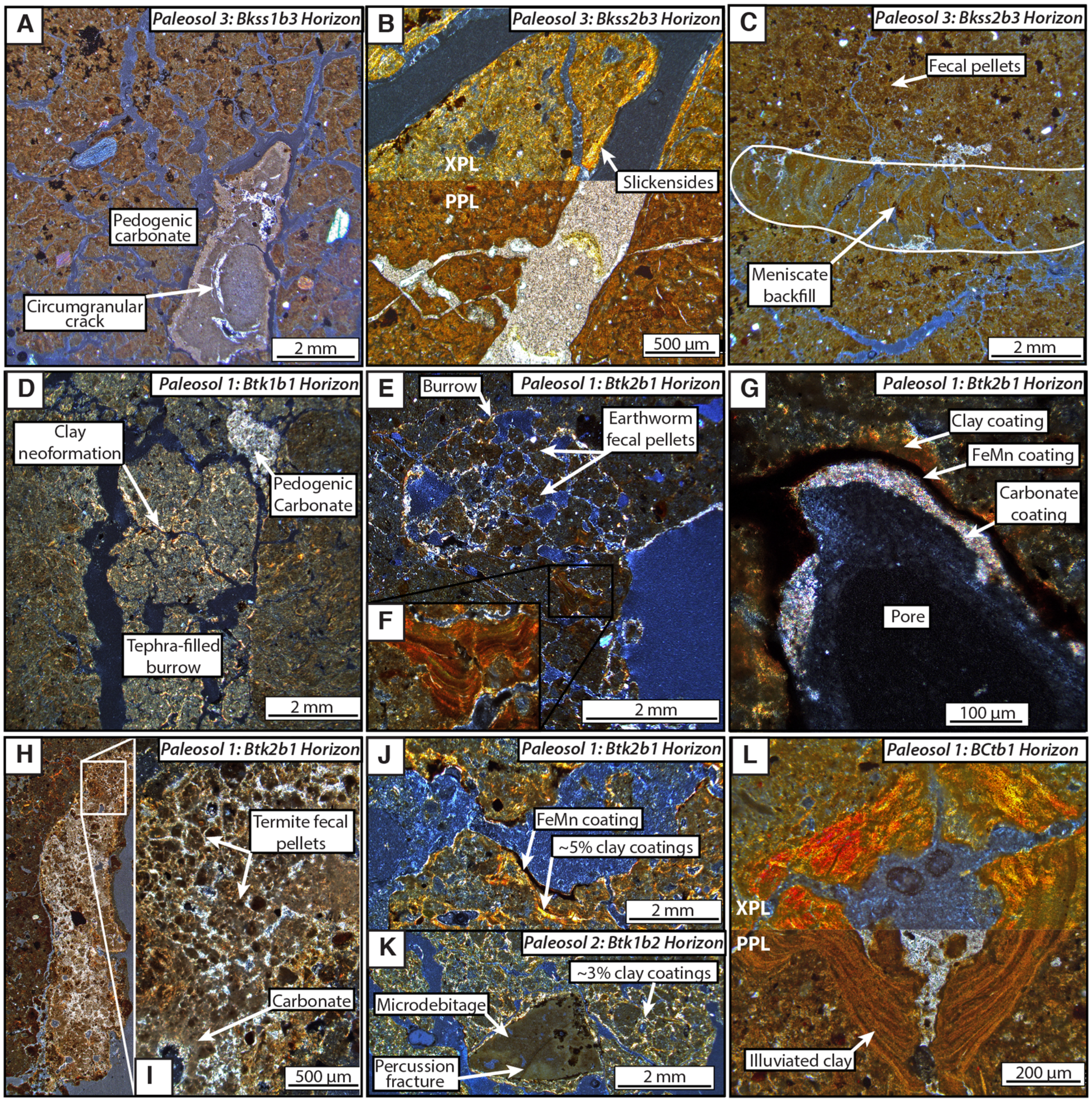

Figure 3.4: Photomicrographs of representative microstructures and biologic features. All photomicrographs are oriented. A) Paleosol 3: Very different soil matrix with little tephra, but very well developed pedogenic carbonates with circumgranular cracking, 1.25x XPL. B) Paleosol 3: Pedogenic slickensides, 4x, upper XPL, lower PPL. C) Paleosol 3: Fecal pellets in the matrix and a burrow with meniscate backfill, 1.25x XPL. D) Paleosol 1: Burrow filled with tephra undergoing neoformation to clay and pedogenic carbonate, 1.25x XPL. E) Paleosol 1: Burrow filled with fecal pellets, likely by earthworms, and illuviated clay, 1.25x XPL. F) Paleosol 1: Close up of illuviated clay, 10x XPL. G) Paleosol 1: Cross cutting relationships of pedogenic features: 1) illuviated clay, 2) FeMn, and 3) carbonate, 20x XPL. H) Paleosol 1: Carbonate rhizolith, 1.25x XPL. I) Paleosol 1: Close-up of fecal pellets, likely from termites, cemented by calcite in rhizolith, 4x XPL. J) Paleosol 1: Illuviated clay (~5%) and FeMn coatings filling pore spaces and coating ped surfaces, 1.25x XPL. K) Paleosol 2: ~3% Illuviated clay coating ped surfaces and microdebitage, 1.25x XPL. L) Paleosol 1: Very well developed illuviated clay with at least 10 generations of illuviation, 10x, upper XPL, lower PPL.

Table 3.1: Summary of field and micromorphological descriptions of type section paleosols at Kisaaka 13.

Horizon	Munsell Color	Pedogenic features	Illuviated clay (%)	B-fabric	Biologic indicators
Paleosol 1: Inceptisol (49 to >33)					
ABkb1	10YR 5/4	• Granular and subangular blocky peds • FeMn redoximorphic redistribution in matrix • Poorly developed carbonate nodules often with diffuse boundaries	<1	None	• Earthworm fecal pellets • Tephra filled burrows • Carbonate rhizoliths
Btk1b1	10YR 5/3	• Subangular blocky peds • FeMn coatings on peds and redoximorphic redistribution in matrix • Poorly developed carbonate nodules often with diffuse boundaries	3	None	• Earthworm fecal pellets • Tephra filled burrows • Carbonate rhizoliths
Btk2b1	10YR 4/2.5	• Subangular blocky peds • FeMn coating on peds and minor redoximorphic redistribution in matrix • Poorly developed carbonate nodules often with diffuse boundaries • Complex history of FeMn, illuviated clay, and carbonate coatings in pores • Pedorelicts	5	None	• Abundant earthworm fecal pellets • Tephra filled burrows, often preferential flowpath for illuviated clay • Carbonate rhizoliths • OM complexed with illuviated clay and disseminated in matrix
BCtb1	10YR 5/4	• Angular blocky peds • Complex history of FeMn, illuviated clay, and carbonate coatings in pores • Tephra increases with depth throughout profile and gradual boundary with Nyamsingula Tuff	3	None	• Abundant earthworm fecal pellets but forming dense microaggregates • Tephra filled burrows • Carbonate rhizoliths
Paleosol 2: Inceptisol (49 to >33)					
Bk1b2	10YR 5/4	• Granular to subangular blocky peds • FeMn coating on peds	<1	None	• Earthworm fecal pellets • Tephra filled burrows • Weakly developed carbonate rhizoliths

Table 3.1: Continued

Horizon	Munsell Color	Pedogenic features	Illuviated clay (%)	B-fabric	Biologic indicators
Btk1b2	10YR 4/3	• Subangular blocky peds • FeMn coating on peds • Complex history of FeMn, illuviated clay, and carbonate coatings in pores • Pedorelicts • Weakly developed pedogenic slickensides	3	None	• Earthworm fecal pellets • Tephra filled burrows • Weakly developed carbonate rhizoliths • Microdebitage
Btk2b2	10YR 5/4	• Subangular blocky peds • FeMn coatings on peds • Poorly developed carbonate nodules often with diffuse boundaries • Complex history of FeMn, illuviated clay, and carbonate coatings in pores • Pedorelicts	3	None	• Earthworm fecal pellets • Tephra filled burrows • Weakly developed carbonate rhizoliths
Bk2b2	10YR 4/3	• Subangular blocky peds • FeMn coatings on peds • Gradual boundary with Nyamita Tuff • Stone line	<1	None	• Bone fragment • Weakly developed carbonate rhizoliths
Paleosol 3: Vertisol (94 to 49 ka)					
ABkb3	10YR 4/3	• Granular to subangular blocky peds • FeMn coatings on peds	0	None	• Tephra filled burrows • Weak to well developed carbonate rhizoliths
Bkb3	10YR 4/2	• Angular blocky peds • FeMn coatings on peds • FeMn glaebules • Tephra weathering to clay but no indication of illuviation	0	Parallel to weakly cross-striated, granostriated	• Earthworm fecal pellets • Tephra filled burrows • Weak to well developed carbonate rhizoliths

Table 3.1: Continued

Horizon	Munsell Color	Pedogenic features	Illuviated clay (%)	B-fabric	Biologic indicators
Bkss1b3	10YR 3/2	• Subangular blocky and wedge peds • Pedogenic slickensides • FeMn coatings on peds and redoximorphic redistribution in matrix • Well developed carbonate nodules with septarian and circumgranular cracks • Tephra weathering to clay but no indication of illuviation	0	Parallel to granostriated	• Earthworm fecal pellets • Tephra filled burrows • Weak to well developed carbonate rhizoliths
Bkss2b3	10YR 3/2	• Subangular blocky and wedge peds • Pedogenic slickensides • Carbonate along master slickensides • FeMn coatings on peds and redoximorphic redistribution in matrix • Carbonate nodules	0	Parallel striated	• Tephra filled burrows • Carbonate rhizoliths and rhizocretions • Burrows with meniscate backfill
Bkss3b3	10YR 4/2	• Subangular blocky and wedge peds • Pedogenic slickensides • Carbonate nodules	0	Granostriated	• Tephra filled burrows • Carbonate rhizoliths and rhizocretions • Burrows with meniscate backfill

The type section of Paleosol 3 is divided into 5 soil horizons: ABkb3, Bkb3, Bkss1b3, Bkss2b3, Bkss3b3 that are described in detail in Table 3.1. At some sites, the A horizon, characterized by granular peds, has been eroded (Kisaaka 4F). In other areas the paleo-Vertisol is significantly thicker (Kisaaka 14A) or thinner (Kisaaka 4F or 12), but the paleosol has remarkably similar features across the landscape (Fig. 3.2). The paleo-Vertisol contains both carbonate nodules and rhizoliths throughout the profile (Figs. 3.2, 3.3D, and 3.4A). The carbonate rhizoliths are commonly poorly developed and powdery, but the nodules are dense micrite with septarian and circumgranular cracks (Fig. 3.4A). Carbonate was also identified along ped boundaries especially master slickenside surfaces (Fig. 3.3C). Rhizocretions are also identified in the lower horizons (Fig. 3.2). Throughout the paleo-Vertisol are tephra-filled burrows often associated with fecal pellets that are likely attributed to earthworms due to their size (200-500 μm) (Figs. 3.2, 3.3D, and 3.4C; Stoops et al., 2010). Burrows with meniscate backfill were also identified in thin section and can also be attributed to earthworms (Fig. 3.4C; Stoops et al., 2010).

Paleosol 2 overlies the Nyamita Tuff and has 4 soil horizons: Bk1b2, Btk1b2, Btk2b2, and Bk2b2. This paleosol is identified as paleo-Inceptisol with Alfisol-like soil characteristics, but the lack of E horizon prevents classification as an Alfisol (Soil Survey Staff, 1999). In outcrop, this paleosol is thin (40-80 cm) and poorly developed with only granular to subangular blocky peds, FeMn coatings on peds, tephra-filled burrows, and weakly developed pedogenic carbonate nodules and rhizoliths (Fig. 3.3G). In thin section, the carbonate often has diffuse boundaries filling in pore spaces and engulfing paleosol matrix. The micromorphology also reveals a much more complex pedogenesis with abundant illuviated clay coatings of up to 3% in the Btk1b2 and Btk2b2 horizons (Fig. 3.4H). These coatings were not visible in outcrop because the majority of the coatings are covered with a second layer of FeMn that prevented field identification (Figs. 3.3G, 3.4G, and 3.4J).

MSA artifacts have been collected from the surface at Kisaaka, but systematic excavations have yet to be conducted and few artifacts have been found *in situ* (Faith et al., 2015). Paleosol 2 has evidence for microdebitage from on-site tool production where several large, angular grains of chert are identified (Fig. 3.4K). Artifacts made from this material were collected at Kisaaka (Faith et al., 2015). These grains are much larger than the dominantly silt- to fine sand-sized coarse fraction and contain percussion fractures typical of microdebitage (Angelucci, 2010).

Paleosol 1 is identified as a paleo-Inceptisol with Alfisol-like soil characteristics, like Paleosol 2. Paleosol 1 is thicker (2.2 m) and better developed and has 4 horizons: ABkb1, Btkb1, Btk2b1, and BC1b1 (Table 3.1). The ABkb1 horizon contains granular peds and all other horizons are dominated by subangular blocky peds (Fig. 3.4G). FeMn coatings, tephra-filled burrows (Fig. 3.4D), carbonate rhizoliths are abundant throughout the profile (Figs. 3.3G, 3.4D, and 3.4H). Similar to Paleosol 2, the micromorphology reveals an abundance of features not visible in outcrop due to the abundance of FeMn coatings. Earthworm fecal pellets (~500 μm) are found throughout the matrix and commonly fill burrows (Fig. 3.4E). These burrows generally allowed for preferential flow and greater accumulations of illuviated clay (Figs. 3.4D-F). Much smaller fecal pellets (50 to 100 μm) are also preserved in carbonate rhizoliths (Figs. 3.4H and I) and were likely made by termites, which produce fecal pellets ~100 μm (Jungerius et al., 1999;

Stoops et al., 2010). The carbonate rhizoliths and nodules are poorly developed in comparison to Paleosol 3 often with diffuse boundaries (i.e. Figs. 3.4A vs. 3.4D and 3.4H). In addition, the crosscutting relationships record the timing of features: 1) illuviated clay, 2) FeMn coatings, and 3) carbonate (Figs. 3.4G and 3.4J). The illuviated clay coatings are well developed and comprise up to 5% of the paleosol in the Btk2b1 horizon (Fig. 3.4G). In some areas, pores have multiple generations of illuviation and >10 bands of illuviated clay, which range from 5 to 10 µm in width (Fig. 3.4F and 3.4L).

Mineralogy

Mineralogy of paleosols was analyzed by horizon but showed little variability, and therefore only examples from Paleosol 1 and 3 are included here. Locations of these samples can be found on Figure 3.2. Figure 3.5A is representative of Paleosols 1 and 2 (Inceptisols) and Figure 3.5B is representative of Paleosol 3 (Vertisols). All paleosols contain abundant smectite with variable contributions of palygorskite, quartz, feldspar, and augite. The broad 16.6 Å peaks are indicative of poorly crystalline smectite (Fig. 3.5B), and the weak intensities in the upper paleosols are attributed to the abundance of amorphous tephra (Fig. 3.5A).

Bulk Geochemistry

Bulk geochemistry is commonly used to determine paleosol weathering trends with depth using molecular weathering ratios, and constitutive mass balance models have been used in the past to quantify these changes (Brimhall and Dietrich, 1987; Chadwick et al., 1990; Sheldon and Tabor, 2009). Mass balance is a powerful tool because it compares the ratio of the weathered material to the parent material and takes into account

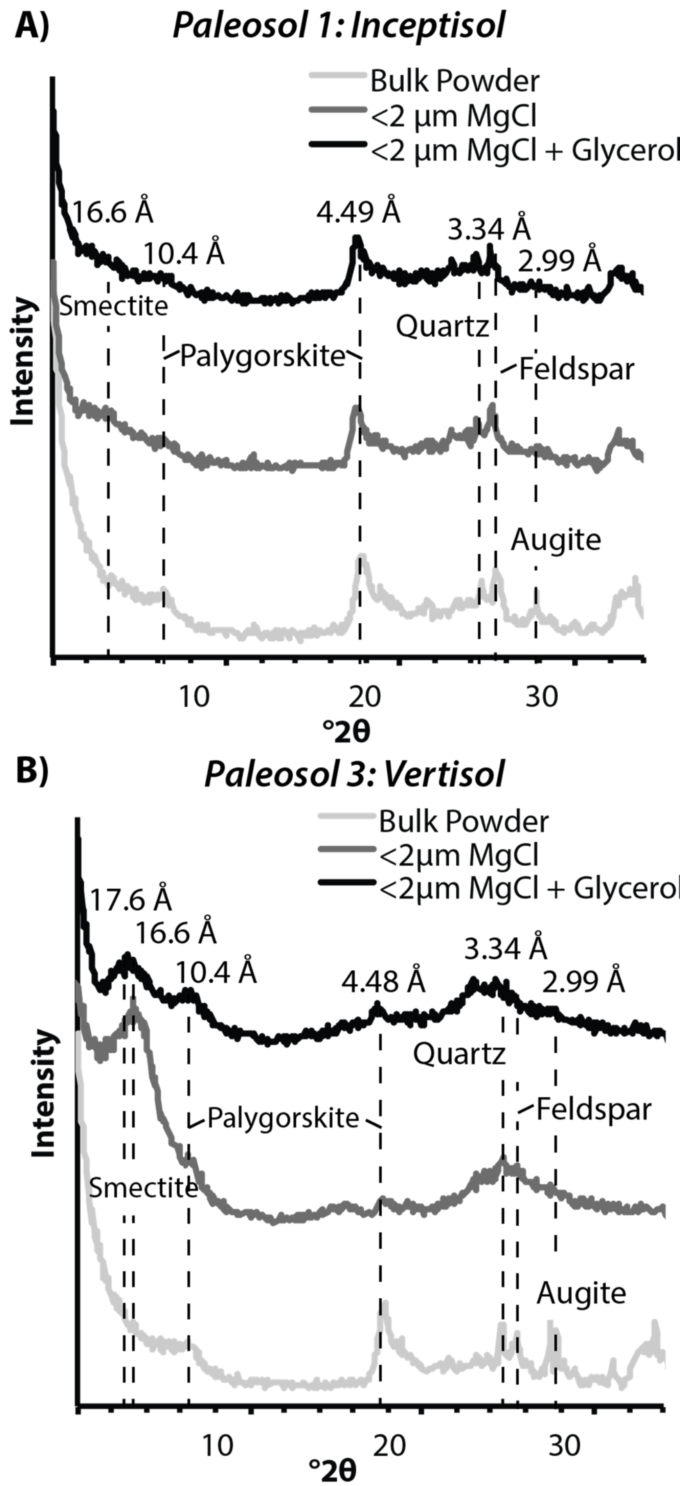

Figure 3.5: Clay mineralogy of paleosols. The abundance of poorly crystalline tephra within this paleosol created poorly defined peaks and made identification difficult. A) Clay mineralogy of Paleosol 1 that is representative of both Inceptisols 1 and 2. Dominated by poorly crystalline smectite and palygorskite with minor amounts of quartz and augite. B) Paleosol 3 dominated by smectite with minor amounts of palygorskite, quartz, and augite.

changes in bulk density (Brimhall and Dietrich, 1987; Chadwick et al., 1990). When bulk density is not accounted for, increasing porosity can have the effect of making it appear that the ratio of weathered material to the parent material is constant (Brimhall and Dietrich, 1987; Chadwick et al., 1990). However, all Kisaaka paleosols were weathered through the profile leaving no unweathered parent material to calculate mass balance. Molecular weathering ratios can only be used to examine relative changes down profile for an individual paleosol because the molecular weathering ratios do not account for parent material and density changes (Retallack, 2001). For this reason, it is difficult to compare between paleosols and across the landscape and through time using molecular weathering ratios. There is little change in parent material across the landscape, but density can fluctuate significantly due to varying contributions of tephra.

The geochemistry of the Kisaaka paleosols show little consistent variability with depth likely due to the limitations of molecular weathering ratios rather than a lack of weathering due to insufficient pedogenesis. Therefore, the bulk geochemistry has been averaged by paleosol, in addition to the molecular weathering ratios and paleoprecipitation proxies calculated from the bulk geochemistry, to show general trends between paleosols and across the landscape (Table 3.2). All paleosols show evidence of pedogenesis, seen by comparing the additions of CaO, MgO, and Fe_2O_3 and losses of Na_2O in the paleosols to the bulk geochemistry of Nyamsingula and Nyamita Tuffs, which are possible parent materials (Table 3.2). Paleosols 1 and 2 show no variability across the landscape, but Paleosol 3 does indicate some variability, such that paleosols at Kisaaka 10 and Kisaaka 13 have higher CaO and lower Fe_2O_3 and Al_2O_3 in comparison to the paleosols at the Kisaaka 4F and 12 localities (Table 3.2). There is also very little

Table 3.2: Average bulk geochemistries of paleosols and tephra in wt%, average of molecular weathering ratios normalized to molecular weight, and averaged by paleosol.

Locality	Unit	Al_2O_3	CaO	MgO	Na_2O	K_2O	SiO_2	BaO	SrO	Fe_2O_3
10	Paleosol 1	13.16	2.51	2.35	1.38	2.12	45.68	0.06	0.04	13.27
13	Paleosol 1	13.36	3.04	2.24	2.12	2.51	49.75	0.07	0.05	11.09
	Average	**13.26**	**2.78**	**2.29**	**1.75**	**2.31**	**47.72**	**0.07**	**0.05**	**12.18**
10	Paleosol 2	14.44	1.37	1.89	1.81	2.46	50.28	0.05	0.03	11.19
13	Paleosol 2	14.06	1.56	2.08	2.18	2.46	51.94	0.05	0.04	10.83
	Average	**14.25**	**1.47**	**1.98**	**1.99**	**2.46**	**51.11**	**0.05**	**0.03**	**11.01**
4F	Paleosol 3	13.44	3.67	2.39	1.60	2.22	45.95	0.16	0.05	14.41
10	Paleosol 3	12.21	5.00	2.16	1.18	2.13	46.16	0.11	0.05	11.54
13	Paleosol 3	12.82	5.09	2.46	1.88	2.21	44.80	0.11	0.05	13.02
12	Paleosol 3	13.53	2.38	2.80	1.22	2.20	47.42	0.07	0.05	14.62
	Average	**13.00**	**4.03**	**2.45**	**1.47**	**2.19**	**46.08**	**0.11**	**0.05**	**13.40**
10	Nyamsingula Tuff	13.3	1.47	1.66	2.26	2.54	52.7	0.07	0.04	10.65
10	Nyamita Tuff	14.95	1.15	1.79	2.36	2.59	49.2	0.05	0.03	10.95

Table 3.2: Continued

Locality	Unit	Leaching	Salinization	Hydrolysis	Hydration	CALMAG (mm/yr) SE ±108	CIA-K (mm/yr) SE ±182
10	Paleosol 1	1.06	0.17	0.17	3.59	-	725
13	Paleosol 1	0.98	0.26	0.16	4.13	-	901
	Average	**1.02**	**0.22**	**0.16**	**3.86**	**-**	**813**
10	Paleosol 2	1.14	0.21	0.17	3.96	-	987
13	Paleosol 2	0.94	0.26	0.16	4.21	-	939
	Average	**1.04**	**0.23**	**0.16**	**4.08**	**-**	**963**
4F	Paleosol 3	1.88	0.20	0.17	3.44	812	726
10	Paleosol 3	1.55	0.16	0.16	4.01	840	915
13	Paleosol 3	1.33	0.24	0.17	3.59	579	685
12	Paleosol 3	1.06	0.15	0.17	3.52	826	967
	Average	**1.46**	**0.19**	**0.17**	**3.64**	**764**	**823**
10	Nyamsingula Tuff	-	-	-	-	-	-
10	Nyamita Tuff	-	-	-	-	-	-

- not applicable

variability through time between Paleosols 1, 2, and 3 with the exception of CaO and leaching, which is calculated using CaO content in the paleosols.

Pedotransfer functions were applied to the paleosols with vertic features (Paleosol 3 only) to reconstruct colloidally based physical and chemical properties used in modern soil characterization (Nordt and Driese, 2010a). Some pedotransfer functions developed by Nordt and Driese (2010a) were not applicable due to the presence of carbonate and only those applicable are presented here: total clay, fine clay, the ratio of fine clay to total clay (FC/TC), coefficient of linear extensibility (COLE), cation exchange capacity (CEC), the ratio of CEC to clay (CEC/clay), pH, base saturation (BS), exchangeable sodium percentage (ESP), electrical conductivity (EC), crystalline Fe oxide (Fe_d), and percent $CaCO_3$. These properties all yield further information on soil fertility and are summarized in Table 3.3. Detailed explanation of these modern soil properties can be found in Burt (2011).

The ratio of FC/TC indicates no translocation with depth, paralleling observations in the field and in thin section (Tables 3.1 and 3.2). The high proportion of clay and specifically smectitic clay (Fig. 3.5B) gives the paleosols a high shrink-swell potential, high COLE of 0.07 to 0.09 cm cm^{-1} (high is defined as 0.06 to 0.09 cm cm^{-1} by the NRCS (Burt, 2011), and high CEC between 30.7 and 44.2 cmolc kg^{-1} (Table 3.3). The CEC is the total number of exchangeable cations that a soil can absorb and depends on the types of clays and amount of organic matter present in the soil that hold these exchangeable cations (Brady and Weil, 2008). Smectite has a high CEC (~80 to 130 cmolc kg^{-1}) and for this reason modern Vertisols often have a high CEC of ~35.6 cmolc kg^{-1} (Brady and Weil, 2008). Base saturation (BS) is a measure of how many base cations the soil

Table 3.3: Pedotransfer functions calculated from the Paleosol 3 Vertisol to reconstruct soil properties across the landscape. See Figure 3.1 for location of sites.

Soil	Depth	Total Clay	Fine Clay	FC/TC	COLE	CEC	CEC/clay	pH	BS	ESP	EC	Fe_d	$CaCO_3$
Horizon	cm	%	%		cm cm^{-1}	cmolc kg^{-1}		H_2O	%	%	dS m^{-1}	%	%
Kisaaka 4F													
Bkss1b3	0-20	57.9	27.0	0.47	0.08	44.2	0.76	7.7	100	18	17	13	3
Bkss2b3	20-40	57.9	28.0	0.48	0.08	44.2	0.76	7.6	99	18	16	13	2
Bkss3b3	40-110	56.4	24.3	0.43	0.08	44.1	0.78	7.7	100	18	17	13	4
Bkss4b3	110-120	55.1	25.5	0.46	0.08	44	0.80	7.8	100	19	18	16	5
BCkb3	120-130	53.6	22.7	0.42	0.08	43.9	0.82	7.9	100	21	21	17	6
Kisaaka 10													
ABkb3	0-5	53.8	23.7	0.44	0.08	43.9	0.82	7.9	100	21	20	8	6
Bk1b3	5-30	56.4	27.5	0.49	0.08	44.2	0.78	7.6	99	16	13	10	3
Bk2b3	30-60	57.1	26.5	0.46	0.08	44.1	0.77	7.7	100	15	13	11	4
Bkss1b3	60-120	58.1	26.1	0.45	0.08	44.1	0.76	7.7	100	15	13	11	4
Bkss2b3	120-180	58.2	26.0	0.45	0.08	44.1	0.76	7.7	100	16	14	12	3
Bkss3b3	180-220	57.5	25.4	0.44	0.08	44.1	0.77	7.7	100	17	15	11	4
Kisaaka 13													
ABkb3	0-20	60.6	30.3	0.50	0.09	39.7	0.66	7.4	96	34	43	8	2
Bkb3	20-60	56.6	23.3	0.41	0.08	35.2	0.62	7.9	100	23	23	10	6
Bkss1b3	60-100	55.2	21.2	0.38	0.08	33.4	0.61	8.1	100	23	23	11	8
Bkss2b3	100-140	52.9	18.9	0.36	0.07	30.7	0.58	8.2	100	22	22	10	11
Bkss3b3	140-190	54.4	20.9	0.38	0.07	33	0.61	8.1	100	23	22	11	8
Bkss4b3	190-220	53.3	21.5	0.40	0.07	33.1	0.62	8	100	21	20	12	7

Table 3.3: Continued

Soil Horizon	Depth cm	Total Clay %	Fine Clay %	FC/TC	COLE cm cm^{-1}	CEC cmolc kg^{-1}	CEC/clay	pH H_2O	BS %	ESP %	EC dS m^{-1}	Fe_d %	$CaCO_3$ %
Kisaaka 12													
ABkb3	0-10	56.2	25.0	0.44	0.08	44	0.78	7.8	100	11	9	12	3
Bkb3	10-40	56.1	25.5	0.45	0.09	44.1	0.79	7.8	100	12	10	13	3
Bkss1b3	40-90	56.4	26.2	0.46	0.08	44.1	0.78	7.7	100	14	11	15	2
Bkss2b3	90-110	55.7	24.9	0.45	0.08	44	0.79	7.8	100	15	13	14	3
BCkb3	110-120	54.6	23.0	0.42	0.08	43.9	0.80	7.9	100	14	11	13	4

FC/TC: ratio of fine clay to total clay; COLE: coeffiecient of linear extensibility; CEC: cation exchange capacity; BS: base saturation; ESP: exchangable sodium percentage; EC: electrical conductivity; Fe_d: crystalline Fe oxide.

potentially holds (Brady and Weil, 2008), and the Kisaaka paleosols are all base saturated at 99 to 100%. A higher pH also increases the effective CEC and the Kisaaka paleosols have alkaline pH of between 7.4 and 8.2. The CEC, BS and pH are all buffered by the presence of carbonate, which ranges from 3 to 11%, with the highest carbonate at Kisaaka 13 and the lowest at Kisaaka 4F and 12 (Table 3.3). ESP is a measure of the sodicity of the soil, which affects both physical and chemical soil properties that are detrimental to plant growth. A soil classified as normal has an ESP of <15% and indicates that plants with a typical tolerance will be unaffected by sodicity. All but the upper horizons in Kisaaka 12 have an ESP >10%, and most horizons are >15%. The Fe_d is often used as a measure of total pedogenic Fe from minerals such as goethite, hematite, lepidocrocite, and ferrihydrite and with >1% indicative of oxidizing soil conditions (Nordt and Driese, 2009; 2010a). The Fe_d ranges from 8 to 14% in Paleosol 3 (Table 3.3).

Paleoprecipitation was also calculated using CALMAG for those paleosols identified as Vertisols (Paleosol 3) and CIA-K for all paleosols. The paleoprecipitation estimates for Paleosol 3 averages 764±108 and 823±182 mm yr^{-1} for CALMAG and CIA-K, respectively. Paleosol 2 is higher with an average of 963±182 mm yr^{-1} and Paleosol 1 has an average of 813±182 mm yr^{-1} (Table 3.2).

Discussion

Depositional Environment

The three laterally continuous tuffs deposited at Kisaaka (the Nyamita Tuff, the Nyamsingula Tuff, and the BTPT) preserve a succession of buried landscapes and allow for the reconstruction of three separate paleocatenas. The Kisaaka paleosols often have a similar grain size (clay-sized) throughout the profile, few erosive scour surfaces, and well-developed pedogenic features. Paleosols with these features often form in a fluvial system, distal to the active fluvial channel, with steady depositional conditions where pedogenesis is able to keep up with constant additions and forming well developed, but cumulative soils (Kraus, 1999).

Gilgai topography. The oldest and best preserved paleocatena (Paleosol 3), formed between 94 and ~49 ka, is a paleo-Vertisol with pedogenic slickensides (Fig. 3.5E) that are indicative of intensive shrink-swell processes due to wetting and drying of smectite (Fig. 3.5B). The shrinking and swelling of the clay during wet and dry seasons formed gilgai topography that is preserved by the rapid deposition of the Nyamita Tuff at ~49 ka. Gilgai topography is rarely preserved in the rock record as the granular peds of the A horizon are easily eroded prior to the next depositional event and eroding the gilgai topography in the process (Caudill et al., 1996; Mora and Driese, 1999; Driese et al., 2000, 2003). The wavelengths and amplitudes of these well-preserved gilgai vary across the landscape and may reflect changes in gilgai type. The wavelengths and amplitudes of gilgai identified at the Kisaaka 12, 4F, 3, and 2 localities (Fig. 3.3H) ranges from 0.8 to 1.6 m. In comparison, the average wavelength from Kisaaka 15 is much larger at 6.4 m with amplitudes of 0.55 m on average. These large wavelengths and amplitudes can form in linear gilgai that form on sloping landscapes, commonly, 1° to 3° (Beckmann et al., 1973, 1970; Hallsworth and Beckman, 1969; Hallsworth et al., 1955).

Linear gilgai are commonly identified in Australia (Beckmann et al., 1973; Hallsworth and Beckman, 1969), but are rare in Africa or not reported in the literature.

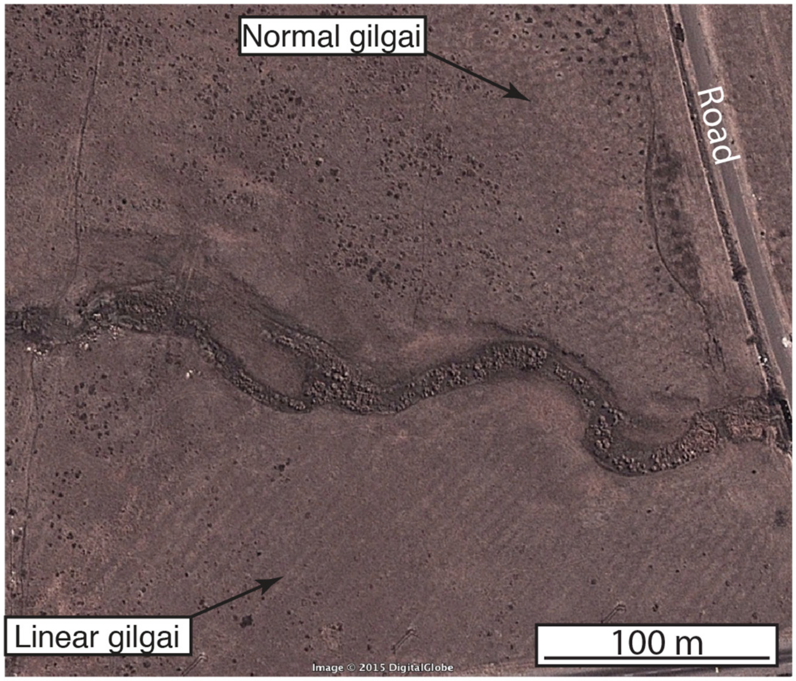

Figure 3.6: Modern examples of linear and normal gilgai from Rustenburg, South Africa from Google Earth (2015) (25.59°S, 27.25°E).

Examples of both normal and linear gilgai have been identified at Rustenburg, South Africa, and the normal gilgai have shorter wavelengths of ≤5 m, but the linear gilgai have wavelengths of ≥8 m (Verster et al., 1973; Fey et al., 2010). This suggests that specific conditions may be needed to form these features. The physical and colloidal soil properties of the modern Rustenburg Vertisols with 62% to 69% clay, a CEC of 34 to 58, pH of 7.7 to 8.6, and a range of carbonate from 0 to 15.5% are remarkably similar to those reconstructed using pedotransfer functions for the Kisaaka paleo-Vertisols (Table 3.2; Verster et al., 1973). This suggests that the Kisaaka paleotopography may have been similar to Rustenburg where specific conditions allow for gilgai formation. Seasonal rainfall ranging from 600 to 700 mm yr^{-1}, and the smectitic mineralogy create ideal conditions for normal gilgai formation. When combined with a sloping landscape of 1 to 3°, these conditions form linear gilgai (Fig. 3.6).

Paleosol characteristics and productivity. There is little variability in the reconstructed soil characteristics in profiles sampled across the landscape with exception of Kisaaka 10 and Kisaaka 13, which have high CaO of 5% (Table 3.2) and are very close to tufa deposits mapped in Fig. 3.1C. The lowest horizons of Paleosol 3 closest to these spring deposits have evidence for a higher proportion of carbonate as syndepositional cement (Beverly et al., 2015). For example, the lowest horizon at Kisaaka 14A is much lighter in color due to the increased carbonate content (Fig. 3.2). Deposition of tufa ceased due to the influx of sediment, but lower horizons were likely still affected by supersaturated groundwater. These effects would disappear up section as cumulative pedogenesis continued, but may have contributed to greater carbonate (up to 11% $CaCO_3$) in the soil matrix at Kisaaka 10 and 13, making the pH more alkaline than at other localities (Table 3.3).

High CEC and BS (30.7 to 43.9 cmolc kg^{-1} and 99 to 100%, respectively) indicate that the Paleosol 3 (paleo-Vertisol) would have been fertile with many plant available nutrients with an alkaline pH (7.4 to 8.2) that would not have affected plant size by limiting nutrient availability, which can be lost with an acidic pH (Brady and Weil, 2008). Burrows from earthworms and termites would have provided macropores favorable to root growth and microbial activity (Figs. 3.3C and 3.4L; Jongmans et al., 2001). Although the paleo-Vertisol was fertile and had a high water storage capacity due to high clay content that would support abundant vegetation, high ESP and EC indicate that this soil was affected by both high salinity and sodicity, which would have limited the types of plants able to grow on the landscape to those that were tolerant of these conditions. A saline-sodic soil is defined by a BS >15%, an EC >4 dS m^{-1}, and pH <8.5 (Brady and Weil, 2008). With the exception of the upper two horizons from Kisaaka 12, all other horizons are classified as saline-sodic. Some plants are affected by as little as 2 dS m^{-1} for EC, and the saline-sodic conditions would have affected nutrient uptake and microbial activity (Brady and Weil, 2008). The saline-sodic conditions would have also caused a decrease in plant size in more tolerant species or have completely prevented the growth of species intolerant to saline-sodic conditions. Due to the trachytic-phonolitic composition of the tephra, which adds sodium-bearing primary minerals to the paleosols, the ESP and EC are likely to be maximal estimations (Nordt and Driese, 2010a). However, the amount of Na_2O in the paleosols is distinctly lower than the amount either in the Nyamsingula Tuff or the Nyamita Tuff (Table 3.2) indicating that it is unlikely that the high saline-sodic values in the paleosols are entirely related to differences in sodium-bearing primary minerals and likely are the result of pedogenesis.

These high-salinity conditions are common in soils in semi-arid climates (Brady and Weil, 2008). Additionally, the high Fe_d of 8 to 17% supports an interpretation of a semi-arid environment and also indicates warm and oxidizing conditions. The Fe_2O_3 concentrations are much higher in the Karungu paleosols than in those used to develop pedotransfer functions (Nordt and Driese, 2010a), which is likely due to contribution of Fe-rich tephra. However, the wt% Fe_2O_3 is between 1 to 4% higher in the paleosols than in the tephra indicating that the Fe_2O_3 content cannot be attributed solely to differences in primary iron-bearing minerals (Table 3.2) and instead is a pedogenic signal.

In Paleosol 3 volcaniclastic material is very limited (Figs. 3.4A-C) and tephra is only occasionally found filling burrows (Fig. 3.3D), which are likely related to burrowing following burial and termination of the soil by the Nyamita Tuff. Burrowing infill is not limited to tephra, and the meniscate backfill is often composed of the clay matrix (Fig. 3.4C). This indicates that the burrowing occurred for the duration of soil formation. However, as Paleosol 3 has very little volcaniclastic material in the matrix, it is unlikely that tephra accumulated throughout the life of the paleosol.

Following the deposition of the Nyamita Tuff at ~49 ka, tephra becomes much more abundant on the landscape and was likely frequently deposited during of the development of Paleosols 1 and 2. Both paleo-Inceptisols (Paleosols 1 and 2) deposited between 49 and >33 ka have significantly more tephra within burrows and the matrix (Fig. 3.4D). The additional tephra had physical effects on these paleosols. Although Paleosols 1 through 3 are smectitic (Figs. 3.5A and B) and MAP estimates suggest that the climate is similar, the addition of tephra into the depositional system seems to have limited the shrink-swell behavior of the smectite within Paleosols 1 and 2, and thus prevented the development of a Vertisol.

The lack of vertic features and less developed carbonates, which are powdery or hard masses with diffuse boundaries, would suggest that Paleosols 1 and 2 underwent shorter periods of pedogenesis (consistent with radiometric estimates of maximum formation times); however, clay coatings indicate the paleosols were forming on the landscape for intervals of time long enough to bring the paleo-Inceptisols into equilibrium with climate. Clay coatings are common in soils with high percentage of volcanic fragments (Jongmans et al. 1994), and clay coatings of up to 3% in Paleosol 2 and 5% in Paleosol 1 indicate perhaps a few thousand years of stability on the paleolandscape (Figs. 3.4B, 3.4C, and 3.4G-I; Soil Survey Staff, 1999; Ufnar, 2007). The age-estimate model for clay coating accumulation by Ufnar (2007) gives an estimate of ~3 kyr for Paleosol 2 and ~7 kyr for Paleosol 1. The illuviated clay chronofunctions developed by Ufnar (2007) were developed using deeply weathered, subtropical soils from southeastern Mississippi, and therefore, a combined value of 10 kyr of deposition may be an overestimation for an East African monsoonal climate. Radiometric estimates from gastropods from correlative deposits on Rusinga and Mfangano Islands (Tryon et al., 2010; Blegen et al., 2015) suggest that both Paleosols 1 and 2 were formed between 49 and >33 ka, consistent with the clay chronofunction estimate. Although Inceptisols are weakly developed soils, the degree of development of clay coatings (an Alfisol-like characteristic) provides evidence for continuous pedogenesis that would have brought the paleosols into equilibrium with the climate, supporting the MAP estimates. In addition, modern Inceptisols were included in the Marbut (1935) database used to develop the CIA-K proxy where CIA-K varied with changes in MAP (Sheldon et al., 2002).

Evidence suggests that with development of additional illuviated clay, Paleosols 1 and 2 would have eventually developed into paleo-Vertisols, as has been demonstrated in modern soils where the clay coatings reach a threshold (Stoops et al., 2010). In the Btk1b2 horizon of Paleosol 2 where the highest concentrations of clay coatings accumulated, weakly developed pedogenic slickensides are present (Table 3.1). Because Paleosols 1 and 2 are identified as paleo-Inceptisols, the pedotransfer functions developed for paleo-Vertisols are not applicable (Nordt and Driese, 2010a). However, the upper paleosols (1 and 2) have similar evidence of earthworms and termites that suggests that soil conditions were similar (Figs.3.4A, 3.4B, 3.4E, and 3.4F; Table 3.1). In addition, with the exception of CaO (discussed earlier) average geochemical compositions and molecular weathering ratios indicate that Paleosols 1 and 2 likely had similar colloidal properties to Paleosol 3 that would have provided abundant nutrients (Table 3.2). High salinity and sodicity also likely affected Paleosols 1 and 2 due to their similarities in wt. % Na_2O and Al_2O_3, which are used to estimate the ESP and EC (Table 3.2).

All three paleosols show evidence of redoximorphic features in which Fe and Mn have been depleted within the matrix, or concentrated as coatings on peds or pores, which suggest that, at times, the soil was poorly drained. Redoximorphic features can form quickly and possibly within one wet season (Vepraskas, 1992, 2001; Vepraskas and Faulkner, 2001), but all three paleosols show evidence for drier periods as well with the precipitation of pedogenic carbonates. Paleosols 1 and 2 also have evidence for the relative timing of these features: 1) illuviated clay coatings indicative of drier climate with low water table, 2) redoximorphic FeMn coatings characteristic of a higher water table and impeded soil drainage, and 3) carbonate coatings suggestive of a return to drier conditions (Figs. 3.4G and 3.5J). The third coating of carbonate is not always present, but where it occurs, it is always in this order. This suggests that the paleosols underwent a long period of drier climate where many layers of illuviated clay coatings were deposited, followed by wetter conditions, and a return to dry conditions with the deposition of carbonate. The features in the micromorphology are likely a result of higher frequency (e.g., decadal) climate changes that occurred within an overall drier period, as indicated by the MAP estimates.

Implications for Paleoclimate and Paleoenvironment

Evidence from Rusinga Island and Karungu suggests that at ~94 ka the Lake Victoria region underwent a significant change in paleoclimate. Spring-fed rivers were present on the Late Pleistocene landscape at Rusinga Island and Karungu, after which MAP crossed a critical recharge threshold such that the springs were choked with fluvial sediments and tufa precipitation was terminated (Beverly et al., 2015). After ~94 ka, the landscape became distinctly more fluvial with fining upward overbank floodplain deposits and paleosols. Mean annual precipitation proxies from these paleosols suggest that between 94 ka and >33 ka the Lake Victoria region experienced a significantly drier climate and environment than today.

The paleosols indicate an average paleoprecipitation range from 813±108 to 963±108 mm yr^{-1} using CIA-K for Paleosols 1 to 3 (Table 3.2). There is no evidence for a distinct change in MAP between 94 and >33 ka when these paleosols were formed, thus climate seems to have been significantly drier than modern for an extended period of time. The estimates from the Vertisol using CALMAG are lower with an average of 764 mm yr^{-1} for Paleosol 3, but CIA-K is known to overestimate paleoprecipitation in Vertisols (Nordt and Driese, 2010b). There is no evidence for diagenesis in these paleosols that would affect the paleoprecipitation estimates. There is a maximum of 2 meters of modern soil above the paleosols, and all features appear to be primary with no recrystallization of pedogenic carbonates or precipitation of secondary sparry calcite that would affect the paleoprecipitation estimates using CALMAG (Figs. 3.4A and 3.4H). In addition, the physical evidence from the paleosols (vertic features, illuviated clay and pedogenic carbonates) and chemical evidence from pedotransfer functions (high salinity and sodicity) all suggest a highly seasonal environment and support the interpretation of an environment significantly drier than modern (~1400 mm yr^{-1}). With average CIA-K values from Paleosols 1 to 3 of 813 to 963 mm yr^{-1}, this represents a considerable reduction in precipitation relative to the present (31-42% reduction), and the first quantitative paleoprecipitation estimate for the region.

However, applying proxies developed in the United States to Eastern Africa may potentially bias the precipitation estimates because of differences in the mineralogy and chemistry of East African soils relative to those from the United States that were used in the paleosol proxy calibration datasets. Mineralogically the paleo-Vertisols from Kisaaka are similar to those from Texas used to develop the proxy: a predominantly smectitic clay mineralogy from a pre-weathered parent material (Fig. 3.5B; Nordt and Driese, 2010b). However, the effect of constant additions of tephra is uncertain because none of the Texas Vertisols used to develop the CALMAG proxy include volcanically influenced soils (Nordt and Driese, 2010b). The Marbut (1935) database used to develop the CIA-K proxy includes some soils with volcanically derived parent materials, but they are not abundant (Sheldon et al., 2002). Further research is needed to determine if the addition of volcaniclastic material into soils has any influence on these geochemical proxies.

Bulk geochemical analyses from each paleosol were duplicated between different localities, and in the case of Paleosol 3, samples from four localities were analyzed to capture any potential variability. The variability between individual paleosols within Paleosol units 1 and 2 is minimal and within the standard error of ±182 for CIA-K. Paleosol 3 has more variability and at the Kisaaka 13 locality has a low MAP estimate (579±108 mm yr^{-1}; CALMAG). The estimate is likely anomalously low and probably due to the proximity of the paleosol to the freshwater springs that were disappearing during the deposition of these sediments that subsequently underwent pedogenesis. The groundwater moving through these sediments would still have been supersaturated with respect to carbonate and would have resulted in additional carbonate precipitation resulting in a high average CaO of 5% in the soil matrix in comparison to other sites. MAP estimates from Paleosol 3 at other sites distal to the spring (i.e. Kisaaka 4F and 12) have CALMAG estimates of 812±108 and 826±108 mm yr^{-1}, respectively. Alternatively, this variability in Paleosol 3 could be attributed to problems with applying the CIA-K and CALMAG proxies to volcanically influenced East African paleosols. Regardless, the proxies still suggest that paleoprecipitation was less than modern, and they are not the only line of evidence supporting this interpretation.

The paleosol evidence is supported by the analysis of tooth enamel using the aridity index of Levin et al. (2006), which suggests a water deficit much higher than modern and a >20% reduction in MAP in the Late Pleistocene (Garrett et al., 2015). Potential evapotranspiration (ET) for the Lake Victoria region greatly exceeds MAP and ranges from 2000 to 2200 mm yr^{-1} (Dagg et al., 1970). Assuming comparable values in the past, these much drier conditions during the Late Pleistocene would have resulted in a negative hydrologic budget and a significantly reduced Lake Victoria due to the sensitivity of the lake to local precipitation (Broecker et al., 1998; Milly, 1999).

In addition, Rusinga and Mfangano Islands and Karungu have the most diverse fauna of any Late Pleistocene site from East Africa and abundant extinct taxa (Tryon et al., 2012; Faith, 2014; Faith et al., 2015, in press). The presence of gregarious and migratory grazers on Mfangano Island, which is too small to support viable populations of large ungulates, suggests a connection to the mainland. This requires a lake level decline of at least 25 m (Tryon et al., 2010, 2012, 2014; Faith et al., 2011, 2012, 2014, 2015) and comparisons with existing models suggest that such a decline is only possible with a significant rainfall reduction (Broecker et al., 1998; Milly, 1999). Analyses by Faith (2013) indicate peak ungulate diversity in sub-Saharan African game reserves at ~800 mm yr^{-1} and evidence from the paleosols provide quantitative support to explain this high diversity of ungulates. Isotopic and mesowear analyses of the teeth of both ungulates and microfauna indicate an animal community dominated by a C_4 grass diet (Faith et al., 2011, 2015; Garrett et al., 2015). This C_4 grassland contrasts with the evergreen bushland, thicket, and forest habitats historically present in the region and supports the paleosol evidence for a significant reduction in precipitation. This paleosol evidence supports the hypothesis that a reduction in precipitation, coupled with expansion of grasslands and a reduced Lake Victoria facilitated the dispersal of fauna – and possibly human populations – across equatorial Africa (Cowling et al., 2008; Lorenzen et al., 2012; Faith et al., 2015; in press).

Modern Analogs

The modern Vertisols of Rustenburg, South Africa have similar physical features such as grain size and gilgai topography and chemical properties such as CEC and pH. These features suggest that Rustenburg may be an appropriate modern analog. In addition, due to their low precipitation and volcanic parent material (Sinclair, 1979; Belsky, 1990), modern soils of the Serengeti (only ~150 km southeast of Karungu) are

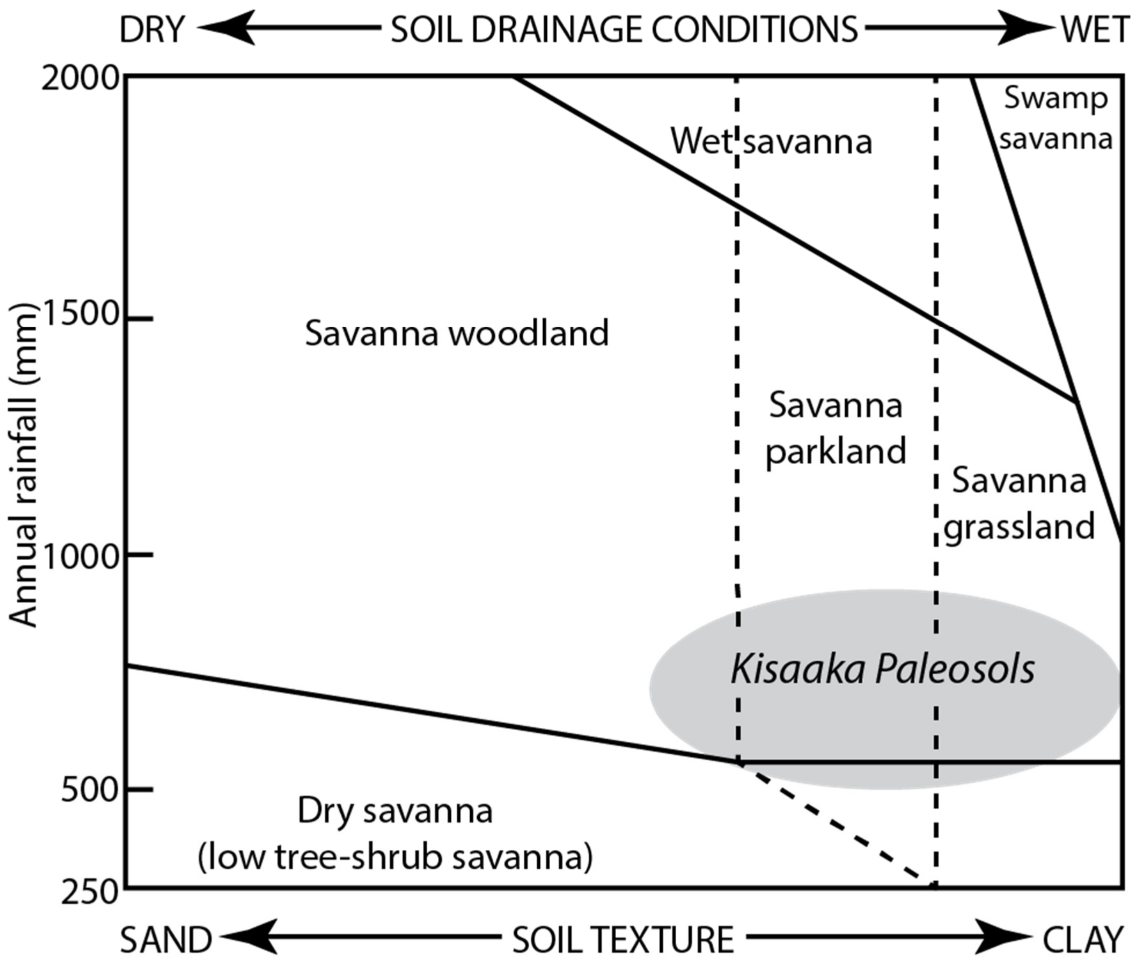

Figure 3.7: The Kisaaka paleosols are plotted on the Johnson/Tothill model of tropical savannas, which uses soil texture and annual precipitation (Modified from Johnson and Tothill, 1985).

similarly saline and alkaline to the saline-sodic paleo-Vertisols and paleo-Inceptisols identified at Kisaaka. Together with MAP, soil texture and the salinity and sodicity of the soils is strongly associated with vegetation type in the Serengeti (Belsky, 1990). Generally, soil catenas in the Serengeti have shallow sandy soils on ridges with short, shallowly rooted grasses and thicker, clay-rich soils (i.e. Vertisols) in the valleys with taller grasses (Bell, 1970; Belsky, 1995). Although parts of the Serengeti have enough precipitation to support trees, trees growth is limited on the Serengeti Plains due to the saline-sodic conditions (Vesey-Fitzgerald, 1973; Belsky, 1990).

The Johnson/Tothill model, a simple abiotic model for African savannas, illustrates how soil texture and precipitation greatly affect the type of vegetation (Fig. 3.7; Johnson and Tothill, 1985) and has been used previously to interpret paleosols in the rock record in northern Kenya (Wynn et al., 2000). With a MAP of ~800 mm yr^{-1}, the Kisaaka paleosols could support either a savanna woodland or grassland, depending on the soil texture (Johnson and Tothill, 1985; Belsky, 1990). With the higher clay contents of soils in the valleys, water penetration is poor and rivers may seasonally flood the soil, which prevents the growth of trees and shrubs (Johnson and Tothill, 1985; Belsky, 1990). Both the high salinity and sodicity and the clay-rich soil texture of Kisaaka may have contributed to the development of open grassland, which is consistent with faunal community composition and the C_4 diet of mammals from Rusinga and Mfangano Islands (Garrett et al., 2015) and Karungu (Faith et al., 2015).

Conclusions

The Kisaaka paleosols provide valuable paleoenvironmental and paleoclimatic information during a critical interval of human evolution. At ~94 ka, reduced precipitation translated to change from spring-fed rivers to soil formation. The paleosols are cumulative such that pedogenesis on the floodplain, and distal to the active channel, exceeded the rate of additions of sediments, and allowed the paleosol to come into equilibrium with the climate. The three paleosols are separated by continuous tuffs that allow for reconstruction of the landscape as a paleocatena. The oldest catena was deposited between ~94 and 49 ka and has paleo-Vertisols with abundant evidence of vertic features and exceptionally well-preserved gilgai. Pedotransfer functions suggest that paleo-Vertisols were fertile, but had saline-sodic conditions that would have affected plant growth and the types of plants growing on the landscape. The upper paleo-Inceptisols were deposited between 49 and >33 ka and the abundance of tephra had significant effects on physical characteristics by inhibiting shrinking and swelling of clays. The weathering tephra formed illuviated clay, and the degree of development of this illuviated clay suggests that these paleo-Inceptisols were in equilibrium with the climate and provides support for the paleoprecipitation estimates.

The paleosol MAP estimates suggest a similar paleoclimate between ~94 and 49 ka with MAP ranges from 764±182 mm yr^{-1} for Vertisols (CALMAG) and 813 to 963±108 mm yr^{-1} for all other paleosols (CIA-K) with no significant changes in paleoprecipitation between paleosols. This reduction in precipitation would have resulted in a significant reduction in the size of Lake Victoria, and represent the first paleoprecipitation estimates for the region during the late Pleistocene. The drop in precipitation and the saline-sodic conditions of these paleosols supports the interpretation of the expansion of semi-arid C_4 grasslands made based on fossil and stable C and O isotope analyses. Together, all lines of evidence suggest that the Serengeti may represent a modern analog for the late Pleistocene paleolandscape at Kisaaka.

References

Ambrose, S.H., Lorenz, K.G., 1990. Social and ecological models for the Middle Stone Age in southern Africa, in: Mellars, P. (Ed.), The Emergence of Modern Humans: And Archaeological Perspective. Edinburgh University Press, Edinburgh, pp. 3–33.

Angelucci, D.E., 2010. The recognition and description of knapped lithic artifacts in thin section. Geoarchaeology 25, 220–232.

Beckmann, G.G., Hubble, G.D., Thompson, C.H., 1970. Gilgai forms, distribution and soil relationships in North-Eastern Australia, in: Proceedings of the Symposium on Soils and Earth Structures in Arid Climates; Adelaide, 21-22, May 1970. Adelaide, pp. 116–121.

Beckmann, G.G., Thompson, C.H., Hubble, G.D., 1973. Linear Gilgai. The Australian Geographer. 12, 363–366.

Bell, R.H.V., 1970. The use of the herb layer by grazing ungulates in the Serengeti, in: Watson, A. (Ed.), Animal Populations in Relation to their Food Resources. Blackwell, Oxford, pp. 111-124.

Belsky, A.J., 1990. Tree/grass ratios in East African savannas: a comparison of existing models. Journal of Biogeography 17, 483–489.

Belsky, J.A., 1995. Spatial and temporal landscape patterns in arid and semi-arid African savannas, in: Hansson, L., Fahrig, L., and Merriam, G. (Eds.), Mosaic Landscapes and Ecological Processes. Chapman & Hall, London, pp. 31-56.

Berke, M. A., Johnson, T.C., Werne, J.P., Grice, K., Schouten, S., Sinninghe Damsté, J.S., 2012. Molecular records of climate variability and vegetation response since the Late Pleistocene in the Lake Victoria basin, East Africa. Quaternary Science Reviews. 55, 59–74.

Beverly, E.J., Driese, S.G., Peppe, D.J., Johnson, C.R., Michel, L.A., Faith, J.T., Tryon, C.A., Sharp, W.D., 2015. Recurrent spring-fed rivers in a Middle to Late Pleistocene semi-arid grassland: Implications for environments of early humans in the Lake Victoria Basin, Kenya. Sedimentology. doi: 10.1111/sed.12199

Birkeland, P.W., 1999. Topography—Soil relations with time in in different climatic settings, in: Soils and Geomorphology. Oxford University Press, New York, pp. 230-267.

Bishop, W.W., Trendall, A.F., 1967. Erosion-surfaces, tectonics and volcanic activity in Uganda. Quarterly Journal of the Geological Society 122, 385–420.

Blegen, N., Tryon, C.A., Faith, J.T., Peppe, D.J., Beverly, E.J., Li, B., Jacobs, Z., 2015. Distal tephras of the eastern Lake Victoria Basin, equatorial East Africa: correlations, chronology, and a context for early modern humans. Quaternary Science Reviews 122, 89-111.

Blome, M.W., Cohen, A.S., Tryon, C.A., Brooks, A.S., Russell, J., 2012. The environmental context for the origins of modern human diversity: A synthesis of regional variability in African climate 150,000-30,000 years ago. Journal of Human Evolution 62, 563-592.

Bootsma, H. A., Hecky, R.E., 2003. A Comparative Introduction to the Biology and Limnology of the African Great Lakes. Journal of Great Lakes Research 29, 3–18.

Brady, N.C., Weil, R.R., 2008. The Nature and Properties of Soils, 14th ed. Pearson Prentice Hall, New Jersey.

Brimhall, G.H., Dietrich, W.E., 1987. Constitutive mass balance relations between chemical composition, volume, density, porosity, and strain in metasomatic hydrochemical systems: Results on weathering and pedogenesis. Geochimica et Cosmochimica Acta 51, 567–587.

Broecker, W.S., Peteet, D., Hajdas, I., Lin, J., Clark, E., 1998. Antiphasing between rainfall in Africa's Rift Valley and North America's Great Basin. Quaternary Research 50, 12–20.

Brown, F.H., McDougall, I., Fleagle, J.G., 2012. Correlation of the KHS Tuff of the Kibish Formation to volcanic ash layers at other sites, and the age of early Homo sapiens (Omo I and Omo II). Journal of Human Evolution 63, 577–85.

Burt, R. (Ed.), 2011, Soil Survey Laboratory Information Manual: Soil Survey Investigations Report No. 45: USDA NRCS, Nebraska.

Caudill, M.R., Driese, S.G., and Mora, C.I., 1996. Preservation of a paleo-Vertisol and an estimate of Late Mississippian paleoprecipitation. Journal of Sedimentary Research 66, 58-70.

Chadwick, O.A., Brimhall, G.H., Hendricks, D.M., 1990. From a black to a gray box - a mass balance interpretation of pedogenesis. Geomorphology 3, 369–390.

Cowling, S.A., Cox, P.M., Jones, C.D., Maslin, M.A., Peros, M., Spall, S.A., 2008. Simulated glacial and interglacial vegetation across Africa: Implications for species phylogenies and trans-African migration of plants and animals. Global Change Biology 14, 827–840.

Crul, R.C.M., 1995. Limnology and hydrology of Lake Victoria. In: Comprehensive and Comparative Study of Great Lakes. UNESCO, p. 79.

Dagg, M., Woodhead, T., Rijks, D. a., 1970. Evaporation in East Africa. Bulletin of the International Association of Scientific Hydrology 15, 61–67.

Doornkamp, J.C., Temple, P.H., 1966. Surface, drainage and tectonic instability in part of southern Uganda. The Geographical Journal 132, 238–252.

Driese, S.G., Jacobs, J.R., Nordt, L.C., 2003. Comparison of modern and ancient Vertisols developed on limestone in terms of their geochemistry and parent material. Sedimentary Geology 157, 49–69.

Driese, S.G., Mora, C.I., Stiles, C.A., Joeckel, R.M., Nordt, L.C., 2000. Mass-balance reconstruction of a modern Vertisol: implications for interpreting the geochemistry and burial alteration of paleo-Vertisols. Geoderma 95, 179–204.

Google Earth, 2015. Rustenburg Linear Gilgai, 25°35'24.30"S, 27°15'11.49"E, elev 3636 ft, July 14, 2011. [Accessed January 20, 2015].

Ebinger, C.J., 1989. Tectonic development of the western branch of the East African rift system. GSA Bulletin 101, 885–903.

Eriksson, A., Betti, L., Friend, A.D., Lycett, S.J., Singarayer, J.S., von Cramon-Taubadel, N., Valdes, P.J., Balloux, F., Manica, A., 2012. Late Pleistocene climate change and the global expansion of anatomically modern humans. Proceedings of the National Academy of Sciences of the United States of America 109, 16089–16094.

Faith, J.T., 2013. Ungulate diversity and precipitation history since the Last Glacial Maximum in the Western Cape, South Africa. Quaternary Science Reviews 68, 191-199.

Faith, J.T., 2014. Late Pleistocene and Holocene mammal extinctions on continental Africa. Earth-Science Reviews 128, 105-121.

Faith, J.T., Choiniere, J.N., Tryon, C.A., Peppe, D.J., Fox, D.L., 2011. Taxonomic status and paleoecology of Rusingoryx atopocranion (Mammalia, Artiodactyla), an extinct Pleistocene bovid from Rusinga Island, Kenya. Quaternary Research 75, 697–707.

Faith, J.T., Potts, R., Plummer, T.W., Bishop, L.C., Marean, C.W., Tryon, C.A., 2012. New perspectives on middle Pleistocene change in the large mammal faunas of East Africa: Damaliscus hypsodon sp. nov. (Mammalia, Artiodactyla) from Lainyamok, Kenya. Palaeogeography, Palaeoclimatology, Palaeoecology 361-362, 84–93.

Faith, J.T., Tryon, C.A., Peppe, D.J., Beverly, E.J., Blegen, N., 2014. Biogeographic and Evolutionary Implications of an Extinct Late Pleistocene Impala from the Lake Victoria Basin , Kenya. Journal of Mammalian Evolution 21, 213–222.

Faith, J.T., Tryon, C.A., and Peppe, D.J., in press. Environmental change, ungulate biogeography, and their implications for early human dispersals in equatorial East Africa. In: Jones, S.C. and Stewart, B.A. (Eds) Africa from MIS 6-2: Population Dynamics and Paleoenvironments, Springer.

Faith, J.T., Tryon, C.A., Peppe, D.J., Beverly, E.J., Blegen, N., Blumenthal, S., Chritz, K., Driese, S.G., Patterson, D., 2015. Paleoenvironmental context of the Middle Stone Age record from Karungu, Lake Victoria Basin, Kenya, and its implications for human and faunal dispersal in East Africa. Journal of Human Evolution 83, 28-45.

Fey, M., Hughes, J., Lambrechts, J., Dohse, T., 2010. Vertic Soils. In: Soils of South Africa. Cambridge University Press, Cape Town, South Africa, pp. 35–45.

Fillinger, U., Sonye, G., Killeen, G.F., Knols, B.G.J., Becker, N., 2004. The practical importance of permanent and semipermanent habitats for controlling aquatic stages of Anopheles gambiae sensu lato mosquitoes: operational observations from a rural town in western Kenya. Tropical Medicine and International Health 9, 1274–1289.

Fitzpatrick, E.A., 1993. Soil microscopy and micromorphology. John Wiley & Sons, New York.

Garrett, N.D., Fox, D.L., Mcnulty, K.P., Tryon, C.A., Faith, J.T., Peppe, D.J., Plantinga, A. Van, 2015. Stable isotope paleoecology of Late Pleistocene Middle Stone Age humans from the equatorial East Africa, Lake Victoria basin, Kenya. Journal of Human Evolution 82, 1-14

Hallsworth, E.G., Beckman, G.G., 1969. Gilgai in the Quaternary. Soil Science 107, 409–420.

Hallsworth, E.G., Robertson, G.K., Gibbons, F.R., 1955. Studies in pedogenesis in New South Wales. Journal of Soil Science 6, 1–31.

Johnson, T.C., Scholz, C.A., Talbot, M.R., Kelts, K., Ricketts, R.D., Ngobi, G., Beuning, K.R., Ssemmanda, I., McGill, J.W., 1996. Late Pleistocene dessication of Lake Victoria and rapid evolution of cichlid fishes. Science 273, 1091–1093.

Johnson, R.W., Tothill, J.C., 1985. Definitions and broad geographic outline of savanna lands. In: Tothill, J.C., Mott, J.J. (Eds.), Ecology and management of the world's savannas. Australian Academy of Science, Canberra, pp.1-13.

Jongmans, a. G., Buurman, P., van Doesburg, J.D.J., van Oort, F., Jaunet, a. M., 1994. Morphology, Chemistry, and Mineralogy of Isotropic Aluminosilicate Coatings in a Guadeloupe Andisol. Soil Science Society of America Journal 58, 501-507.

Jongmans, A.G., Pulleman, M.M., Marinissen, J.C.Y., 2001. Soil structure and earthworm activity in a marine silt loam under pasture versus arable land. Biology and Fertility of Soils 33, 279–285.

Jungerius, P.D., Ancker, J.A.M. Van Den, Mucher, H.J., 1999. The contribution of termites to the microgranular structure of soils on the Uasin Gishu Plateau, Kenya. Catena 34, 349–363.

Kendall, R.L., 1969. An ecological history of the Lake Victoria Basin. Ecological Monograph 39, 121–176.

Kent, P.E., 1944. The age and tectonic relationships of East African Volcanic Rocks. Geological Magazine 81, 15–27.

Kraus, M.J., 1999. Paleosols in clastic sedimentary rocks: their geologic applications. Earth-Science Reviews 47, 41–70.

Levin, N.E., Cerling, T.E., Passey, B.H., Harris, J.M., Ehleringer, J.R., 2006. A stable isotope aridity index for terrestrial environments. PNAS 103, 11201-11205.

Lorenzen, E.D., Heller, R., Siegismund, H.R., 2012. Comparative phylogeography of African savannah ungulates. Molecular Ecology 21, 3656-3670.

McBrearty, S., Brooks, A.S., 2000. The revolution that wasn't: a new interpretation of the origin of modern human behavior. Journal of Human Evolution 39, 453–563.

McDougall, I., Brown, F.H., Fleagle, J.G., 2005. Stratigraphic placement and age of modern humans from Kibish, Ethiopia. Nature 433, 733–736.

Marbut, C.F., 1935, Atlas of American. III. Soils of the United States. Government Printing Office, Washington, D.C.

Milly, P.C.D., 1999. Comment on "Antiphasing between Rainfall in Africa's Rift Valley and North America's Great Basin." Quaternary Research 51, 104–107.

Milne, G., 1936. Natural Erosion as a Factor in Soil Profile Development. Nature 138, 548–549.

Moore, D.M., Reynolds, R.C., 1997. X-Ray diffraction and the identification and analysis of clay minerals. Oxford University Press, New York, p. 378.

Mora, C.I., and Driese, S.G., 1999, Palaeoclimatic significance and stable carbon isotopes of Palaeozoic red bed paleosols, Appalachian Basin, USA and Canada. In: Thiry, M., and Simon-Coinçon, R. (eds.), Palaeoweathering, palaeosurfaces and related continental deposits. International Association of Sedimentologists Special Publication No. 27, pp. 61-84.

Nordt, L.C., Driese, S.G., 2009. Hydropedological assessment of a vertisol climosequence on the Gulf Coast Prairie Land Resource Area of Texas. Hydrology and Earth System Science 13, 2039–2053.

Nordt, L.C., Driese, S.G., 2010a. A modern soil characterization approach to reconstructing physical and chemical properties of paleo-Vertisols. American Journal of Science 310, 37–64.

Nordt, L.C., Driese, S.G., 2010b. New weathering index improves paleorainfall estimates from Vertisols. Geology 38, 407–410.

Owen, W.E., 1937. Draft of tentative preliminary report on the July 1937 investigations at Ng'ira Karungu. Unpublished manuscript housed in the archives of the Natural History Museum, London.

Owen, W.E., 1938. The Kombewa Culture, Kenya Colony. Man 38, 203-205.

Owen, W.E., 1939. An amateur field collector in Kavirondo, Part II. Journal of the Royal African Society 38, 220-226.

Pickford, M.H., 1984. An aberrant new bovid (Mammalia) in subrecent deposits from Rusinga island, Kenya. Proceedings of the Koninklijke Nederlandse Akademie Van Wetenschappen Series B: Palaeontology, Geology, Physics, Chemistry, Anthropology 87, 441–452.

Retallack, G.J., 2001. Soils of the past: An introduction to paleopedology, 2nd ed. Blackwell Science Ltd, Oxford.

Rito, T., Richards, M.B., Fernandes, V., Alshamali, F., Cerny, V., Pereira, L., Soares, P., 2013. The first modern human dispersals across Africa. PLoS One 8, 1-16.

Scholz, C.A., Johnson, T.C., Cohen, A.S., King, J.W., Peck, J.A., Overpeck, J.T., Talbot, M.R., Brown, E.T., Kalindekafe, L., Amoako, P.Y., Lyons, R.P., Shanahan, T.M., Castaneda, I.S., Heil, C.W., Forman, S.L., McHargue, L.R., Beuning, K.R., Gomez, J., Pierson, J., 2007. East African megadroughts between 135 and 75 thousand years ago and bearing on early-modern human origins. Proceedings of the National Academy of Sciences of the United States of America 104, 16416–16421.

Sheldon, N.D., Retallack, G.J., Tanaka, S., 2002. Geochemical climofunctions from North America soils and applications to paleosols across the Eocene-Oligocene Boundary in Oregon. Journal of Geology 110, 687–696.

Sheldon, N.D., Tabor, N.J., 2009. Quantitative paleoenvironmental and paleoclimatic reconstruction using paleosols. Earth-Science Reviews 95, 1–52.

Sinclair, A.R.E., 1979. The Serengeti Environment, in: Sinclair, A.R.E. and Norton-Griffiths M. (Eds.). The University of Chicago Press, Chicago, pp. 31-45.

Soares, P., Alshamali, F., Pereira, J.B., Fernandes, V., Silva, N.M., Afonso, C., Costa, M.D., Musilova, E., Macaulay, V., Richards, M.B. Cerny, V., Pereira, L., 2012. The expansion of mtDNA Haplogroup L3 within and out of Africa. Molecular Biology and Evolution 29, 915-927.

Song, Y., Semazzi, F.H.M., Xie, L., Ogallo, L.J., 2004. A coupled regional climate model for the Lake Victoria Basin of East Africa. International Journal of Climatology 24, 57–75.

Soil Survey Staff, 1999. Soil Taxonomy: A Basic System of Soil Classification for Making and Interpreting Soil Surveys, 2nd ed. USDA NRCS, Washington D.C.

Stager, J.C., Mayewski, L., Meeker, L.D., 2002. Cooling cycles, Heinrich event 1, and the desiccation of Lake Victoria. Palaeogeography, Palaeoclimatology Palaeoecology 183, 169–178.

Stager, J.C., Johnson, T.C., 2008. The late Pleistocene desiccation of Lake Victoria and the origin of its endemic biota. Hydrobiologia 596, 5–16.

Stager, J.C., Ryves, D.B., Chase, B.M., Pausata, F.S.R., 2011. Catastrophic drought in the Afro-Asian monsoon region during Heinrich Event 1. Science 331, 1299–1302.

Stoops, G., 2003. Guidelines for Analysis and Description of Soil and Regolith Thin Sections. Soil Science Society of America, Inc., Madison, Wisconsin.

Stoops, G., Marcelino, V., Mees, F. (Eds.), 2010. Interpretation of Micromorphological Features of Soils and Regoliths, 1st ed. Elsevier, Netherlands.

Tabor, N.J. and Myers, T.S., 2015. Paleosols as indicators of paleoenvironment and paleoclimate. Annual Reviews of Earth and Planetary Science 43, 11.1-11.29.

Talbot, M.R., Laerdal, T., 2000. The late Pleistocene - Holocene palaeolimnology of Lake Victoria, East Africa, based upon elemental and isotopic analyses of sedimentary organic matter. Journal of Paleolimnology 23, 141–164.

Talbot, M.R., Williams, M.A.J., 2009. Cenozoic evolution of the Nile Basin. In: Dumont, H.J. (Ed.), The Nile: Origin, Environments, Limnology and Human Use. Springer Science + Business Media B.V., pp. 37–60.

Tryon, C.A., Faith, J.T., 2013. Variability in Middle Stone Age of Eastern Africa. Current Anthropology 54, S234-S254.

Tryon, C.A., Faith, J.T., Peppe, D.J., Fox, D.L., McNulty, K.P., Jenkins, K., Dunsworth, H., Harcourt-Smith, W., 2010. The Pleistocene archaeology and environments of the Wasiriya Beds, Rusinga Island, Kenya. Journal of Human Evolution 59, 657–671.

Tryon, C.A., Faith, J.T., Peppe, D.J., Keegan, W.F., Keegan, K.N., Jenkins, K.H., Nightingale, S., Patterson, D., Van Plantinga, A., Driese, S., Johnson, C.R., Beverly, E.J., 2014. Sites on the landscape: Paleoenvironmental context of late Pleistocene archaeological sites from the Lake Victoria basin, equatorial East Africa. Quaternary International 331, 20–30.

Tryon, C.A., Peppe, D.J., Faith, J.T., Van Plantinga, A., Nightingale, S., Ogondo, J., Fox, D.L., 2012. Late Pleistocene artefacts and fauna from Rusinga and Mfangano islands, Lake Victoria, Kenya. Azania: Archaeological Research in Africa 47, 14–38.

Ufnar, D., 2007. Clay coatings from a modern soil chronosequence: A tool for estimating the relative age of well-drained paleosols. Geoderma 141, 181–200.

Van Plantinga, A.A., 2011. Geology of the Late Pleistocene artifact-bearing WAsiriya Beds at the Nyamita locality, Rusinga Island, Kenya. M.S. Thesis, Baylor Unviersity.

Vepraskas, M.J., 1992, Redoximorphic features for identifying aquic conditions: North Carolina Agricultural Research Service, Technical Bulletin 301, 33 p.

Vepraskas, M.J., 2001, Morphological features of seasonally reduced soils. In: Richardson, J.L., and Vepraskas, M.J. (eds.), Wetland Soils: Genesis, Hydrology, Landscapes, and Classification. Lewis Publishers, New York, pp. 163-182.

Vepraskas, M.J., and Faulkner, S.P., 2001, Redox chemistry of hydric soils. In: Richardson, J.L., and Vepraskas, M.J. (eds.), Wetland Soils: Genesis, Hydrology, Landscapes, and Classification. Lewis Publishers, New York, pp. 85-105.

Verster, E., de Villiers, J.M., Scheepers, J.C., 1973. Gilgai in the Rustenburg Area. Agrochemophysica 4, 57–62.

Vesey-Fitzgerald, D., 1973. East African grasslands. East African Publishing House, Nairobi.

Wynn, J.G., 2000. Paleosols, stable carbon isotopes, and paleoenvironmental interpretation of Kanapoi, Northern Kenya. Journal of Human Evolution 39, 411–432.

CHAPTER FOUR

Lake Victoria Megadrought and Equatorial
Grassland Expansion during the Late Pleistocene

Summary

Lake Victoria is the largest freshwater lake in the tropics by surface area (68,800 km^2) and is currently a biogeographic barrier between the eastern and western branches of the East African Rift (EAR). Lake Victoria has desiccated several times in the past, most recently at ~17 ka and at ~15 ka[1], but little is known about its history prior to the Last Glacial Maximum (LGM). We present new data from thirteen Late Pleistocene paleosols from deposits adjacent to the lake that indicate mean annual precipitation (MAP) was 44% of modern between ~94 ka and >33 ka. This paleoprecipitation estimate, when input into a water budget model, projects that Lake Victoria may desiccates within a few centuries but refills very slowly (e.g., >10 kyr) if precipitation is <94% of modern. This information supports that Lake Victoria was likely desiccated for most, if not all, of the interval between 94 and >33 ka. This also indicates aridity extended much longer than the megadroughts elsewhere in tropical Africa generally accepted to be caused by eccentricity-enhanced precession. With the return of high-latitude forcing, low sea surface temperatures (SSTs) affected the Congo Air Boundary (CAB) convergence, keeping precipitation below levels that sustain Lake Victoria and extended aridity. Prolonged desiccation would have removed a major barrier for the movement of fauna, including early modern humans, between the rifts and across the equator, providing a long-term dispersal corridor. Inputting future climate projections into this water budget

model yields results that indicae Lake Victoria could have no outlet to the White Nile in 10 years, and Kenya loses access to the lake within 400 years, which would significantly impact subsistence and economic resources supplied by Lake Victoria for the East African Community.

Text

Climate change in the tropics results in large-scale changes in precipitation but not temperature. The location of the Intertropical Convergence Zone (ITCZ) affects precipitation and crosses Lake Victoria twice a year, creating two rainy seasons in March and in October[2]. The MAP varies across the catchment ranging from 1.4-1.8 m yr^{-1} [[3]]. Because MAP is almost equal to average evaporation (1.46 m y^{-1}) with local precipitation derived primarily from the lake itself, the lake level responds directly to rainfall[3–6]. The lake is not within a rift basin and is wide and shallow (maximum depth 79 m) in comparison to other African Great Lakes[4] (Fig. 1A and B). This bathymetry results in small changes in lake level causing large changes in surface area.

Precipitation is also controlled by the movement of the CAB, the strength of the Indian and Atlantic monsoons, and topography[2]. Throughout the Pleistocene, precipitation in tropical Africa varied due to orbital forcing, high latitude processes, regional tectonics, and changes in ocean circulation and SSTs[2,7]. However, the paleolimnological record for Lake Victoria extends no farther than the LGM, with two paleosols indicating desiccation at ~17 ka and 15 ka[1,8].

We present new paleoprecipitation data from six Late Pleistocene sites from northeastern Lake Victoria in Kenya: Rusinga Island, Mfangano Island, and Karungu[9–14], and model the effect of precipitation changes on the surface area of Lake Victoria (Fig.

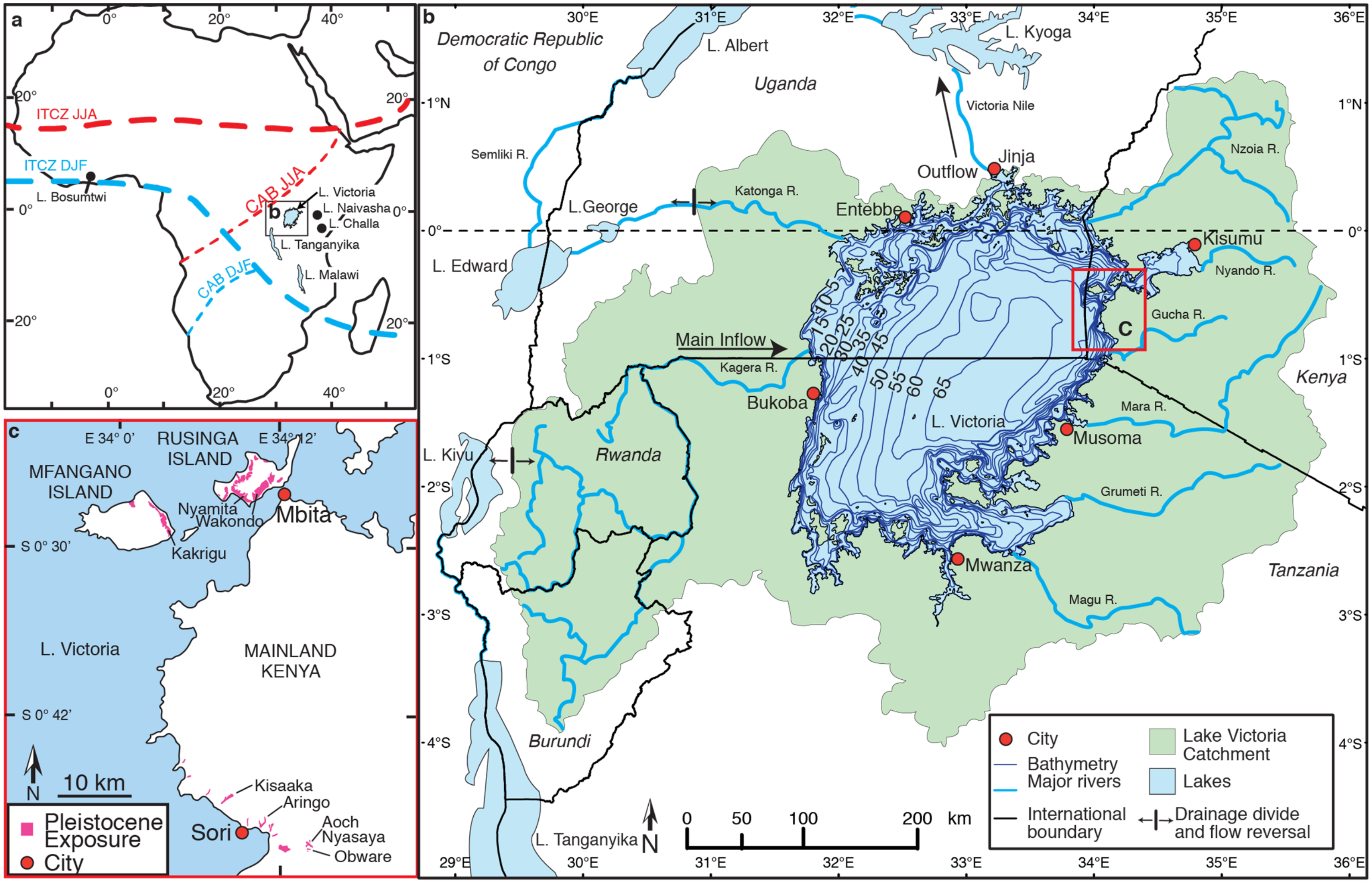

Figure 4.1: Location of study. A) Location of Lake Victoria and other African Lakes with a record from the Late Pleistocene. The position of the ITCZ and CAB during June, July, and August and during December, January, and February are indicated. B) The catchment of Lake Victoria with major rivers indicated and bathymetry of the lake. C) Exposure of Late Pleistocene sites along the eastern shoreline of Lake Victoria. Those used in this study are labeled.

1C). These deposits have been dated to ~94 to >33 ka[9,10,13] and sample an approximately ~55 km north to south transect along the eastern margin of the modern lake. Fossils and Middle Stone Age artifacts are preserved within a sequence of tuffaceous alluvial and fluvial sediments intercalated with paleosols, primary fall-out and variably reworked tephra, and tufa[9–14] (Fig. 4.2; Supplementary Discussion 1).

Bulk geochemistry from 13 paleo-Inceptisols and paleo-Vertisols was used to estimate MAP using two different proxies: CALMAG[15] (for Vertisols only) and CIA-K[16] for all other paleosol types (Table 4.1; Methods). The MAP for these paleosols ranges from 0.552 to 1.000 m yr^{-1} with an average of 0.800 m yr^{-1} (CIA-K) for all paleosols, with no statistical difference throughout the 11-m thick sequence. The stratigraphy is dominated by paleosols that based on various dating methods[9] and paleosol features[11] likely represents the entire ~60 kyr interval (Supplementary Discussion 2). Previous water budget models[5,6] indicate that Lake Victoria would be reduced to <10% of current surface area with a MAP of 0.800 m yr^{-1}, but these models do not assess how changes in temperature or insolation influenced lake level, or the rate of surface area loss.

We use this estimate of paleoprecipitation as input for a simple water budget model to project lake levels in Lake Victoria during this past interval of prolonged aridity (see Methods). Using reconstructed precipitation levels (44% of modern precipitation), we model Lake Victoria would be completely desiccated within a few centuries regardless of change in insolation and temperature (Fig. 4.3A). At precession maxima (+40 W m^{-2} relative to today), Lake Victoria will not refill to modern levels until there is enough precipitation to generate runoff, which occurs at ~96% of modern MAP (Fig.

Table 4.1: Pleistocene paleosol MAP estimates.

Locality	Site	CALMAG m yr^{-1} SE ±108	CIA-K m yr^{-1} SE ±182
Above Nyamita Tuff			
Kakrigu	DP1011	-	0.552
Kisaaka	10	-	1.000
Kisaaka	10	-	0.716
Kisaaka	13	-	0.894
Kisaaka	13	-	0.946
Aringo	5	-	0.864
Obware	2	-	0.698
Nyamita	AV1002	-	0.614
	Mean	-	0.786
	SE	-	0.058
	Range	-	0.552-1.000
Below Nyamita Tuff			
Kisaaka	4F	0.735	0.812
Kisaaka	10	0.847	0.920
Kisaaka	12	0.813	0.954
Kisaaka	13	0.620	0.713
Aringo	3	0.911	0.812
Aoch Nyasaya	5	0.557	0.657
Wakondo	Bovid Hill	0.767	0.819
Nyamita	1	0.750	0.829
	Mean	0.750	0.815
	SE	0.041	0.034
	Range	0.557-0.911	0.657-0.954
	All Paleosols CIA-K Range		0.552-1.000
	All Paleosols CIA-K Average		0.800

- not applicable to Paleosol order

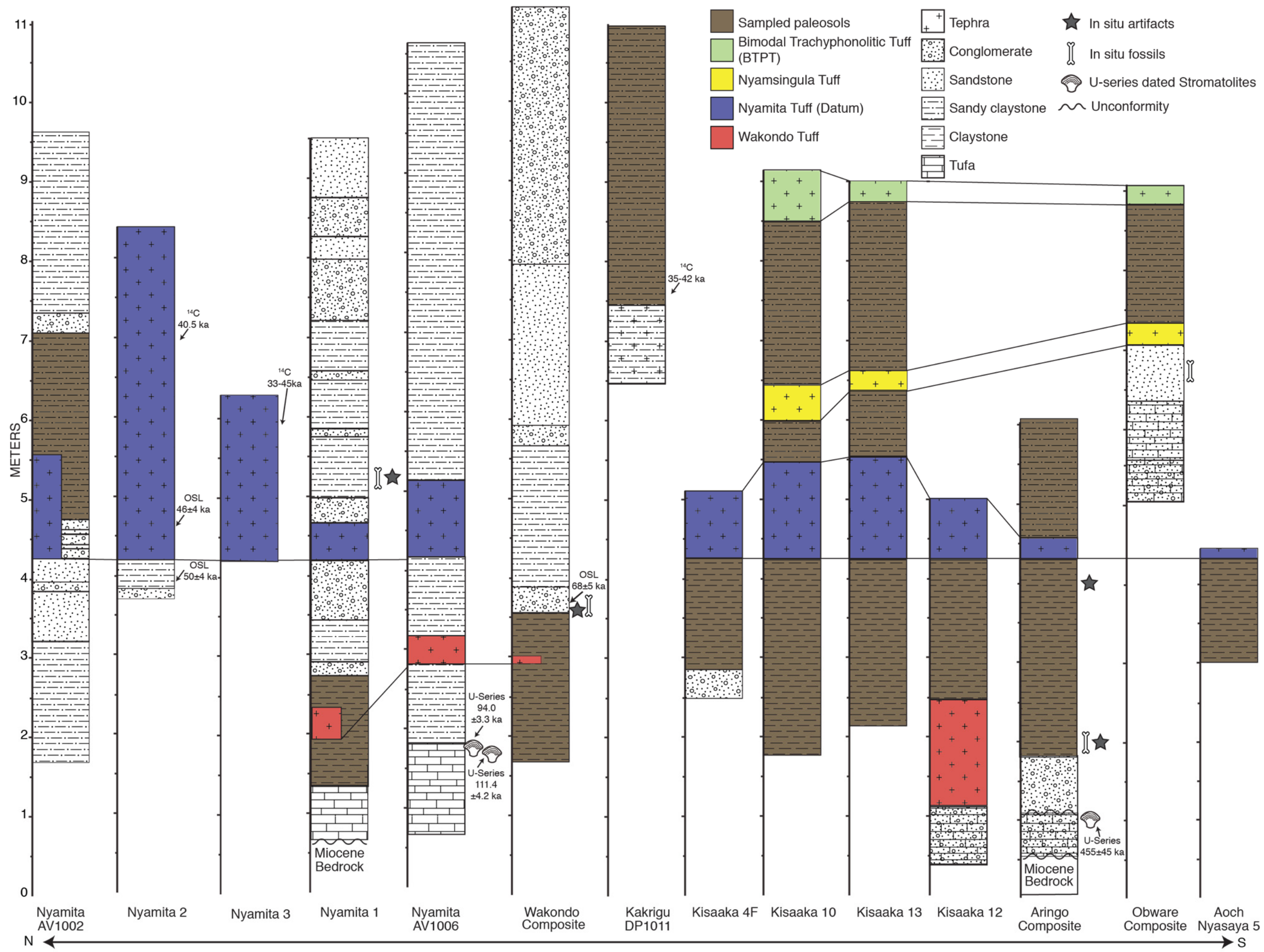

Figure 4.2: Stratigraphy of paleosols used in this study. The dates identified on this figure are discussed further in Blegen et al.[9] and Beverly et al.[10]. The Nyamita and Wakondo Tuffs at the Nyamita AV1002, Nyamita 1, and Wakondo localities are discontinuous due to their proximity to fluvial channels and are shown in their correlated positions within the paleosols. The localities were sampled to access the most complete paleosol record.

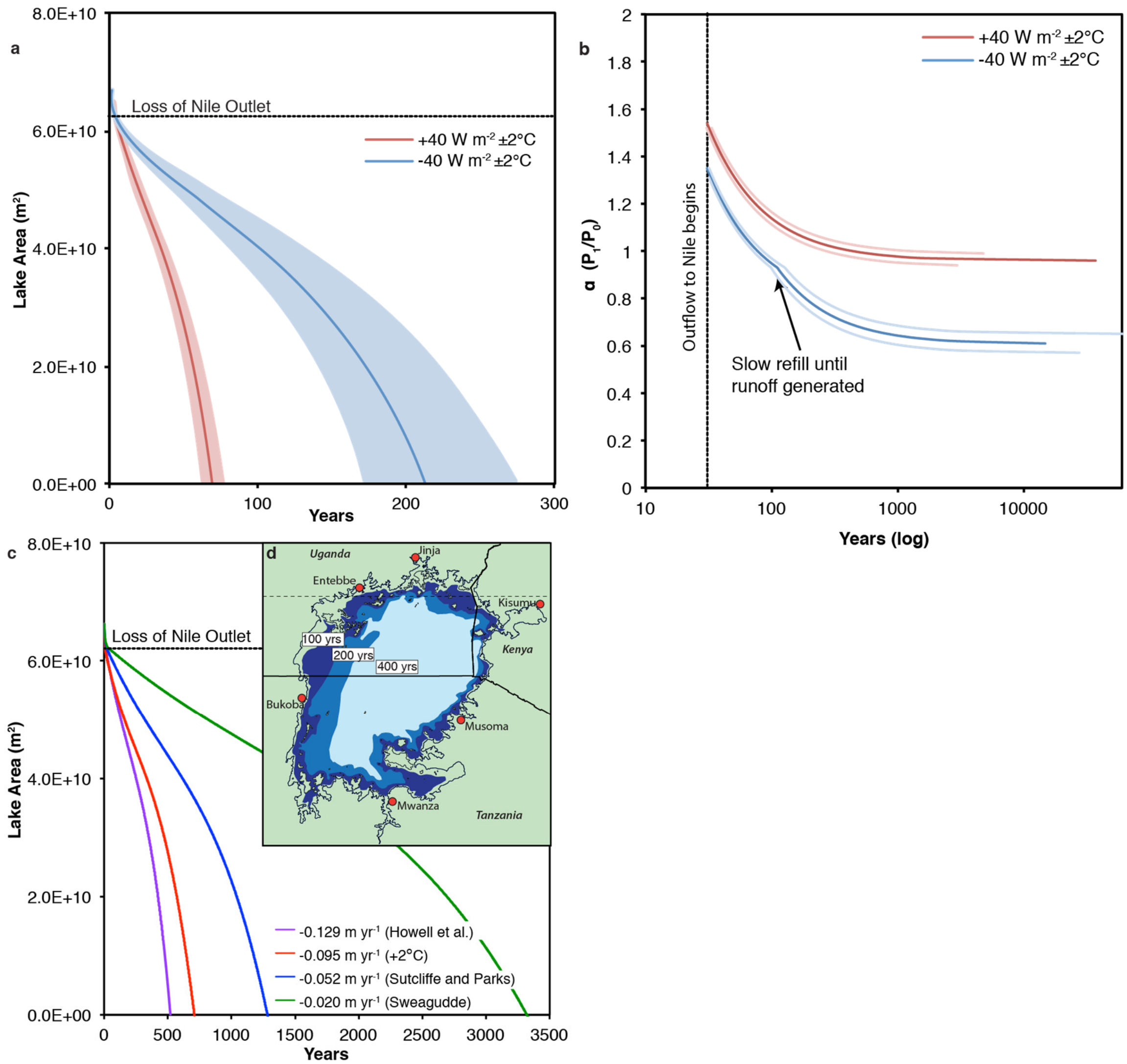

Figure 4.3: A) Drying of Lake Victoria. B) Filling of Lake Victoria. C) Modern drying of Lake Victoria. D) Areal extent of Lake Victoria after 100, 200, and 400 years based on modern drying rates.

4.3B). Under precession maxima conditions, the lake would refill within centuries when precipitation is >97% of modern. At precession minima (-40 W m^{-2}), Lake Victoria can be refilled with lower precipitation (>60%), but refill is slow (>10 kyr) until there is enough rainfall to generate runoff (~94% of modern). These rates of draining and refilling are similar to the post-LGM desiccation events where the lake drained and refilled twice between 14 ka and 18 ka[1]. Our modeling results indicate precipitation levels were significantly less than the minimum needed to maintain a lake and agrees with a Late Pleistocene dessication surface of unknown duration at ~80 ka in Lake Victoria estimated using sedimentation rates and seismic stratigraphy[8].

The Late Pleistocene decrease in precipitation with desiccation of Lake Victoria is a regional phenomenon suggesting a regional forcing mechanism. Between 135 ka and 70 ka, equatorial Africa was more arid than the post-LGM[17]. Lake levels in Lakes Malawi, Tanganyika, and Botsumtwi were all very low[17] (Figs. 4.4F and G). Zonal shifts in the ITCZ are often used to explain precipitation changes in tropical Africa. However, it is unlikely that the ITCZ could be shifted so far south to prevent the bi-annual crossing of the ITCZ over Lake Victoria. Widespread climatic variability likely peaked between 145 and 60 ka[17] (Fig. 4.4A) due to eccentricity-enhanced precession. Climate modeling[18] indicates that when eccentricity is high, precessional forcing is greater at low compared to high latitudes[19]. This effect is seen in tropical marine records from the Atlantic[20] and Indian Oceans[21] as well as the East Asian monsoon[22] (Figs. 4.4H and I). This orbital mechanism explains the aridity for Lakes Malawi, Tanganyika, Botsumtwi, and Victoria during the megadrought. After 70 ka, all these lakes, except Lake Victoria (based on model) begin to refill. The refilling of the EAR Lakes is attributed stable precipitation conditions as eccentricity decreased[17]. We propose that the shift to high-latitude forcing affected Lake Victoria differently.

Evidence presented here indicates that Lake Victoria remaines desiccated, or nearly so, until ~33 ka, similar to Lake Naivasha, ~250 km to the east. This suggests that the cause for extended aridity from ~70-33 ka is due to factors other than eccentricity-enhanced precession. Lake Naivasha level is low to intermediate between 105 to 60 ka

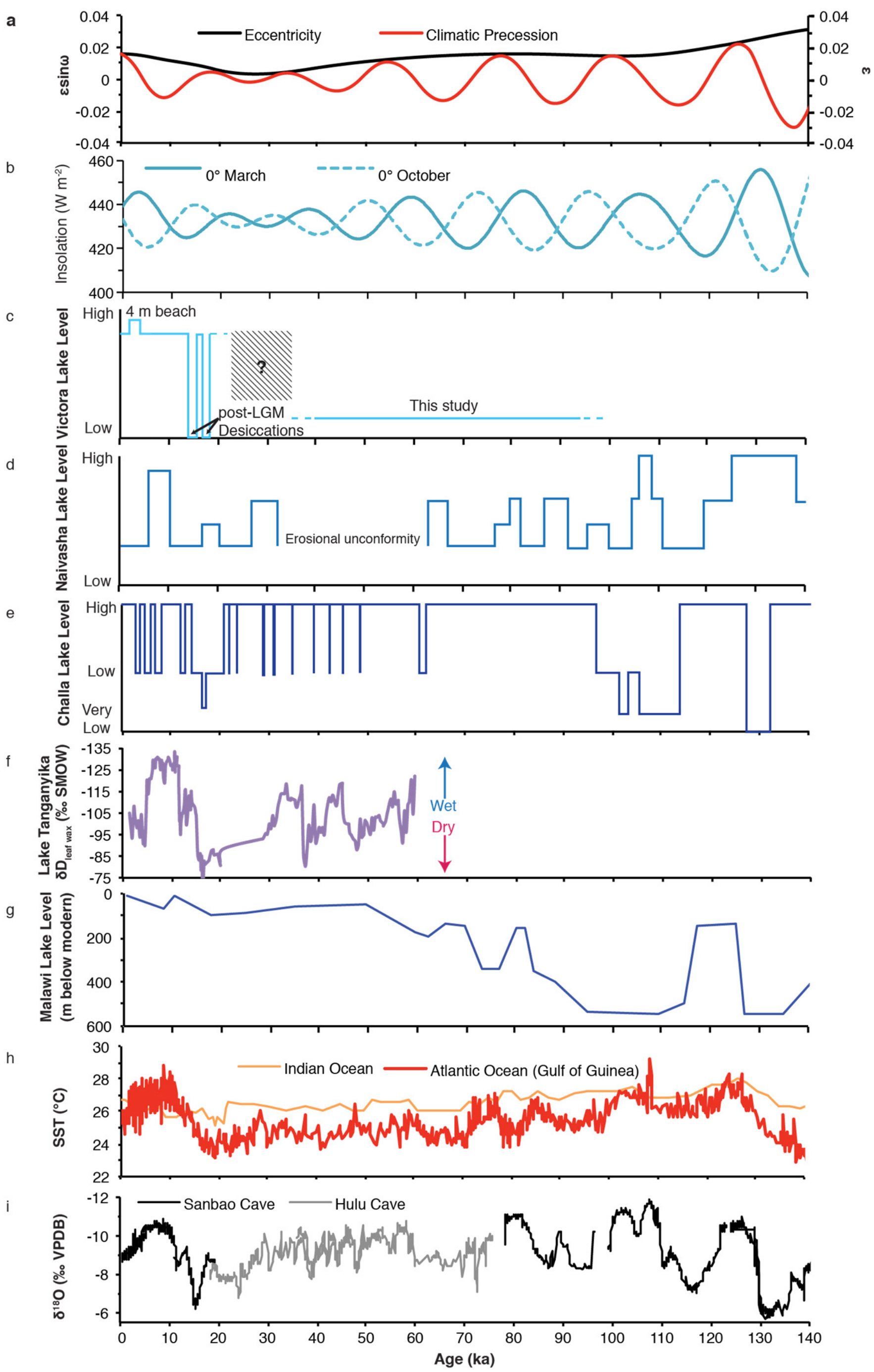

Figure 4.4: A) Eccentricity and climatic precession between and present and 140 kyr[30]. B) Mean monthly insolation at the equator for March and October[30]. C) Relative level of Lake Victoria [1, this study]. D) Relative level of Lake Naivasha [23]. E) Relative level of Lake Challa[24]. F) $\delta D_{leaf\ wax}$ from Lake Tanganika showing the relative changes from wet to dry during the past 60 ka[26]. G) Level of Lake Malawi in meters below modern[17]. H) Sea surface temperature records for the Indian and Atlantic monsoons. SSTs calibrated from the $U_{37}^{K'}$ record for the MD85668 core in the Indian Ocean off the coast of Somalia[21] and Mg/Ca SSTs estimates from the Gulf of Guinea in the Atlantic Ocean[20]. I) $\delta^{18}O$ record of the Asian monsoon from the Sanbao and Hulu Caves from China[22]. The Hulu record is plotted 1.6‰ more negative to account for the higher values in the Hulu Cave [22].

and dry between 60 ~35 ka based on an erosional unconformity[23]. Low lake levels are attributed to low SSTs in the Indian Ocean that weakened the monsoon[21,23] (Fig. 4.4D). In contrast, Lake Challa is only dry for a short duration of the megadrought between 114 and 97 ka with high levels until the LGM[24] (Fig. 4.4E). The post-LGM aridity is the only analog for low lake levels at Lakes Malawi, Tanganyika, and Challa and a desiccated Lake Victoria (Fig. 4.4C-G). Post-LGM, Lake Victoria desiccates twice[1], but equivalent lake level drops at Lakes Challa[24], Malawi, and Tangayika[17] are less severe than the megadrought.

$\delta D_{leaf\ wax}$ records from the last 25 kyr indicate that this east-west moisture gradient across tropical Africa is related to strength of the CAB, which may be more important to the climate of tropical Africa than previously realized[24–27]. Lakes Malawi and Challa are both on the Indian Ocean side of the CAB, and therefore, unaffected by changes in the Atlantic moisture supply. The CAB converges over Lake Victoria and contributes moisture from both the Atlantic and Indian Oceans to Lake Victoria precipitation. Lake Naivasha is close to the CAB but ~250 km closer to the Indian Ocean potentially explaining the intermediate aridity of Lake Naivasha. Cooler SSTs in both the Indian[21] and Atlantic[20] Oceans are responsible for the aridity during the post-LGM due to reduction of moisture transport[1]. Changes in the tropical-subtropical SST gradient in the SE Atlantic are linked to high latitude forcing[20] (Fig. 4.4H-J). Therefore, we suggest that the extended period of aridity at Lake Victoria between 94 and >33 ka was maintained below a precipitation threshold that could sustain Lake Victoria. This aridity was caused by the eccentricity-enhanced precession creating a megadrought from 94 - ~70 ka followed by high-latitude forcing causing low SSTs affecting CAB convergence from ~70 - ~35 ka.

Desiccation of Lake Victoria during the MIS 5 megadrought and into MIS 4 and 3 would have affected migrations of early modern humans and other fauna. Grasslands expanded simultaneously with the retreat of the lake. Fossil fauna from Rusinga Island, Mfangano Island, and Karungu document a >20% decrease in MAP[14], a C_4 grass-dominated ecosystem, and a diverse population of grazing herbivores[12–14]. Arid-adapted ungulates such Grevy's zebra (*Equus grevyi*) and oryx (*Oryx beisa*) are found far outside their modern range of arid eastern and northeastern Africa. The removal of Lake Victoria as a biogeographic barrier and the expansion of grasslands indicated by the fauna enhances the Nilotic corridor as an avenue for the movement of modern humans out of and within Africa between 94 and >33 ka.

These results also have significant implications for the future of the East African Community, which is projected to experience an increase in temperature between 1 and 5°C over the next 100 years[28]. Our model indicates that Lake Victoria is most sensitive to the evaporation-precipitation balance. Increased temperature will effect evaporation regardless of precipitation change, for which climate models disagree[28]. At minimum estimated rates, the lake could be desiccated in 3500 years[29] and at maximum rates the Nile outlet is gone within 10 years and Kenya loses access to the lake within 400 years (Fig. 4.3C and D; Methods). Any decrease in precipitation would accelerate the rate of decline of modern Lake Victoria similar to what occurred during the post-LGM and Late Pleistocene Megadrought interval.

Methods

Paleopedology

All outcrop locations were recorded and mapped using a hand-held GPS (Appendix D), the exposures were trenched to expose bedding unaffected by modern processes, and the stratigraphic sequence measured and described at the cm scale. All lithologic and pedogenic features were recorded and photographed. Samples were collected for bulk geochemistry at 10 cm vertical intervals through the paleosols, and where applicable, samples were collected from gilgai topography micro-lows of paleo-Vertisols where erosion is less likely and pedogenic processes are greatest[31]. Samples were pulverized for mineralogical and geochemical analysis. Bulk geochemical samples were pulverized at Baylor University prior to being sent for commercial analysis to ALS Geochemistry (Reno, NV) for major, rare, and trace element analyses using a combination of inductively coupled plasma atomic emission spectroscopy (ICP-AES) and inductively coupled plasma mass spectrometry (ICP-MS). The complete geochemical analyses of all samples are available in Appendix C. Bulk geochemical data were used to calculate paleoprecipitation using the chemical index of alteration minus potassium (CIA-K), applicable for all soil types[16], and the CALMAG proxy, specific to paleo-Vertisols[15]. For both proxies, all oxides are normalized to their molar ratios and were calculated by averaging the oxides over the critical depth, defined as 20 to 100 cm [[15]]. If the BC or C horizon fell within the critical depth, only B horizons were used. CIA-K is defined as:

$$Al_2O_3/\,(Al_2O_3 + CaO + Na_2O) \times 100 \qquad (1)$$

and is a weathering index that measures clay formation and base loss associated with feldspar weathering and was designed to be universal for all paleosol types in which there has been sufficient time of soil formation to equilibrate with climate conditions[16].

CALMAG is a weathering index specifically for paleo-Vertisols[15] defined as:

$$Al_2O_3/(Al_2O_3 + CaO + MgO) \times 100. \quad (2)$$

Vertisols are formed from preweathered parent material, and therefore limited hydrolysis occurs in this soil type, and for this reason, CIA-K often overpredicts precipitation in Vertisols. The CALMAG proxy improves the paleoprecipitation estimates of paleo-Vertisols by focusing on tracking the flux of Ca and Mg, which better describe the weathering occurring in Vertisols[15]. Both the CIA-K and CALMAG weathering indices in modern soils have a strong correlations to MAP and these indices can be used to estimate paleo-rainfall[15,16].

Water Balance of Lake Victoria

Lake Victoria is not within a rift basin and therefore very shallow (maximum depth 79 m) in comparison to other African Great Lakes[4], and this geometry results in large changes in surface area with small changes in depth. This is effect is amplified because ~80% of the inflow to the lake is direct input from recycled lake water with only ~20% contributed by rivers. Lake Victoria also comprises 26% of the total catchment area in comparison to Lakes Turkana (5%), Tanganyika (13%), and Malawi (19%) [[32]]. Therefore, catchment processes including precipitation interception and runoff are less important than direct precipitation interception and evaporation of the lake. The Kagera River is the main inflow with a drainage basin of 60,000 km^2, which drains the highlands of Rwanda and Burundi, and which accounts for >10% of the overall inflow into the lake[3,33,34] (Fig.1B). The lake is hydrologically open, and the only outflow is through the Victoria or White Nile at Jinja. Outflow is now controlled by the Nalubaale Dam, which was constructed in 1954, using the "agreed curve" that mimics natural discharge due to fluctuations in climate[35].

A simple water budget model approach has been applied to the Lake Victoria catchment. Researchers have been trying to understand the water balance of Lake Victoria since the 1930s[36] and the resulting models often have an imbalance of inflows and outflows[8]. Yin and Nicholson[3] summarize the widely varying input parameters that have been used in the past. The main problems with the water balance are calculating the two largest variables: precipitation and evaporation and to a lesser degree the lack of stream inflow measurements[3]. Calculating precipitation over the Lake Victoria is difficult due to the lack of consistent station coverage because most stations are concentrated in Kenya and Tanzania and interruptions in recording periods[3]. As a result, early models often balanced the water budget by increasing or decreasing precipitation[37–39] and later models modified evaporation[3]. Here we use an adapted Penman equation to model evaporation for the Lake Victoria region.

Adapted Penman equation for evaporation. The Penman equation was adapted for modeling the water balance of Lake Victoria:

$$\lambda E = \frac{\Delta R_n + \rho c_p (e_s - e_a) f(U_2)}{\Delta + \gamma} \tag{3}$$

where λ is the latent heat of water evaporation (J g^{-1} K^{-1}), E is the evaporative mass flux density (g m^{-2} s^{-1}), Δ is the slope of saturated vapor pressure with temperature (Pa K^{-1}), R_n is net short and longwave radiation (W m^{-2}), ρ is the density of saturated air (g m^{-3}), c_p is the specific heat of air (J g^{-1} K^{-1}), e_s is the saturated vapor pressure for the daily mean temperature (Pa), e_a is the daily ambient vapor pressure (Pa), $f(U_2)$ is a wind speed function utilizing wind speed data collected at a 2 m height (m s^{-1} Pa^{-1}), and γ is the psychometric "constant" (Pa K^{-1}).

We estimated R_n by:

$$R_n = (1 - \alpha)SW - LW. \tag{4}$$

Shortwave radiation (SW; W m^{-2}) is estimated as 220 W m^{-2} based on satellite observations[40] and annual averages for Jinja, Entebbe, Kisumu, Bukoba, and Mwanza that range from 185 to 230 W m^{-2} [[34]]. Albedo (α) of shortwave radiation was estimated to be a value of 0.07 based on the latitude of Lake Victoria[41]. For emitted longwave radiation (LW; W m^{-2}), we estimated the flux density based on the method presented by Budyko[42]:

$$LW = \varepsilon\sigma T_K^4\left(0.39 - 0.058\sqrt{e_s/1.33.322}\right)(1 - 0.54C^2) \tag{5}$$

where ε is the emissivity set here at a value 0.96 [[42]], σ is the Stefan Boltzmann constant (5.67×10^{-8} W m^{-2} K^{-4}), T_K is the daily mean temperature (K), e_s is the saturated vapor pressure in mm Hg, and C is the cloudiness in fraction of sky cover which is assumed to be 0.50 based on previous water budget studies of Lake Victoria[3,43] and averages from shoreline meteorological stations[44–46].

The value of Δ for equation (3) was calculated by:

$$\Delta = \frac{\lambda M_w e_s}{RT_K} \tag{6}$$

where M_w is the molecular mass of water (18.02 g mol^{-1}) and R is the gas constant (8.3143 J mol^{-1} K^{-1}). The value of λ was derived by polynomial approximation[47] as a function of daily mean temperature (T_C, °C):

$$\lambda = 2500.8 - 2.36T_C + 0.0016T_C^2 - 0.00006T_C^3 \quad (7)$$

The values of e_s and e_a were approximated from the Tetens formula where:

$$e_s = 611e^{\left(\frac{17.502T_{C_{mean}}}{240.97+T_{C_{mean}}}\right)} \quad (8)$$

And

$$e_a = 611e^{\left(\frac{17.502T_{C_{min}}}{240.97+T_{C_{min}}}\right)} \quad (9)$$

where $T_{C_{mean}}$ is the mean maximum temperature (°C) and $T_{C_{min}}$ is the mean minimum temperature. The mean maximum temperature from 6 stations (Entebbe, Jinja, Kisumu, Musoma, Mwanza, and Bukoba) around the basin is 21.3°C[3] and the mean minimum temperature is 17.1°C [44–46]. The minimum temperature is used here as a surrogate estimate of dew point temperature and correlates well in non-arid climates[48]. The air directly above a large body of water like Lake Victoria is likely to be near saturation. Therefore the density of air (ρ) was calculated as moist air, or air near saturation, that changes as a function of temperature:

$$\rho = \{M_w e_a + M_a(P - e_a)\}/RT_K \quad (10)$$

where M_a is the mean mass of dry air (28.96 g mol^{-1}) and P is the mean air pressure (Pa) with the air pressure was approximated by:

$$P = 101300\, e^{(\text{-elev}/8200)} \quad (11)$$

where *elev* is the mean elevation of the surface of Lake Victoria. The mean lake elevation since the building of the Nalubaale Dam is approximately 1135 m. For the model, the value changes with changes in lake storage and the resultant changes in elevation.

The value of γ in (3) varies slightly with temperature due to the influence on λ. The value was estimated by:

$$\gamma = \frac{c_p P}{\lambda \left({M_w}/{M_a} \right)} \tag{12}$$

where a constant value of 1.012 J g^{-1} K^{-1} was assumed for c_p.

The use of the wind function (i.e. $f(U_2)$) as a modifier of vapor pressure difference in equation (3) 1) avoids the need for specific estimation of heat transfer, radiative, and vapor transfer resistance, 2) is consistent with the original formulation of the Penman equation, and 3) allows for the inclusion of lake morphology as a variable affecting open water evaporation estimation. McJannet et al.[49] proposed a wind function for open water that included lake area (A_L) as a variable where:

$$f(U_2) = (2.36 + 1.67\ U_2) A_L^{-0.05} \tag{13}$$

with an average wind speed of 2.2 m s^{-1} [3] measured at a 2 m reference height (U_2) with output units of the $f(U_2)$ in mm d^{-1} k Pa^{-1}. For unit consistency in our adapted Penman equation, the units of the original McJannet et al.[49] formula were converted into units of m s^{-1} Pa^{-1}. The value of using this function for the analysis rather than utilizing resistance formulations (*sensu* [50]) is that the change in area of the lake over time can be included as a potential feedback variable on evaporation rate in the water balance calculation.

Modeling the present lake level. The lake water was modeled based on a simple water balance approach:

$$\Delta h = P_C \gamma_0 + P_L - E_L - R_L \tag{14}$$

where Δh is the change in annual height of the water (m yr^{-1}), P_C is the annual catchment precipitation interception (m), γ_0 is the catchment precipitation runoff ratio (dimensionless) for time=0, P_L is the annual lake precipitation interception (m), E_L is the lake precipitation ([$E_L = (E/\lambda)(1/\rho_w)(365 \cdot 86400)$]) in m yr^{-1}, and R_L is the discharge from the lake (m) assuming that the lake is the outlet structure of the catchment where 365 is the number of days per year and 86,400 is the number of seconds per day. Groundwater inflow or outflow is assumed to be negligible because in relation to other water balance fluxes (precipitation and evaporation) groundwater interaction is insignificant[29,39]. The density of liquid water (ρ_w) was calculated as a function of temperature where:

$$\rho_w = 999.84847 + 0.006337563\, T_{C_{mean}} - 0.008523829 T_{C_{mean}}{}^2 + 0.00006943248 T_{C_{mean}}{}^3 - 0.0000003821216\, T_{C_{mean}}{}^4 \quad (15)$$

To test this model, two sets of observed precipitation and lake discharge data from 1956 to 1978 [[33,51]] were used, but the model was only tested using data from 1965 to 1978 to avoid changes in lake level due to the damming of Lake Victoria in 1954 [[33]]. P_C is assumed to be the same value for P_L. For R_L, observed values for the Jinja station were derived from the "agreed-upon curve"[35]. For γ_0, a value of 0.08 was used for the Lake Victoria catchment [34], which is close to the value of 0.10 for the entire Nile River[52]. With these input data, the value of Δh was calculated and compared with observed values (Fig. 4.5A). Least square regression analysis revealed that the modeled and Δh were correlated highest with the simulated Sutcliffe and Parks[33] input data with an $r^2 = 0.78$, which indicates that lake elevation is driven by a fairly straightforward budget, which is highly constrained by P_L and E_L and is consistent with other studies[3–6,35,39] (Fig. 4.5A and B). For the simulation using Howell et al.[51] data, the $r^2 = 0.73$.

Bathymetric analysis of Lake Victoria. While the water budget approach of this study was based on water depth values, the change of the area and volume of the lake is also of interest because the size of Lake Victoria has fluctuated significantly in the past from +4 meter above current lake level[53,54] to desiccation at ~17 ka and again at ~15 ka[[1,8,55,56]]. Because the depth to area/volume relationship is specific to each lake's geomorphology, the area/volume characteristics were first derived for increasing depth for Lake Victoria using a georeferenced and digitized bathymetric map[57]. This is meant to be an estimate for the depth/area relationship because the depth and shape of Lake Victoria has likely changed in the last 100 ka. The contours were mapped at 5 m intervals and these digitized data were captured in the form of a shapefile. All analyses were conducted in ArcGIS® (version 10.0; ESRI, Redlands, CA). To calculate area and volume values by depth, the shapefile was analyzed using the Polygon Volume function based on analysis of the individual bathymetric contours below the reference height of 1135 m. Using these data, we fit a fourth-order polynomial function using bathymetric depth as the independent variable and lake area (A_L) as the dependent variable:

$$y = -8.424999988041810 \times 10^2 x^4 + 3.931696313072550 \times 10^6 x^3 - 6.862506670194270 \times 10^9 x^2 + 5.311594269525770 \times 10^{12} x - 1.538663756789360 \times 10^{15} . \qquad (16)$$

This equation is used to predict discharge in the past (Fig. 4.5C). Changes in depth (Δh) were then used to calculate annual depth values that when applied to the derived depth to area relationship (15) can be used to estimate A_L. This new annual value of A_L was then used as input for $f(U_2)$ affecting subsequent derived values of λE.

Calculating lake discharge of the past. As part of the water budget, discharge from the lake is required. Values of R_L for the analysis of lake levels for 1965 to 1978 were derived from observed values, though inferred from the derived values of the "agreed curve"[35]. This curve is assumed to reflect natural discharge of the lake prior to construction of the Nalubaale Dam:

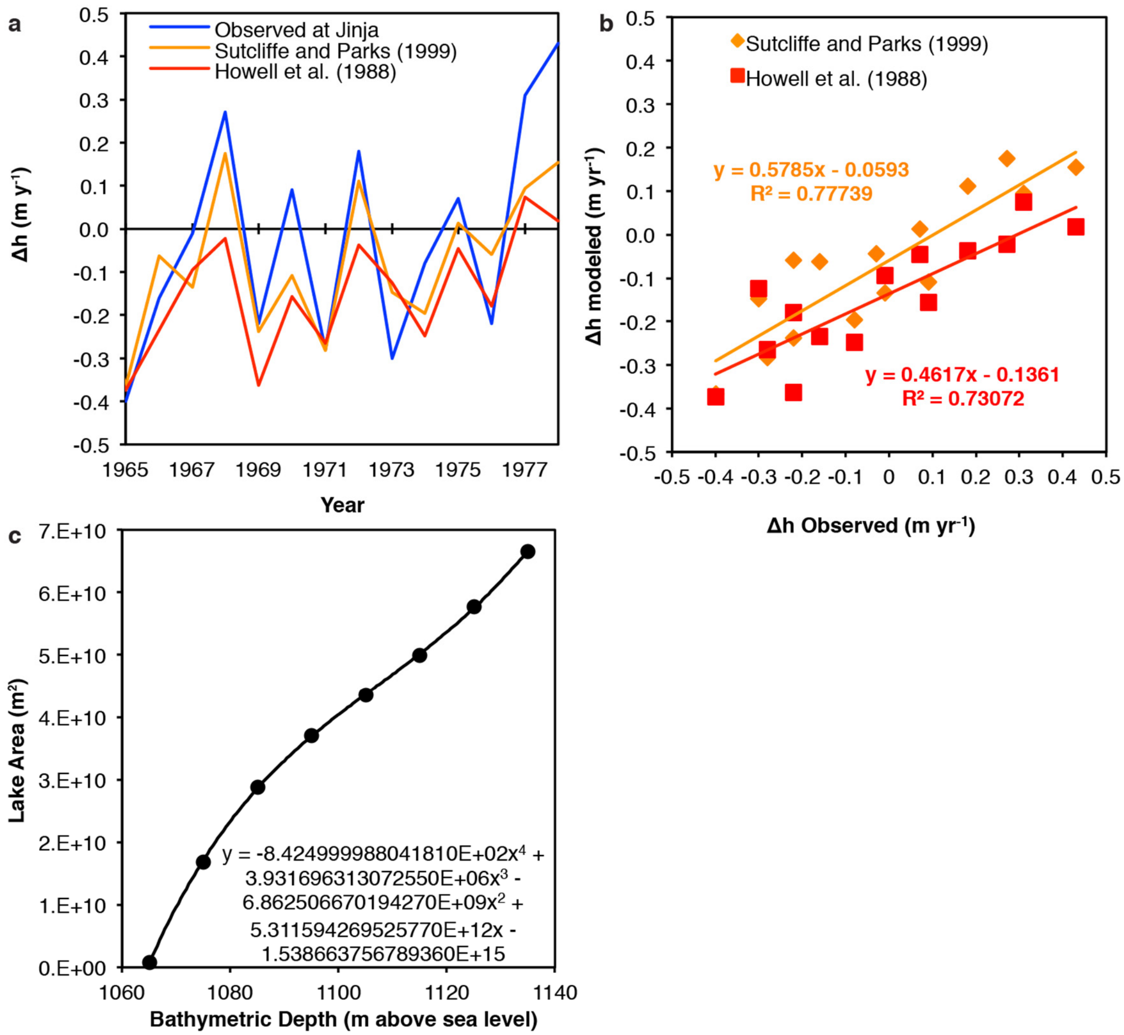

Figure 4.5: A) Change in annual height of the lake (Δh) with modeled results from two different datasets: Sutcliffe and Parks [33] and Howell et al. [51], and the observed values measured at Jinja [35] for the years 1965 to 1978. B) Observed Δh vs. modeled Δh with simple linear regression resulting in a slightly better R^2 value of 0.78 for the Sutcliffe and Parks [33] dataset that is therefore used in development of the model. C) Bathymetric analysis of Lake Victoria that relates depth in m above sea level to lake area using a fourth-order polynomial function.

$$Q = 132.923(\Delta h - 8.486)^{1.686} \tag{17}$$

where Q is the Nile River discharge at Jinja in $m^3\ s^{-1}$. To convert Q values to annual depth values for the water budget analysis,

$$R_L = (Q/A_L)(365)(86400) \tag{18}$$

where 365 is the number of days per year and 86,400 is the number of seconds per day.

However, at some point the value of Δh would result in complete cessation of flow into the Victoria Nile using the present morphologic characteristics of Jinja outlet. Linearization of the "agreed curve" function followed by solving for Δh where $Q = 0.0$ yields a values of 1130.5 m for the cessation of Nile flow. For the model of the past, lake height value (h, where $h = 1122 \cdot \Delta h$ assuming 1122 m is the Jinja elevation as a reference point), and $R_L = 0.0$ where calculated values of $h \leq 1130.5$ m.

Uplift and tilting during the Middle Pleistocene, shifted the center of the Lake Victoria basin ~50 km to the east and exposed fluvio-lacustrine sediments in the Kagera River Valley[53]. There is no evidence for tectonic modification of Lake Victoria since the Middle Pleistocene, suggesting that the modern Lake had formed by this time, but uplift in the Toro-Ankole volcanic province (≤50 ka) in Uganda likely modified the drainage of the two tributaries, the Katonga and Kagera Rivers[58]. Prior to uplift and volcanism in the Toro-Ankole province[58] outflow for Lake Victoria was likely through the Katonga and Kagera Rivers towards Lakes Albert and Edwards[59]. This uplift caused a flow reversal of these tributaries, likely between 35 and 25 ka and the formation of the modern outflow to the north through the Victoria Nile[59,60]. It is uncertain when this modern connection occurred but probably in the last 13 ka [[60]]. The effect of any outlet on water budget of Lake Victoria would be to increase the rate of desiccation. Therefore, knowing whether the Katonga or Kagera Rivers were the outlet during the Late Pleistocene is not necessary because these outlets would only have the effect of increasing the rate of desiccation, and the Jinja outlet is used to demonstrate this effect for our model. The relationship between precipitation and evaporation is much more important to understanding the water balance of Lake Victoria.

Modeling past lake levels and time to drain and refill Lake Victoria. The Nyamita Tuff is used as a division between the upper and lower paleosols because it is precisely dated to ~49 (OSL) and because it is distinct on the landscape and present at most sites. Because most of the upper paleosols are paleo-Inceptisols, and therefore, the CALMAG index is not applicable, the CIA-K index is used for calculations in the water budget. Paleosols above the Nyamita Tuff have an average MAP of 0.786±0.182 m yr^{-1} and paleosols below have an average of 0.815±0.182 m yr^{-1}. For convenience in the modeling and because paleo-precipitation does not vary through time, an overall CIA-K average of 0.8 m yr^{-1} for all paleosols is applied to water budget calculations for the Late Pleistocene (Table 4.1).

For the estimation of the water budget of Lake Victoria and subsequent storage changes in the past, the MAP of the past (P_p) was assumed to be 0.8 m y^{-1} based on the paleosol precipitation estimates or 44% of the average MAP for 1965 to 1978 [[33]]. Next, using the methods proposed by Wigley and Jones [52], the value of the past catchment runoff (R_1) was approximated by the equation:

$$\frac{R_1 - R_0}{R_0} = \frac{\alpha - (1 - \gamma_0)\beta}{\gamma_0} \tag{19}$$

that can be simplified to:

$$R_1 = R_0\left(\frac{\alpha - (1 - \gamma_0)\beta}{\gamma_0} - 1\right) \tag{20}$$

where α is the fraction of precipitation in the past relative to the current (0.44) and β is a function that represents the change in catchment evapotranspiration under a different climate than the present. For simplification, the β function was estimated as:

$$\beta \cong 1 - 0.3a \tag{21}$$

where a is the fraction of catchment area covered by vegetation. In this case, we assumed under drier conditions of the past, that only 25% of available catchment land area had vegetation cover similar to the large scale drying of the sub-Sahelian savanna[61].

In addition to changes in precipitation and fractional vegetation, changes in incident radiation were modeled as insolation has varied throughout the Pleistocene. Precession has the greatest influence over climate in tropical Africa and has created fluctuations in insolation over periods of 19 to 23 ka throughout the Pleistocene, which have a great effect on the strength of the East African monsoon[62]. For the simulations, changes in insolation translated into simulations in which input values of SW, as part of the calculation of E_L, were varied from present mean values of 220 W m^{-2} by ± 40 W m^{-2} to form the boundaries of precession maximum and minimum. The effects changing temperature of ±2°C were also simulated based changes in temperature from the Burundi highlands over the past 40 ka, which is the closest available temperature data[63–65]. Using these values to calculate lake evaporation, coupled with annual updated values of A_L and resultant R_L, annual values of Δh were calculated, starting with an assumed lake elevation 1135 m (full lake), to determine the trend in elevation and potential long-term effects on the lake. The annual values of Δh were subtracted from a starting lake elevation of 1135 m to determine time to desiccation of the lake.

According to the model, Lake Victoria will not refill without a certain amount of precipitation. To model the time and precipitation needed to refill Lake Victoria to achieve outflow through Jinja, the fractional precipitation was adjusted by 1% for ± 40 W m^{-2} and ±2°C until the lake began to refill with a positive Δh value. Then, the total depth of the lake (1130.5 m – 1065 m) was divided by Δh to calculate the effective time to fill Lake Victoria.

Modeling future lake levels. The future of Lake Victoria is also of interest for this region and several modern rates were used to calculate the time to desiccation for Lake Victoria if current drops in lake level were to continue. Limited observational data indicates that precipitation in the East African Community has decreased over the last 50 years, but the projected precipitation for the next 100 years is complex due to contrasting predictions between Global Climate Models (GCMs) and regional models[28]. Predictions of precipitation range from no change to a 20% increase in precipitation in GCMs, to a decrease in regional models[28]. The Δh values calculated from the two modern datasets[33,51] from 1965 to 1978 are used to determine the time to loss of the Nile outlet and desiccation of the lake from a starting elevation of 1135 m. Using Sutcliffe and Parks[33] dataset, the effect of +2°C on evaporation was also modeled to simulate a minimum estimate of climate change effects. Our model indicates that a +2°C increase in temperature accelerates the rate of lake level drop from -0.052 to -0.095 m yr^{-1} (Fig. 4.3C). Another model, derived using the IPCC A2 scenario[29], predicts historically low lake levels (1133 m) by the end of the century, and an extension of this rate (0.020 m yr^{-1}) indicates lake desiccation within 3500 years. Below 1130.5 m, Lake Victoria has no outlet to the White Nile, depriving Uganda of its main source of electricity, and the water that sustains the Nile during non-flood stage[60]. Therefore, we use 0.020 m yr^{-1} as a potential minimum estimate and our model as a maximum estimate. In this maximum estimate (-0.129 m yr^{-1}), cities such as Kisumu and Jinja lose access to the lake within 100 years and within 400 years Kenya loses all access to Lake Victoria (Fig. 3D).

Supplementary Discussion

1. Background to Karungu and Rusinga and Mfangano Islands

The Late Pleistocene geology, fossils, and Middle Stone Age (MSA) artifacts from Rusinga and Mfangano Islands have been the focus of research since 2009 [9,13,66–71]. More recently, this research has expanded to include the deposits around Karungu ~40 km to the south near the town of Sori[9–12] (Fig. 1C). Abundant fossils and MSA artifacts have long been reported[72,73] from Karungu and Rusinga and Mfangano Islands, but until recently only limited geological mapping and reconstructions of the paleoclimate or paleoenvironment have been conducted. Karungu and Rusinga and Mfangano Islands were originally mapped by Pickford[72] and have been more extensively mapped by Beverly et al.[10,11], Blegen et al.[9], and Tryon et al.[13,66,67].

Tephra deposits can be correlated between sites on the basis of geochemical compositional similarity where they have been dated by multiple radiometric methods[25,32,34]. Four tuffs are used to correlate the sections between Rusinga Island and Karungu: Wakondo, Nyamita, Nyamsingula, and the Bimodal Trachyphonolitic Tuff (BTPT). The Wakondo Tuff is >68±5 ka based on overlying optically stimulated luminescence (OSL) dates and <94.0±3.3 based on the age of the underlying tufa deposits[9,10]. Additional data on the tufas are presented in Beverly et al.[10]. The Nyamita Tuff is the best constrained by OSL dates above and below that indicate deposition at ~49 ka. It is also thick, distinct, and found at almost all Pleistocene sites in this region, making it an ideal datum (Fig. 4.2). The Nyamsingula Tuff and the BTPT, and are both dated between >33 and 49 ka based on their stratigraphic relationship with the underlying Nyamita Tuff and AMS radiocarbon dates on the shells of gastropods that post-depositionally burrowed into the sediment[13,67]. See Blegen et al.[9] for an extensive discussion of tephra correlations and dates.

2. Stratigraphy

Up until ~94 ka riverine tufa deposits were a recurring feature on eastern margin of Lake Victoria, when the system became choked with fluvial sediments and tufa precipitation ceased at ~94 ka [10]. A well-developed paleo-Vertisol with pedogenic slickensides, wedge peds, and smectitic mineralogy overlies these tufa deposits[11]. This paleo-Vertisol was long-lived and formed between ~94 and 49 ka, with the upper age constraint corresponding to deposition of the Nyamita Tuff [9]. Overlying the Nyamita Tuff, one to two paleosols were preserved depending on the stability of the landscape and are identified as paleo-Inceptiols due to their lack of vertic features and angular blocky ped structure and FeMn coatings. Most of these paleo-Inceptisols are also tuffaceous and contain illuviated clay coatings that indicate each paleosol was forming on the landscape for several thousand years[11,74,75]. The paleo-Inceptisols from Kisaaka contain up to 3 to 5% illuviated clay and using the age-estimate model for clay coating accumulation by Ufnar[74] indicates that pedogenesis occurred for ~3 to 7 kyr per paleosol[11], for a total of ~10 kyr of deposition. This may be an overestimation for an East African monsoonal climate because the illuviated clay chronofunctions were developed using deeply weathered, subtropical soils from southeastern Mississippi formed from loess parented material[74]. Radiometric estimates from gastropods on Rusinga and Mfangano Islands[9,66] indicate that the paleo-Inceptisols were formed between 49 and >33 ka, which is consistent with the clay chronofunction estimate. This degree of development of clay coatings also provides evidence that the paleo-Inceptisols were in equilibrium with the climate[11]. Therefore, these paleosols likely represent a time-averaged, but complete record of ~60 kyr between 94 and >33 ka. Therefore, we suggest that Lake Victoria was likely dry for this entire interval and acknowledge that sub-millenial trends are not possible to differentiate in this type of record. Short-term wet periods may not have been recorded by the paleosols, but the record suggests that Lake Victoria was overwhelming dry for most, if not the entire interval.

References

1. Stager, J. C., Ryves, D. B., Chase, B. M. & Pausata, F. S. R. Catastrophic drought in the Afro-Asian monsoon region during Heinrich Event 1. *Science* **331,** 1299–1302 (2011).

2. Nicholson, S. E. in *The limnology, climatology and paleoclimatology of the East African Lakes* (eds. Johnson, T. C. & Odada, E. O.) 25–56 (Gordon and Breach Publishers, 1996).

3. Yin, X. & Nicholson, S. E. The water balance of Lake Victoria. *Hydrological Sciences Journal* **43,** 789–811 (1998).

4. Bootsma, H. a. & Hecky, R. E. A Comparative Introduction to the Biology and Limnology of the African Great Lakes. *J. Great Lakes Res.* **29,** 3–18 (2003).

5. Broecker, W. S., Peteet, D., Hajdas, I., Lin, J. & Clark, E. Antiphasing between rainfall in Africa's Rift Valley and North America's Great Basin. *Quat. Res.* **50,** 12–20 (1998).

6. Milly, P. C. D. Comment on 'Antiphasing between Rainfall in Africa's Rift Valley and North America's Great Basin'. *Quat. Res.* **51,** 104–107 (1999).

7. Bergonzini, L., Richard, Y., Petit, L. & Camberlin, P. Zonal circulations over the Indian and Pacific oceans and the level of Lakes Victoria and Tanganyika. *Int. J. Climatol.* **24,** 1613–1624 (2004).

8. Stager, J. C. & Johnson, T. C. The late Pleistocene desiccation of Lake Victoria and the origin of its endemic biota. *Hydrobiologia* **596,** 5–16 (2008).

9. Blegen, N. *et al.* Distal tephras of the eastern Lake Victoria Basin, equatorial East Africa: correlations, chronology, and a context for early modern humans. *Quarternary Sci. Rev.* (2015).

10. Beverly, E. J. *et al.* Recurrent spring-fed rivers in a Middle to Late Pleistocene semi-arid grassland: Implications for environments of early humans in the Lake Victoria Basin, Kenya. *Sedimentology* (2015). doi:10.1111/sed.12199

11. Beverly, E. J. *et al.* Reconstruction of a semi-arid Late Pleistocene paleocatena from the Lake Victoria region, Kenya. *Quat. Res.* (2015).

12. Faith, J. T. *et al.* Paleoenvironmental context of the Middle Stone Age record from Karungu, Lake Victoria Basin, Kenya, and its implications for human and faunal dispersal in East Africa. *J. Hum. Evol.* **83,** 28–45 (2015).

13. Tryon, C. A. *et al.* Sites on the landscape: Paleoenvironmental context of late Pleistocene archaeological sites from the Lake Victoria basin, equatorial East Africa. *Quat. Int.* **331,** 20–30 (2014).

14. Garrett, N. D. *et al.* Stable isotope paleoecology of late pleistocene middle stone age humans from the equatorial East Africa, Lake Victoria basin, Kenya. *J. Hum. Evol.* **82,** 1–14 (2015).

15. Nordt, L. C. & Driese, S. G. New weathering index improves paleorainfall estimates from Vertisols. *Geology* **38,** 407–410 (2010).

16. Sheldon, N. D., Retallack, G. J. & Tanaka, S. Geochemical climofunctions from North America soils and applications to paleosols across the Eocene-Oligocene Boundary in Oregon. *J. Geol.* **110,** 687–696 (2002).

17. Scholz, C. a *et al.* East African megadroughts between 135 and 75 thousand years ago and bearing on early-modern human origins. *Proc. Natl. Acad. Sci. U. S. A.* **104,** 16416–16421 (2007).

18. Clement, A. C., Hall, A. & Broccoli, A. J. The importance of precessional signals in the tropical climate. *Clim. Dyn.* **22,** 327–341 (2004).

19. Verschuren, D. *et al.* Half-precessional dynamics of monsoon rainfall near the East African Equator. *Nature* **462,** 637–641 (2009).

20. Weldeab, S., Lea, D. W., Schneider, R. R. & Andersen, N. 155,000 years of West African monsoon and ocean thermal evolution. *Science* **316,** 1303–1307 (2007).

21. Bard, E., Rostek, F. & Sonzogni, C. Interhemispheric synchrony of the last deglaciation inferred from alkenone palaeothermometry. *Nature* **385,** 707–710 (1997).

22. Wang, Y. *et al.* Millennial- and orbital-scale changes in the East Asian monsoon over the past 224,000 years. *Nature* **451,** 1090–1093 (2008).

23. Trauth, M. H., Deino, A. L., Bergner, A. G. N. & Strecker, M. R. East African climate change and orbital forcing during the last 175 kyr BP. *Earth Planet. Sci. Lett.* **206,** 297–313 (2003).

24. Moernaut, J. *et al.* The seismic-stratigraphic record of lake-level fluctuations in Lake Challa: Hydrological stability and change in equatorial East Africa over the last 140kyr. *Earth Planet. Sci. Lett.* **290,** 214–223 (2010).

25. Tierney, J. E., Russell, J. M., Sinninghe Damsté, J. S., Huang, Y. & Verschuren, D. Late Quaternary behavior of the East African monsoon and the importance of the Congo Air Boundary. *Quat. Sci. Rev.* **30,** 798–807 (2011).

26. Tierney, J. E. *et al.* Northern hemisphere controls on tropical southeast African climate during the past 60,000 years. *Science (80-.).* **322,** 252–255 (2008).

27. Costa, K., Russell, J., Konecky, B. & Lamb, H. Isotopic reconstruction of the African Humid Period and Congo Air Boundary migration at Lake Tana, Ethiopia. *Quat. Sci. Rev.* **83,** 58–67 (2014).

28. Niang, I. *et al.* in *Climate Change 2014: Impacts, Adaptation, and Vulnerability. Part B: Regional Aspects. Contribution of Working Group II to the Fifth Assessment Report of the Intergovernmental Panel on Climate Change* (eds. Barros, V. R. et al.) 1199–1265 (Cambridge University Press, 2014).

29. Sweagudde, S. M. Lake Victoria ' s Water Budget and the Potential Effects of Climate Change in the 21st Century ↔ Paper presented to the Lake Victoria. *African J. Trop. Hydrobiol. Fish.* **30,** 22–30 (2009).

30. Laskar, J. *et al.* A long-term numerical solution for the insolation quantities of the Earth. *Astron. Astrophys.* **428,** 261–285 (2004).

31. Driese, S. G., Mora, C. I., Stiles, C. A., Joeckel, R. M. & Nordt, L. C. Mass-balance reconstruction of a modern Vertisol: implications for interpreting the geochemistry and burial alteration of paleo-Vertisols. *Geoderma* **95,** 179–204 (2000).

32. Becker, M., LLovel, W., Cazenave, A., Güntner, A. & Crétaux, J. F. Recent hydrological behavior of the East African great lakes region inferred from GRACE, satellite altimetry and rainfall observations. *Comptes Rendus - Geosci.* **342,** 223–233 (2010).

33. Sutcliffe, J. V. & Parks, Y. P. The Hydrology of the Nile. *IAHS Spec. Publ.* **5,** 192 (1999).

34. Shahin, M. *Hydrology of the Nile Basin*. (Elsevier, 1985).

35. Sutcliffe, J. V & Petersen, G. Lake Victoria: derivation of a corrected natural water level series. *Hydrol. Sci. J.* **52,** 1316–1321 (2007).

36. Hurst, H. E. & Phillips, P. *The Nile Basin, vol III. Ten-day mean and monthly mean gauge readings of the Nile and its tributaries*. (Government Press, 1933).

37. Kite, G. W. Recent changes in level of Lake Victoria. *Hydrol. Sci. Bull.* **26,** 233–243 (1981).

38. Kite, G. W. Analysis of Lake Victoria levels. *Hydrol. Sci. J.* **27,** 99–110 (1982).

39. Piper, B. S., Plinston, D. T. & Barton, H. The water balance of Lake Victoria. *Hydrol. Sci. J.* **31,** 25–37 (1986).

40. Ba, M. B. & Nicholson, S. E. Satellite-Derived surface Radiation Budget over the African Continent. Part II: Climatologies of the Various Components. *J. Clim.* **14,** 60–76 (2001).

41. Cogley, J. G. The albedo of water as a function of latitude. *Mon. Weather Rev.* **107,** 775–781 (1979).

42. Budyko, M. I. *Climate and Life*. (Academic Press, 1974).

43. Nicholson, S. E., Yin, X. & Ba, M. B. On the feasibility of using a lake water balance model to infer rainfall: an example from Lake Victoria. *Hydrol. Sci. J.* **45,** 75–95 (2000).

44. East African Meteorological Department. *Part I - Kenya*. *Climatological Statistics for East Africa* (1975).

45. East African Meteorological Department. *Part II Uganda*. *Climatological Statistics for East Africa* (1975).

46. East African Meteorological Department. *Part III - Tanzania*. *Climatological Statistics for East Africa* (1975).

47. Rogers, R. R. & Yau, M. K. *A Short Course in Cloud Physics*. (Butterworth-Heinemann, 1989).

48. Glassy, J. M. & Running, S. W. Validating diurnal climatology logic of the MT-CLIM model across a climatic gradient in Oregon. *Ecol. Appl.* **4,** 248–257 (1994).

49. McJannet, D. L., Webster, I. T. & Cook, F. J. An area-dependent wind function for estimating open water evaporation using land-based meteorological data. *Environ. Model. Softw.* **31,** 76–83 (2012).

50. Monteith, J. & Unsworth, M. *Principles of Environmental Physics*. (Academic Press, 2008).

51. *The Jonglei Canal: Impact and Opportunity*. (Cambridge University Press, 1988).

52. Wigley, T. M. L. & Jones, P. D. Influences of precipitation changes and direct CO2 effects on streamflow. *Nature* **314,** 149–152 (1985).

53. Doornkamp, J. C. & Temple, P. H. Surface, drainage and tectonic instability in part of southern Uganda. *Geogr. J.* **132,** 238–252 (1966).

54. Temple, P. H. Evidence of changes in the level of Lake Victoria and their significance. (University of London, 1966).

55. Talbot, M. R. & Laerdal, T. The late Pleistocene - Holocene palaeolimnology of Lake Victoria, East Africa, based upon elemental and isotopic analyses of sedimentary organic matter. *J. Paleolimnol.* **23,** 141–164 (2000).

56. Johnson, T. C. *et al.* Late Pleistocene dessication of Lake Victoria and rapid evolution of cichlid fishes. *Science (80-.).* **273,** 1091–1093 (1996).

57. Verschuren, D. *et al.* History and timing of human impact on Lake Victoria, East Africa. *Proc. R. Soc. London Biol.* **269,** 289–294 (2002).

58. Boven, A., Pasteels, P., Punzalan, L. E., Yamba, T. K. & Musisi, J. H. Quaternary perpotassic magmatism in Uganda (Toro-Ankole volcanic province): age assessment and significance for magmatic evolution along the East African Rift. *J. African Earth Sci.* **26,** 463–476 (1998).

59. Bishop, W. W. *Pleistocene stratigraphy in Uganda*. *Geological Survey of Uganda Memoir X* (1969).

60. Talbot, M. R. & Williams, M. A. J. in *The Nile: Origin, Environments, Limnology and Human Use* (ed. Dumont, H. J.) **89,** 37–60 (Springer Science + Business Media B.V., 2009).

61. Claussen, M. *et al.* Simulation of an abrupt change in Saharan vegetation in the mid-Holocene. *Geopysical Res. Lett.* **26,** 2037–2040 (1999).

62. Blome, M. W., Cohen, A. S., Tryon, C. A., Brooks, A. S. & Russell, J. The environmental context for the origins of modern human diversity: A synthesis of regional variability in African climate 150,000-30,000 years ago. *J. Hum. Evol.* (2012). doi:10.1016/j.jhevol.2012.01.011

63. Bonnefille, R., Chalié, F., Guiot, J. & Vincens, A. Quantitative estimates of full glacial temperatures in equatorial Africa from palynological data. *Clim. Dyn.* **6,** 251–257 (1992).

64. Bonnefille, R., Roeland, J. C. & Guiot, J. Temperature and rainfall estimates for the past 40,000 years in equatorial Africa. *Nature* **346,** 347–349 (1990).

65. Bonnefille, R. & Chalie, F. Pollen-inferred precipitation time-series from equatorial mountains, Africa, the last 40 kyr B.P. *Glob. Planet. Change* **26,** 25–50 (2000).

66. Tryon, C. a. *et al.* The Pleistocene archaeology and environments of the Wasiriya Beds, Rusinga Island, Kenya. *J. Hum. Evol.* **59,** 657–671 (2010).

67. Tryon, C. A. *et al.* Late Pleistocene artefacts and fauna from Rusinga and Mfangano islands, Lake Victoria, Kenya. *Azania Archaeol. Res. Africa* **47,** 14–38 (2012).

68. Van Plantinga, A. A. Geology of the Late Pleistocene artifact-bearing WAsiriya Beds at the Nyamita locality, Rusinga Island, Kenya. (Baylor Unviersity, 2011).

69. Faith, J. T., Choiniere, J. N., Tryon, C. A., Peppe, D. J. & Fox, D. L. Taxonomic status and paleoecology of Rusingoryx atopocranion (Mammalia, Artiodactyla), an extinct Pleistocene bovid from Rusinga Island, Kenya. *Quat. Res.* **75,** 697–707 (2011).

70. Faith, J. T. *et al.* New perspectives on middle Pleistocene change in the large mammal faunas of East Africa: Damaliscus hypsodon sp. nov. (Mammalia, Artiodactyla) from Lainyamok, Kenya. *Palaeogeogr. Palaeoclimatol. Palaeoecol.* **361-362,** 84–93 (2012).

71. Faith, J. T., Tryon, C. A., Peppe, D. J., Beverly, E. J. & Blegen, N. Biogeographic and Evolutionary Implications of an Extinct Late Pleistocene Impala from the Lake Victoria Basin , Kenya. *J. Mamm. Evol.* **21,** 213–222 (2014).

72. Pickford, M. H. An aberrant new bovid (Mammalia) in subrecent deposits from Rusinga island, Kenya. *Proc. K. Ned. Akad. Van Wet. Ser. B Palaeontol. Geol. Physics, Chem. Anthropol.* **87,** 441–452 (1984).

73. Owen, W. E. *Draft of tentative preliminary report on the July 1937 investigations at Ng'ira Karungu*. (1937).

74. Ufnar, D. Clay coatings from a modern soil chronosequence: A tool for estimating the relative age of well-drained paleosols. *Geoderma* **141,** 181–200 (2007).

75. Soil Survey Staff. *Soil Taxonomy: A Basic System of Soil Classification for Making and Interpreting Soil Surveys*. (USDA NRCS, 1999).

CHAPTER FIVE

Conclusion

Rather than focusing solely on one aspect of the landscape such as paleosols, this research has demonstrated that by analyzing all aspects of a paleolandscape a great deal more information can be recovered. Spring-fed rivers were a recurrent feature on this landscape between 455 and 94 ka when tufa precipitation ceases. The isotopes from these riverine tufas indicate that they precipitated within a C_4 grassland that is supported by isotopes from fossil teeth and pedogenic carbonates (Faith and others, 2015; Garrett and others, 2015). This is very different from the modern landscape with shrubs and trees and suggests that climate was much drier than modern. The disappearance of the tufas indicates that precipitation dropped below a threshold able to sustain the springs (Beverly and others, 2015a). After these tufas disappear, fluvial processes and soil formation dominate the landscape for almost 60 ka (Beverly and others, 2015b).

The number of paleosols varies depending on landscape stability and proximity to the fluvial channel, but at the best-exposed site, Kisaaka, three paleosols are exposed intercalated with tuffs that allow for correlation reconstruction of the landscape as a catena. These oldest paleosol, a paleo-Vertisol, is fertile but has saline-sodic properties that would have affected the types of plants able to grow in this soil. The upper paleosols are both paleo-Inceptisols with Alfisol-like characteristics (illuviated clay). Using the bulk geochemistry from the paleosols, paleoprecipitation can be estimated. The paleoprecipitation does not change statistically through time and the average for this time interval is 0.8 m yr^{-1}. These paleoprecipitation estimates from paleosol sites are spread across a transect of ~55 km and suggest that climate was significantly drier in the Lake Victoria region than modern (1.4 to 1.8 m yr^{-1}) (Yin and Nicholson, 1998).

This paleoprecipitation data is then used in a water budget model to understand how a reduction in precipitation would affect the level of Lake Victoria during the Late Pleistocene. This water budget suggests that Lake Victoria is very sensitive to the evaporation-precipitation balance. The lake has dried up multiple times in the past 20 ka (Johnson and others, 1996; Stager and others, 2002, 2011) and new evidence from the paleosol paleoprecipitation evidence combined with a simple water budget model suggests that it was also dry for most of the Late Pleistocene as the lake cannot be sustained precipitation levels <98% of modern. The desiccation of Lake Victoria between ~94 and >33 ka opens a biogeographic barrier between the eastern and western branches of the rift during a critical interval of human evolution when humans began migrating throughout Africa and into Eurasia.

This model also has repercussions for the future of the East African Community. East Africa is predicted to warm between 1 and 5°C over the next 100 years. This research has shown that temperature has a significant effect on evaporation in the Lake Victoria region and will likely upset the delicate evaporation-precipitation balance. The effect of global warming on precipitation in East Africa is unknown because regional and global climate models disagree on whether precipitation will increase or decrease in the next 100 years. The level of Lake Victoria has been steadily declining since the 1960s (Sweagudde, 2009) and regional climate models predict that precipitation will decrease, but global climate models indicate the precipitation will increase or remain the same (Niang and others, 2014). Regardless, the change in temperature will affect the evaporation and therefore lake level. The maximum rates from this model predict a loss of the Jinja outlet, where most of Uganda's electricity is produced hydroelectrically, within 10 years. Major cities like Entebbe and Kisumu, which depend on Lake Victoria for subsistence and economic resources, could lose access to the lake within 100 years and Kenya could lose access within 400 years. Any decrease in precipitation would exacerbate the rate of decline of modern Lake Victoria similar to what occurred during the post-LGM and Late Pleistocene megadrought interval.

APPENDICES

APPENDIX A

Table A.1: Raw Stable Isotope Data

Sample	$\delta^{13}C$ (‰VPDB)	$\delta^{18}O$ (‰VPDB)	Location	Site	Description
CRJ-11-5A	-6.86	-6.50	Nyamita	Nyamita 5	Stromatolite
CRJ-11-5B	-6.56	-6.62	Nyamita	Nyamita 5	Stromatolite
CRJ-11-5C	-6.79	-6.90	Nyamita	Nyamita 5	Syndepositional cement
CRJ-11-5D	-6.80	-6.98	Nyamita	Nyamita 5	Syndepositional cement
CRJ-11-5E	-6.52	-6.85	Nyamita	Nyamita 5	Syndepositional cement
CRJ-11-10-1	-5.45	-5.12	Nyamita	AV1006	Stromatolite
CRJ-11-10-2	-5.38	-4.87	Nyamita	AV1006	Stromatolite
CRJ-11-10-3	-5.16	-5.89	Nyamita	AV1006	Stromatolite
CRJ-11-10-4	-5.07	-5.49	Nyamita	AV1006	Stromatolite
CRJ-11-10-5	-5.57	-5.45	Nyamita	AV1006	Stromatolite
CRJ-11-10A	-3.22	-5.06	Nyamita	AV1006	Stromatolite
CRJ-11-10B	-3.23	-5.03	Nyamita	AV1006	Stromatolite
CRJ-11-10C	-6.23	-5.77	Nyamita	AV1006	Stromatolite
CRJ-11-10D	-4.79	-4.83	Nyamita	AV1006	Stromatolite
CRJ-11-10E	-5.91	-4.28	Nyamita	AV1006	Stromatolite
CRJ-11-15-1	-6.08	-5.16	Nyamita	AV1006	Stromatolite
CRJ-11-15-2	-5.93	-5.54	Nyamita	AV1006	Stromatolite
CRJ-11-15-3	-5.81	-5.42	Nyamita	AV1006	Stromatolite
CRJ-11-15-4	-5.76	-5.83	Nyamita	AV1006	Stromatolite
CRJ-11-15-5	-6.13	-5.73	Nyamita	AV1006	Stromatolite

Table A.1: (Continued)

Sample	$\delta^{13}C$ (‰VPDB)	$\delta^{18}O$ (‰VPDB)	Location	Site	Description
CRJ-11-15-6	-5.85	-5.67	Nyamita	AV1006	Stromatolite
CRJ-11-15-7	-6.07	-5.77	Nyamita	AV1006	Stromatolite
CRJ-11-15-8	-6.49	-6.07	Nyamita	AV1006	Stromatolite
CRJ-11-15-9	-6.03	-5.55	Nyamita	AV1006	Stromatolite
CRJ-11-15-10	-5.59	-4.81	Nyamita	AV1006	Stromatolite
CRJ-11-15-11	-5.81	-5.18	Nyamita	AV1006	Stromatolite
CRJ-11-15-12	-5.83	-5.55	Nyamita	AV1006	Stromatolite
CRJ-11-15-13	-5.68	-5.34	Nyamita	AV1006	Stromatolite
CRJ-11-15-14	-5.96	-5.01	Nyamita	AV1006	Stromatolite
CRJ-11-15-15	-6.11	-5.19	Nyamita	AV1006	Stromatolite
CRJ-11-15-16	-5.92	-5.27	Nyamita	AV1006	Stromatolite
CRJ-11-15-17	-6.31	-5.66	Nyamita	AV1006	Stromatolite
CRJ-11-15-18	-6.42	-5.97	Nyamita	AV1006	Stromatolite
CRJ-11-15-19	-5.77	-5.47	Nyamita	AV1006	Stromatolite
CRJ-11-15-20	-6.44	-5.47	Nyamita	AV1006	Stromatolite
CRJ-11-15-21	-5.87	-5.31	Nyamita	AV1006	Stromatolite
CRJ-11-15-22	-5.88	-5.48	Nyamita	AV1006	Stromatolite
CRJ-11-15-23	-6.14	-5.50	Nyamita	AV1006	Stromatolite
CRJ-11-15-24	-6.54	-5.58	Nyamita	AV1006	Stromatolite
CRJ-11-15-25	-6.35	-5.58	Nyamita	AV1006	Stromatolite
CRJ-11-15-26	-6.04	-5.51	Nyamita	AV1006	Stromatolite
CRJ-11-15-27	-5.72	-5.40	Nyamita	AV1006	Stromatolite
CRJ-11-15-28	-5.79	-5.36	Nyamita	AV1006	Stromatolite

Table A.1: (Continued)

Sample	$\delta^{13}C$ (‰VPDB)	$\delta^{18}O$ (‰VPDB)	Location	Site	Description
CRJ-11-15-29	-5.48	-5.04	Nyamita	AV1006	Stromatolite
CRJ-11-15-30	-5.38	-5.09	Nyamita	AV1006	Stromatolite
CRJ-11-15-31	-5.47	-4.99	Nyamita	AV1006	Stromatolite
CRJ-11-15-32	-5.52	-4.82	Nyamita	AV1006	Stromatolite
CRJ-11-15-33	-5.59	-5.45	Nyamita	AV1006	Stromatolite
CRJ-11-15-34	-5.69	-5.14	Nyamita	AV1006	Stromatolite
CRJ-11-15-35	-5.67	-5.28	Nyamita	AV1006	Stromatolite
CRJ-11-15-36	-5.45	-5.05	Nyamita	AV1006	Stromatolite
CRJ-11-15-37	-5.73	-5.00	Nyamita	AV1006	Stromatolite
CRJ-11-15-38	-5.77	-4.96	Nyamita	AV1006	Stromatolite
AVP-1	**-6.57**	**-4.44**	**Nyamita**	**AV1006**	**Stromatolite**
AVP-2	**-8.25**	**-4.32**	**Nyamita**	**AV1006**	**Stromatolite**
AVP-3	-4.61	-5.46	Nyamita	AV1006	Stromatolite
AVP-4	-4.08	-5.22	Nyamita	AV1006	Stromatolite
AVP-5	-5.13	-5.08	Nyamita	AV1006	Stromatolite
AVP-6	-5.12	-5.33	Nyamita	AV1006	Stromatolite
AVP-7	-5.59	-5.66	Nyamita	AV1006	Stromatolite
AVP-8	-5.02	-5.52	Nyamita	AV1006	Stromatolite
AVP-9	-5.74	-5.49	Nyamita	AV1006	Stromatolite
AVP-10	-5.97	-5.65	Nyamita	AV1006	Stromatolite
AVP-11	-5.43	-5.57	Nyamita	AV1006	Stromatolite
AVP-12	-6.06	-5.99	Nyamita	AV1006	Stromatolite
AVP-13	-6.29	-5.79	Nyamita	AV1006	Stromatolite

Table A.1: (Continued)

Sample	$\delta^{13}C$ (‰VPDB)	$\delta^{18}O$ (‰VPDB)	Location	Site	Description
AVP-14	-6.17	-5.60	Nyamita	AV1006	Stromatolite
AVP-15	-6.29	-5.80	Nyamita	AV1006	Stromatolite
AVP-16	-6.09	-5.78	Nyamita	AV1006	Stromatolite
AVP-17	-6.00	-5.90	Nyamita	AV1006	Stromatolite
AVP-18	-5.36	-5.86	Nyamita	AV1006	Stromatolite
CRJ-11-14-0	-6.60	-5.76	Nyamita	AV1006	Stromatolite
CRJ-11-14-1	-6.54	-5.60	Nyamita	AV1006	Stromatolite
CRJ-11-14-2	-6.45	-5.68	Nyamita	AV1006	Stromatolite
CRJ-11-14-3	-6.69	-5.52	Nyamita	AV1006	Stromatolite
CRJ-11-14-4	-6.76	-5.51	Nyamita	AV1006	Stromatolite
CRJ-11-14-5	-6.32	-5.37	Nyamita	AV1006	Stromatolite
CRJ-11-14-6	-6.53	-5.31	Nyamita	AV1006	Stromatolite
CRJ-11-14-7	-6.60	-5.73	Nyamita	AV1006	Stromatolite
CRJ-11-14-8	-6.46	-5.54	Nyamita	AV1006	Stromatolite
CRJ-11-14-9	-6.39	-5.59	Nyamita	AV1006	Stromatolite
CRJ-11-14-10	-6.28	-5.84	Nyamita	AV1006	Stromatolite
CRJ-11-14-11	-6.64	-5.76	Nyamita	AV1006	Stromatolite
CRJ-11-14-12	-6.49	-5.44	Nyamita	AV1006	Stromatolite
CRJ-11-14-13	-6.42	-5.08	Nyamita	AV1006	Stromatolite
CRJ-11-14-14	-6.05	-5.43	Nyamita	AV1006	Stromatolite
CRJ-11-14-15	-6.17	-5.56	Nyamita	AV1006	Stromatolite
CRJ-11-14-16	-5.95	-5.42	Nyamita	AV1006	Stromatolite
CRJ-11-14-17	-6.17	-5.70	Nyamita	AV1006	Stromatolite

Table A.1: (Continued)

Sample	$\delta^{13}C$ (‰VPDB)	$\delta^{18}O$ (‰VPDB)	Location	Site	Description
CRJ-11-14-18	-5.45	-4.84	Nyamita	AV1006	Stromatolite
CRJ-11-14-19	-4.54	-5.23	Nyamita	AV1006	Stromatolite
CRJ-11-14-20	-3.56	-4.50	Nyamita	AV1006	Stromatolite
CRJ-11-14-21	-4.51	-5.17	Nyamita	AV1006	Stromatolite
CRJ-11-14-22	-4.54	-5.27	Nyamita	AV1006	Stromatolite
CRJ-11-14-23	-4.58	-5.43	Nyamita	AV1006	Stromatolite
CRJ-11-14-24	-4.91	-5.52	Nyamita	AV1006	Stromatolite
CRJ-11-14-25	-6.06	-6.22	Nyamita	AV1006	Stromatolite
CRJ-11-14-26	-5.67	-6.81	Nyamita	AV1006	Stromatolite
CRJ-11-14-27	-5.50	-5.04	Nyamita	AV1006	Stromatolite
CRJ-11-14-28	-5.29	-5.18	Nyamita	AV1006	Stromatolite
CRJ-11-14-29	-5.65	-5.79	Nyamita	AV1006	Stromatolite
CRJ-11-14-30	-5.72	-5.55	Nyamita	AV1006	Stromatolite
CRJ-11-14-31	-5.88	-4.73	Nyamita	AV1006	Stromatolite
CRJ-11-14-32	-5.69	-4.49	Nyamita	AV1006	Stromatolite
CRJ-11-14-33	-6.09	-5.78	Nyamita	AV1006	Stromatolite
CRJ-11-14-34	-6.59	-5.14	Nyamita	AV1006	Stromatolite
CRJ-11-14-35	**-6.33**	**-11.76**	**Nyamita**	**AV1006**	**Stromatolite**
CRJ-11-14-36	-6.43	-5.60	Nyamita	AV1006	Stromatolite
CRJ-11-14-37	-6.17	-4.75	Nyamita	AV1006	Stromatolite
CRJ-11-14-38	-6.28	-4.81	Nyamita	AV1006	Stromatolite
CRJ-11-14-39	-6.55	-4.88	Nyamita	AV1006	Stromatolite
CRJ-11-22A	-9.96	-7.27	Nyamita	Nyamita 22	Syndepositional cement

Table A.1: (Continued)

Sample	$\delta^{13}C$ (‰VPDB)	$\delta^{18}O$ (‰VPDB)	Location	Site	Description
CRJ-11-22B	-9.21	-4.78	Nyamita	Nyamita 22	Syndepositional cement
CRJ-11-22C	-9.63	-5.86	Nyamita	Nyamita 22	Syndepositional cement
CRJ-11-22D	-9.17	-5.29	Nyamita	Nyamita 22	Pisoids
CRJ-11-22E	-9.37	-5.61	Nyamita	Nyamita 22	Pisoids
CRJ-11-22F	-9.33	-5.58	Nyamita	Nyamita 22	Pisoids
CRJ-11-22G	-9.40	-4.53	Nyamita	Nyamita 22	Syndepositional cement
CRJ-11-22H	-9.54	-4.97	Nyamita	Nyamita 22	Syndepositional cement
CRJ-11-25A	-10.18	-5.89	Nyamita	Nyamita 25	Pisoids
CRJ-11-25B	-10.10	-6.28	Nyamita	Nyamita 25	Pisoids
CRJ-11-25C	-9.77	-5.78	Nyamita	Nyamita 25	Pisoids
CRJ-11-25D	-9.47	-6.00	Nyamita	Nyamita 25	Syndepositional cement
CRJ-11-25E	-9.78	-5.83	Nyamita	Nyamita 25	Syndepositional cement
CRJ-11-25F	-9.99	-5.77	Nyamita	Nyamita 25	Syndepositional cement
13-KIS-TS1A	-4.70	-2.96	Kisaaka	Kisaaka 20	Syndepositional cement
13-KIS-TS1B	-4.65	-2.79	Kisaaka	Kisaaka 20	Syndepositional cement
13-KIS-TS1C	-4.20	-3.25	Kisaaka	Kisaaka 20	Syndepositional cement
13-KIS-TS1D	-11.46	-5.04	Kisaaka	Kisaaka 20	Nodule
13-KIS-TS1E	-11.12	-4.83	Kisaaka	Kisaaka 20	Nodule
13-KIS-TS1F	-11.07	-5.17	Kisaaka	Kisaaka 20	Nodule
13-KIS-TS1G	-4.75	-2.64	Kisaaka	Kisaaka 20	Syndepositional cement
13-KIS-TS1H	-5.40	-4.73	Kisaaka	Kisaaka 20	Syndepositional cement
13-KIS-TS2A	-5.11	-3.01	Kisaaka	Kisaaka 20	Reworked clast
13-KIS-TS2B	-5.41	-2.81	Kisaaka	Kisaaka 20	Reworked clast

Table A.1: (Continued)

Sample	$\delta^{13}C$ (‰VPDB)	$\delta^{18}O$ (‰VPDB)	Location	Site	Description
13-KIS-TS2C	-4.55	-2.59	Kisaaka	Kisaaka 20	Reworked clast
13-KIS-TS2D	-4.59	-2.76	Kisaaka	Kisaaka 20	Syndepositional cement
13-KIS-TS2E	-4.42	-3.18	Kisaaka	Kisaaka 20	Syndepositional cement
13-KIS-TS2F	-5.27	-2.46	Kisaaka	Kisaaka 20	Syndepositional cement
13-KIS-TS2G	-5.21	-2.55	Kisaaka	Kisaaka 20	Syndepositional cement
13-KIS-TS3A	-2.84	-2.52	Kisaaka	Kisaaka 20	Syndepositional cement
13-KIS-TS3B	-4.67	-3.26	Kisaaka	Kisaaka 20	Syndepositional cement
13-KIS-TS3C	-6.11	-3.88	Kisaaka	Kisaaka 20	Syndepositional cement
13-KIS-TS3D	-2.46	-2.66	Kisaaka	Kisaaka 20	Syndepositional cement
13-KIS-TS3E	-10.57	-5.09	Kisaaka	Kisaaka 20	Nodule
13-KIS-TS3F	-10.28	-4.92	Kisaaka	Kisaaka 20	Nodule
13-KIS-TS3G	-10.59	-5.31	Kisaaka	Kisaaka 20	Nodule
13-KIS-TS13A	-1.30	-3.66	Kisaaka	Kisaaka 20	Rhizolith
13-KIS-TS13B	-0.85	-3.49	Kisaaka	Kisaaka 20	Rhizolith
13-KIS-TS13C	-1.19	-3.70	Kisaaka	Kisaaka 20	Rhizolith
13-KIS-TS13D	-2.93	-3.79	Kisaaka	Kisaaka 20	Syndepositional cement
13-KIS-TS13E	-2.62	-3.64	Kisaaka	Kisaaka 20	Syndepositional cement
13-KIS-TS13F	-1.98	-3.71	Kisaaka	Kisaaka 20	Syndepositional cement
13-KIS-TS13G	-2.43	-3.98	Kisaaka	Kisaaka 20	Nodule
13-AR-TS1-0	-3.85	-3.35	Aringo	Aringo 9	Stromatolite
13-AR-TS1-1	-3.61	-3.60	Aringo	Aringo 9	Stromatolite
13-AR-TS1-2	-3.18	-3.48	Aringo	Aringo 9	Stromatolite
13-AR-TS1-3	-4.01	-5.65	Aringo	Aringo 9	Stromatolite

Table A.1: (Continued)

Sample	**$\delta^{13}C$ (‰VPDB)**	**$\delta^{18}O$ (‰VPDB)**	**Location**	**Site**	**Description**
13-AR-TS1-4	-4.47	-3.81	Aringo	Aringo 9	Stromatolite
13-AR-TS1-5	-3.95	-3.55	Aringo	Aringo 9	Stromatolite
13-AR-TS1-6	-5.41	-4.12	Aringo	Aringo 9	Stromatolite
13-AR-TS1-7	-3.80	-3.67	Aringo	Aringo 9	Stromatolite
13-AR-TS1-8	-3.51	-3.61	Aringo	Aringo 9	Stromatolite
13-AR-TS1-9	-3.28	-3.32	Aringo	Aringo 9	Stromatolite
13-AR-TS1-10	-3.33	-3.77	Aringo	Aringo 9	Stromatolite
13-AR-TS1-11	-3.79	-4.01	Aringo	Aringo 9	Stromatolite
13-AR-TS1-12	-3.72	-6.45	Aringo	Aringo 9	Stromatolite
13-AR-TS1-13	*-3.92*	*-5.74*	*Aringo*	*Aringo 9*	*Stromatolite*
13-AR-TS1-14	-3.07	-4.55	Aringo	Aringo 9	Stromatolite
13-AR-TS1-15	-3.45	-3.44	Aringo	Aringo 9	Stromatolite
13-AR-TS1-16	-3.52	-5.00	Aringo	Aringo 9	Stromatolite
13-AR-TS1-17	-3.21	-3.78	Aringo	Aringo 9	Stromatolite
13-AR-TS1-18	-3.47	-4.02	Aringo	Aringo 9	Stromatolite
13-AR-TS1-19	-3.58	-3.68	Aringo	Aringo 9	Stromatolite
13-AR-TS1-20	-3.97	-3.27	Aringo	Aringo 9	Stromatolite
13-AR-TS1-21	-4.26	-4.01	Aringo	Aringo 9	Stromatolite
13-AR-TS1-22	-4.18	-3.79	Aringo	Aringo 9	Stromatolite
13-AR-TS1-23	-3.55	-3.84	Aringo	Aringo 9	Stromatolite
13-AR-TS1-24	-3.39	-4.23	Aringo	Aringo 9	Stromatolite
13-AR-TS1-25	-3.51	-4.31	Aringo	Aringo 9	Stromatolite
13-AR-TS1-26	-3.30	-4.39	Aringo	Aringo 9	Stromatolite

Table A.1: (Continued)

Sample	$\delta^{13}C$ (‰VPDB)	$\delta^{18}O$ (‰VPDB)	Location	Site	Description
13-AR-TS1-27	-2.64	-3.70	Aringo	Aringo 9	Stromatolite
13-AR-TS1-28	-2.81	-3.47	Aringo	Aringo 9	Stromatolite
13-AR-TS1-29	-2.45	-3.16	Aringo	Aringo 9	Stromatolite
13-AR-TS1-30	-3.26	-3.79	Aringo	Aringo 9	Stromatolite
13-AR-TS1-31	-3.32	-3.81	Aringo	Aringo 9	Stromatolite
13-AR-TS1-32	-3.34	-3.14	Aringo	Aringo 9	Stromatolite
13-AR-TS1-33	-3.12	-3.48	Aringo	Aringo 9	Stromatolite
13-AR-TS1-34	-3.39	-3.44	Aringo	Aringo 9	Stromatolite
13-AR-TS1-35	-3.82	-3.44	Aringo	Aringo 9	Stromatolite
13-AR-TS1-36	*-3.72*	*-8.51*	*Aringo*	*Aringo 9*	*Stromatolite*
13-AR-TS1-37	-4.04	-3.94	Aringo	Aringo 9	Stromatolite
13-AR-TS1-38	-4.56	-3.26	Aringo	Aringo 9	Stromatolite
13-AR-TS1-39	-4.52	-3.61	Aringo	Aringo 9	Stromatolite
13-AR-TS1-40	-4.84	-3.31	Aringo	Aringo 9	Stromatolite
13-AR-TS1-41	-3.72	-3.75	Aringo	Aringo 9	Stromatolite
13-AR-TS1-42	-4.23	-3.97	Aringo	Aringo 9	Stromatolite
13-AR-TS1-43	-3.61	-4.16	Aringo	Aringo 9	Stromatolite
13-AR-TS1-44	-3.44	-4.02	Aringo	Aringo 9	Stromatolite
13-AR-TS1-45	-3.54	-3.87	Aringo	Aringo 9	Stromatolite
13-AR-TS1-46	-3.68	-3.52	Aringo	Aringo 9	Stromatolite
13-AR-TS1-47	-2.26	-2.78	Aringo	Aringo 9	Stromatolite
13-AR-TS1-48	-2.82	-3.05	Aringo	Aringo 9	Stromatolite
13-AR-TS1-49	-2.50	-3.34	Aringo	Aringo 9	Stromatolite

Table A.1: (Continued)

Sample	**$\delta^{13}C$ (‰VPDB)**	**$\delta^{18}O$ (‰VPDB)**	**Location**	**Site**	**Description**
13-AR-TS1-50	-2.95	-3.56	Aringo	Aringo 9	Stromatolite
13-AR-TS1-51	-2.80	-3.66	Aringo	Aringo 9	Stromatolite
13-AR-TS1-52	-2.80	-3.45	Aringo	Aringo 9	Stromatolite
13-AR-TS1-53	-3.20	-3.64	Aringo	Aringo 9	Stromatolite
13-AR-TS1-54	-4.17	-7.04	Aringo	Aringo 9	Stromatolite
13-AR-TS2-0	-3.37	-3.68	Aringo	Aringo 9	Stromatolite
13-AR-TS2-1	*-4.30*	*-5.96*	*Aringo*	*Aringo 9*	*Stromatolite*
13-AR-TS2-2	-3.89	-4.79	Aringo	Aringo 9	Stromatolite
13-AR-TS2-3	-4.24	-3.66	Aringo	Aringo 9	Stromatolite
13-AR-TS2-4	-3.08	-3.20	Aringo	Aringo 9	Stromatolite
13-AR-TS2-5	-3.48	-2.97	Aringo	Aringo 9	Stromatolite
13-AR-TS2-6	-3.34	-3.29	Aringo	Aringo 9	Stromatolite
13-AR-TS2-7	-3.04	-3.46	Aringo	Aringo 9	Stromatolite
13-AR-TS2-8	-2.70	-3.17	Aringo	Aringo 9	Stromatolite
13-AR-TS2-9	-3.30	-3.37	Aringo	Aringo 9	Stromatolite
13-AR-TS2-10	-3.37	-3.63	Aringo	Aringo 9	Stromatolite
13-AR-TS2-11	-3.55	-3.10	Aringo	Aringo 9	Stromatolite
13-AR-TS2-12	-2.41	-3.03	Aringo	Aringo 9	Stromatolite
13-AR-TS2-13	-2.82	-3.31	Aringo	Aringo 9	Stromatolite
13-AR-TS2-14	-2.92	-2.81	Aringo	Aringo 9	Stromatolite
13-AR-TS2-15	-3.23	-3.18	Aringo	Aringo 9	Stromatolite
13-AR-TS2-16	-3.16	-2.98	Aringo	Aringo 9	Stromatolite
13-AR-TS5-0	-2.37	-3.74	Aringo	Aringo 9	Stromatolite

Table A.1: (Continued)

Sample	$\delta^{13}C$ (‰VPDB)	$\delta^{18}O$ (‰VPDB)	Location	Site	Description
13-AR-TS5-1	-2.03	-4.82	Aringo	Aringo 9	Stromatolite
13-AR-TS5-2	-3.97	-3.82	Aringo	Aringo 9	Stromatolite
13-AR-TS5-3	-4.36	-4.57	Aringo	Aringo 9	Stromatolite
13-AR-TS5-4	-3.64	-3.70	Aringo	Aringo 9	Stromatolite
13-AR-TS5-5	-2.93	-5.19	Aringo	Aringo 9	Stromatolite
13-AR-TS5-6	-1.09	-4.10	Aringo	Aringo 9	Stromatolite
13-AR-TS5-7	-2.63	-3.04	Aringo	Aringo 9	Stromatolite
13-AR-TS5-8	-2.54	-3.12	Aringo	Aringo 9	Stromatolite
13-AR-TS5-9	-4.11	-2.88	Aringo	Aringo 9	Stromatolite
13-AR-TS5-10	-3.71	-3.76	Aringo	Aringo 9	Stromatolite
13-AR-TS5-11	-3.14	-3.42	Aringo	Aringo 9	Stromatolite
13-AR-TS5-12	-3.17	-3.48	Aringo	Aringo 9	Stromatolite
13-AR-TS5-13	-3.79	-3.78	Aringo	Aringo 9	Stromatolite
13-AR-TS5-14	-3.36	-3.90	Aringo	Aringo 9	Stromatolite
13-AR-TS5-15	-1.96	-4.49	Aringo	Aringo 9	Stromatolite
13-AR-TS5-16	-2.19	-3.75	Aringo	Aringo 9	Stromatolite
13-AR-TS5-17	-2.20	-3.61	Aringo	Aringo 9	Stromatolite
13-AR-TS5-18	-2.37	-3.84	Aringo	Aringo 9	Stromatolite
13-AR-TS5-19	-2.57	-3.40	Aringo	Aringo 9	Stromatolite
13-AR-TS5-20	-2.82	-4.22	Aringo	Aringo 9	Stromatolite
13-AR-TS5-21	-2.53	-3.56	Aringo	Aringo 9	Stromatolite
13-AR-TS5-22	-3.21	-3.42	Aringo	Aringo 9	Stromatolite
13-AR-TS5-23	-2.54	-3.23	Aringo	Aringo 9	Stromatolite

Table A.1: (Continued)

Sample	$\delta^{13}C$ (‰VPDB)	$\delta^{18}O$ (‰VPDB)	Location	Site	Description
13-AR-TS5-24	-2.45	-3.13	Aringo	Aringo 9	Stromatolite
13-AR-TS5-25	-2.53	-3.44	Aringo	Aringo 9	Stromatolite
13-AR-TS5-26	-3.20	-3.96	Aringo	Aringo 9	Stromatolite
13-AR-TS5-27	-3.46	-3.65	Aringo	Aringo 9	Stromatolite
13-AR-TS5-28	-4.13	-3.92	Aringo	Aringo 9	Stromatolite
13-AR-TS5-29	-3.77	-4.73	Aringo	Aringo 9	Stromatolite
13-AR-TS5-30	-3.46	-3.67	Aringo	Aringo 9	Stromatolite
13-AR-TS5-31	-2.79	-3.58	Aringo	Aringo 9	Stromatolite
13-AR-TS5-32	-1.16	-3.09	Aringo	Aringo 9	Stromatolite
13-AR-TS5-33	-1.21	-3.13	Aringo	Aringo 9	Stromatolite
13-AR-TS5-34	-1.59	-3.45	Aringo	Aringo 9	Stromatolite
13-AR-TS5-35	-2.97	-3.33	Aringo	Aringo 9	Stromatolite
13-AR-TS5-36	-1.65	-3.69	Aringo	Aringo 9	Stromatolite
13-AR-TS5-37	-2.66	-3.49	Aringo	Aringo 9	Stromatolite
13-AR-TS5-38	-1.99	-3.26	Aringo	Aringo 9	Stromatolite
13-AR-TS5-39	-2.98	-3.43	Aringo	Aringo 9	Stromatolite
13-AR-TS5-40	-4.05	-3.18	Aringo	Aringo 9	Stromatolite
13-OB-TS1A	-7.34	-4.58	Obware	Obware 1	Syndepositional cement
13-OB-TS1B	-7.07	-4.24	Obware	Obware 1	Syndepositional cement
13-OB-TS1C	-7.16	-4.82	Obware	Obware 1	Syndepositional cement
13-OB-TS2A	-7.13	-3.97	Obware	Obware 1	Syndepositional cement
13-OB-TS2B	-6.89	-4.62	Obware	Obware 1	Syndepositional cement

Table A.1: (Continued)

Sample	$\delta^{13}C$ (‰VPDB)	$\delta^{18}O$ (‰VPDB)	Location	Site	Description
13-OB-TS2C	-8.63	-4.31	Obware	Obware 1	Syndepositional cement

Those in **bold** are recrystallized and therefore were not used in any analysis.
Those in *italics* not included because of low CO2 peaks during analysis.

APPENDIX B

Table B.1: GPS coordinates of geologic localities

Locality	Latitude	Longitude	Elevation (m)
Kisaaka 11	-0.803438695	34.140071	1176
Kisaaka 12	-0.802341085	34.141207	1173
Kisaaka 13	-0.805622935	34.137066	1165
Kisaaka 13B	-0.806530947	34.135932	1148
Kisaaka 13D	-0.806013364	34.137386	1178
Kisaaka 14	-0.804410828	34.138431	1174
Kisaaka 14A	-0.804667482	34.138127	1160
Kisaaka 15	-0.803894168	34.139335	1182
Kisaaka 20	-0.805907082	34.136554	1152
Kisaaka 3A	-0.810143128	34.130270	1158
Kisaaka 4F	-0.809698049	34.131172	1119
Kisaaka 7C	-0.807418087	34.134296	1165
KRL	-0.807378357	34.133744	1162
Kisaaka 8A	-0.807754202	34.133614	1173
Kisaaka 9A	-0.806388622	34.133602	1174
Datum: WGS 84			

APPENDIX C

Table C.1: Raw Bulk Geochemical Data

Depth (cm)	Site	Unit	Paleosol Horizon	Sample	Ba (ppm)	Ce (ppm)	Cr (ppm)	Cs (ppm)	Dy (ppm)	Eu (ppm)	Ga (ppm)	Gd (ppm)
0	Kisaaka 4F	Paleosol 3	Bkss1b3	13-KIS-57	796	281	90	1.34	11.5	4.06	26.1	14.65
10	Kisaaka 4F	Paleosol 3	Bkss2b3	13-KIS-58	1460	283	100	1.47	10.85	4.03	29.5	14.3
20	Kisaaka 4F	Paleosol 3	Bkss2b3	13-KIS-59	752	295	100	1.49	11.15	4.12	29.8	14.9
30	Kisaaka 4F	Paleosol 3	Bkss2b3	13-KIS-60	863	294	90	1.43	11.3	4.32	29.3	14.75
40	Kisaaka 4F	Paleosol 3	Bkss3b3	13-KIS-61	600	291	100	1.45	11.35	4.18	29.1	14.9
50	Kisaaka 4F	Paleosol 3	Bkss3b3	13-KIS-62	2220	248	80	1.26	10.05	3.66	24.3	12.65
60	Kisaaka 4F	Paleosol 3	Bkss3b3	13-KIS-63	608	302	100	1.37	11	4.12	28.9	14.45
70	Kisaaka 4F	Paleosol 3	Bkss3b3	13-KIS-64	1230	294	90	1.4	11.25	4.22	27.9	14.05
80	Kisaaka 4F	Paleosol 3	Bkss3b3	13-KIS-65	998	308	90	1.39	11.15	4.29	28.5	14.7
90	Kisaaka 4F	Paleosol 3	Bkss3b3	13-KIS-66	1400	308	100	1.33	11.2	4.26	28.4	14.85
100	Kisaaka 4F	Paleosol 3	Bkss3b3	13-KIS-67	814	337	100	1.33	11.55	4.47	29.2	15.1
110	Kisaaka 4F	Paleosol 3	Bkss4b3	13-KIS-68	1965	333	100	1.31	12.05	4.38	28.5	15.2
120	Kisaaka 4F	Paleosol 3	Bkss4b3	13-KIS-69	886	352	130	1.26	12.05	4.46	28.7	15.95
130	Kisaaka 4F	Paleosol 3	BCkb3	13-KIS-70	5870	363	120	1.15	12.2	4.62	28	16.05
0	Kisaaka 10	Paleosol 3	ABb3	12-KIS-25	522	241	80	1.42	12.55	3.59	29.9	15.5
10	Kisaaka 10	Paleosol 3	Bkb3	12-KIS-24	501	244	90	1.38	11	3.48	26.3	14.2
20	Kisaaka 10	Paleosol 3	Bkb3	12-KIS-23	541	259	90	1.41	11.4	4.01	27.3	15.35
30	Kisaaka 10	Paleosol 3	Bkb3	12-KIS-22	2360	258	90	1.38	11.25	3.85	26.6	14.95
40	Kisaaka 10	Paleosol 3	Bkb3	12-KIS-21	515	260	90	1.36	11.4	3.91	27.8	15.4
50	Kisaaka 10	Paleosol 3	Bkb3	12-KIS-20	653	268	100	1.38	11.3	3.97	27.1	14.9

Table C.1: (Continued)

Depth (cm)	Site	Unit	Paleosol Horizon	Sample	Ba (ppm)	Ce (ppm)	Cr (ppm)	Cs (ppm)	Dy (ppm)	Eu (ppm)	Ga (ppm)	Gd (ppm)
60	Kisaaka 10	Paleosol 3	Bkss1b3	12-KIS-19	539	264	100	1.37	11.2	3.91	26.7	14.95
70	Kisaaka 10	Paleosol 3	Bkss1b3	12-KIS-18	582	261	90	1.32	11.7	3.97	26.2	15.35
80	Kisaaka 10	Paleosol 3	Bkss1b3	12-KIS-17	489	252	90	1.3	10.65	3.69	25	14.05
90	Kisaaka 10	Paleosol 3	Bkss1b3	12-KIS-16	517	260	90	1.31	10.85	3.78	26.2	14.5
100	Kisaaka 10	Paleosol 3	Bkss1b3	12-KIS-15	511	257	100	1.32	10.8	3.92	25.5	15.05
110	Kisaaka 10	Paleosol 3	Bkss1b3	12-KIS-14	525	266	100	1.3	11	4.03	26	15.1
120	Kisaaka 10	Paleosol 3	Bkss2b3	12-KIS-13	514	267	100	1.28	11.3	4.13	25.7	15.05
130	Kisaaka 10	Paleosol 3	Bkss2b3	12-KIS-12	501	262	90	1.25	11.1	4.06	25	14.9
140	Kisaaka 10	Paleosol 3	Bkss2b3	12-KIS-11	514	272	100	1.26	10.8	4.01	25.7	15
150	Kisaaka 10	Paleosol 3	Bkss2b3	12-KIS-10	555	267	100	1.21	10.8	3.95	24.8	14.3
160	Kisaaka 10	Paleosol 3	Bkss2b3	12-KIS-9	481	263	100	1.19	10.7	3.91	24.5	14.45
170	Kisaaka 10	Paleosol 3	Bkss2b3	12-KIS-8	519	269	90	1.21	10.6	3.9	24.4	14.6
180	Kisaaka 10	Paleosol 3	Bkss3b3	12-KIS-7	537	259	100	1.16	10.75	3.94	24.5	14.6
190	Kisaaka 10	Paleosol 3	Bkss3b3	12-KIS-6	499	264	110	1.16	10.8	3.94	24.1	14.7
200	Kisaaka 10	Paleosol 3	Bkss3b3	12-KIS-5	500	272	100	1.17	11.05	3.97	25.1	14.5
210	Kisaaka 10	Paleosol 3	Bkss3b3	12-KIS-4	504	275	100	1.12	10.3	3.86	23.7	14.35
220	Kisaaka 10	Paleosol 3	Bkss3b3	12-KIS-3	469	265	100	1.13	10.4	3.83	24.1	14.15
230	Kisaaka 10	Paleosol 3	Bkss3b3	12-KIS-2	897	265	110	1.13	10.5	3.91	24.1	14.2
240	Kisaaka 10	Paleosol 3	Bkss3b3	12-KIS-1	755	257	110	1.08	10.55	3.8	23.3	13.85
0	Kisaaka 10	Paleosol 2	Btkb2	12-KIS-33	538	260	70	1.49	12.55	3.11	29.1	15.15
10	Kisaaka 10	Paleosol 2	Btkb2	12-KIS-32	511	244	70	1.57	12.25	3.31	30.2	15.35
20	Kisaaka 10	Paleosol 2	Btkb2	12-KIS-31	460	233	70	1.58	11.85	3.08	30.9	14.85
30	Kisaaka 10	Paleosol 2	Btkb2	12-KIS-30	467	233	70	1.53	12.15	3.06	30.8	14.7
40	Kisaaka 10	Paleosol 2	Btkb2	12-KIS-29	395	227	60	1.56	12.15	2.85	30	14.25

Table C.1: (Continued)

Depth (cm)	Site	Unit	Paleosol Horizon	Sample	Ba (ppm)	Ce (ppm)	Cr (ppm)	Cs (ppm)	Dy (ppm)	Eu (ppm)	Ga (ppm)	Gd (ppm)
0	Kisaaka 10	Paleosol 1	Btk1b1	12-KIS-58	1200	192.5	50	1.06	8.39	2.64	21.3	10.5
10	Kisaaka 10	Paleosol 1	Btk1b1	12-KIS-57	1780	223	50	1.17	9.59	3.08	23.6	12.05
20	Kisaaka 10	Paleosol 1	Btk1b1	12-KIS-56	1295	233	60	1.22	10.3	3.34	24.4	12.7
30	Kisaaka 10	Paleosol 1	Btk1b1	12-KIS-55	1425	254	60	1.29	10.7	3.59	26.1	13.05
40	Kisaaka 10	Paleosol 1	Btk1b1	12-KIS-54	1005	250	60	1.29	10.6	3.53	26.2	13.35
50	Kisaaka 10	Paleosol 1	Btk1b1	12-KIS-53	1020	248	60	1.28	10.65	3.42	25.6	13
60	Kisaaka 10	Paleosol 1	Btk1b1	12-KIS-52	1035	243	60	1.22	10.65	3.4	24.9	12.9
70	Kisaaka 10	Paleosol 1	Btk1b1	12-KIS-51	1040	246	60	1.24	10.45	3.3	25.4	12.7
90	Kisaaka 10	Paleosol 1	Btk1b1	12-KIS-48	1025	258	60	1.3	10.6	3.39	26.8	12.9
100	Kisaaka 10	Paleosol 1	Btk1b1	12-KIS-47	1380	268	70	1.19	10.95	3.48	26.2	13.25
120	Kisaaka 10	Paleosol 1	Btk1b1	12-KIS-46	1175	264	70	1.23	10.8	3.54	26.1	13.45
130	Kisaaka 10	Paleosol 1	Btk2b1	12-KIS-45	1450	290	70	1.27	11.35	3.72	27	14.15
140	Kisaaka 10	Paleosol 1	Btk2b1	12-KIS-44	1055	259	70	1.28	10.85	3.58	27	13.6
150	Kisaaka 10	Paleosol 1	Btk2b1	12-KIS-42	1040	283	90	1.27	11.4	3.97	27.8	14.25
160	Kisaaka 10	Paleosol 1	Btk2b1	12-KIS-41	1530	267	80	1.27	10.7	3.72	26.6	13.65
170	Kisaaka 10	Paleosol 1	Btk2b1	12-KIS-40	1020	265	80	1.25	10.6	3.63	25.8	13.45
180	Kisaaka 10	Paleosol 1	Btk2b1	12-KIS-39	961	269	80	1.31	10.65	3.86	27.7	13.45
190	Kisaaka 10	Paleosol 1	Btk2b1	12-KIS-38	840	257	80	1.31	10.55	3.69	27.8	13.35
200	Kisaaka 10	Paleosol 1	Btk2b1	12-KIS-37	823	247	80	1.33	11.6	3.56	27.5	15.05
210	Kisaaka 10	Paleosol 1	Btk2b1	12-KIS-36	925	259	90	1.33	11.65	3.66	27.2	15
220	Kisaaka 10	Paleosol 1	BCb1	12-KIS-35	746	265	90	1.34	11.65	3.6	28.5	14.7
0	Kisaaka 13	Paleosol 1	ABkb1	13-KIS-2	794	234	50	1.29	10.7	3.12	23.1	12.5
10	Kisaaka 13	Paleosol 1	ABkb1	13-KIS-3	848	250	60	1.33	11.55	3.53	24.8	13.7
20	Kisaaka 13	Paleosol 1	Btk1b1	13-KIS-4	865	251	60	1.5	11.05	3.27	25.8	13.5

Table C.1: (Continued)

Depth (cm)	Site	Unit	Paleosol Horizon	Sample	Ba (ppm)	Ce (ppm)	Cr (ppm)	Cs (ppm)	Dy (ppm)	Eu (ppm)	Ga (ppm)	Gd (ppm)
30	Kisaaka 13	Paleosol 1	Btk1b1	13-KIS-5	708	227	60	1.59	11.15	3.17	26.6	13.1
40	Kisaaka 13	Paleosol 1	Btk1b1	13-KIS-6	651	245	60	1.64	11.35	3.38	27.2	14.35
50	Kisaaka 13	Paleosol 1	Btk2b1	13-KIS-7	927	268	60	1.6	11.8	3.38	27.5	14.45
60	Kisaaka 13	Paleosol 1	Btk2b1	13-KIS-8	657	263	60	1.66	12.1	3.38	27	14.25
65	Kisaaka 13	Paleosol 1	Btk2b1	13-KIS-9	560	260	60	1.71	12	3.43	27	14.3
70	Kisaaka 13	Paleosol 1	Btk2b1	13-KIS-10	500	272	60	1.88	12.55	3.27	26.5	14.95
80	Kisaaka 13	Paleosol 1	BCtb1	13-KIS-11	489	288	60	2.02	13.25	3.38	28.1	15.4
90	Kisaaka 13	Paleosol 1	BCtb1	13-KIS-12	516	296	60	2.06	13.95	3.23	29.1	15.75
100	Kisaaka 13	Paleosol 1	BCtb1	13-KIS-13	452	298	60	2.12	14.85	3.16	30.1	16.45
110	Kisaaka 13	Paleosol 1	BCtb1	13-KIS-14	508	297	60	2.15	14.7	3.3	29.8	16.35
120	Kisaaka 13	Paleosol 1	BCtb1	13-KIS-15	943	277	60	2.04	12.8	3.29	27.7	15.2
140	Kisaaka 13	Paleosol 1	BCtb1	13-KIS-17	845	256	70	1.84	11.45	3.35	24.1	14.15
150	Kisaaka 13	Paleosol 1	BCtb1	13-KIS-18	743	266	70	1.94	11.65	3.45	25.8	13.35
0	Kisaaka 13	Paleosol 2	ABk1b2	13-KIS-20	563	270	70	1.81	12.15	3.44	25.7	14.55
10	Kisaaka 13	Paleosol 2	Btk1b2	13-KIS-21	458	285	60	1.87	12.15	3.36	26.6	14.5
20	Kisaaka 13	Paleosol 2	Btk1b2	13-KIS-22	444	261	60	2.04	11.6	3.17	28.2	13.5
30	Kisaaka 13	Paleosol 2	Btk1b2	13-KIS-23	386	245	60	1.96	12	3.05	28.3	14.05
40	Kisaaka 13	Paleosol 2	Btk2b2	13-KIS-24	486	232	60	1.98	11.6	2.96	28.7	13.25
50	Kisaaka 13	Paleosol 2	Btk2b2	13-KIS-25	539	234	60	2.09	11.45	3.03	29.3	13.4
60	Kisaaka 13	Paleosol 2	Btk2b2	13-KIS-26	551	247	60	2.1	11.85	3.08	28.9	13.75
70	Kisaaka 13	Paleosol 2	Bktb2	13-KIS-27	582	222	50	1.95	11.05	2.95	27.9	12.65
80	Kisaaka 13	Paleosol 2	Bktb2	13-KIS-28	441	221	50	1.96	11.3	2.88	28.2	12.8
0	Kisaaka 13	Paleosol 3	ABkb3	13-KIS-30	456	237	60	1.83	11.6	2.88	29.9	13.25
10	Kisaaka 13	Paleosol 3	ABkb3	13-KIS-31	611	256	80	1.64	11.3	3.44	27.2	14

Table C.1: (Continued)

Depth (cm)	Site	Unit	Paleosol Horizon	Sample	Ba (ppm)	Ce (ppm)	Cr (ppm)	Cs (ppm)	Dy (ppm)	Eu (ppm)	Ga (ppm)	Gd (ppm)
20	Kisaaka 13	Paleosol 3	ABkb3	13-KIS-32	685	266	80	1.69	11.25	3.73	27.5	14.3
40	Kisaaka 13	Paleosol 3	Bkb3	13-KIS-34	678	261	90	1.61	10.75	3.93	26.3	13.95
50	Kisaaka 13	Paleosol 3	Bkb3	13-KIS-35	839	261	80	1.56	10.65	3.9	24.2	13.85
60	Kisaaka 13	Paleosol 3	Bkb3	13-KIS-36	1215	253	80	1.52	10.35	3.68	23.5	13.4
70	Kisaaka 13	Paleosol 3	Bkss1b3	13-KIS-37	808	262	80	1.46	10.3	3.86	23.8	13.7
80	Kisaaka 13	Paleosol 3	Bkss1b3	13-KIS-38	900	270	90	1.56	10.6	4.08	24.3	14.15
90	Kisaaka 13	Paleosol 3	Bkss1b3	13-KIS-39	808	260	80	1.44	10.3	3.65	22.7	12.95
100	Kisaaka 13	Paleosol 3	Bkss1b3	13-KIS-40	856	268	90	1.31	10.8	4.01	26.2	13.8
110	Kisaaka 13	Paleosol 3	Bkss1b3	13-KIS-41	1005	280	90	1.32	10.8	4.15	26.8	14.35
120	Kisaaka 13	Paleosol 3	Bkss1b3	13-KIS-42	847	272	90	1.28	10.65	4.24	26.1	14.05
130	Kisaaka 13	Paleosol 3	Bkss2b3	13-KIS-43	890	253	90	1.2	10.5	3.83	24.7	13.5
140	Kisaaka 13	Paleosol 3	Bkss2b3	13-KIS-44	911	270	90	1.21	10.45	4	24.9	13.6
150	Kisaaka 13	Paleosol 3	Bkss2b3	13-KIS-45	1450	281	90	1.26	10.85	4.13	26.1	14.25
160	Kisaaka 13	Paleosol 3	Bkss3b3	13-KIS-46	939	269	90	1.38	10.25	4.13	26.5	14.15
180	Kisaaka 13	Paleosol 3	Bkss3b3	13-KIS-48	901	259	100	1.23	10.45	3.91	25.8	13.75
190	Kisaaka 13	Paleosol 3	Bkss3b3	13-KIS-49	1840	263	90	1.32	10.45	4.03	25.2	13.75
200	Kisaaka 13	Paleosol 3	Bkss3b3	13-KIS-50	1160	282	90	1.37	10.65	4.16	28.2	14.35
210	Kisaaka 13	Paleosol 3	Bkss3b3	13-KIS-51	1030	269	110	1.22	10.5	3.84	26.3	13.9
220	Kisaaka 13	Paleosol 3	Bkss3b3	13-KIS-52	1165	283	100	1.19	10.95	4.13	25.7	14
230	Kisaaka 13	Paleosol 3	Bkss3b3	13-KIS-53	935	306	100	1.3	11	4.36	27.7	14.7
240	Kisaaka 13	Paleosol 3	Bkss3b3	13-KIS-54	1290	292	90	1.23	10.7	4.16	26.5	14
250	Kisaaka 13	Paleosol 3	Bkss3b3	13-KIS-55	1000	308	110	1.27	11.3	4.41	26.5	15.1
260	Kisaaka 13	Paleosol 3	Bkss3b3	13-KIS-56	1115	281	110	0.98	10.1	4.07	22.8	13.55
0	Kisaaka 12	Paleosol 3	ABkb3	13-KIS-71	643	267	160	1.37	10.5	3.87	28.3	13.7

Table C.1: (Continued)

Depth (cm)	Site	Unit	Paleosol Horizon	Sample	Ba (ppm)	Ce (ppm)	Cr (ppm)	Cs (ppm)	Dy (ppm)	Eu (ppm)	Ga (ppm)	Gd (ppm)
10	Kisaaka 12	Paleosol 3	Bk1b3	13-KIS-72	717	280	150	1.32	11.3	4.03	29.1	14.2
20	Kisaaka 12	Paleosol 3	Bk1b3	13-KIS-73	873	288	180	1.43	11.05	3.99	28.1	14.45
30	Kisaaka 12	Paleosol 3	Bk1b3	13-KIS-74	600	281	200	1.63	10.8	4.19	27.5	14.5
40	Kisaaka 12	Paleosol 3	Bkss1b3	13-KIS-75	601	288	210	1.57	10.5	3.96	28.3	14.05
50	Kisaaka 12	Paleosol 3	Bkss1b3	13-KIS-76	628	287	220	1.66	10.65	3.83	28.5	13.55
60	Kisaaka 12	Paleosol 3	Bkss1b3	13-KIS-77	621	281	210	1.55	10.45	3.88	27.9	13.95
70	Kisaaka 12	Paleosol 3	Bkss1b3	13-KIS-78	517	272	200	1.61	10.55	3.91	27.4	13.45
80	Kisaaka 12	Paleosol 3	Bkss1b3	13-KIS-79	570	278	200	1.48	10.65	3.89	27.9	13.8
90	Kisaaka 12	Paleosol 3	Bkss2b3	13-KIS-80	527	279	200	1.61	10.1	3.91	28.2	13.75
100	Kisaaka 12	Paleosol 3	Bkss2b3	13-KIS-81	789	280	550	1.59	10.2	3.88	27.5	13
110	Kisaaka 12	Paleosol 3	Bkss2b3	13-KIS-82	716	285	200	1.45	10.1	3.94	27.7	13.85
120	Kisaaka 12	Paleosol 3	BCkb3	13-KIS-83	781	282	200	1.72	10.6	3.81	27.7	13.55
60	Kakrigu DP1011	Paleosol 2	Bk	DP1011H	1465	294	70	2.13	9.94	4.81	22.5	14.45
195	Kakrigu DP1011	Paleosol 2	Bk	DP1011F	1355	284	60	1.96	10.1	4.6	21.8	13.75
255	Kakrigu DP1011	Paleosol 2	Bk	DP1011E	1475	289	60	1.96	10.05	4.69	22.1	13.65
315	Kakrigu DP1011	Paleosol 2	Bk	DP1011D	1460	298	60	2.3	10.4	4.87	23.8	13.8
365	Kakrigu DP1011	Paleosol 2	Bk	DP1011C	1765	329	80	2.03	10.75	5.45	23.2	15.9
415	Kakrigu DP1011	Paleosol 2	Bk	DP1011B	1745	349	80	2	11.8	5.57	24	16.55
0	Aringo 5	Paleosol 2	ABkb2	13-AR-6	634	249	30	1.99	11	2.91	30.1	12.65
10	Aringo 5	Paleosol 2	ABkb2	13-AR-7	1175	248	30	1.92	11.25	2.94	28.6	12.95
20	Aringo 5	Paleosol 2	ABkb2	13-AR-8	638	247	30	1.97	10.9	2.84	28.6	12.4
30	Aringo 5	Paleosol 2	ABkb2	13-AR-9	1140	250	20	1.86	11.3	2.81	29.1	13.2
40	Aringo 5	Paleosol 2	ABkb2	13-AR-10	1090	249	20	1.75	10.8	2.69	28.9	12.7
50	Aringo 5	Paleosol 2	Bk1b2	13-AR-11	945	291	30	1.51	11.95	3.18	27.1	14.05

Table C.1: (Continued)

Depth (cm)	Site	Unit	Paleosol Horizon	Sample	Ba (ppm)	Ce (ppm)	Cr (ppm)	Cs (ppm)	Dy (ppm)	Eu (ppm)	Ga (ppm)	Gd (ppm)
60	Aringo 5	Paleosol 2	Bk1b2	13-AR-12	787	302	30	1.66	13	2.93	27.6	15.4
70	Aringo 5	Paleosol 2	Bk1b2	13-AR-13	816	261	20	1.78	11.8	2.75	29.3	13.15
80	Aringo 5	Paleosol 2	Bk2b2	13-AR-14	560	255	30	1.9	10.7	2.84	30.4	12.65
90	Aringo 5	Paleosol 2	Bk2b2	13-AR-15	768	247	20	1.76	10.25	2.73	29.9	12.3
100	Aringo 5	Paleosol 2	Bk2b2	13-AR-16	619	250	20	1.77	11.5	2.89	30	12.7
110	Aringo 5	Paleosol 2	Bk2b2	13-AR-17	545	247	20	1.8	10.25	2.81	30.5	12.9
120	Aringo 5	Paleosol 2	Bk2b2	13-AR-18	652	249	30	1.75	10.7	2.78	29.7	12.5
130	Aringo 5	Paleosol 2	Bk2b2	13-AR-19	745	258	20	1.7	11.2	2.9	30	12.95
140	Aringo 5	Paleosol 2	Bk2b2	13-AR-20	751	253	20	1.82	12.45	2.7	31.6	13.65
0	Aringo 3	Paleosol 3	Bkss1b3	13-AR-37	973	274	30	1.21	11.15	3.16	23.7	13.05
20	Aringo 3	Paleosol 3	Bkss1b3	13-AR-38	1350	350	30	1.43	10.55	3.54	26.1	13
50	Aringo 3	Paleosol 3	Bkss2b3	13-AR-21	1055	290	30	1.29	11.35	3.41	23.1	14
60	Aringo 3	Paleosol 3	Bkss2b3	13-AR-22	1625	301	40	1.47	10.4	3.35	25	12.65
70	Aringo 3	Paleosol 3	Bkss2b3	13-AR-23	1340	317	40	1.58	9.75	3.37	27.7	12.65
80	Aringo 3	Paleosol 3	Bkss3b3	13-AR-24	1400	308	40	1.62	9.9	3.31	25.8	12.6
90	Aringo 3	Paleosol 3	Bkss3b3	13-AR-25	953	280	40	1.59	9.55	3.34	26.2	11.45
100	Aringo 3	Paleosol 3	Bkss3b3	13-AR-26	1465	302	40	1.59	9.18	3.17	26.6	11.85
110	Aringo 3	Paleosol 3	Bkss3b3	13-AR-27	1385	291	40	1.65	9.54	3.28	26.7	11.75
120	Aringo 3	Paleosol 3	Bkss3b3	13-AR-28	927	276	40	1.65	9.7	3.15	25.8	11.8
130	Aringo 3	Paleosol 3	Bkss3b3	13-AR-29	1015	302	40	1.55	11.45	3.65	25.8	14.05
160	Aringo 3	Paleosol 3	Bkss4b3	13-AR-32	1335	290	30	1.48	13.35	3.76	24	15.55
170	Aringo 3	Paleosol 3	Bkss4b3	13-AR-33	1360	327	30	1.49	12.8	3.73	25.4	15.75
190	Aringo 3	Paleosol 3	Bkss5b3	13-AR-34	1750	330	30	1.57	13.25	3.99	26.2	15.85
200	Aringo 3	Paleosol 3	Bkss5b3	13-AR-35	1035	300	40	1.66	8.93	3.21	27.1	12.1

Table C.1: (Continued)

Depth (cm)	Site	Unit	Paleosol Horizon	Sample	Ba (ppm)	Ce (ppm)	Cr (ppm)	Cs (ppm)	Dy (ppm)	Eu (ppm)	Ga (ppm)	Gd (ppm)
210	Aringo 3	Paleosol 3	Bkss5b3	13-AR-36	1685	432	30	1.3	17.55	5.07	23	21.7
0	Aoch Nyasaya 5	Paleosol 3	Bk1b3	13-AOCH-2	693	211	40	1.42	10.3	2.75	26.3	11.5
10	Aoch Nyasaya 5	Paleosol 3	Bkss1b3	13-AOCH-3	798	210	50	1.43	9.74	2.98	23.1	10.9
20	Aoch Nyasaya 5	Paleosol 3	Bkss1b3	13-AOCH-4	766	195.5	60	1.51	7.81	2.63	21.3	9.54
30	Aoch Nyasaya 5	Paleosol 3	Bkss1b3	13-AOCH-5	882	200	60	1.4	8.04	2.81	20.5	9.46
40	Aoch Nyasaya 5	Paleosol 3	Bkss1b3	13-AOCH-6	995	208	60	1.42	8.82	2.98	21.2	10.65
50	Aoch Nyasaya 5	Paleosol 3	Bkss1b3	13-AOCH-7	955	218	80	1.42	8.86	3.1	20.9	11.2
65	Aoch Nyasaya 5	Paleosol 3	Bkss2b3	13-AOCH-8	1055	221	60	1.38	9.04	3.13	20.9	11.25
75	Aoch Nyasaya 5	Paleosol 3	Bkss2b3	13-AOCH-9	1290	241	60	1.3	10.4	3.54	21	12.55
85	Aoch Nyasaya 5	Paleosol 3	Bkss2b3	13-AOCH-10	1235	243	60	1.42	10.4	3.59	21	12.5
95	Aoch Nyasaya 5	Paleosol 3	BCkb3	13-AOCH-11	1115	239	50	1.33	10.75	3.76	20	12.85
105	Aoch Nyasaya 5	Paleosol 3	BCkb3	13-AOCH-12	1255	255	60	1.26	10.55	3.85	21.7	13.3
0	Obware 1	Paleosol 1	Bk1b1	13-OB-1	828	185.5	70	1.66	7.16	2.84	21.5	9.57
20	Obware 1	Paleosol 1	Bk2b1	13-OB-3	704	180	80	1.57	7.5	2.87	21.5	9.42
50	Obware 1	Paleosol 1	Bk2b1	13-OB-6	936	164.5	70	1.23	6.68	2.63	18.6	9.03
0	Wakondo Bovid Hill	Paleosol 3	Bkb3	13-WOK-1	1835	296	50	3.76	11.45	5.11	28	15.1
10	Wakondo Bovid Hill	Paleosol 3	Bkb3	13-WOK-2	1310	278	50	3.53	10.9	4.76	26.4	14.25
30	Wakondo Bovid Hill	Paleosol 3	Bkss1b3	13-WOK-4	1385	295	50	3.87	11.2	5.16	28	14.85
40	Wakondo Bovid Hill	Paleosol 3	Bkss1b3	13-WOK-5	1225	294	50	3.86	11.65	5.32	27.8	15.5
50	Wakondo Bovid Hill	Paleosol 3	Bkss1b3	13-WOK-6	1225	303	50	3.57	10.45	4.85	26.3	14.1

Table C.1: (Continued)

Depth (cm)	Site	Unit	Paleosol Horizon	Sample	Ba (ppm)	Ce (ppm)	Cr (ppm)	Cs (ppm)	Dy (ppm)	Eu (ppm)	Ga (ppm)	Gd (ppm)
50	Wakondo Bovid Hill	Paleosol 3	Bkss2b3	13-WOK-7	1655	317	50	3.46	10.65	4.89	26.8	14.75
60	Wakondo Bovid Hill	Paleosol 3	Bkss2b3	13-WOK-8	1250	296	50	3.57	11.1	4.97	26.8	14.8
70	Wakondo Bovid Hill	Paleosol 3	Bkss2b3	13-WOK-9	1075	289	50	3.44	10.35	4.96	26.1	13.85
80	Wakondo Bovid Hill	Paleosol 3	Bkss3b3	13-WOK-10	1115	308	50	3.45	11.75	5.53	27.1	16
90	Wakondo Bovid Hill	Paleosol 3	Bkss3b3	13-WOK-11	1335	332	60	3.62	12.55	5.73	27.3	16.75
100	Wakondo Bovid Hill	Paleosol 3	Bkss3b3	13-WOK-12	1195	319	60	3.39	12.5	5.72	27.5	16.6
10	Nyamita 1	Paleosol 3	Bkb3	13-NY-2	1315	279	90	3.34	9.85	4.5	26.5	13.95
20	Nyamita 1	Paleosol 3	Bkss1b3	13-NY-3	1090	195	80	2.59	10.9	4.47	19.3	14.3
30	Nyamita 1	Paleosol 3	Bkss1b3	13-NY-4	1195	280	90	3.73	9.42	4.27	27.9	12.3
40	Nyamita 1	Paleosol 3	Bkss1b3	13-NY-5	1140	254	80	3.54	9.25	4.24	26.1	13.4
60	Nyamita 1	Paleosol 3	BCkb3	13-NY-6	1270	185.5	50	1.82	11.2	4.3	15.6	14.45
0	Nyamita AV1002	Paleosol 2	Bk1b2	13-NY-7	1395	213	70	2.27	9.61	4.07	21.1	12.6
10	Nyamita AV1002	Paleosol 2	Bk1b2	13-NY-8	1210	221	60	2.58	9.71	4.47	21.8	12.95
20	Nyamita AV1002	Paleosol 2	Bk1b2	13-NY-9	1260	237	60	2.8	9.92	4.23	23.2	13.4
30	Nyamita AV1002	Paleosol 2	Bk1b2	13-NY-10	1430	268	70	3.04	9.59	4.44	26.5	13.7
40	Nyamita AV1002	Paleosol 2	Bk1b2	13-NY-11	1405	263	80	2.78	10.55	4.77	24.2	14.75
50	Nyamita AV1002	Paleosol 2	Bk2b2	13-NY-12	1470	279	80	2.96	11.1	5.08	26.1	14.7
60	Nyamita AV1002	Paleosol 2	BCb2	13-NY-13	2180	215	60	2.59	8.67	3.89	21	11.85

Table C.1: (Continued)

Sample	Hf (ppm)	Ho (ppm)	La (ppm)	Lu (ppm)	Nb (ppm)	Nd (ppm)	Pr (ppm)	Rb (ppm)	Sn (ppm)	Sr (ppm)	Ta (ppm)	Tb (ppm)	Th (ppm)	Tm (ppm)
13-KIS-57	10.9	2.2	129	0.77	151	99.7	26.9	96.7	3	491	8.9	2.16	15.05	0.87
13-KIS-58	12	2.05	127	0.75	164	101	27	109	4	471	9.7	2.09	16.25	0.81
13-KIS-59	12.4	2.03	132	0.71	169	104	28.1	111.5	4	434	9.8	2.12	16.45	0.8
13-KIS-60	12.2	2.06	131	0.73	167.5	103.5	27.7	108.5	4	425	9.8	2.12	16.4	0.81
13-KIS-61	12.1	2.05	131	0.76	167.5	104.5	27.6	108	4	402	9.8	2.11	16.5	0.78
13-KIS-62	10.3	1.77	113	0.68	140.5	88.9	24	90.3	3	571	8	1.82	13.9	0.75
13-KIS-63	11.8	2.05	129.5	0.74	167.5	102	27.5	104.5	4	412	10	2.1	16.4	0.81
13-KIS-64	11.6	2.01	128	0.71	164.5	102.5	27.3	102.5	3	450	9.8	2.11	16.1	0.79
13-KIS-65	11.8	2.08	131	0.74	168.5	104	27.6	102.5	4	437	10	2.14	16.95	0.84
13-KIS-66	12.1	2.11	133	0.73	168.5	105	28.3	98.6	3	466	10.1	2.14	16.55	0.82
13-KIS-67	11.9	2.15	135	0.74	175	108	28.9	97.5	4	432	10.6	2.21	17.4	0.85
13-KIS-68	11.9	2.2	136.5	0.77	175	108	28.9	93.7	3	489	10.8	2.13	17.5	0.87
13-KIS-69	12.3	2.18	139.5	0.83	179	112	30	94	3	438	11.2	2.23	18.05	0.88
13-KIS-70	11.4	2.3	142	0.79	175.5	114	30.4	85.4	3	608	10.7	2.26	17.75	0.84
12-KIS-25	12.6	2.53	123.5	0.83	149.5	91.6	26	114.5	4	435	9.4	2.29	17.55	0.94
12-KIS-24	11.4	2.15	119	0.68	145.5	88.7	24.6	105	4	360	8.7	2.02	16.15	0.75
12-KIS-23	11.5	2.28	127	0.7	154	95.1	26.3	109.5	4	396	9.3	2.16	16.85	0.8
12-KIS-22	11.1	2.27	123	0.68	146.5	93.7	25.7	105.5	4	464	9	2.14	16.3	0.81
12-KIS-21	12	2.26	126	0.69	152	94.9	26.1	108.5	4	376	9.4	2.12	17.2	0.82
12-KIS-20	11.3	2.21	129	0.69	151	96.6	27.1	108.5	4	401	9.2	2.11	16.75	0.77
12-KIS-19	11.2	2.22	124	0.66	148.5	94.5	26.1	106.5	4	382	9	2.09	16.9	0.78
12-KIS-18	10.6	2.26	125	0.69	146	95.5	26.2	103.5	3	424	9	2.12	16.5	0.81
12-KIS-17	10.4	2.08	120	0.64	140	89.2	24.6	101.5	3	373	8.7	1.97	15.65	0.72

Table C.1: (Continued)

Sample	Hf (ppm)	Ho (ppm)	La (ppm)	Lu (ppm)	Nb (ppm)	Nd (ppm)	Pr (ppm)	Rb (ppm)	Sn (ppm)	Sr (ppm)	Ta (ppm)	Tb (ppm)	Th (ppm)	Tm (ppm)
12-KIS-16	11.5	2.11	120.5	0.65	148.5	91.4	25	103	4	377	8.9	2	16.3	0.74
12-KIS-15	11	2.14	121.5	0.64	146.5	93.9	25.8	102.5	3	385	8.8	2.06	16.4	0.75
12-KIS-14	10.9	2.14	124	0.64	153.5	93.4	26.1	103	3	395	8.9	2.06	16.55	0.74
12-KIS-13	11.3	2.21	125.5	0.69	149.5	95.7	26.3	103.5	3	403	9.1	2.11	16.9	0.77
12-KIS-12	11.1	2.17	123.5	0.66	149.5	94.1	25.8	102	3	381	9.1	2.08	16.5	0.75
12-KIS-11	11.1	2.11	125.5	0.63	152.5	96.1	26.2	102.5	3	383	9.3	2.08	17.15	0.74
12-KIS-10	10.7	2.13	122.5	0.62	146.5	93.2	25.6	97.5	3	382	9.1	2.02	16.55	0.72
12-KIS-9	10.5	2.07	122	0.65	144.5	94.1	25.8	96.6	3	382	8.9	2.05	16.5	0.73
12-KIS-8	10.8	2.07	119.5	0.61	147.5	93	25.5	97	3	372	9.1	2.03	16.65	0.73
12-KIS-7	10.8	2.1	121.5	0.64	146	93.6	25.2	94.4	3	371	8.9	2.03	16.75	0.72
12-KIS-6	10.6	2.1	121.5	0.61	145	94.2	25.7	94.5	3	373	8.8	2.03	16.35	0.72
12-KIS-5	10.6	2.13	124	0.64	148	94.7	26.2	95.7	3	384	9	2.04	16.45	0.77
12-KIS-4	10.2	2.03	117.5	0.6	144	90.7	25.1	92.9	3	370	8.9	1.98	16.3	0.71
12-KIS-3	10.3	2.02	118.5	0.6	145	91.5	25.4	92.7	3	361	8.6	1.95	16.15	0.71
12-KIS-2	10.5	2.09	121.5	0.62	144.5	93.2	25.3	94	3	391	8.9	2.01	16.35	0.73
12-KIS-1	10	2.06	117	0.61	142.5	90.7	24.6	90.6	3	390	8.7	1.94	16.05	0.73
12-KIS-33	15	2.51	125.5	0.83	171.5	92.5	25.7	114.5	5	293	10.3	2.24	19.05	0.94
12-KIS-32	14.7	2.45	123	0.8	162	90.6	25.3	119	5	303	9.9	2.25	18.25	0.91
12-KIS-31	15.1	2.4	117	0.81	156.5	88	24.3	119	5	279	9.3	2.14	17.2	0.9
12-KIS-30	15.3	2.45	120	0.82	158	86.8	23.9	117	5	275	9.7	2.22	17.8	0.94
12-KIS-29	15.3	2.5	114.5	0.83	151.5	83.9	23.5	112	5	251	9.3	2.17	17.35	0.94
12-KIS-58	9.1	1.66	93.2	0.66	117.5	68.1	19.1	80.1	3	536	6.9	1.55	12.15	0.69
12-KIS-57	10.4	1.88	105.5	0.73	131	78.4	21.4	90	3	515	7.7	1.75	13.7	0.79
12-KIS-56	10.9	1.99	110	0.8	137.5	82.1	22.4	94.7	4	466	8.3	1.88	14.55	0.82

Table C.1: (Continued)

Sample	Hf (ppm)	Ho (ppm)	La (ppm)	Lu (ppm)	Nb (ppm)	Nd (ppm)	Pr (ppm)	Rb (ppm)	Sn (ppm)	Sr (ppm)	Ta (ppm)	Tb (ppm)	Th (ppm)	Tm (ppm)
12-KIS-55	11.5	2.06	117.5	0.8	148	88.8	24.1	100.5	4	464	8.9	1.95	15.05	0.85
12-KIS-54	11.3	2.05	117	0.8	149.5	88.3	24	99.7	4	431	8.8	1.97	15.25	0.85
12-KIS-53	11.4	2.04	115.5	0.79	145	85.6	23.5	98.3	4	455	8.6	1.94	15	0.85
12-KIS-52	11.4	2.04	113.5	0.8	140.5	84.3	23.2	95.7	4	501	8.6	1.91	14.95	0.85
12-KIS-51	11.6	2.01	115	0.8	147	86	24	100	4	461	8.8	1.9	15.05	0.86
12-KIS-48	11.9	2.05	118.5	0.8	151	88.2	24.7	101.5	4	491	8.9	1.94	15.65	0.84
12-KIS-47	11.7	2.1	123	0.83	150	91.7	25.5	98.1	4	538	9	1.95	15.55	0.89
12-KIS-46	11.8	2.1	120	0.82	148.5	89.7	24.2	96.2	4	507	9.2	1.95	15.15	0.87
12-KIS-45	12	2.2	125	0.85	153	91.7	25.9	102	4	500	9.5	2.1	16	0.89
12-KIS-44	12	2.1	119	0.81	152	89.1	24.4	102.5	4	441	9.1	1.97	15.8	0.87
12-KIS-42	12.4	2.16	127	0.83	161	95.9	26	105	4	477	9.8	2.1	16.8	0.89
12-KIS-41	11.6	2.05	123.5	0.8	153	92.7	25.7	101	4	522	9.2	1.99	15.65	0.83
12-KIS-40	11.5	2.04	119.5	0.77	147	89.4	25.1	100	4	533	9.2	1.98	15.65	0.84
12-KIS-39	12	2	124	0.75	157	94.2	26	103.5	4	488	9.5	1.96	16.35	0.81
12-KIS-38	12.4	1.98	118	0.74	154	90.4	25.2	103	4	470	9.7	1.94	16.2	0.8
12-KIS-37	12.7	2.26	121	0.73	153.5	90.2	25	108.5	4	523	9.4	2.12	16.5	0.84
12-KIS-36	12.4	2.3	124.5	0.72	151	93.3	25.9	105	4	527	9.5	2.14	17.1	0.83
12-KIS-35	12.6	2.25	123	0.69	154.5	94.7	26.2	107.5	4	494	9.5	2.12	17.4	0.82
13-KIS-2	11.9	1.95	109	0.74	134.5	84.2	22.4	92.2	4	640	7.7	1.84	14.5	0.8
13-KIS-3	13.2	2.2	120	0.84	149.5	91.1	24.9	101	4	535	8.7	2.12	16.35	0.91
13-KIS-4	13.9	2.19	118	0.76	149.5	89.2	24.5	103	4	496	8.7	2.06	16.25	0.92
13-KIS-5	13.6	1.99	113.5	0.76	144.5	87	23.5	108	4	434	8.7	1.94	15.8	0.83
13-KIS-6	14.4	2.19	119	0.84	150.5	89.9	24.5	110.5	5	419	9.1	2.08	16.6	0.96
13-KIS-7	14.6	2.23	124	0.85	155.5	95.6	26.2	106.5	5	445	9.5	2.16	17.3	0.94

Table C.1: (Continued)

Sample	Hf (ppm)	Ho (ppm)	La (ppm)	Lu (ppm)	Nb (ppm)	Nd (ppm)	Pr (ppm)	Rb (ppm)	Sn (ppm)	Sr (ppm)	Ta (ppm)	Tb (ppm)	Th (ppm)	Tm (ppm)
13-KIS-8	14.5	2.27	124.5	0.85	153.5	94.8	25.8	108	5	413	9.3	2.1	17.1	0.96
13-KIS-9	14.7	2.25	124	0.87	153	94.2	25.5	105.5	5	366	9.3	2.18	17.35	0.96
13-KIS-10	15.3	2.37	129.5	0.9	158.5	97.5	26.2	106	5	351	9.7	2.23	17.9	1.04
13-KIS-11	17.2	2.59	135.5	1.02	173.5	102	27.8	111.5	5	320	10.6	2.36	20	1.09
13-KIS-12	17.5	2.66	140	1.08	181.5	104	28.7	117.5	6	356	11	2.5	20.6	1.1
13-KIS-13	19.2	2.83	143	1.14	187	106.5	29.4	121.5	6	299	11.8	2.57	21.8	1.21
13-KIS-14	19.2	2.84	145.5	1.14	184.5	108	29.4	123	6	339	11.4	2.63	21.3	1.21
13-KIS-15	16.2	2.49	131	0.97	164.5	98.9	27.1	111.5	5	575	9.9	2.26	18.6	1.06
13-KIS-17	12.5	2.24	118.5	0.83	135	88.9	24.5	97.8	4	680	8.3	2.07	15.35	0.9
13-KIS-18	13	2.17	120.5	0.82	139	93.2	24.7	100.5	4	525	8.5	2.15	15.35	0.91
13-KIS-20	13.6	2.32	125.5	0.87	151	96.3	26.3	100	4	322	9.3	2.15	16.85	0.91
13-KIS-21	13.7	2.31	126	0.86	153	97.7	26.5	103.5	4	301	9.3	2.24	16.8	0.93
13-KIS-22	14	2.2	118	0.86	145.5	91.8	25.1	112	4	304	9.1	2.04	16.4	0.89
13-KIS-23	14.5	2.33	119	0.9	143	91.3	25.1	110.5	5	288	8.9	2.02	16.05	0.97
13-KIS-24	14.4	2.21	116	0.83	138.5	88.6	24.1	114.5	4	317	8.6	2.01	15.6	0.9
13-KIS-25	14.4	2.19	117	0.87	141	88.9	24.4	117	5	427	8.6	2.05	15.95	0.98
13-KIS-26	14.9	2.22	120	0.86	144	91.2	24.5	115.5	5	390	9.1	2.06	16.25	0.94
13-KIS-27	13.9	2.13	110	0.8	130.5	84	23	108	4	445	8.1	1.94	15.05	0.89
13-KIS-28	13.5	2.2	111	0.82	132.5	84.4	23.1	106	4	367	8.2	1.94	14.55	0.88
13-KIS-30	14.7	2.27	115.5	0.87	140.5	89.4	24	108.5	5	213	8.8	2.06	15.45	0.94
13-KIS-31	12.9	2.09	121.5	0.83	138	94.4	25.5	102.5	4	314	8.5	1.99	15.6	0.83
13-KIS-32	12.7	2.13	125	0.74	141	97.1	26.1	105.5	4	355	8.7	2.08	15.8	0.85
13-KIS-34	12.4	1.98	124	0.76	142	97.7	26.2	104	4	401	8.8	2.08	15.8	0.82
13-KIS-35	11.6	1.98	121.5	0.68	134	94.9	25.5	96.2	4	416	8.1	1.95	14.75	0.8

Table C.1: (Continued)

Sample	Hf (ppm)	Ho (ppm)	La (ppm)	Lu (ppm)	Nb (ppm)	Nd (ppm)	Pr (ppm)	Rb (ppm)	Sn (ppm)	Sr (ppm)	Ta (ppm)	Tb (ppm)	Th (ppm)	Tm (ppm)
13-KIS-36	11.2	1.96	120.5	0.69	130.5	94.1	24.9	94.5	3	465	8	1.9	14.15	0.79
13-KIS-37	11.3	1.9	120.5	0.69	132	93.1	25.1	93.7	4	467	8.1	1.86	14.5	0.72
13-KIS-38	11.3	1.99	123.5	0.7	137	96.7	26.1	97.1	3	454	8.6	1.98	15.05	0.74
13-KIS-39	10.1	1.92	119	0.68	127.5	91.2	24.4	89	3	475	7.9	1.87	14.1	0.81
13-KIS-40	11.1	1.96	122	0.64	153.5	95.3	25.7	94.4	4	462	9	1.93	15.15	0.74
13-KIS-41	10.9	2.03	126.5	0.73	155.5	99	26.9	94.5	3	479	9.1	2.03	14.95	0.79
13-KIS-42	10.9	1.96	123.5	0.67	153.5	96.9	25.9	93.2	3	469	9.1	1.96	15.05	0.77
13-KIS-43	10.2	1.97	120.5	0.72	143	93.8	25.1	85.8	3	492	8.2	2.01	14.1	0.79
13-KIS-44	10.2	1.91	121.5	0.7	147	95.4	25.6	87.4	3	516	8.7	1.95	14.25	0.78
13-KIS-45	10.6	2.03	129	0.73	154.5	99.6	27	89.1	3	543	9.1	2.03	14.95	0.79
13-KIS-46	11	1.98	122.5	0.67	152	95	25.6	94.8	3	489	9	1.98	15	0.74
13-KIS-48	10.3	1.9	120.5	0.68	150	94.9	25.5	91.1	3	495	8.9	1.92	14.6	0.73
13-KIS-49	10.4	1.87	121	0.68	146.5	94.3	25.4	87.5	3	573	8.6	1.91	14.4	0.79
13-KIS-50	11.4	1.95	126.5	0.71	159	101	27	95.4	3	491	9.5	2.08	15.6	0.79
13-KIS-51	10.5	2.01	124	0.71	150	97	25.8	87.8	3	514	8.8	1.97	14.65	0.71
13-KIS-52	10.8	1.94	126	0.7	155	99.7	26.6	88.5	3	517	9.2	1.98	15.3	0.77
13-KIS-53	10.9	2	131.5	0.68	163.5	105	28.3	93.7	3	484	9.9	2.14	16.05	0.8
13-KIS-54	10.8	1.99	128	0.69	159	102	27.4	90.1	3	548	9.4	1.99	15.55	0.74
13-KIS-55	11.2	2.1	135	0.73	163	108	28.9	90	4	515	10	2.22	16.35	0.84
13-KIS-56	9.5	1.86	124.5	0.67	143.5	97.8	26.2	76.4	3	570	8.6	1.99	14.65	0.76
13-KIS-71	11.5	1.84	121	0.68	150	96.2	25.5	103.5	4	431	9.1	1.91	15.2	0.77
13-KIS-72	12.1	2	125.5	0.77	157.5	99.3	26.6	101	4	427	9.5	2.05	15.7	0.84
13-KIS-73	11.7	2.02	125.5	0.74	156	100	27	101.5	4	460	9.1	2.06	15.3	0.76
13-KIS-74	11.1	1.97	124.5	0.8	155	99.4	26.3	99.9	4	377	9.1	2.21	16.25	0.83

Table C.1: (Continued)

Sample	Hf (ppm)	Ho (ppm)	La (ppm)	Lu (ppm)	Nb (ppm)	Nd (ppm)	Pr (ppm)	Rb (ppm)	Sn (ppm)	Sr (ppm)	Ta (ppm)	Tb (ppm)	Th (ppm)	Tm (ppm)
13-KIS-75	11.5	2	122	0.76	158	96.7	26.3	100	4	375	9.4	2.07	16.4	0.82
13-KIS-76	11.6	1.93	124.5	0.7	158.5	99	26.5	99.7	4	377	9.7	2.04	16.7	0.79
13-KIS-77	11.3	1.95	121.5	0.7	156.5	97.3	26.1	98.1	4	378	9.6	2.04	16.3	0.78
13-KIS-78	11.3	1.87	121	0.66	155	96.6	25.6	98.3	4	359	9.4	2.03	16.15	0.76
13-KIS-79	11.2	1.97	122	0.7	155	96.7	25.7	96.6	4	376	9.3	2.06	16.25	0.76
13-KIS-80	11.3	2	122.5	0.71	154	97.6	26.3	97.2	4	366	9.2	2.05	16.05	0.81
13-KIS-81	11.3	1.87	118.5	0.68	155.5	96	25.4	95.8	4	393	9.4	1.96	16.35	0.74
13-KIS-82	11.4	1.97	121.5	0.69	156	96.6	26.1	96.8	4	384	9.1	2.04	16.6	0.76
13-KIS-83	11.1	1.96	118.5	0.69	153.5	96.6	25.4	93.4	4	403	9.2	2.09	16.4	0.79
DP1011H	9.3	1.8	157.5	0.47	191.5	110.5	30.8	86.6	3	740	7.8	1.84	21.1	0.62
DP1011F	9.2	1.75	152.5	0.52	173.5	108	29.4	81.7	3	684	7.4	1.76	19.6	0.58
DP1011E	9	1.8	154	0.52	173.5	111.5	29.7	80.9	3	691	7.3	1.76	19.75	0.6
DP1011D	10.1	1.87	163	0.53	178	112	31.1	91.7	3	671	7.8	1.89	19.85	0.66
DP1011C	10.3	2	171	0.55	198	122	33.4	88.3	3	816	8.6	2	21.4	0.62
DP1011B	10.2	2.04	177.5	0.59	215	127	35	90	3	789	8.8	2.17	22.8	0.66
13-AR-6	14.2	2.04	119	0.75	165.5	88.5	24.6	120	5	451	9.6	2.04	17.95	0.84
13-AR-7	14.1	2.14	118	0.9	160	86.7	23.7	115	5	659	9.3	2.11	17.25	0.98
13-AR-8	13.3	2.17	117	0.85	158	86.4	23.7	114.5	4	439	9.1	2.14	17.2	0.98
13-AR-9	13.9	2.17	118.5	0.9	159	88.1	24	111.5	4	759	9.3	2.05	17.05	0.96
13-AR-10	13.6	2.14	114	0.82	154.5	85.4	23.1	107.5	5	801	9	2.06	16.5	0.92
13-AR-11	13.5	2.39	126	0.93	172.5	94.2	26	97.8	5	661	10	2.22	18	1.05
13-AR-12	14.8	2.48	133.5	1	186	98.4	27.2	104	5	475	10.5	2.46	20.2	1.11
13-AR-13	14.6	2.23	121	0.84	169	89.8	24.7	112.5	5	471	9.8	2.19	18.3	0.97
13-AR-14	14.5	2.08	121	0.76	166	90	24.6	116.5	5	306	9.8	2.07	17.9	0.89

Table C.1: (Continued)

Sample	Hf (ppm)	Ho (ppm)	La (ppm)	Lu (ppm)	Nb (ppm)	Nd (ppm)	Pr (ppm)	Rb (ppm)	Sn (ppm)	Sr (ppm)	Ta (ppm)	Tb (ppm)	Th (ppm)	Tm (ppm)
13-AR-15	13.7	1.93	113.5	0.78	156.5	85	23.5	115.5	5	374	9.1	1.99	17.05	0.86
13-AR-16	13.8	2.28	117.5	0.88	154.5	86.5	23.6	111.5	5	350	8.9	2.1	16.8	0.97
13-AR-17	14.7	1.99	116	0.8	162	86.6	23.8	115	5	289	9.4	1.95	17.5	0.86
13-AR-18	13.6	2.07	115.5	0.87	156.5	85.3	23.5	112	5	342	9.2	2.05	17.25	0.9
13-AR-19	13.7	2.09	118.5	0.85	160	87.5	24.2	110.5	5	594	9.2	2.02	17.5	0.89
13-AR-20	14.6	2.5	121	1.04	157.5	89.6	24.6	105	6	530	9.1	2.19	16.85	1.14
13-AR-37	10.4	2.19	120	0.84	133	89.5	25.1	85.6	3	533	7.3	2.11	14.2	0.89
13-AR-38	11.8	1.93	129	0.74	153	96.7	27	94.3	4	476	8.4	1.99	15.75	0.83
13-AR-21	10.8	2.22	123.5	0.88	134	93	25	89.5	3	731	7.1	2.07	14.35	0.95
13-AR-22	11	1.94	117.5	0.8	140.5	90.9	24.4	96.3	3	597	7.8	1.93	15.3	0.84
13-AR-23	11.6	1.89	118.5	0.68	154	92.6	24.8	105	4	464	8.5	1.88	16	0.79
13-AR-24	11.3	1.83	114.5	0.67	145.5	89.1	24	100.5	4	662	8	1.79	15.4	0.75
13-AR-25	11.9	1.66	115.5	0.62	150	87.4	24.5	104.5	4	503	8.4	1.79	15.9	0.72
13-AR-26	11.8	1.83	109.5	0.63	149.5	83.6	23	102.5	4	549	8.3	1.72	16.2	0.77
13-AR-27	11.5	1.78	110.5	0.63	150	83.7	23.5	101.5	4	572	8.3	1.74	16.2	0.74
13-AR-28	11.5	1.75	112	0.69	149.5	86.1	23.8	101.5	4	512	7.9	1.72	15.7	0.71
13-AR-29	11.6	2.17	125.5	0.84	153.5	96.4	25.8	101	4	531	8.4	2.1	17.05	0.88
13-AR-32	11.4	2.65	142.5	0.99	153.5	103	28.8	88.6	4	934	8.1	2.41	17.05	1.13
13-AR-33	12.1	2.47	134.5	0.92	158.5	102.5	28	93.9	4	578	9	2.39	18.55	1.01
13-AR-34	12.9	2.55	141	1.04	168.5	107.5	29.3	98.8	4	651	9	2.38	19	1.08
13-AR-35	11.9	1.65	116.5	0.61	152.5	89	24.6	107	4	448	8.5	1.67	16.25	0.7
13-AR-36	10.7	3.39	220	1.3	141.5	149	41.2	84.5	3	1000	7.9	3.19	16.15	1.43
13-AOCH-2	12.4	1.97	104	0.75	142.5	80.3	22.2	95.3	5	427	7.8	1.85	14.15	0.86
13-AOCH-3	11.8	1.82	101	0.63	129	73.7	21.5	90.4	3	473	8	1.61	14.85	0.77

Table C.1: (Continued)

Sample	Hf (ppm)	Ho (ppm)	La (ppm)	Lu (ppm)	Nb (ppm)	Nd (ppm)	Pr (ppm)	Rb (ppm)	Sn (ppm)	Sr (ppm)	Ta (ppm)	Tb (ppm)	Th (ppm)	Tm (ppm)
13-AOCH-4	10.1	1.42	86.7	0.51	119	64.2	18.55	87.5	3	500	7.4	1.33	13.7	0.63
13-AOCH-5	9.7	1.52	90.3	0.52	113	65.5	19	82.6	3	541	7.1	1.34	13.05	0.6
13-AOCH-6	10.3	1.57	98.1	0.55	118.5	72.2	20.7	84.6	3	559	7.5	1.48	13.7	0.69
13-AOCH-7	10.1	1.65	99.9	0.54	123.5	74.2	21.4	82.7	3	532	7.8	1.49	14.35	0.64
13-AOCH-8	10.5	1.71	100.5	0.58	124	75.6	21.5	81	3	564	7.9	1.57	14.45	0.68
13-AOCH-9	10.3	1.84	112.5	0.71	131	84.1	23.8	79.9	3	576	8.2	1.77	14.75	0.75
13-AOCH-10	10.5	1.97	114	0.67	133.5	84.2	24.2	80.8	3	580	8.4	1.77	15.05	0.78
13-AOCH-11	10.1	1.99	118.5	0.72	128.5	86.2	24.2	78.4	3	595	8	1.81	14.4	0.81
13-AOCH-12	10.8	1.93	118.5	0.66	133.5	87.7	24.9	79.9	3	559	8.7	1.82	15.5	0.77
13-OB-1	9.2	1.27	95.9	0.44	120.5	70.9	19.1	92.1	3	528	6	1.3	13.7	0.47
13-OB-3	9.8	1.34	94.5	0.45	120	71.4	19.75	92.4	3	498	6.4	1.34	13.3	0.52
13-OB-6	9.3	1.22	86.9	0.43	106.5	63.9	17.5	80.5	2	534	5.6	1.22	11.75	0.48
13-WOK-1	11.4	2.07	166.5	0.57	185	105.5	31	112.5	3	710	8.1	2.03	20.1	0.71
13-WOK-2	10	1.88	166.5	0.56	170.5	103	30.3	105	3	682	7.3	1.88	19.75	0.7
13-WOK-4	11.3	1.99	165	0.59	185.5	106	31.1	113.5	3	679	8.4	1.93	20.7	0.74
13-WOK-5	11.8	2.08	166.5	0.61	191	108	31.3	110.5	3	657	8.7	2.06	20.3	0.75
13-WOK-6	11.1	1.83	157	0.51	184.5	101	29.7	107	3	646	8.2	1.89	19.7	0.67
13-WOK-7	11	1.93	164.5	0.53	184.5	105.5	30.8	107	3	661	8.1	1.99	20	0.71
13-WOK-8	11.4	1.97	158	0.53	185.5	103	29.9	110	3	632	8.5	2.03	20.2	0.7
13-WOK-9	10.8	1.84	152.5	0.52	179.5	101.5	28.9	104	3	590	8.2	1.89	19.45	0.67
13-WOK-10	11.6	2.11	159	0.58	185	109.5	31.4	107	3	633	9.2	2.11	19.7	0.76
13-WOK-11	12.6	2.28	168	0.59	196.5	114	33.1	109	3	655	9.9	2.29	21	0.76

Table C.1: (Continued)

Sample	Hf (ppm)	Ho (ppm)	La (ppm)	Lu (ppm)	Nb (ppm)	Nd (ppm)	Pr (ppm)	Rb (ppm)	Sn (ppm)	Sr (ppm)	Ta (ppm)	Tb (ppm)	Th (ppm)	Tm (ppm)
13-WOK-12	12	2.16	165	0.56	191.5	114.5	32.6	107	3	633	9.8	2.2	20.4	0.78
13-NY-2	9.7	1.78	150	0.47	219	102.5	28.4	102	3	701	7.3	1.76	20.8	0.62
13-NY-3	7.1	2.03	187	0.55	149.5	103.5	29.5	76.3	2	1210	4.9	1.91	15.05	0.64
13-NY-4	9.7	1.61	145.5	0.46	216	95.4	27.9	109	3	657	7.1	1.69	21.5	0.54
13-NY-5	8.9	1.65	152	0.48	213	98.8	28	103.5	3	688	6.8	1.76	21.3	0.56
13-NY-6	5.4	2.22	191	0.68	117.5	102.5	28.5	62.1	2	2410	4.2	1.89	12.95	0.83
13-NY-7	9.1	1.77	116.5	0.44	155.5	82.9	21.9	80.2	3	1120	6	1.71	12.95	0.57
13-NY-8	9.1	1.86	131.5	0.48	163	88	23.9	84.6	3	1140	6	1.78	13.65	0.64
13-NY-9	9.3	1.8	135	0.49	166	90.4	25	91.8	3	949	6.6	1.84	14.9	0.62
13-NY-10	10.4	1.72	135	0.5	199	93.7	25.6	102.5	3	900	7.1	1.77	17.45	0.62
13-NY-11	9.7	1.91	142	0.55	183	97.2	27	95.2	3	984	7.2	1.99	16.55	0.6
13-NY-12	10.7	1.89	142	0.5	206	101	27.8	101	3	896	8	1.98	17.85	0.63
13-NY-13	7.7	1.54	131	0.45	157	83.6	23	82.3	2	1230	5.4	1.62	14.3	0.53

Table C.1: (Continued)

Sample	U (ppm)	V (ppm)	W (ppm)	Y (ppm)	Yb (ppm)	Zr (ppm)	Al_2O_3 (wt %)	Fe_2O_3 (wt %)	CaO (wt %)	MgO (wt %)	Na_2O (wt %)	K_2O (wt %)	Cr_2O_3 (wt %)	TiO_2 (wt %)
13-KIS-57	3.15	257	2	57.7	5.08	470	12.4	12.75	7.35	2.21	1.54	2.2	0.01	2.51
13-KIS-58	2.7	285	2	54.8	4.73	518	14.3	14.3	2.24	2.46	1.68	2.44	0.01	2.77
13-KIS-59	2.46	292	2	56.1	4.95	537	14.45	14.5	1.71	2.48	1.67	2.43	0.01	2.82
13-KIS-60	2.65	285	2	55	4.97	528	14.15	14.25	1.64	2.42	1.64	2.41	0.01	2.81
13-KIS-61	2.94	286	2	55.9	4.89	520	14.25	14.4	1.66	2.45	1.64	2.41	0.01	2.85
13-KIS-62	3.6	239	2	49.1	4.44	438	11.9	12.1	9.91	2.19	1.38	1.99	0.01	2.37
13-KIS-63	3.41	292	2	54.6	4.86	517	13.9	14.35	2.69	2.47	1.6	2.32	0.01	2.84
13-KIS-64	3.64	283	2	54.6	4.79	508	13.65	14.15	3.51	2.41	1.58	2.27	0.01	2.82
13-KIS-65	4.02	294	2	54.6	4.85	518	13.5	14.25	2.98	2.39	1.56	2.23	0.01	2.85
13-KIS-66	4.21	304	2	56.3	4.88	505	13.25	14.55	3.97	2.42	1.58	2.16	0.01	2.89
13-KIS-67	4.59	325	2	57.1	4.9	524	13.5	15.2	2.82	2.38	1.6	2.15	0.01	3.06
13-KIS-68	4.45	317	2	61.1	5.15	520	13.3	15.15	3.37	2.25	1.64	2.04	0.01	3.05
13-KIS-69	4.58	335	2	59.3	5.2	520	13	15.75	3.3	2.42	1.58	2.1	0.02	3.19
13-KIS-70	4.61	355	2	60.6	5.29	497	12.55	16	4.23	2.44	1.68	1.99	0.02	3.25
12-KIS-25	3.2	204	2	64.1	5.89	486	13.55	11.75	4.42	2.16	1.77	2.35	0.01	2.14
12-KIS-24	2.35	230	2	52.6	4.84	444	13.8	12.55	1.91	2.3	1.44	2.24	0.01	2.37
12-KIS-23	2.56	259	2	55.2	5.08	446	13.8	13.15	1.94	2.4	1.37	2.24	0.01	2.58
12-KIS-22	2.72	260	2	53.6	4.91	432	13.5	12.95	3.12	2.39	1.32	2.19	0.01	2.57
12-KIS-21	2.59	252	2	53.6	5.14	451	14	13.25	1.89	2.35	1.41	2.26	0.01	2.58
12-KIS-20	2.7	272	2	54.9	5.06	439	13.8	13.55	2.32	2.34	1.35	2.23	0.01	2.7
12-KIS-19	2.73	270	2	53.3	4.91	439	13.75	13.45	1.79	2.33	1.46	2.23	0.01	2.66
12-KIS-18	3.15	262	2	55.6	5.15	424	13.05	12.9	4.33	2.36	1.29	2.12	0.01	2.59
12-KIS-17	2.99	261	2	50.5	4.61	405	13.6	13.5	2.69	2.36	1.34	2.18	0.01	2.71
12-KIS-16	2.79	263	2	51.4	4.65	450	13.6	13.3	1.96	2.38	1.36	2.19	0.01	2.65

Table C.1: (Continued)

Sample	U (ppm)	V (ppm)	W (ppm)	Y (ppm)	Yb (ppm)	Zr (ppm)	Al_2O_3 (wt %)	Fe_2O_3 (wt %)	CaO (wt %)	MgO (wt %)	Na_2O (wt %)	K_2O (wt %)	Cr_2O_3 (wt %)	TiO_2 (wt %)
12-KIS-15	3.02	273	2	52.1	4.65	429	13.3	13.4	2.11	2.38	1.31	2.15	0.01	2.72
12-KIS-14	3.43	284	2	52.3	4.68	430	13.25	13.5	2.35	2.39	1.32	2.13	0.01	2.77
12-KIS-13	3.67	280	2	53.5	4.97	436	13.2	13.5	2.42	2.38	1.34	2.11	0.01	2.78
12-KIS-12	3.77	274	2	51.6	4.69	427	13	13.5	2.09	2.36	1.32	2.08	0.01	2.78
12-KIS-11	4.17	285	2	51.5	4.71	429	13.6	14.2	2.33	2.43	1.4	2.15	0.01	2.95
12-KIS-10	4.21	280	2	50.6	4.63	418	13.45	14	2.58	2.43	1.4	2.13	0.01	2.93
12-KIS-9	4.1	275	2	51.1	4.74	414	12.9	13.6	2.59	2.41	1.35	2.04	0.01	2.84
12-KIS-8	4.05	276	2	49.3	4.61	417	13.05	13.45	2.46	2.3	1.38	2.07	0.01	2.84
12-KIS-7	3.97	272	2	51.2	4.72	420	12.8	13.2	2.2	2.36	1.39	2.03	0.01	2.78
12-KIS-6	4.05	276	2	51.4	4.62	404	12.5	13.25	2.42	2.38	1.35	1.98	0.01	2.8
12-KIS-5	4.15	289	2	51.6	4.68	420	12.45	13.3	2.16	2.35	1.37	1.99	0.01	2.83
12-KIS-4	4.03	285	2	49.3	4.48	399	12.25	13.25	2.2	2.34	1.35	1.97	0.01	2.8
12-KIS-3	4.06	272	2	48.9	4.48	406	12.4	13.25	2.12	2.37	1.36	1.97	0.01	2.82
12-KIS-2	4.17	277	2	50.4	4.55	404	12.35	13.2	2.42	2.3	1.34	1.98	0.01	2.79
12-KIS-1	4.31	270	2	50	4.48	396	11.95	12.7	4.02	2.28	1.32	1.92	0.01	2.7
12-KIS-33	2.41	182	2	60.5	6.09	586	13.7	11.1	1.32	1.82	1.95	2.48	0.01	2.01
12-KIS-32	2.31	190	2	59.1	5.77	567	14.45	11.6	1.29	1.93	1.63	2.48	0.01	2.01
12-KIS-31	2.13	171	2	58.3	5.84	575	14.75	11.3	1.23	1.92	1.72	2.42	0.01	1.81
12-KIS-30	2.19	173	2	58.3	5.92	566	14.7	11.25	1.21	1.95	1.75	2.46	0.01	1.83
12-KIS-29	2.14	136	2	56.9	5.91	560	14.6	10.7	1.78	1.82	1.99	2.47	0.01	1.63
12-KIS-58	3.05	178	2	43.6	3.98	376	9.97	8.93	13.45	1.86	0.78	1.79	0.01	1.63
12-KIS-57	2.79	198	2	49.6	4.52	419	11.05	9.94	8.95	1.92	1	1.95	0.01	1.85
12-KIS-56	2.61	202	2	52.9	4.82	446	11.45	10.35	5.91	1.97	1.01	2.03	0.01	1.94
12-KIS-55	2.33	228	2	55.5	4.92	474	12.1	11.1	4.34	2.01	1.12	2.16	0.01	2.13

Table C.1: (Continued)

Sample	U (ppm)	V (ppm)	W (ppm)	Y (ppm)	Yb (ppm)	Zr (ppm)	Al_2O_3 (wt %)	Fe_2O_3 (wt %)	CaO (wt %)	MgO (wt %)	Na_2O (wt %)	K_2O (wt %)	Cr_2O_3 (wt %)	TiO_2 (wt %)
12-KIS-54	2.23	224	2	55.5	4.89	470	12.25	11.35	3.46	2.04	1.12	2.17	0.01	2.16
12-KIS-53	2.27	221	2	55.1	4.92	469	12.1	11	4.18	1.99	1.04	2.15	0.01	2.09
12-KIS-52	2.48	212	2	53.1	4.85	464	11.85	10.8	5.53	1.99	1.02	2.11	0.01	2.04
12-KIS-51	2.37	217	2	54.8	4.82	471	11.95	11	4.51	1.98	1.04	2.14	0.01	2.08
12-KIS-48	2.37	236	2	55	5.05	489	12.2	11.2	4.37	2.07	1.13	2.15	0.01	2.11
12-KIS-47	2.81	243	2	57.4	5.16	473	11.75	11.6	7.15	2.26	1.3	2.06	0.01	2.21
12-KIS-46	2.66	235	2	56.7	5.02	471	12.05	11.55	5.8	2.23	1.14	2.1	0.01	2.18
12-KIS-45	2.55	265	3	58.4	5.35	493	12.2	12.05	4.52	2.23	1.14	2.13	0.01	2.28
12-KIS-44	2.04	241	2	54.8	4.95	490	12.45	12.05	2.66	2.23	1.16	2.15	0.01	2.24
12-KIS-42	2.14	271	2	56.3	4.98	498	12.45	12.9	2.85	2.44	1.18	2.18	0.01	2.46
12-KIS-41	2.37	262	2	55.9	4.95	475	12.25	12.1	4.92	2.32	1.18	2.14	0.01	2.32
12-KIS-40	2.56	252	2	52.8	4.81	463	12.4	12	5.13	2.38	1.22	2.1	0.01	2.29
12-KIS-39	2.41	269	2	52.8	4.66	486	13.15	12.9	3.9	2.4	1.29	2.19	0.01	2.49
12-KIS-38	2.4	251	2	50.4	4.63	498	13.2	12.85	2.73	2.25	1.34	2.26	0.01	2.42
12-KIS-37	2.49	237	2	55.3	5.32	474	13.35	12.3	3.21	2.19	1.35	2.26	0.01	2.34
12-KIS-36	2.79	245	2	54.8	5.31	467	13.25	12.65	4.51	2.4	1.34	2.18	0.01	2.41
12-KIS-35	2.49	240	2	54	5.15	487	13.15	12.35	3.14	2.37	1.83	2.22	0.01	2.34
13-KIS-2	2.56	165	2	54.1	5.31	519	12.2	10.35	6.45	2.21	1.68	2.31	0.01	1.85
13-KIS-3	2.56	182	2	59.5	5.98	577	12.95	11.05	3.98	2.35	1.75	2.44	0.01	2.05
13-KIS-4	2.33	187	2	58.1	5.63	592	13.35	11.3	3.11	2.34	1.74	2.48	0.01	2.04
13-KIS-5	2.21	174	2	56.1	5.52	587	13.85	11.45	2.26	2.42	1.74	2.47	0.01	1.95
13-KIS-6	2.19	176	2	57.6	5.49	619	14.05	11.5	1.81	2.36	1.8	2.53	0.01	1.99
13-KIS-7	2.49	192	2	61.3	5.97	618	13.35	11.3	2.07	2.23	1.79	2.44	0.01	2.02
13-KIS-8	2.43	186	2	62	5.92	615	13.6	11.5	1.75	2.3	1.8	2.47	0.01	2.04

Table C.1: (Continued)

Sample	U (ppm)	V (ppm)	W (ppm)	Y (ppm)	Yb (ppm)	Zr (ppm)	Al_2O_3 (wt %)	Fe_2O_3 (wt %)	CaO (wt %)	MgO (wt %)	Na_2O (wt %)	K_2O (wt %)	Cr_2O_3 (wt %)	TiO_2 (wt %)
13-KIS-9	2.44	176	2	61.7	6.17	622	13.6	11.25	1.74	2.24	1.96	2.5	0.01	2
13-KIS-10	2.87	170	2	66.5	6.92	652	12.95	10.9	2.84	2.12	2.32	2.45	0.01	1.85
13-KIS-11	2.74	167	2	69.4	6.93	733	13.65	11.05	1.65	2.07	2.64	2.69	0.01	1.94
13-KIS-12	2.94	166	2	72.7	7.37	774	13.65	11	2.05	2.06	2.64	2.7	0.01	1.89
13-KIS-13	3.05	151	2	77.3	7.85	830	13.95	10.85	1.28	1.96	3.03	2.82	0.01	1.78
13-KIS-14	3.03	155	2	79	7.78	830	14.15	11.1	1.46	2.08	2.92	2.79	0.01	1.81
13-KIS-15	3.13	163	2	68.2	6.95	698	13.25	10.85	3.73	2.24	2.37	2.51	0.01	1.84
13-KIS-17	3.39	167	2	60.1	5.89	540	12.2	10.5	7.44	2.35	1.76	2.23	0.01	1.84
13-KIS-18	3.41	164	2	60.6	5.62	553	12.65	10.75	6.02	2.22	1.99	2.41	0.01	1.86
13-KIS-20	2.47	173	2	62.1	5.85	593	12.75	10.9	1.52	2.03	2.38	2.48	0.01	2.07
13-KIS-21	2.39	172	2	60.9	6.02	604	13.35	11	1.1	1.87	2.17	2.51	0.01	2.01
13-KIS-22	2.25	157	2	58.8	5.81	609	13.95	10.85	1.11	2	2.07	2.45	0.01	1.78
13-KIS-23	2.13	149	2	61	5.82	602	14.1	10.75	0.99	1.98	2.08	2.42	0.01	1.71
13-KIS-24	2.04	145	2	59.1	5.82	602	14.5	10.85	1.08	2.14	2.07	2.42	0.01	1.65
13-KIS-25	2.23	146	2	60.8	6.03	605	14.75	11	1.53	2.31	2.13	2.46	0.01	1.65
13-KIS-26	2.05	150	2	59.9	5.93	618	14.65	11.05	1.45	2.18	2.2	2.51	0.01	1.71
13-KIS-27	2.17	138	2	57	5.65	572	14.15	10.55	3.26	2.25	2.1	2.37	0.01	1.61
13-KIS-28	2.05	132	1	58	5.57	571	14.35	10.5	2.04	1.96	2.39	2.48	0.01	1.57
13-KIS-30	2.31	121	2	60.2	6.36	621	14.8	10.25	1.06	1.63	3.98	3.29	0.01	1.53
13-KIS-31	1.94	182	2	58.3	5.41	559	14.4	12.05	1.26	2.24	2.63	2.68	0.01	2.1
13-KIS-32	1.99	213	2	56.7	5.25	541	14.5	12.95	1.41	2.44	2.26	2.55	0.01	2.32
13-KIS-34	2.06	245	2	54	4.92	513	14.15	13.45	2.36	2.59	1.9	2.4	0.01	2.55
13-KIS-35	2.13	244	2	54.3	4.86	479	13.15	12.85	3.88	2.48	1.87	2.23	0.01	2.46
13-KIS-36	2.27	237	2	53.3	4.78	471	12.55	12.35	6.45	2.46	1.88	2.16	0.01	2.39

Table C.1: (Continued)

Sample	U (ppm)	V (ppm)	W (ppm)	Y (ppm)	Yb (ppm)	Zr (ppm)	Al_2O_3 (wt %)	Fe_2O_3 (wt %)	CaO (wt %)	MgO (wt %)	Na_2O (wt %)	K_2O (wt %)	Cr_2O_3 (wt %)	TiO_2 (wt %)
13-KIS-37	2.39	246	2	52	4.71	465	12.75	12.5	6.95	2.47	1.77	2.15	0.01	2.4
13-KIS-38	2.38	263	2	53.2	4.98	474	13.1	13.25	5.06	2.55	1.76	2.22	0.01	2.59
13-KIS-39	2.45	247	2	51.1	4.7	437	12.25	12.3	8	2.39	1.65	2.06	0.01	2.38
13-KIS-40	2.49	268	2	52.3	4.56	474	12.9	13.3	4.71	2.53	1.92	2.19	0.01	2.61
13-KIS-41	2.54	279	2	54.4	4.72	477	13.05	13.55	4.36	2.56	1.96	2.19	0.01	2.69
13-KIS-42	2.51	276	2	53.6	4.84	474	12.85	13.4	4.59	2.52	1.87	2.16	0.01	2.65
13-KIS-43	2.76	250	2	54.4	4.73	446	11.8	12.4	8.51	2.42	1.74	1.99	0.01	2.39
13-KIS-44	2.9	272	2	52.5	4.74	450	12.1	12.85	7.7	2.43	1.6	2.02	0.01	2.57
13-KIS-45	2.89	278	2	56.2	4.74	461	12.4	13.45	5.91	2.51	1.66	2.08	0.01	2.7
13-KIS-46	2.55	268	2	52	4.43	474	13	13.3	4.93	2.56	1.89	2.19	0.01	2.6
13-KIS-48	2.82	262	2	51.8	4.58	462	12.5	13.05	5.42	2.53	1.76	2.11	0.01	2.55
13-KIS-49	2.84	266	2	51.2	4.54	447	12.05	12.9	7.09	2.53	1.7	2.03	0.01	2.55
13-KIS-50	2.53	283	2	53.7	4.75	495	13.35	13.8	3.26	2.59	1.81	2.22	0.01	2.74
13-KIS-51	2.84	268	2	52.7	4.6	455	12.15	12.9	6.6	2.47	1.62	2.04	0.01	2.56
13-KIS-52	2.75	283	2	52.8	4.58	465	12.35	13.45	5.11	2.5	1.6	2.07	0.01	2.72
13-KIS-53	2.54	306	2	53.4	4.66	483	12.85	14.3	2.48	2.54	1.66	2.17	0.01	2.93
13-KIS-54	2.68	279	2	52.5	4.52	476	12.65	13.7	4.15	2.52	1.66	2.12	0.01	2.76
13-KIS-55	2.92	306	2	56.5	4.8	476	12.5	14.45	4.13	2.61	1.62	2.12	0.01	2.98
13-KIS-56	3.57	279	2	51.2	4.42	410	10.75	13	9.95	2.52	1.41	1.84	0.02	2.69
13-KIS-71	3.02	278	2	51.7	4.73	497	13.6	14	2.61	2.73	1.06	2.33	0.02	2.61
13-KIS-72	2.96	272	2	54.5	5.09	521	13.55	13.65	2.36	2.67	1.11	2.3	0.02	2.56
13-KIS-73	3.08	292	2	54.2	4.95	503	13.4	14.05	3.35	2.73	1.05	2.3	0.02	2.7
13-KIS-74	2.9	313	2	52.2	5.18	448	13.7	14.9	1.7	2.79	1.25	2.27	0.03	2.88
13-KIS-75	2.8	318	2	50.8	5.16	459	13.75	15.1	1.74	2.91	1.26	2.2	0.03	2.89

Table C.1: (Continued)

Sample	U (ppm)	V (ppm)	W (ppm)	Y (ppm)	Yb (ppm)	Zr (ppm)	Al_2O_3 (wt %)	Fe_2O_3 (wt %)	CaO (wt %)	MgO (wt %)	Na_2O (wt %)	K_2O (wt %)	Cr_2O_3 (wt %)	TiO_2 (wt %)
13-KIS-76	2.72	321	2	49.9	4.81	460	13.85	15.35	1.66	2.88	1.23	2.22	0.03	2.94
13-KIS-77	2.51	315	2	49.7	5.05	450	13.8	15.05	1.61	2.84	1.24	2.2	0.03	2.89
13-KIS-78	2.47	307	2	49.8	4.84	446	13.7	14.85	1.65	2.78	1.23	2.17	0.03	2.85
13-KIS-79	2.54	302	2	50.6	5.42	453	13.35	14.6	2.84	2.8	1.25	2.16	0.03	2.79
13-KIS-80	2.56	302	2	50.8	5.15	444	13.7	15	2.35	2.82	1.35	2.2	0.03	2.89
13-KIS-81	2.58	308	2	48.1	4.68	448	13.4	15	2.73	2.94	1.36	2.15	0.03	2.87
13-KIS-82	2.73	306	2	48.8	4.79	449	13.1	14.35	2.75	2.75	1.28	2.06	0.03	2.73
13-KIS-83	2.9	299	2	50	5	447	12.95	14.2	3.62	2.73	1.18	2.03	0.03	2.69
DP1011H	2.64	230	2	46	3.74	427	11.25	10.55	8.11	3.47	1.33	2.31	0.01	2.16
DP1011F	2.75	208	2	45	3.66	412	11.2	10.5	7.77	3.31	1.31	2.24	0.01	2.15
DP1011E	2.89	208	2	44.4	3.59	409	10.8	10.3	7.56	3.24	1.27	2.21	0.01	2.11
DP1011D	2.92	217	2	46.5	3.65	442	12.6	10.7	6.45	3.46	1.22	2.45	0.01	2.15
DP1011C	3.22	245	2	48.9	3.82	440	11.25	11.3	8.92	3.47	1.38	2.45	0.01	2.38
DP1011B	3.44	248	2	50.6	3.78	451	11.55	12	7.56	3.58	1.47	2.57	0.01	2.61
13-AR-6	11.2	147	2	53.1	5.32	577	14.9	10.45	1.35	2.08	2.07	2.95	<0.01	1.62
13-AR-7	11.75	145	2	58	5.97	558	14.1	9.95	3.34	2.01	2.48	2.83	<0.01	1.55
13-AR-8	11.8	143	2	57.4	5.77	552	14.4	10.1	2.56	2.01	2.65	2.82	<0.01	1.55
13-AR-9	11.95	141	2	59.1	6.31	557	14.45	10	2.93	1.97	2.6	2.76	<0.01	1.54
13-AR-10	11.15	141	2	55.8	5.77	540	14.2	9.83	3.19	1.91	2.59	2.72	<0.01	1.5
13-AR-11	7.7	146	2	61.8	6.88	557	13.15	8.82	2.16	1.39	2.66	3.04	<0.01	1.65
13-AR-12	8	139	2	67.1	7.48	614	13.55	8.98	0.89	1.4	3.09	2.96	<0.01	1.61
13-AR-13	8.86	134	2	58.5	6.18	604	14.7	9.92	1.29	1.78	3.11	2.76	<0.01	1.47
13-AR-14	9.79	143	2	54.3	5.66	592	14.45	9.95	0.91	1.82	3.21	2.74	<0.01	1.51
13-AR-15	9.56	138	2	51.4	5.52	570	15.05	10.3	1.08	1.9	3.19	2.79	<0.01	1.48

Table C.1: (Continued)

Sample	U (ppm)	V (ppm)	W (ppm)	Y (ppm)	Yb (ppm)	Zr (ppm)	Al_2O_3 (wt %)	Fe_2O_3 (wt %)	CaO (wt %)	MgO (wt %)	Na_2O (wt %)	K_2O (wt %)	Cr_2O_3 (wt %)	TiO_2 (wt %)
13-AR-16	9.57	132	2	58.5	6.5	552	14.65	10.05	2.73	1.86	3.04	2.75	<0.01	1.45
13-AR-17	8.5	141	2	53.5	5.77	589	15.15	10.3	0.96	1.88	3.44	2.79	<0.01	1.53
13-AR-18	9.02	140	2	55.1	6	558	14.7	9.95	1.42	1.78	3.4	2.66	<0.01	1.47
13-AR-19	8.59	141	2	55.6	5.93	571	14.65	9.88	1.58	1.7	3.37	2.62	<0.01	1.47
13-AR-20	8.32	121	2	66	7.07	582	14.6	9.31	3.43	1.53	3.24	2.41	<0.01	1.23
13-AR-37	7.62	151	2	57.1	5.46	437	12.05	9.3	10.05	1.83	2.63	1.97	<0.01	1.52
13-AR-38	8.4	194	2	51.8	5.01	496	13.85	11.05	4.06	2	2.97	2.24	0.01	1.9
13-AR-21	3.68	191	2	60.3	5.57	424	12.9	10.45	6.43	1.92	2.69	2.09	<0.01	1.77
13-AR-22	3.33	213	2	52.6	4.96	452	13.85	11.5	3.18	1.87	3.13	2.23	0.01	1.93
13-AR-23	3.18	242	2	50	4.56	489	14.55	12.05	1.12	1.86	3.04	2.3	0.01	2.01
13-AR-24	3.05	221	2	47.2	4.42	464	14.6	12.1	1.87	1.88	2.93	2.27	0.01	2.01
13-AR-25	2.98	209	2	44	4.05	484	14.85	12.3	1.1	1.87	2.85	2.29	0.01	2.05
13-AR-26	3.07	223	2	44.8	4.24	481	15.05	12.45	1.27	1.87	2.76	2.31	0.01	2.07
13-AR-27	2.96	227	2	45.8	4.23	481	14.65	12.3	1.22	1.83	2.66	2.28	0.01	2.05
13-AR-28	2.92	215	2	47.9	4.48	471	14.6	12	1.8	1.82	2.52	2.22	0.01	2.03
13-AR-29	2.81	205	2	55.9	5.25	484	14.35	11.9	2.01	1.82	2.52	2.22	0.01	2.04
13-AR-32	2.51	185	2	74.3	6.9	491	12.55	10.05	6.14	1.69	2.25	1.93	<0.01	1.88
13-AR-33	2.08	196	2	65.5	6.02	519	13.95	11.25	1.4	1.74	2.77	2.14	0.01	2.09
13-AR-34	2.34	212	2	69.8	6.64	538	13.55	10.95	1.67	1.66	2.72	2.13	0.01	2.05
13-AR-35	3.01	216	2	42.3	4.23	482	14.9	12.4	0.7	1.85	2.85	2.3	0.01	2.05
13-AR-36	2.78	206	2	98.8	8.65	443	11.75	10.4	7.37	1.8	2.21	1.94	<0.01	1.79
13-AOCH-2	2.44	116	2	53.8	4.94	514	13.25	9.15	3.12	1.72	2.33	2.41	0.01	1.47
13-AOCH-3	2.26	151	2	44.6	4.48	478	12.45	9.46	2.96	1.99	1.59	2.16	0.01	1.59
13-AOCH-4	2.54	189	2	33.6	3.71	420	11.75	9.59	5.3	2	1.47	2.08	0.01	1.63

Table C.1: (Continued)

Sample	U (ppm)	V (ppm)	W (ppm)	Y (ppm)	Yb (ppm)	Zr (ppm)	Al_2O_3 (wt %)	Fe_2O_3 (wt %)	CaO (wt %)	MgO (wt %)	Na_2O (wt %)	K_2O (wt %)	Cr_2O_3 (wt %)	TiO_2 (wt %)
13-AOCH-5	2.77	181	2	35.2	3.65	390	11.4	9.42	6.72	1.97	1.41	2.03	0.01	1.62
13-AOCH-6	2.68	185	2	39	3.7	413	11.75	9.85	6.1	2.07	1.52	2.07	0.01	1.74
13-AOCH-7	2.51	184	2	38.7	4.07	415	11.4	9.59	4.58	2.01	1.5	2.09	0.01	1.8
13-AOCH-8	2.6	176	2	40.7	4.08	425	11.65	9.76	4.66	2.1	1.6	2.14	0.01	1.83
13-AOCH-9	3.1	187	2	46.8	4.47	427	11.4	9.71	4.99	2.07	1.62	2.12	0.01	1.95
13-AOCH-10	3.13	189	2	48.1	4.63	438	11.25	9.62	4.88	1.98	1.62	2.09	0.01	1.94
13-AOCH-11	3.23	196	2	51.6	4.52	417	11.15	10.05	7	2.07	1.56	2.03	0.01	1.98
13-AOCH-12	3.31	222	2	48.3	4.59	430	11.65	11	5.38	2.22	1.6	2.14	0.01	2.19
13-OB-1	3.89	192	2	33.9	3.02	390	12.45	9.41	4.24	2.71	1.24	2.63	0.01	1.76
13-OB-3	3.45	187	2	35.8	3.11	415	12	9.01	3.45	2.46	1.22	2.54	0.01	1.68
13-OB-6	3.06	167	2	33.2	2.85	367	11	8.58	7.41	2.46	1.18	2.28	0.01	1.62
13-WOK-1	3.02	229	2	51.3	4.46	516	15.25	11.9	4.05	2.27	1.48	2.88	0.01	2.05
13-WOK-2	2.81	208	2	49.7	4.23	466	14.3	11.15	7.48	2.21	1.35	2.61	0.01	1.86
13-WOK-4	2.96	232	3	50.2	4.13	516	14.9	11.5	4.13	2.2	1.36	2.73	0.01	2.09
13-WOK-5	2.92	248	2	51.7	4.32	537	14.95	11.8	3.89	2.18	1.31	2.7	0.01	2.2
13-WOK-6	2.81	231	2	45	3.81	504	14.8	11.6	3.72	2.17	1.32	2.66	0.01	2.11
13-WOK-7	2.78	226	2	47.5	3.85	500	14.5	11.2	5.32	2.15	1.32	2.71	0.01	1.96
13-WOK-8	2.84	229	2	49.7	4.04	518	14.65	11.45	3.92	2.09	1.28	2.81	0.01	2.13
13-WOK-9	2.69	222	2	46.5	3.78	495	14.7	11.6	4.57	2.14	1.23	2.66	0.01	2.15
13-WOK-10	3.32	240	2	52.2	4.3	526	14.65	11.6	4.36	2.05	1.44	2.75	0.01	2.3
13-WOK-11	3.19	263	2	53.8	4.57	563	14.65	11.95	4.73	2.1	1.35	2.73	0.01	2.42
13-WOK-12	2.95	255	2	50.8	4.32	544	14.5	11.65	3.97	2.06	1.33	2.75	0.02	2.36
13-NY-2	3.41	223	2	43.7	3.69	499	13.55	12.55	3.82	3.22	2.54	2.6	0.01	2.12

Table C.1: (Continued)

Sample	U (ppm)	V (ppm)	W (ppm)	Y (ppm)	Yb (ppm)	Zr (ppm)	Al_2O_3 (wt %)	Fe_2O_3 (wt %)	CaO (wt %)	MgO (wt %)	Na_2O (wt %)	K_2O (wt %)	Cr_2O_3 (wt %)	TiO_2 (wt %)
13-NY-3	3.41	154	1	62.4	3.69	353	10.1	8.81	18.1	2.7	1.88	1.94	0.01	1.4
13-NY-4	3.18	212	2	40	3.34	499	14.6	12.85	2.05	3.1	2.6	2.77	0.01	2.01
13-NY-5	3.15	198	2	42.5	3.56	476	14.05	12.2	2.31	3.03	2.49	2.67	0.01	1.92
13-NY-6	3.66	130	1	71.9	4.89	288	8.36	7.23	21.8	3.57	1.74	1.76	0.01	1.16
13-NY-7	4.75	221	1	43.4	3.36	436	11.45	11.2	15.2	2.81	1.7	2.46	0.01	2.3
13-NY-8	4.4	215	2	48.5	3.39	443	11.35	10.5	13.9	2.67	1.58	2.21	0.01	2.06
13-NY-9	4.17	209	2	46.7	3.69	453	12.85	11.3	10.35	2.81	1.75	2.42	0.01	2.17
13-NY-10	3.98	229	2	44.4	3.5	510	13.6	12	6.34	2.9	1.82	2.63	0.01	2.27
13-NY-11	3.74	244	2	48.8	3.52	482	12.9	11.95	8.09	2.91	1.88	2.52	0.01	2.36
13-NY-12	3.92	267	2	46.9	3.61	521	13.2	12.8	6.54	2.99	1.92	2.63	0.01	2.57
13-NY-13	4	193	2	43.8	3.69	398	11.45	10.35	13.65	2.9	1.64	2.27	0.01	1.94

Table C.1: (Continued)

Sample	MnO (wt %)	P_2O_5 (wt %)	SrO (wt %)	BaO (wt %)	LOI (wt %)	Total (wt %)
13-KIS-57	0.5	0.52	0.05	0.09	14.65	99.38
13-KIS-58	0.47	0.55	0.05	0.16	11.85	100.98
13-KIS-59	0.48	0.56	0.05	0.08	11.45	100.49
13-KIS-60	0.47	0.57	0.05	0.09	11.25	99.16
13-KIS-61	0.49	0.58	0.04	0.06	11.5	99.94
13-KIS-62	0.42	0.49	0.06	0.24	16.9	99.16
13-KIS-63	0.54	0.58	0.05	0.06	11.75	99.76
13-KIS-64	0.5	0.58	0.05	0.13	12.15	100.01
13-KIS-65	0.56	0.59	0.05	0.1	11.75	98.92
13-KIS-66	0.62	0.61	0.05	0.15	11.8	99.96
13-KIS-67	0.76	0.63	0.05	0.09	10.95	100.70
13-KIS-68	0.71	0.65	0.06	0.21	10.95	100.39
13-KIS-69	0.73	0.69	0.05	0.1	10.5	100.03
13-KIS-70	0.94	0.73	0.07	0.63	10.7	100.33
12-KIS-25	0.36	0.49	0.05	0.06	15.7	99.61
12-KIS-24	0.37	0.51	0.05	0.06	17.15	99.56
12-KIS-23	0.39	0.56	0.05	0.06	15.25	101.40
12-KIS-22	0.41	0.61	0.06	0.27	15.7	101.70
12-KIS-21	0.39	0.56	0.05	0.06	14.95	99.36
12-KIS-20	0.43	0.63	0.05	0.08	15.15	99.84
12-KIS-19	0.43	0.59	0.05	0.06	14.85	99.66
12-KIS-18	0.42	0.59	0.05	0.07	16.2	101.68
12-KIS-17	0.42	0.64	0.05	0.06	15.35	99.61
12-KIS-16	0.44	0.60	0.05	0.06	15.1	101.30

Table C.1: (Continued)

Sample	MnO (wt %)	P_2O_5 (wt %)	SrO (wt %)	BaO (wt %)	LOI (wt %)	Total (wt %)
12-KIS-15	0.44	0.63	0.05	0.06	16	101.06
12-KIS-14	0.44	0.64	0.05	0.06	15.35	100.96
12-KIS-13	0.44	0.66	0.05	0.06	15.35	101.20
12-KIS-12	0.44	0.64	0.05	0.06	15.65	100.48
12-KIS-11	0.48	0.68	0.05	0.06	15.25	101.29
12-KIS-10	0.46	0.68	0.05	0.07	15.35	100.54
12-KIS-9	0.46	0.63	0.05	0.06	15.9	101.04
12-KIS-8	0.47	0.63	0.05	0.06	17.15	99.52
12-KIS-7	0.45	0.66	0.05	0.06	17.25	101.44
12-KIS-6	0.45	0.64	0.05	0.06	17.3	100.29
12-KIS-5	0.5	0.66	0.05	0.06	17.2	100.43
12-KIS-4	0.55	0.62	0.05	0.06	17.3	99.75
12-KIS-3	0.44	0.62	0.05	0.06	17.25	100.32
12-KIS-2	0.44	0.62	0.05	0.11	17.3	100.21
12-KIS-1	0.45	0.60	0.05	0.09	18.3	100.09
12-KIS-33	0.36	0.44	0.04	0.06	14.45	101.94
12-KIS-32	0.34	0.43	0.04	0.06	14.6	100.67
12-KIS-31	0.3	0.38	0.03	0.05	16.05	99.67
12-KIS-30	0.31	0.37	0.03	0.05	14.85	101.97
12-KIS-29	0.28	0.31	0.03	0.05	14.75	100.92
12-KIS-58	0.59	0.69	0.07	0.13	21.6	101.10
12-KIS-57	0.62	0.81	0.07	0.2	18.7	100.97
12-KIS-56	0.56	0.79	0.06	0.14	17.25	98.77
12-KIS-55	0.54	0.82	0.06	0.16	16.1	100.55

Table C.1: (Continued)

Sample	MnO (wt %)	P_2O_5 (wt %)	SrO (wt %)	BaO (wt %)	LOI (wt %)	Total (wt %)
12-KIS-54	0.46	0.8	0.06	0.11	15.65	100.74
12-KIS-53	0.51	0.75	0.06	0.11	16.95	101.04
12-KIS-52	0.48	0.75	0.06	0.12	16.4	100.56
12-KIS-51	0.46	0.71	0.06	0.12	15.65	99.51
12-KIS-48	0.54	0.72	0.06	0.11	15.4	99.67
12-KIS-47	0.57	0.72	0.07	0.15	16.85	101.50
12-KIS-46	0.53	0.7	0.07	0.13	16.05	100.24
12-KIS-45	0.81	0.68	0.06	0.16	15.4	99.47
12-KIS-44	0.54	0.62	0.06	0.12	15.95	98.34
12-KIS-42	0.42	0.7	0.06	0.11	13.55	98.61
12-KIS-41	0.65	0.74	0.07	0.17	15.45	99.62
12-KIS-40	0.45	0.66	0.07	0.11	15.15	98.97
12-KIS-39	0.52	0.68	0.06	0.11	14.3	100.20
12-KIS-38	0.51	0.66	0.06	0.1	16.15	101.94
12-KIS-37	0.46	0.66	0.06	0.1	15.3	99.99
12-KIS-36	0.52	0.64	0.06	0.11	15.2	99.58
12-KIS-35	0.44	0.6	0.06	0.09	15.8	101.30
13-KIS-2	0.3	0.6	0.07	0.09	15.2	99.92
13-KIS-3	0.37	0.57	0.06	0.09	13.85	101.62
13-KIS-4	0.43	0.55	0.06	0.1	13.9	101.01
13-KIS-5	0.28	0.47	0.05	0.08	13.6	100.73
13-KIS-6	0.25	0.49	0.05	0.07	12.85	101.06
13-KIS-7	0.47	0.54	0.05	0.1	13.05	98.82
13-KIS-8	0.29	0.53	0.05	0.07	12.6	99.21

Table C.1: (Continued)

Sample	MnO (wt %)	P_2O_5 (wt %)	SrO (wt %)	BaO (wt %)	LOI (wt %)	Total (wt %)
13-KIS-9	0.38	0.53	0.04	0.06	12.7	99.61
13-KIS-10	0.4	0.51	0.04	0.05	13.1	98.64
13-KIS-11	0.4	0.5	0.04	0.05	11.5	100.49
13-KIS-12	0.38	0.5	0.04	0.05	11.05	99.72
13-KIS-13	0.36	0.47	0.03	0.05	10.4	99.19
13-KIS-14	0.35	0.53	0.04	0.05	10.55	100.54
13-KIS-15	0.38	0.48	0.06	0.1	12.35	98.37
13-KIS-17	0.43	0.55	0.08	0.09	14.55	98.73
13-KIS-18	0.42	0.54	0.06	0.08	13.2	99.81
13-KIS-20	0.32	0.48	0.04	0.06	12.8	99.74
13-KIS-21	0.45	0.39	0.03	0.05	12.65	100.29
13-KIS-22	0.38	0.37	0.03	0.05	13.8	99.85
13-KIS-23	0.36	0.38	0.03	0.04	13.95	99.90
13-KIS-24	0.3	0.4	0.04	0.05	14.45	100.86
13-KIS-25	0.35	0.43	0.05	0.06	12.1	100.63
13-KIS-26	0.26	0.43	0.04	0.06	11.45	101.80
13-KIS-27	0.27	0.48	0.05	0.06	12.6	100.56
13-KIS-28	0.23	0.5	0.04	0.05	11.25	100.87
13-KIS-30	0.34	0.32	0.03	0.05	8.69	100.48
13-KIS-31	0.37	0.47	0.04	0.06	10.2	99.31
13-KIS-32	0.43	0.54	0.04	0.07	10.8	101.12
13-KIS-34	0.33	0.62	0.05	0.07	11.3	101.28
13-KIS-35	0.42	0.63	0.05	0.09	12.6	98.42
13-KIS-36	0.35	0.63	0.05	0.13	14.05	99.46

Table C.1: (Continued)

Sample	MnO (wt %)	P_2O_5 (wt %)	SrO (wt %)	BaO (wt %)	LOI (wt %)	Total (wt %)
13-KIS-37	0.39	0.6	0.06	0.09	14.4	100.34
13-KIS-38	0.4	0.63	0.05	0.1	13.2	100.32
13-KIS-39	0.45	0.58	0.06	0.09	15.05	99.07
13-KIS-40	0.46	0.64	0.05	0.09	12.95	99.06
13-KIS-41	0.52	0.65	0.05	0.11	12.4	98.90
13-KIS-42	0.53	0.64	0.05	0.09	12.75	98.41
13-KIS-43	0.42	0.58	0.06	0.1	15	98.32
13-KIS-44	0.52	0.6	0.06	0.1	14.55	98.71
13-KIS-45	0.48	0.68	0.06	0.16	13.3	98.80
13-KIS-46	0.47	0.64	0.05	0.1	12.9	99.24
13-KIS-48	0.44	0.62	0.05	0.1	14.05	98.79
13-KIS-49	0.43	0.63	0.06	0.2	15.2	99.08
13-KIS-50	0.49	0.62	0.06	0.12	12.95	100.02
13-KIS-51	0.48	0.6	0.06	0.11	14.8	98.50
13-KIS-52	0.52	0.64	0.06	0.12	14	98.35
13-KIS-53	0.56	0.69	0.05	0.1	12.4	98.14
13-KIS-54	0.52	0.65	0.06	0.14	13.55	99.29
13-KIS-55	0.52	0.71	0.06	0.11	12.9	100.32
13-KIS-56	0.48	0.63	0.06	0.12	16.45	99.02
13-KIS-71	0.42	0.57	0.05	0.07	12.25	100.32
13-KIS-72	0.46	0.56	0.05	0.08	11.9	99.97
13-KIS-73	0.55	0.6	0.05	0.09	12.5	101.29
13-KIS-74	0.53	0.58	0.04	0.06	11.75	101.38
13-KIS-75	0.54	0.53	0.04	0.06	12.05	100.90

Table C.1: (Continued)

Sample	MnO (wt %)	P_2O_5 (wt %)	SrO (wt %)	BaO (wt %)	LOI (wt %)	Total (wt %)
13-KIS-76	0.54	0.53	0.04	0.07	12.2	101.64
13-KIS-77	0.53	0.52	0.04	0.07	11.5	100.62
13-KIS-78	0.49	0.5	0.04	0.06	11.9	100.05
13-KIS-79	0.47	0.51	0.05	0.06	12.9	99.11
13-KIS-80	0.52	0.59	0.05	0.06	13.55	101.41
13-KIS-81	0.53	0.51	0.05	0.09	13.75	101.81
13-KIS-82	0.51	0.5	0.04	0.07	12.4	98.87
13-KIS-83	0.55	0.52	0.05	0.08	12.9	100.23
DP1011H	0.31	0.94	0.09	0.15	15.25	99.73
DP1011F	0.26	0.97	0.08	0.15	14.45	101.10
DP1011E	0.36	0.99	0.08	0.16	14.2	98.39
DP1011D	0.36	0.9	0.08	0.16	13.35	98.49
DP1011C	0.45	1.01	0.09	0.18	13.95	98.54
DP1011B	0.43	1.14	0.09	0.19	12.25	99.35
13-AR-6	0.25	0.37	0.05	0.07	10.8	101.36
13-AR-7	0.42	0.37	0.08	0.12	12.2	99.25
13-AR-8	0.34	0.33	0.05	0.07	11.85	101.23
13-AR-9	0.39	0.34	0.09	0.12	11.65	101.04
13-AR-10	0.5	0.35	0.09	0.12	11.7	100.70
13-AR-11	0.53	0.37	0.08	0.1	8.97	101.62
13-AR-12	0.44	0.3	0.06	0.08	9.01	100.77
13-AR-13	0.35	0.25	0.05	0.09	10.9	100.27
13-AR-14	0.26	0.26	0.04	0.06	10.85	96.66
13-AR-15	0.4	0.24	0.05	0.08	10.95	98.81

Table C.1: (Continued)

Sample	MnO (wt %)	P_2O_5 (wt %)	SrO (wt %)	BaO (wt %)	LOI (wt %)	Total (wt %)
13-AR-16	0.36	0.24	0.04	0.07	12	99.24
13-AR-17	0.36	0.27	0.03	0.06	10.85	99.52
13-AR-18	0.36	0.24	0.04	0.07	11.35	99.54
13-AR-19	0.4	0.22	0.07	0.08	11.45	99.49
13-AR-20	0.33	0.18	0.06	0.08	12.55	98.05
13-AR-37	0.32	0.17	0.06	0.11	17.75	98.36
13-AR-38	0.57	0.21	0.06	0.15	14.3	100.47
13-AR-21	0.58	0.32	0.09	0.12	14.35	98.51
13-AR-22	0.61	0.35	0.07	0.19	12.8	98.42
13-AR-23	0.69	0.35	0.05	0.14	11.85	98.02
13-AR-24	0.66	0.36	0.08	0.16	12.2	98.33
13-AR-25	0.4	0.31	0.06	0.11	11.8	98.40
13-AR-26	0.68	0.34	0.06	0.17	12.4	99.94
13-AR-27	0.59	0.33	0.07	0.16	12.75	99.20
13-AR-28	0.42	0.32	0.06	0.11	13.25	98.26
13-AR-29	0.45	0.31	0.06	0.12	13.5	99.31
13-AR-32	0.58	0.29	0.11	0.15	15	98.52
13-AR-33	0.63	0.31	0.07	0.16	12.35	99.77
13-AR-34	0.82	0.3	0.07	0.19	12.4	99.42
13-AR-35	0.49	0.31	0.05	0.12	12.25	98.68
13-AR-36	0.82	0.29	0.12	0.19	15.4	99.78
13-AOCH-2	0.31	0.3	0.05	0.08	11.65	99.05
13-AOCH-3	0.35	0.31	0.05	0.09	12	98.31
13-AOCH-4	0.29	0.26	0.06	0.09	12.55	98.78

Table C.1: (Continued)

Sample	MnO (wt %)	P_2O_5 (wt %)	SrO (wt %)	BaO (wt %)	LOI (wt %)	Total (wt %)
13-AOCH-5	0.38	0.26	0.06	0.1	14.15	99.13
13-AOCH-6	0.4	0.31	0.06	0.12	12.85	101.15
13-AOCH-7	0.39	0.33	0.06	0.11	11.9	98.67
13-AOCH-8	0.42	0.38	0.07	0.12	11.3	100.04
13-AOCH-9	0.51	0.47	0.06	0.15	11.15	100.31
13-AOCH-10	0.43	0.5	0.07	0.14	11.1	98.53
13-AOCH-11	0.36	0.57	0.07	0.13	12.85	99.43
13-AOCH-12	0.41	0.53	0.07	0.15	11.3	99.65
13-OB-1	0.25	0.47	0.06	0.1	11.25	101.68
13-OB-3	0.25	0.43	0.06	0.08	10	101.09
13-OB-6	0.25	0.44	0.06	0.11	13.2	100.00
13-WOK-1	0.39	0.76	0.08	0.22	10.35	101.69
13-WOK-2	0.37	0.68	0.08	0.16	12.65	101.11
13-WOK-4	0.37	0.69	0.08	0.16	11	100.82
13-WOK-5	0.38	0.69	0.08	0.14	10.6	100.23
13-WOK-6	0.41	0.68	0.08	0.15	10.65	98.96
13-WOK-7	0.47	0.67	0.08	0.19	11.6	100.58
13-WOK-8	0.37	0.72	0.08	0.15	10.4	99.76
13-WOK-9	0.36	0.68	0.08	0.13	11.45	101.96
13-WOK-10	0.36	0.73	0.08	0.13	9.4	100.06
13-WOK-11	0.49	0.74	0.08	0.15	9.67	100.87
13-WOK-12	0.42	0.71	0.08	0.14	9.09	98.48
13-NY-2	0.26	0.56	0.08	0.15	8.91	100.07

Table C.1: (Continued)

Sample	MnO (wt %)	P_2O_5 (wt %)	SrO (wt %)	BaO (wt %)	LOI (wt %)	Total (wt %)
13-NY-3	0.19	0.4	0.14	0.13	19	100.20
13-NY-4	0.28	0.53	0.08	0.15	9.19	101.72
13-NY-5	0.26	0.53	0.08	0.14	9.84	99.13
13-NY-6	0.22	0.41	0.3	0.15	22.6	100.91
13-NY-7	0.32	0.64	0.14	0.17	13.85	101.85
13-NY-8	0.3	0.59	0.13	0.14	14.8	98.44
13-NY-9	0.33	0.64	0.11	0.15	12.4	100.19
13-NY-10	0.33	0.68	0.1	0.17	10	99.05
13-NY-11	0.34	0.69	0.11	0.16	10.25	99.27
13-NY-12	0.34	0.77	0.1	0.17	8.85	99.89
13-NY-13	0.28	0.64	0.15	0.26	15.15	99.79

APPENDIX D

Table D.1: GPS Coordinates of Paleosols Used in Chapter Four

Locality	Site	Latitude (°S)	Longitude (°E)
Aringo	3	0.838	34.18
Aringo	5	0.838	34.18
Aoch Nyasaya	5	0.865	34.24
Kakrigu	DP1011	0.460	34.06
Kisaaka	4F	0.810	34.13
Kisaaka	10	0.807	34.13
Kisaaka	13	0.806	34.14
Kisaaka	12	0.802	34.14
Nyamita	1	0.423	34.16
Nyamita	AV1002	0.419	34.16
Obware	2	0.868	34.24
Wakondo	Bovid Hill	0.426	34.17

Datum WGS 1984

REFERENCES

Ambrose, S.H., and Lorenz, K.G., 1990, Social and ecological models for the Middle Stone Age in southern Africa, *in* Mellars, P. ed., The emergence of modern humans: and archaeological perspective: Edinburgh University Press, Edinburgh, p. 3–33.

Andrews, J.E., 2006, Palaeoclimatic records from stable isotopes in riverine tufas: Synthesis and review: Earth-Science Reviews, v. 75, p. 85–104.

Andrews, J.E., and Brasier, A.T., 2005, Seasonal records of climatic change in annually laminated tufas: short review and future prospects: Journal of Quaternary Science, v. 20, no. 5, p. 411–421.

Andrews, J.E., Riding, R., and Dennis, P.F., 1993, Stable isotopic compositions of recent freshwater cyanobacterial carbonates from the British Isles: Local and regional environmental controls: Sedimentology, v. 40, p. 303–314.

Andrews, J., Riding, R., and Dennis, P., 1997, The stable isotope record of environmental and climatic signals in modern terrestrial microbial carbonates from Europe: Palaeogeography, Palaeoclimatology, Palaeoecology, v. 129, p. 171–189.

Angelucci, D.E., 2010, The recognition and description of knapped lithic artifacts in thin section: Geoarchaeology, v. 25, p. 220–232.

Arenas, C., Vázquez-Urbez, M., Auqué, L., Sancho, C., Osácar, C., and Pardo, G., 2014, Intrinsic and extrinsic controls of spatial and temporal variations in modern fluvial tufa sedimentation: A thirteen-year record from a semi-arid environment (M. Pedley, Ed.): Sedimentology, v. 61, p. 90–132.

Arenas-Abad, C., Vázquez-Urbez, M., Pardo-Tirapu, G., and Sancho-Marcén, C., 2010, Fluvial and Associate Carbonate Deposits, *in* Alonso-Zarza, A.M. and Tanner, L.H. eds., Carbonates in Continental Settings: Facies, Environments, and Processes: Elsevier, New York, p. 133–175.

Ashley, G.M., Barboni, D., Domínguez-Rodrigo, M., Bunn, H.T., Mabulla, A.Z.P., Diez-Martin, F., Barba, R., and Baquedano, E., 2010a, A spring and wooded habitat at FLK Zinj and their relevance to origins of human behavior: Quaternary Research, v. 74, no. 3, p. 304–314.

Ashley, G.M., Barboni, D., Domínguez-Rodrigo, M., Bunn, H.T., Mabulla, A.Z.P., Diez-Martin, F., Barba, R., and Baquedano, E., 2010b, Paleoenvironmental and paleoecological reconstruction of a freshwater oasis in savannah grassland at FLK North, Olduvai Gorge, Tanzania: Quaternary Research, v. 74, no. 3, p. 333–343.

Ashley, G.M., Bunn, H.T., Delaney, J.S., Barboni, D., Domínguez-Rodrigo, M., Mabulla, A.Z.P., Gurtov, A.N., Baluyot, R., Beverly, E.J., and Baquedano, E., 2014, Paleoclimatic and paleoenvironmental framework of FLK North archaeological site, Olduvai Gorge, Tanzania: Quaternary International, v. 322-323, p. 54–65.

Ashley, G.M., Domínguez-Rodrigo, M., Bunn, H.T., Mabulla, A.Z.P., and Baquedano, E., 2010c, Sedimentary geology and human origins: A fresh look at Olduvai Gorge, Tanzania: Journal of Sedimentary Research, v. 80, no. 8, p. 703–709.

Ashley, G., Tactikos, J., and Owen, R., 2009, Hominin use of springs and wetlands: Paleoclimate and archaeological records from Olduvai Gorge (~1.79–1.74 Ma): Palaeogeography, Palaeoclimatology, Palaeoecology, v. 272, p. 1–16.

Ba, M.B., and Nicholson, S.E., 2001, Satellite-derived surface radiation budget over the African Continent. Part II: Climatologies of the various components: Journal of Climate, v. 14, p. 60–76.

Bard, E., Rostek, F., and Sonzogni, C., 1997, Interhemispheric synchrony of the last deglaciation inferred from alkenone palaeothermometry: Nature, v. 385, p. 707–710.

Barich, B.E., and Garcea, E.A.A., 2008, Ecological Patterns in the Upper Pleistocene and Holocene in the Jebel Gharbi, Northern Libya: Chronology, Climate and Human Occupation: African Archaeological Review, v. 25, p. 87–97.

Barnaby, R.J., and Rimstidt, J.D., 1989, Redox conditions of calcite cementation interpreted from Mn and Fe contents of authigenic calcites: Geological Society of America Bulletin, v. 101, p. 795–804.

Becker, M., LLovel, W., Cazenave, A., Güntner, A., and Crétaux, J.F., 2010, Recent hydrological behavior of the East African great lakes region inferred from GRACE, satellite altimetry and rainfall observations: Comptes Rendus Geoscience, v. 342, p. 223–233.

Beckmann, G.G., Thompson, C.H., and Hubble, G.D., 1973, Linear Gilgai: The Australian Geographer, v. 12, p. 363–366.

Behrensmeyer, A., Potts, R., and Plummer, T., 1995, The Pleistocene locality of Kanjera, Western Kenya: stratigraphy, chronology and paleoenvironments: Journal of Human Evolution, v. 29, p. 247–274.

Bell, R.H.V., 1970, The use of the herb layer by grazing ungulates in the Serengeti, *in* Watson, A. ed., Animal Populations in Relation to their Food Resources: Blackwell, Oxford, p. 111–124.

Belsky, A.J., 1990, Tree/grass ratios in East African savannas: a comparison of existing models: Journal of Biogeography, v. 17, p. 483–489.

Belsky, A.J., 1995, Spatial and temporal landscape patterns in arid and semi-arid Africa savannas, *in* Mosaic Landscapes and Ecological Processes:, p. 31–56.

Bergonzini, L., Richard, Y., Petit, L., and Camberlin, P., 2004, Zonal circulations over the Indian and Pacific oceans and the level of Lakes Victoria and Tanganyika: International Journal of Climatology, v. 24, p. 1613–1624.

Berke, M.A., Johnson, T.C., Werne, J.P., Grice, K., Schouten, S., and Sinninghe Damsté, J.S., 2012, Molecular records of climate variability and vegetation response since the Late Pleistocene in the Lake Victoria basin, East Africa: Quaternary Science Reviews, v. 55, p. 59–74.

Beuning, R.M., Kelts, K., Russell, J., and Wolfe, B.B., 2002, Reassessment of Lake Victoria-Upper Nile River paleohydrology from oxygen isotopes records of lake-sediment cellulose: Geology, v. 30, p. 559–562.

Beuning, K.R.M., Kelts, K., and Stager, J.C., 1998, Abrubt climate changes associated with the arid Younger Dryas interval in Africa, *in* Lehman, J.T. ed., Environmental Change and Response in East African Lakes: Springer, Netherlands, p. 147–156.

Beverly, E.J., Driese, S.G., Peppe, D.J., Arellano, L.N., Blegen, N., Faith, J.T., and Tryon, C.A., 2015a, Reconstruction of a semi-arid Late Pleistocene paleocatena from the Lake Victoria region, Kenya: Quaternary Research.

Beverly, E.J., Driese, S.G., Peppe, D.J., Johnson, C.R., Michel, L.A., Faith, J.T., Tryon, C.A., and Sharp, W.D., 2015b, Recurrent spring-fed rivers in a Middle to Late Pleistocene semi-arid grassland: Implications for environments of early humans in the Lake Victoria Basin, Kenya: Sedimentology.

Birkeland, P.W., 1999, Soils and Geomorphology: Oxford University Press, New York, 448 p.

Bishop, W.W., 1969, Pleistocene stratigraphy in Uganda: 128 p.

Bishop, W.W., and Trendall, A.F., 1967, Erosion-surfaces, tectonics and volcanic activity in Uganda: Quarterly Journal of the Geological Society of London, v. 122, p. 385–420.

Blegen, N., Tryon, C.A., Faith, J.T., Peppe, D.J., Beverly, E.J., Li, B., and Jacobs, Z., 2015, Distal tephras of the eastern Lake Victoria Basin, equatorial East Africa: correlations, chronology, and a context for early modern humans: Quarternary Science Reviews.

Blome, M.W., Cohen, A.S., Tryon, C.A., Brooks, A.S., and Russell, J., 2012, The environmental context for the origins of modern human diversity: A synthesis of regional variability in African climate 150,000-30,000 years ago: Journal of Human Evolution, v. 62, p. 563-592.

Bonnefille, R., and Chalie, F., 2000, Pollen-inferred precipitation time-series from equatorial mountains, Africa, the last 40 kyr B.P.: Global and Planetary Change, v. 26, p. 25–50.

Bonnefille, R., Chalié, F., Guiot, J., and Vincens, A., 1992, Quantitative estimates of full glacial temperatures in equatorial Africa from palynological data: Climate Dynamics, v. 6, p. 251–257.

Bonnefille, R., Roeland, J.C., and Guiot, J., 1990, Temperature and rainfall estimates for the past 40,000 years in equatorial Africa: Nature, v. 346, no. 6282, p. 347–349.

Bootsma, H. a., and Hecky, R.E., 2003, A Comparative Introduction to the Biology and Limnology of the African Great Lakes: Journal of Great Lakes Research, v. 29, p. 3–18.

Boven, A., Pasteels, P., Punzalan, L.E., Yamba, T.K., and Musisi, J.H., 1998, Quaternary perpotassic magmatism in Uganda (Toro-Ankole volcanic province): age assessment and significance for magmatic evolution along the East African Rift: Journal of African Earth Sciences, v. 26, p. 463–476.

Brady, N.C., and Weil, R.R., 2008, The Nature and Properties of Soils: Pearson Prentice Hall, New Jersey, 975 p.

Brasier, A.T., Andrews, J.E., Marca-Bell, A.D., and Dennis, P.F., 2010, Depositional continuity of seasonally laminated tufas: Implications for $\delta^{18}O$ based palaeotemperatures: Global and Planetary Change, v. 71, p. 160–167.

Brimhall, G.H., and Dietrich, W.E., 1987, Constitutive mass balance relations between chemical composition, volume, density, porosity, and strain in metasomatic hydrochemical systems: Results on weathering and pedogenesis: Geochimica et Cosmochimica Acta, v. 51, p. 567–587.

Broecker, W.S., Peteet, D., Hajdas, I., Lin, J., and Clark, E., 1998, Antiphasing between rainfall in Africa’s Rift Valley and North America's Great Basin: Quaternary Research, v. 50, p. 12–20.

Brown, F.H., McDougall, I., and Fleagle, J.G., 2012, Correlation of the KHS Tuff of the Kibish Formation to volcanic ash layers at other sites, and the age of early *Homo sapiens* (Omo I and Omo II).: Journal of Human Evolution, v. 63, p. 577–85.

Budyko, M.I., 1974, Climate and Life: Academic Press, New York, 508 p.

Burt, R. (Ed.), 2011, Soil Survey Laboratory Information Manual: Soil Survey Investigations Report No. 45: USDA NRCS, Nebraska, 506 p.

Carthew, K., Taylor, M., and Drysdale, R., 2002, Aquatic insect larval constructions in tropical freshwater limestone deposits (tufa): preservation of depositional environments: General & Applied Entomology, v. 31, p. 35–42.

Carthew, K.D., Taylor, M.P., and Drysdale, R.N., 2006, An environmental model of fluvial tufas in the monsoonal tropics, Barkly karst, northern Australia: Geomorphology, v. 73, p. 78–100.

Caudill, M.R., Driese, S., and Mora, C.I., 1996, Preservation of a paleo-Vertisol and an estimate of Late Mississippian paleoprecipitation: Journal of Sedimentary Research, v. 66, no. 1, p. 58–70.

Cerling, T.E., 1991, Carbon dioxide in the atmosphere: Evidence from Cenozoic and Mesozoic paleosols: American Journal of Science, v. 291, p. 377–400.

Cerling, T.E., Harris, J.M., and Passey, B.H., 2003, Diets of East African bovidae based on stable isotope analysis: Journal of Mammalogy, v. 84, p. 456–470.

Chadwick, O.A., Brimhall, G.H., and Hendricks, D.M., 1990, From a black to a gray box - a mass balance interpretation of pedogenesis: Geomorphology, v. 3, p. 369–390.

Chafetz, H., and Folk, R., 1984, Travertines: depositional morphology and the bacterially constructed constituents: Journal of Sedimentary Petrology, v. 54, no. 1, p. 289–316.

Chafetz, H., Rush, P., and Utech, N., 1991, Microenvironmental controls on mineralogy and habit of CaCO3 precipitates: an example from an active travertine system: Sedimentology, v. 38, p. 107–126.

Cheng, H., Ewards, R.L., Shen, C.-C., Polyak, V.J., Asmerom, Y., Woodhead, J., Hellstrom, J., Wang, Y., Kong, X., Spotl, C., Wang, X., and Alexander, E.C., 2013, Improvements in ^{230}Th dating, ^{230}Th and ^{234}U half-live values, and U-Th isotopic measurements by multi-collector inductively coupled plasma mass spectrometry: Earth and Planetary Science Letters, v. 371-372, p. 82–91.

Claussen, M., Kubatzki, C., Brovkin, V., Ganopolski, A., Hoelzmann, P., and Pachur, 1999, Simulation of an abrupt change in Saharan vegetation in the mid-Holocene: Geopysical Research Letters, v. 26, p. 2037–2040.

Clement, A.C., Hall, A., and Broccoli, A.J., 2004, The importance of precessional signals in the tropical climate: Climate Dynamics, v. 22, p. 327–341.

Cogley, J.G., 1979, The albedo of water as a function of latitude: Monthly Weather Review, v. 107, p. 775–781.

Costa, K., Russell, J., Konecky, B., and Lamb, H., 2014, Isotopic reconstruction of the African Humid Period and Congo Air Boundary migration at Lake Tana, Ethiopia: Quaternary Science Reviews, v. 83, p. 58–67.

Van Couvering, J.A., 1972, Geology of Rusinga Island and Correlation of the Kenya Mid-Tertiary Fauna: Cambridge, Cambridge University, Ph.D. dissertation, 208 p.

Cowling, S.A., Cox, P.M., Jones, C.D., Maslin, M.A., Peros, M., and Spall, S.A., 2008, Simulated glacial and interglacial vegetation across Africa: Implications for species phylogenies and trans-African migration of plants and animals: Global Change Biology, v. 14, p. 827–840.

Crul, R.C.M., 1995, Limnology and hydrology of Lake Victoria, *in* Comprehensive and Comparative Study of Great Lakes: UNESCO Publishing, Dijon, 79 p.

Cuthbert, M.O., and Ashley, G.M., 2014, A spring forward for hominin evolution in East Africa: PLoS ONE, v. 9, p. 1–9.

Dagg, M., Woodhead, T., and Rijks, D. a., 1970, Evaporation in East Africa: Bulletin of the International Association of Scientific Hydrology, v. 15, p. 61–67.

Dansgard, W., 1964, Stable isotopes in precipitation: Tellus, v. 16, p. 436–468.

Ditchfield, P., Hicks, J., Plummer, T., Bishop, L.C., and Potts, R., 1999, Current research on the Late Pliocene and Pleistocene deposits north of Homa Mountain, southwestern Kenya: Journal of Human Evolution, v. 36, p. 123–150.

Doornkamp, J.C., and Temple, P.H., 1966, Surface, drainage and tectonic instability in part of southern Uganda: The Geographical Journal, v. 132, p. 238–252.

Driese, S.G., Jacobs, J.R., and Nordt, L.C., 2003, Comparison of modern and ancient Vertisols developed on limestone in terms of their geochemistry and parent material: Sedimentary Geology, v. 157, p. 49–69.

Driese, S.G., Mora, C.I., Stiles, C.A., Joeckel, R.M., and Nordt, L.C., 2000, Mass-balance reconstruction of a modern Vertisol: implications for interpreting the geochemistry and burial alteration of paleo-Vertisols: Geoderma, v. 95, p. 179–204.

East African Meteorological Department, 1975a, Part I - Kenya: E.A. Community, Nairobi, Kenya, 1-92 p.

East African Meteorological Department, 1975b, Part II Uganda: E.A. Community, Nairobi, Kenya, 1-53 p.

East African Meteorological Department, 1975c, Part III - Tanzania: E.A. Community, Nairobi, Kenya, 1-92 p.

Ebinger, C.J., 1989, Tectonic development of the western branch of the East African rift system: Geological Society of America Bulletin, v. 101, p. 885–903.

Eriksson, A., Betti, L., Friend, A.D., Lycett, S.J., Singarayer, J.S., von Cramon-Taubadel, N., Valdes, P.J., Balloux, F., and Manica, A., 2012, Late Pleistocene climate change and the global expansion of anatomically modern humans.: Proceedings of the National Academy of Sciences of the United States of America, v. 109, p. 16089–16094.

Faith, J.T., 2014, Late Pleistocene and Holocene mammal extinctions on continental Africa: Earth-Science Reviews, v. 128, p. 105–121.

Faith, J.T., Choiniere, J.N., Tryon, C.A., Peppe, D.J., and Fox, D.L., 2011, Taxonomic status and paleoecology of Rusingoryx atopocranion (Mammalia, Artiodactyla), an extinct Pleistocene bovid from Rusinga Island, Kenya: Quaternary Research, v. 75, p. 697–707.

Faith, J.T., Potts, R., Plummer, T.W., Bishop, L.C., Marean, C.W., and Tryon, C.A., 2012, New perspectives on middle Pleistocene change in the large mammal faunas of East Africa: Damaliscus hypsodon sp. nov. (Mammalia, Artiodactyla) from Lainyamok, Kenya: Palaeogeography, Palaeoclimatology, Palaeoecology, v. 361-362, p. 84–93.

Faith, J.T., Tryon, C.A., and Peppe, D.J. Environmental change, ungulate biogeography, and their implications for early human dispersals in equatorial East Africa, *in* Jones, S.C. and Stewart, B.A. eds., Africa from MIS 6-2: Population Dynamics and Paleoenvironments: Springer.

Faith, J.T., Tryon, C.A., Peppe, D.J., Beverly, E.J., and Blegen, N., 2014, Biogeographic and Evolutionary Implications of an Extinct Late Pleistocene Impala from the Lake Victoria Basin , Kenya: Journal of Mammalian Evolution, v. 21, p. 213–222.

Faith, J.T., Tryon, C. a., Peppe, D.J., Beverly, E.J., Blegen, N., Blumenthal, S., Chritz, K.L., Driese, S.G., and Patterson, D., 2015, Paleoenvironmental context of the Middle Stone Age record from Karungu, Lake Victoria Basin, Kenya, and its implications for human and faunal dispersal in East Africa: Journal of Human Evolution, v. 83, no. 28-45, p. 28–45.

Faure, G., 1986, Oxygen and hydrogen in the lithosphere, *in* Principles of Isotope Geology: Wiley & Sons, New York, p. 460–462.

Fey, M., Hughes, J., Lambrechts, J., and Dohse, T., 2010, Vertic Soils, *in* Soils of South Africa: Cambridge University Press, Cape Town, South Africa, p. 35–45.

Fillinger, U., Sonye, G., Killeen, G.F., Knols, B.G.J., and Becker, N., 2004, The practical importance of permanent and semipermanent habitats for controlling aquatic stages of Anopheles gambiae sensu lato mosquitoes: operational observations from a rural town in western Kenya: Tropical Medicine and International Health, v. 9, no. 12, p. 1274–1289.

Fitzpatrick, E.A., 1993, Soil microscopy and micromorphology: John Wiley & Sons, New York, 304 p.

Freytet, P., Kerp, H., and Broutin, J., 1996, Permian freshwater stromatolites associated with the conifer shoots Cassinisia orobica Kerp et al . - a very peculiar type of fossilization: Review of Palaeobotany and Palynology, v. 91, p. 85–105.

Freytet, P., and Plet, A., 1996, Modern freshwater microbial carbonates: The Phormidium stromatolites (tufa-travertine) of Southeastern Burgundy (Paris Basin, France): Facies, v. 34, p. 219–237.

Freytet, P., and Verrecchia, E.P., 1998, Freshwater organisms that build stromatolites: a synopsis of biocrystallization by prokaryotic and eukaryotic algae: Sedimentology, v. 45, p. 535–563.

Freytet, P., and Verrecchia, E.P., 2007, Lacustrine and palustrine carbonate petrography: an overview: Journal of Paleolimnology, v. 27, p. 221–237.

Garcea, E.A.A., and Giraudi, C., 2006, Late Quaternary human settlement patterning in the Jebel Gharbi.: Journal of Human Evolution, v. 51, p. 411–421.

Garrett, N.D., Fox, D.L., Mcnulty, K.P., Tryon, C.A., Faith, J.T., Peppe, D.J., and Plantinga, A. Van, 2015, Stable isotope paleoecology of late pleistocene middle stone age humans from the equatorial East Africa, Lake Victoria basin, Kenya: Journal of Human Evolution, v. 82, p. 1–14.

Gasse, F., Chalié, F., Vincens, A., Williams, M.A.J., and Williamson, D., 2008, Climatic patterns in equatorial and southern Africa from 30,000 to 10,000 years ago reconstructed from terrestrial and near-shore proxy data: Quaternary Science Reviews, v. 27, no. 25-26, p. 2316–2340.

Glassy, J.M., and Running, S.W., 1994, Validating diurnal climatology logic of the MT-CLIM model across a climatic gradient in Oregon: Ecological Applications, v. 4, p. 248–257.

Hallsworth, E.G., and Beckman, G.G., 1969, Gilgai in the Quaternary: Soil Science, v. 107, no. 6, p. 409–420.

Hallsworth, E.G., Robertson, G.K., and Gibbons, F.R., 1955, Studies in pedogenesis in New South Wales: Journal of Soil Science, v. 6, no. 1, p. 1–31.

Haynes, C.V., Maxwell, T.A., Hawart, A.E., Nicoll, K.A., and Stokes, C.E., 1997, An Acheulian site near Bir Kiseiba in the Darb el Arb'in Desert: Geoarchaeology, v. 12, p. 819–832.

Holden, N.E., 1990, Total half-lives for selected nuclides: Pure and Applied Chemistry, v. 62, p. 941–958.

Horvatinčić, N., Krajcar Bronić, I., and Obelić, B., 2003, Differences in the 14C age, δ13C and δ18O of Holocene tufa and speleothem in the Dinaric Karst: Palaeogeography, Palaeoclimatology, Palaeoecology, v. 193, p. 139–157.

Howell, P., Lock, M., and Cobb, S. (Eds.), 1988, The Jonglei Canal: Impact and Opportunity: Cambridge University Press, New York, 572 p.

Hurst, H.E., and Phillips, P., 1933, The Nile Basin, vol III. Ten-day mean and monthly mean gauge readings of the Nile and its tributaries: Government Press, Cairo.

Ihlenfeld, C., Norman, M.D., Gagan, M.K., Drysdale, R.N., Maas, R., and Webb, J., 2003, Climatic significance of seasonal trace element and stable isotope variations in a modern freshwater tufa: Geochimica et Cosmochimica Acta, v. 67, no. 13, p. 2341–2357.

Jaffey, A.H., Flynn, K.F., Glendenin, L.E., Bentley, W.C., and Essling, A.M., 1971, Precise measurement of half-lives and specific activities of 235U and 238U: Physical Review Series C, v. 4, p. 1889–1906.

Johnson, C.R., Ashley, G.M., De Wet, C.B., Dvoretsky, R., Park, L., Hover, V.C., Bernhart Owen, R., and Mcbrearty, S., 2009, Tufa as a record of perennial fresh water in a semi-arid rift basin, Kapthurin Formation, Kenya: Sedimentology, v. 56, p. 1115–1137.

Johnson, C.R., and McBrearty, S., 2012, Archaeology of middle Pleistocene lacustrine and spring paleoenvironments in the Kapthurin Formation, Kenya: Journal of Anthropological Archaeology, v. 31, no. 4, p. 485–499.

Johnson, T.C., Scholz, C.A., Talbot, M.R., Kelts, K., Ricketts, R.D., Ngobi, G., Beuning, K.R., Ssemmanda, I., and McGill, J.W., 1996, Late Pleistocene dessication of Lake Victoria and rapid evolution of cichlid fishes: Science, v. 273, p. 1091–1093.

Johnson, R.W., and Tothill, J.C., 1985, Definition and broad geographic outline of savanna lands, *in* Ecology and management of the world's savannas: Australian Academy of Science, Canberra, p. 1–13.

Jongmans, a. G., Buurman, P., van Doesburg, J.D.J., van Oort, F., and Jaunet, a. M., 1994, Morphology, Chemistry, and Mineralogy of Isotropic Aluminosilicate Coatings in a Guadeloupe Andisol: Soil Science Society of America Journal, v. 58, p. 501–507.

Jongmans, A.G., Pulleman, M.M., and Marinissen, J.C.Y., 2001, Soil structure and earthworm activity in a marine silt loam under pasture versus arable land: Biology and Fertility of Soils, v. 33, p. 279–285.

Jungerius, P.D., van den Ancker, J.A.M., and Mucher, H.J., 1999, The contribution of termites to the microgranular structure of soils on the Uasin Gishu Plateau, Kenya: Catena, v. 34, p. 349–363.

Kendall, R.L., 1969, An ecological history of the Lake Victoria Basin: Ecological Monographs, v. 39, p. 121–176.

Kent, P.E., 1944, The age and tectonic relationships of East African Volcanic Rocks: Geological Magazine, v. 81, p. 15–27.

Kite, G.W., 1981, Recent changes in level of Lake Victoria: Hydrological Sciences Bulletin, v. 26, no. 3, p. 233–243.

Kite, G.W., 1982, Analysis of Lake Victoria levels: Hydrological Sciences Journal, v. 27, no. 2, p. 99–110.

Kraus, M.J., 1999, Paleosols in clastic sedimentary rocks: their geologic applications: Earth-Science Reviews, v. 47, p. 41–70.

Laskar, J., Robutel, P., Joutel, F., Gastineau, M., Correia, a. C.M., and Levrard, B., 2004, A long-term numerical solution for the insolation quantities of the Earth: Astronomy and Astrophysics, v. 428, p. 261–285.

Lee, R.K.L., Owen, R.B., Renaut, R.W., Behrensmeyer, A.K., Potts, R., and Sharp, W.D., 2013, Facies, geochemistry and diatoms of late Pleistocene Olorgesailie tufas, southern Kenya Rift: Palaeogeography, Palaeoclimatology, Palaeoecology, v. 374, p. 197–217.

Levin, N.E., Cerling, T.E., Passey, B.H., Harris, J.M., and Ehleringer, J.R., 2006, A stable isotope aridity index for terrestrial environments: Proceedings of the National Academy of Sciences of the United States of America, v. 103, no. 30, p. 11201–11205.

Liu, Z., Li, Q., Sun, H., Liao, C., Li, H., Wang, J., and Wu, K., 2006a, Diurnal Variations of Hydrochemistry in a Travertine-depositing Stream at Baishuitai, Yunnan, SW China: Aquatic Geochemistry, v. 12, p. 103–121.

Liu, H., Prugnolle, F., Manica, A., and Balloux, F., 2006b, A geographically explicit genetic model of worldwide human-settlement history: The American Journal of Human Genetics, v. 79, no. August, p. 230–237.

Lorenzen, E.D., Heller, R., and Siegismund, H.R., 2012, Comparative phylogeography of African savannah ungulates: Molecular Ecology, v. 21, p. 3656–3670.

Ludwig, K.R., Wallace, A.R., and Simmons, K.R., 1985, The Schwartzwalder uranium deposit, II: age of uranium mineralization and Pb-isotope constraints on genesis: Economic Geology, v. 80, p. 1858–1871.

Machel, H.G., Mason, R.A., Mariano, A.N., and Mucci, A., 1991, Causes and emission of luminescence in calcite and dolomite, *in* Barker, C.E. and Kopp, O.C. eds., Luminescence Microscopy and Spectroscopy: Quatitative and Qualitative Applications (SC25): SEPM, p. 9–25.

Marbut, C.F., 1935, Atlas of American Agriculture: Part III Soils of the United States: Goverment Printing Office, Washington D.C., 98 p.

Martini, I., and Capezzuoli, E., 2014, Interdigitated fluvial clastic deposits and calcareous tufa testifying an uplift of the catchment area: An example from the Pianizzoli area (southern Tuscany, Italy): Sedimentary Geology, v. 299, p. 60–73.

Matsuoka, J., Kano, A., Oba, T., Watanabe, T., Sakai, S., and Seto, K., 2001, Seasonal variation of stable isotopic compositions recorded in a laminated tufa, SW Japan: Earth and Planetary Science Letters, v. 192, p. 31–44.

Mcbrearty, S., and Brooks, A.S., 2000, The revolution that wasn't: a new interpretation of the origin of modern human behavior.: Journal of Human Evolution, v. 39, p. 453–563.

McDougall, I., Brown, F.H., and Fleagle, J.G., 2005, Stratigraphic placement and age of modern humans from Kibish, Ethiopia.: Nature, v. 433, p. 733–736.

McJannet, D.L., Webster, I.T., and Cook, F.J., 2012, An area-dependent wind function for estimating open water evaporation using land-based meteorological data: Environmental Modelling and Software, v. 31, p. 76–83.

McKenzie, J., 1993, Pluvial conditions in the eastern Sahara following the penultimate deglaciation: implications for changes in atmospheric circulation patterns with global warming: Palaeogeography, Palaeoclimatology, Palaeoecology, v. 103, p. 95–105.

Miall, A.D., 2010, Alluvial deposits, *in* James, N.P. and Dalrymple, R.W. eds., Facies Models 4: Geological Association of Canada, St John's, Newfoundland, p. 105–137.

Milly, P.C.D., 1999, Comment on “Antiphasing between Rainfall in Africa’s Rift Valley and North America's Great Basin”: Quaternary Research, v. 51, p. 104–107.

Milne, G., 1936, Normal Erosion as a Factor in Soil Profile Development: Nature, v. 138, p. 548–549.

Moernaut, J., Verschuren, D., Charlet, F., Kristen, I., Fagot, M., and De Batist, M., 2010, The seismic-stratigraphic record of lake-level fluctuations in Lake Challa: Hydrological stability and change in equatorial East Africa over the last 140kyr: Earth and Planetary Science Letters, v. 290, no. 1-2, p. 214–223.

Monteith, J., and Unsworth, M., 2008, Principles of Environmental Physics: Academic Press, Amsterdam, 418 p.

Moore, D.M., and Reynolds, R.C., 1997, X-Ray diffraction and the identification and analysis of clay minerals, *in* Oxford University Press, New York, p. 378.

Mora, C.I., and Driese, S., 1999, Palaeoenvironment, palaeoclimate, and stable carbon isotopes of Palaeozoic red-bed palaeosols, Appalachian Basin, USA and Canada, *in* Thiry, M. and Simon-Coinçon, R. eds., Palaeoweathering, Palaeosurfaces and Related Continental Deposits: Blackwell Publishing Ltd, Oxford.

Niang, I., Ruppel, O.C., Abdrabo, M.A., Essel, A., Lennard, C., Padgham, J., and Urquhart, P., 2014, Africa, *in* Barros, V.R., Field, C.B., Dokken, D.J., Mastrandrea, M.D., Mach, K.J., Bilir, T.E., Chatterjee, M., Ebi, K.L., Estrada, Y.O., Genova, R.C., Girma, B., Kissel, E.S., Levy, A.N., MacCracken, S., and others eds., Climate Change 2014: Impacts, Adaptation, and Vulnerability. Part B: Regional Aspects. Contribution of Working Group II to the Fifth Assessment Report of the Intergovernmental Panel on Climate Change: Cambridge University Press, New York, p. 1199–1265.

Nicholson, S.E., 1996, A review of climate dynamics and climate variability in Eastern Africa, *in* Johnson, T.C. and Odada, E.O. eds., The limnology, climatology and paleoclimatology of the East African Lakes: Gordon and Breach Publishers, Netherlands, p. 25–56.

Nicholson, S.E., Yin, X., and Ba, M.B., 2000, On the feasibility of using a lake water balance model to infer rainfall: an example from Lake Victoria: Hydrological Sciences Journal, v. 45, no. 1, p. 75–95.

Nicoll, K., Giegengack, R., and Kleindienst, M., 1999, Petrogenesis of artifact-bearing fossil-spring tufa deposits from Kharga Oasis, Egypt: Geoarchaeology, v. 14, no. 8, p. 849–863.

Nordt, L.C., and Driese, S.G., 2009, Hydropedological assessment of a vertisol climosequence on the Gulf Coast Prairie Land Resource Area of Texas: Hydrology and Earth System Sciences, v. 13, p. 2039–2053.

Nordt, L.C., and Driese, S.G., 2010a, A modern soil characterization approach to reconstructing physical and chemical properties of paleo-Vertisols: American Journal of Science, v. 310, no. 1, p. 37–64.

Nordt, L.C., and Driese, S.G., 2010b, New weathering index improves paleorainfall estimates from Vertisols: Geology, v. 38, no. 5, p. 407–410.

Ordóñez, S., González Martín, J. a., García del Cura, M. a., and Pedley, H.M., 2005, Temperate and semi-arid tufas in the Pleistocene to Recent fluvial barrage system in the Mediterranean area: The Ruidera Lakes Natural Park (Central Spain): Geomorphology, v. 69, p. 332–350.

Ortiz, J.E., Torres, T., Delgado, A., Reyes, E., and Diaz-Bautista, A., 2009, A review of the Tagus river tufa deposits (central Spain): age and palaeoenvironmental record: Quaternary Science Reviews, v. 28, p. 947–963.

Owen, W.E., 1937, Draft of tentative preliminary report on the July 1937 investigations at Ng'ira Karungu.:

Owen, W.E., 1938, The Kombewa Culture, Kenya Colony: Man, v. 38, p. 203–205.

Owen, W.E., 1939, An amateur field collector in Kavirondo, Part II: Journal of the Royal African Society, v. 38, no. 2250-226.

Pavlović, G., Prohić, E., Miko, S., and Tibljaš, D., 2002, Geochemical and petrographic evidence of meteoric diagenesis in tufa deposits in Northern Dalmatia (Zrmanja and Krupa Rivers, Croatia): Facies, v. 46, p. 27–34.

Pedley, H.M., 1990, Classification and environmental models of cool freshwater tufas: Sedimentary Geology, v. 68, p. 143–154.

Pedley, M., Martín, J.A.G., Delogado, S.O., and García del Cura, M.A., 2003, Sedimentology of Quaternary perched springline and paludal tufas: criteria for recognition, with examples from Guadalajara Province, Spain: Sedimentology, v. 50, p. 23–44.

Pentecost, A., and Spiro, B., 1990, Stable carbon and oxygen isotope composition of calcites associated with modern freshwater cyanobacteria and algae: Geomicrobiology Journal, v. 8, no. 1, p. 17–26.

Pickford, M.H., 1984, An aberrant new bovid (Mammalia) in subrecent deposits from Rusinga island, Kenya: Proceedings of the Koninklijke Nederlandse Akademie Van Wetenschappen Series B: Palaeontology, Geology, Physics, Chemistry, Anthropology, v. 87, p. 441–452.

Piper, B.S., Plinston, D.T., and Barton, H., 1986, The water balance of Lake Victoria: Hydrological Sciences Journal, v. 31, p. 25–37.

Van Plantinga, A.A., 2011, Geology of the Late Pleistocene artifact-bearing WAsiriya Beds at the Nyamita locality, Rusinga Island, Kenya:.

Plummer, T., Bishop, L.C., Ditchfield, P., and Hicks, J., 1999, Research on Late Pliocene Oldowan Sites at Kanjera South, Kenya: Journal of Human Evolution, v. 36, p. 151–170.

Retallack, G.J., 2001, Soils of the past: An introduction to paleopedology: Blackwell Science Ltd, Oxford, 512 p.

Riding, R., 2000, Microbial carbonates: the geological record of calcified bacterial-algal mats and biofilms: Sedimentology, v. 47, p. 179–214.

Rito, T., Richards, M.B., Fernandes, V., Alshamali, F., Cerny, V., Pereira, L., and Soares, P., 2013, The first modern human dispersals across Africa.: PloS one, v. 8, no. 11, p. e80031.

Rogers, R.R., and Yau, M.K., 1989, A Short Course in Cloud Physics: Butterworth-Heinemann, 304 p.

Romanek, C.S., Grossman, E.L., and Morse, J.W., 1992, Carbon isotopic fractionation in synthetic aragonite and calcite: Effects of temperature and precipitation rate: Geochimica et Cosmochimica Acta, v. 56, no. 1, p. 419–430.

Rozanski, K., Araguas-Araguas, L., and Gonfiantini, R., 1993, Isotopic patterns in modern global precipitation: Geophysical Monograph, v. 78, p. 1–36.

Rozanski, K., Araguas-Araguas, L., and Gonfiantini, R., 1996, Isotope patterns of precipitation in the East African Region, *in* Johnson, T.C. and Odada, E.O. eds., The limnology, climatology and paleoclimatology of the East African Lakes: Gordon and Breach Publishers, Netherlands, p. 79–93.

Scholz, C. a, Johnson, T.C., Cohen, A.S., King, J.W., Peck, J. a, Overpeck, J.T., Talbot, M.R., Brown, E.T., Kalindekafe, L., Amoako, P.Y.O., Lyons, R.P., Shanahan, T.M., Castañeda, I.S., Heil, C.W., and others, 2007, East African megadroughts between 135 and 75 thousand years ago and bearing on early-modern human origins.: Proceedings of the National Academy of Sciences of the United States of America, v. 104, no. 42, p. 16416–16421.

Shahin, M., 1985, Hydrology of the Nile Basin: Elsevier, Amsterdam, 575 p.

Sheldon, N.D., Retallack, G.J., and Tanaka, S., 2002, Geochemical climofunctions from North America soils and applications to paleosols across the Eocene-Oligocene Boundary in Oregon: The Journal of Geology, v. 110, no. 6, p. 687–696.

Sheldon, N.D., and Tabor, N.J., 2009, Quantitative paleoenvironmental and paleoclimatic reconstruction using paleosols: Earth-Science Reviews, v. 95, no. 1-2, p. 1–52.

Sinclair, A.R.E., 1979, The Serengeti Environment, *in* Sinclair, A.R.E. and Norton-Griffiths, M. eds., Serengeti: Dynamics of an ecosystem: The University of Chicago Press, Chicago, p. 31–45.

Smith, J., Giegengack, R., and Schwarcz, H., 2004, Constraints on Pleistocene pluvial climates through stable-isotope analysis of fossil-spring tufas and associated gastropods, Kharga Oasis, Egypt: Palaeogeography, Palaeoclimatology, Palaeoecology, v. 206, p. 157–175.

Smith, J.R., Hawkins, A.L., Asmerom, Y., Polyak, V., and Giegengack, R., 2007, New age constraints on the Middle Stone Age occupations of Kharga Oasis, Western Desert, Egypt.: Journal of Human Evolution, v. 52, no. 6, p. 690–701.

Soares, P., Alshamali, F., Pereira, J.B., Fernandes, V., Silva, N.M., Afonso, C., Costa, M.D., Musilová, E., Macaulay, V., Richards, M.B., Cerny, V., and Pereira, L., 2012, The Expansion of mtDNA Haplogroup L3 within and out of Africa.: Molecular Biology and Evolution, v. 29, no. 3, p. 915–927.

Soil Survey Staff, 1999, Soil Taxonomy: A Basic System of Soil Classification for Making and Interpreting Soil Surveys: USDA NRCS, Washington D.C., 871 p.

Song, Y., Semazzi, F.H.M., Xie, L., and Ogallo, L.J., 2004, A coupled regional climate model for the Lake Victoria Basin of East Africa: International Journal of Climatology, v. 24, p. 57–75.

Stager, J.C., and Johnson, T.C., 2008, The late Pleistocene desiccation of Lake Victoria and the origin of its endemic biota: Hydrobiologia, v. 596, no. 1, p. 5–16.

Stager, J.C., Mayewski, L., and Meeker, L.D., 2002, Cooling cycles, Heinrich event 1, and the desiccation of Lake Victoria: Palaeogeography, Palaeoclimatology, Palaeoecology, v. 183, p. 169–178.

Stager, J.C., Ryves, D.B., Chase, B.M., and Pausata, F.S.R., 2011, Catastrophic drought in the Afro-Asian monsoon region during Heinrich Event 1: Science, v. 331, no. 6022, p. 1299–1302.

Stoops, G., 2003, Guidelines for Analysis and Description of Soil and Regolith Thin Sections (M. J. Vepraskas, Ed.): Soil Science Society of America, Inc. , Madison, Wisconsin, 184 p.

Stoops, G., Marcelino, V., and Mees, F. (Eds.), 2010, Interpretation of Micromorphological Features of Soils and Regoliths: Elsevier, Netherlands, 720 p.

Sundborg, A., 1956, The River Klaralven: A Study of Fluvial Processes: Geografiska Annaler, v. 38, no. 3, p. 238–316.

Sutcliffe, J.V., and Parks, Y.P., 1999, The Hydrology of the Nile: IAHS Special Publication, v. 5, no. 5, p. 192.

Sutcliffe, J. V, and Petersen, G., 2007, Lake Victoria: derivation of a corrected natural water level series: Hydrological Sciences Journal, v. 52, p. 1316–1321.

Sweagudde, S.M., 2009, Lake Victoria ' s Water Budget and the Potential Effects of Climate Change in the 21st Century ↔ Paper presented to the Lake Victoria: African Journal of Tropical Hydrobiology and Fisheries, v. 30, no. October 2008, p. 22–30.

Tabor, N.J., and Myers, T.S., 2015, Paleosols as Indicators of Paleoenvironment and Paleoclimate: Annual Review of Earth and Planetary Sciences, v. 43, p. 11.1–11.29.

Talbot, M.R., and Laerdal, T., 2000, The late Pleistocene - Holocene palaeolimnology of Lake Victoria, East Africa, based upon elemental and isotopic analyses of sedimentary organic matter: Journal of Paleolimnology, v. 23, p. 141–164.

Talbot, M.R., and Williams, M.A.J., 2009, Cenozoic evolution of the Nile Basin, *in* Dumont, H.J. ed., The Nile: Origin, Environments, Limnology and Human Use: Springer Science + Business Media B.V., p. 37–60.

Temple, P.H., 1966, Evidence of changes in the level of Lake Victoria and their significance:.

Tierney, J.E., Russell, J.M., Huang, Y., Damsté, J.S.S., Hopmans, E.C., and Cohen, A.S., 2008, Northern hemisphere controls on tropical southeast African climate during the past 60,000 years: Science, v. 322, no. 5899, p. 252–255.

Tierney, J.E., Russell, J.M., Sinninghe Damsté, J.S., Huang, Y., and Verschuren, D., 2011, Late Quaternary behavior of the East African monsoon and the importance of the Congo Air Boundary: Quaternary Science Reviews, v. 30, p. 798–807.

Trauth, M.H., Deino, A.L., Bergner, A.G.N., and Strecker, M.R., 2003, East African climate change and orbital forcing during the last 175 kyr BP: Earth and Planetary Science Letters, v. 206, no. 3-4, p. 297–313.

Tryon, C. a., Faith, J.T., Peppe, D.J., Fox, D.L., McNulty, K.P., Jenkins, K., Dunsworth, H., Harcourt-Smith, W., Tyler Faith, J., Peppe, D.J., Fox, D.L., McNulty, K.P., Jenkins, K., Dunsworth, H., and others, 2010, The Pleistocene archaeology and environments of the Wasiriya Beds, Rusinga Island, Kenya: Journal of Human Evolution, v. 59, p. 657–671.

Tryon, C.A., Faith, J.T., Peppe, D.J., Keegan, W.F., Keegan, K.N., Jenkins, K.H., Nightingale, S., Patterson, D., Van Plantinga, A., Driese, S., Johnson, C.R., and Beverly, E.J., 2014, Sites on the landscape: Paleoenvironmental context of late Pleistocene archaeological sites from the Lake Victoria basin, equatorial East Africa: Quaternary International, v. 331, p. 20–30.

Tryon, C.A., Peppe, D.J., Faith, J.T., Van Plantinga, A., Nightingale, S., Ogondo, J., and Fox, D.L., 2012, Late Pleistocene artefacts and fauna from Rusinga and Mfangano islands, Lake Victoria, Kenya: Azania: Archaeological Research in Africa, v. 47, no. 1, p. 14–38.

Ufnar, D., 2007, Clay coatings from a modern soil chronosequence: A tool for estimating the relative age of well-drained paleosols: Geoderma, v. 141, no. 3-4, p. 181–200.

Vepraskas, M.J., 1992, Redoximorphic features for identifying aquic conditions: North Carolina State University Technical Bulletin 301: North Carolina Agricultural Research Service, Raleigh, NC, 33 p.

Vepraskas, M.J., 2001, Morphological features of seasonally reduced soils, *in* Wetland Soils: Genesis, Hydrology, Landscapes, and Classification: Lewis Publishers, New York, p. 163–182.

Vepraskas, M.J., and Faulkner, S.P., 2001, Redox chemistry of hydric soils, *in* Richardson, J.L. and Vepraskas, M.J. eds., Wetland Solis; Genesis, Hydrology, Landscapes, and Classification: Lewis Publishers, New York, p. 85–105.

Verschuren, D., Johnson, T.C., Kling, H.J., Edgington, D.N., Leavitt, P.R., Brown, E.T., Talbot, M.R., and Hecky, R.E., 2002, History and timing of human impact on Lake Victoria, East Africa.: Proceedings of the Royal Society of London Biology, v. 269, no. 1488, p. 289–294.

Verschuren, D., Sinninghe Damsté, J.S., Moernaut, J., Kristen, I., Blaauw, M., Fagot, M., and Haug, G.H., 2009, Half-precessional dynamics of monsoon rainfall near the East African Equator.: Nature, v. 462, p. 637–641.

Verster, E., de Villiers, J.M., and Scheepers, J.C., 1973, Gilgai in the Rustenburg Area: Agrochemophysica, v. 4, p. 57–62.

Vesey-Fitzgerald, D., 1973, East African Grasslands: East African Publishing House, Nairobi, Kenya.

Viles, H.A., Taylor, M.P., Nicoll, K., and Neumann, S., 2007, Facies evidence of hydroclimatic regime shifts in tufa depositional sequences from the arid Naukluft Mountains, Namibia: Sedimentary Geology, v. 195, no. 1-2, p. 39–53.

Wang, Y., Cheng, H., Edwards, R.L., Kong, X., Shao, X., Chen, S., Wu, J., Jiang, X., Wang, X., and An, Z., 2008, Millennial- and orbital-scale changes in the East Asian monsoon over the past 224,000 years: Nature, v. 451, no. 7182, p. 1090–1093.

Weldeab, S., Lea, D.W., Schneider, R.R., and Andersen, N., 2007, 155,000 years of West African monsoon and ocean thermal evolution.: Science (New York, N.Y.), v. 316, p. 1303–1307.

Wendorf, F., 1993, Egypt during the Last Interglacial: The Middle Paleolithic of Bir Tarfawi and Bir Sahara East: Springer Science + Business Media, New York, 596 p.

Wigley, T.M.L., and Jones, P.D., 1985, Influences of precipitation changes and direct CO2 effects on streamflow: Nature, v. 314, no. 6007, p. 149–152.

Wynn, J.G., 2000, Paleosols, stable carbon isotopes, and paleoenvironmental interpretation of Kanapoi, Northern Kenya.: Journal of Human Evolution, v. 39, p. 411–432.

Yin, X., and Nicholson, S.E., 1998, The water balance of Lake Victoria: Hydrological Sciences Journal, v. 43, no. 5, p. 789–811.

Zamarreño, I., Anadón, P., and Utrilla, R., 1997, Sedimentology and isotopic composition of Upper Palaeocene to Eocene non-marine stromatolites, eastern Ebro Basin, NE Spain: Sedimentology, v. 44, p. 159–176.

Zimmerman, U., Ehhalt, D., and Munnich, K.O., 1967, Soil-water movement and evapotranspiration: changes in the isotopic composition of the water, *in* Isotopes in Hydrology: International Atomic Energy Agency, Vienna, Austria, p. 567–585.